Characterisation of a parallel microbioreactor system and its application to accelerate cell culture process development

An EngD Thesis submitted to
University College London

by

Vincent Wiegmann

Declaration

I, Vincent Wiegmann, confirm that the work presented in this thesis is my own. Where information has been derived from other sources, I confirm that this has been indicated in the thesis.

Vincent Wiegmann, 18 June 2021

Acknowledgement

First and foremost, I am thankful to Dr Frank Baganz for his exemplary mentorship throughout the project. His scientific guidance has been invaluable and I am particularly grateful for his encouragement to explore areas and ideas that were originally outside the scope of this project. In conversation with him, I learned to think with scientific curiosity about the world of biochemical engineering and the world in general.

When I started at the Department of Biochemical Engineering, my understanding of microbioreactors, and the micro-Matrix in particular, was mostly theoretical. In Delft, Dr Cristina Bernal Martinez gave me the best practical introduction to the micro-Matrix I could have asked for and has been fantastic in supporting the project ever since. Further, I would also like to thank Dr Alexandros Kiparissides for his guidance as secondary supervisor and for making sure that the mammalian lab stays the organised and friendly place it is.

For their help and friendship I would like to express my gratitude to Hai-Yuan Goh, Roman Zakrzewski, Molly Tregidgo, Milena Rivera Trujillo, Maximilian Lularevic, Viktoria Gkoutzioupa, Dipankar Borgayari, Artemis Charalambidou, and Chileab Redwood-Sawyer who paved the way for this thesis to develop and generously provided practical support out of their own time.

I am grateful to Dr Richard Gardner and Dr Daniel Spencer from Ludger Ltd for performing the glycoanalysis shown in this work as part of a collaborative project. This data provided an important puzzle piece of the thesis and I am thankful for the opportunity to learn more about the exciting field of glycobiology.

I thank Dr Arman Amini for introducing me to the fascinating opportunities and challenges of CAR T cell bioprocessing in a highly synergistic collaboration that was both fun and productive.

Throughout this project, the Vineyard office has been a superb place to exchange scholarly ideas and forge friendships. I would like to thank especially Rosalia, Neha, Alex, Becci, Victor, Matt, Pedro, Akash, Mau, and Bapi for being the great companions they are.

Finding your way around a new institution in a different country can be an intimidating task. Kate Sym ensured that my fellow doctoral cohort and I felt welcome from the start and she continued to give excellent advice in all administrative matters.

Special thanks goes to my parents Marion and Uwe Wiegmann for their love, encouragement and support, my grandparents, who I hold accountable for my scientific interest, and my sister for her great sense of humour. Finally, I wish to dedicate this work to my son Jack Stuart, who has taught me to never stop asking “Why?”.

Abstract

Recent advancements in the field of microbioreactor technologies have transformed early- and mid-stage process development. Microbioreactor systems benefit from monitoring and control capabilities akin to larger scale bioreactors that have been realised at a much smaller working volume, thereby promoting the quick accumulation of process knowledge early on in the development timeline. Furthermore, the control of key process parameters at the small scale led to improved scalability when compared to traditionally used systems such as shake flasks and microtitre plates. Ultimately, the successful implementation of microbioreactor systems in a bioprocess development workflow can reduce the time to market and decrease the price of biotechnology products.

This thesis sought to investigate whether the micro-Matrix microbioreactor (Applikon-Biotechnology BV) is a suitable instrument for cell culture process development. The system is based on a shaken 24 deep square well microtitre plate format with a working volume between 2 - 5 mL in which each well can be individually controlled for temperature, pH, and dissolved oxygen (DO) concentration.

The system was first characterised to gain a better understanding of the cultivation environment within each well and to identify a suitable scaling criterion to a reference benchtop-scale bioreactor system. Mixing times were found to range between 1 – 42 s, while the volumetric mass transfer coefficient (k_La) was 2.4 – 240.8 h^{-1}. Computational fluid dynamics was used to derive the power input, which was found to range between 4 W m^{-3} – 765 W m^{-3}. Initial cell cultivations revealed considerable evaporation rates and well-to-well variabilities, which were successfully addressed by establishing a method for the periodic replacement of evaporated liquid.

Mixing time was identified as suitable scaling criterion and a GS-CHO fed-batch process was scaled down from a reference stirred tank reactor (STR) with a working volume of 5 L to the micro-Matrix system. A problem specific to pH controlled small- and benchtop-scale bioreactors was highlighted, where the removal of CO_2 from the cultivation broth is very efficient and eventually CO_2 is stripped out completely. A low CO_2 concentration was shown to negatively affect the

maximum viable cell concentration in either system. A combination of matched mixing time and matched minimum CO_2 fraction in the inflowing gas was therefore proposed as suitable scaling criterion. Scalability of growth and production kinetics as well as antibody glycosylation were demonstrated between micro-Matrix and the 5 L reference STR system.

Subsequently, the micro-Matrix was used for the rapid optimisation of a GS-CHO feeding strategy. First, several bolus, continuous, and dynamic feed addition strategies were compared and bolus feeding was shown to be sufficient for the cell line under investigation. With the help of response surface methodology, the bolus feeding regime was optimised, which led to a 25.4% increase of the space-time yield and a 25 % increase of the final titre. Following a highly replicated validation of the results in the micro-Matrix, the optimised feeding strategy was scaled up to the 5 L STR system and shown to yield equivalent results.

In the final chapter of the thesis, the focus was shifted to an emerging application for small-scale process development systems by investigating the effect of the cultivation environment on the growth and differentiation of the primary T cells. Initially, a perfusion-mimic process was identified as suitable mode of operation, necessitated by the need to repeatedly replenish nutrients and remove waste metabolites. Using this perfusion-mimic process, pH, DO, and shaking speed setpoints were then investigated as part of a full-factorial design and explored for their effect on growth kinetics and differentiation of primary T cells. The numerical optimisation established a locally optimal final cell concentration and differentiation profile for a shaking speed of 200 rpm, a pH of 7.4, and a DO of 25%.

In summary, this work demonstrates the utility of the micro-Matrix microbioreactor in two bioprocess development applications and provides a toolbox and framework to aide with the implementation of the micro-Matrix in further bioprocessing applications.

Impact Statement

The work presented in this thesis is aimed to provide scientific insights and a framework that can be adopted by other researchers in both industry and academia and thereby contribute to the furthering of public health matters related to the manufacturing of biologics and cell therapies.

Initially, an engineering characterisation of Applikon's microbioreactor, the micro-Matrix, is conducted to investigate the cultivation environment in this platform and to provide the basis for ensuing process translations to larger scale systems. These characteristics are fundamental to the micro-Matrix system but can be time-consuming to establish. Their dissemination can therefore speed up development timelines of other researchers working with the same system and in turn positively affect research output.

The thesis then seeks to troubleshoot problems of variability and evaporation commonly encountered during fermentations and cell cultivations in small-scale bioreactor systems. The outlined advices and methodologies can be applied by other researchers to decrease experiment failures and increase the quality of the obtained experimental data.

A framework for rapid cell culture process optimisation presented as a case study, combines the individual objectives of the project and forms the central element of the thesis. The example illustrates how statistical tools can be used to leverage the high-throughput micro-Matrix system and how the results can then be translated to larger scale cultivation systems. Scale-up remains a challenging aspect of bioprocessing that is often accompanied by considerable expenditure of resources and time. The framework outlined here is generic as well as adaptable and may therefore be applied to the specific optimisation challenges of other research groups working with the same system.

The final chapter of the thesis considers challenges of the cell therapy sector by investigating the effect of different cultivation conditions on the expansion and differentiation of primary T cells. Currently, the T cell expansion process is largely uncharacterised and most studies have been conducted under uncontrolled and static cultivation conditions. The results provided in this thesis

demonstrate superior process outcomes under controlled and agitated conditions, which is an important step towards dissolving preconceptions regarding the shear sensitivity of T cells and it highlights the applicability of traditional bioprocessing concepts to T cell manufacturing. The results can not only help other researchers cut down development timelines, but potentially also reduce process durations, which is of particular importance in autologous therapies.

This work has been disseminated in four peer-reviewed publications, a book chapter, two webinar presentations, and two national as well as one international conference poster presentations. All peer-reviewed publications and webinar presentations are free of charge and therefore accessible to researchers as well as the wider public.

Table of Contents

List of Tables

List of Figures

Nomenclature

24 SRW	24 Standard round well microtiter plate
ADCC	Antibody-dependent cell-mediated cytotoxicity
a_i	Initial specific surface area of the gas phase
Asn-297	Asparagine residue at position 297
ATMP	Advanced therapy medicinal products
ATP	Adenine triphosphate
Bo	Bond number ($(\rho d^2 vg) / W$), dimensionless
C	Measured concentration of dissolved oxygen
C_0	Concentration of oxygen at t = 0
C_1	Dissolved oxygen concentration under saturated conditions
CAD	Computer-aided design
CAR	Chimeric antigen receptor
CCD	Circumscribed central composite design
CCF	Face-centred central composite design
CDC	Complement-dependent cytotoxicity
CD CHO	Chemically defined CHO cell medium
CFD	Computational fluid dynamics
CHO	Chinese Hamster Ovary
cIVCC	Cumulative integral viable cell concentration (cells d mL^{-1})
C_p	Dissolved oxygen concentration as measured by the probe
cv	Coefficient of variance
CV	Column volume
D	Diameter of impeller
d	Maximum inner diameter of a shake flask
DHFR	Dihydrofolate reductase
D_i	Diffusion coefficient
DISMT	Dual indicator system for mixing time
DNS	Direct numerical simulation
DO	Dissolved oxygen
D_{O2}	Diffusion coefficient of oxygen ($m^2\ s^{-1}$)
DoE	Design of Experiment
d_v	Inner well diameter
E. Coli	*Escherichia Coli*
Epo-Fc	Erythropoietin-Fc fusion protein
Fab	Antigen binding fragment
Fc	Crystallisable region fragment
Fl	Flow number (Q_G / ND^3), dimensionless
Fr	Froude number ($d_t(2\pi n)^2 / 2g$), dimensionless
G0/G1	Checkpoint between cell-cycle phases G1 and G0
GS	Glutamine synthetase
GU	Glucose unit
H(t)	Homogeneity index

HEPES	4-(2-Hydroxyethyl)-1-Piperazineethanesulfonic acid
HPLC	High-performance liquid chromatograph
IgX	Immunoglobulin of the isotope X
IVCC	Integral viable cell concentration (cells d mL^{-1})
k_La	Volumetric mass transfer coefficient
LAFB	micro-Matrix liquid addition feed bottle
LBE	Lattice-Boltzmann equation
LES	Large eddy simulation
mAb	Monoclonal antibody
MSX	Methionine sulphoximine
MTP	Microtiter plate
MTX	Methotrexate
MVDA	Multivariate data analysis
N	Rotational speed of impeller
n	Shaking frequency
NH_4^+	Ammonia
OFAT	One-factor-at-a-time
P/V	Volumetric power input
P_0	Power number ($P / \rho n^3 d^5$), dimensionless
P_0'	Modified power number ($P / \rho n^3 d^4 VL^{1/3}$), dimensionless
PBMCs	Peripheral blood mononuclear cells
PCA	Principal component analysis
pH(f)	Final pH
pH(i)	Initial pH
q_{mab}	Specific productivity (pg $cell^{-1}$ d^{-1})
q_{Nut}	Specific consumption rate (pg $cell^{-1}$ d^{-1})
Re	Reynolds number (ρnd2v / μ), dimensionless
RNA	Ribonucleic acid
rpm	Revolutions per minute
RSM	Response surface methodology
S	Strain rate (s^{-1})
Sc	Schmidt number (μ / (ρD)), dimensionelss
SRW	Standard round-well plate
STR	Stirred tank reactor
SUB	Single-use bioreactor
t_m	Mixing time
t_{mt}	$1 / k_La$
u	Superficial gas velocity
USD	Ultra scale-down
V_0	Total volume of shake flask
VCC	Viable cell concentration (cells mL^{-1})
V_L	Flask fill volume
vvm	Vessel volumes of gas per minute
$Y_{Lac/Gluc}$	Lactate yield (-)

η	Dynamic viscosity (Pa s)
μ	Growth rate (h^{-1})
ρ_L	Liquid density (kg m^{-3})
τ_p	Probe response time (s)
ω	Angular velocity (rad s^{-1})

Chapter 1. Introduction

1.1 Overview

The longstanding clinical and commercial success of monoclonal antibody (mAbs) products have motivated extensive academic and industrial research and led to substantial progress in the field. However, the development and manufacturing of mAb therapies remains expensive. Recent advances in microbioreactor technologies promise a more scalable early- and mid-stage upstream process development, which has the potential of accelerating development timelines and reducing the cost of goods. In this thesis, the micro-Matrix microbioreactor (Applikon-Biotechnology BV) is examined for its suitability as such a process development tool for mammalian cell culture applications.

1.2 Monoclonal Antibodies

1.2.1 Market and clinic

After making their first appearance in hybridoma cells in 1975 (Köhler and Milstein, 1975), monoclonal antibodies attracted a considerable amount of interest during the 1980s and quickly became both a clinical and financial success, particularly in the field of oncology (Reichert *et al.*, 2005). Antibody products promise fewer side effects than conventional systemic treatments of cancer as the toxicity is directed towards the cancer cells specifically by either employing the endogenous immune response or delivering a cytotoxic agent to the malicious cell (Dillman, 2001; Reichert and Valge-Archer, 2007; Simons *et al.*, 2013). Additionally, antibody drugs are not solely restricted to the treatment of cancer but can be applied to the treatment of autoimmune diseases, coronary syndromes, infections, and as a method of suppressing immune responses following a transplantation (Capriotti, 2001). Most of the mAbs currently on the market, however, target oncology and haematology diseases (Grilo and Mantalaris, 2019).

With a combined sales revenue of almost US$75 billion in 2013, monoclonal antibody products hold a strong position in the current biopharmaceuticals market and dominated the 2014 market with a 25.8% share (Ecker, Jones and Levine, 2015). Furthermore, the average annual growth

rate for the monoclonal antibodies segment was found to be approximately 9.3% between 2011 – 2014 (P&S Market Research, 2015) and will likely continue to grow annually by roughly 8% in the years to come. Since 2014, 47 monoclonal antibody products have been approved and a further 300 are still in development (Ecker, Jones and Levine, 2015). Since 2015, a total of 54 mAb products have reached phase 3 studies, which reveals a US$104 increase when compared to the number of phase 3 studies from 2009 (Reichert, 2016). This shows, the monoclonal antibodies market is still an innovative field with considerable medical and economical potential.

1.2.2 Structure

As part of the adaptive immune system, antibodies are produced as a defence mechanism against foreign substances. Antibodies recognise and bind intruding structures through the recognition of antigens. Antigens can be, but are not restricted to biopolymers such as proteins, glycoproteins, and polysaccharides, and are displayed on the surface of particles. Binding to these antigens initiates further immune responses and ultimately leads to the clearance of the foreign particle (Murphy, 2011). Antibodies are segmented into the immunoglobulin isotopes IgA, IgD, IgE, IgG, and IgM and further divided into several subclasses (Jefferis, 2007). IgG is the isotope most abundant in blood plasma and is also commonly used as a framework for therapeutic antibodies (Weiner, Surana and Wang, 2010; Murphy, 2011). Generally, IgG (Figure 1.1) is a monomer that consists of two identical antigen-binding fragments (Fab) and one crystallisable region fragment (Fc). Together they form a Y-shape in which the two Fab regions are attached to the Fc region through a flexible linker called the hinge-region (Jefferis, 2007). The variable domain at the amino-terminal section of each Fab region promotes binding to the antigen and in turn, promotes the recognition of any intruding body carrying an antigen. The Fc region can interact with effector molecules of the complement system (complement-dependent cytotoxicity, short CDC) or Fc receptors on phagocytes and natural killer cells (antibody-dependent cell-mediated cytotoxicity, short ADCC), both of which entail further immune responses and conclude in the clearance of the targeted particle. Additionally, foreign particles can be neutralised by antibody binding. The resulting coat of antibodies sterically prevents, for instance, pathogens from binding to cell surfaces and consequently leads to a loss of function of the pathogen (Woof and Burton, 2004; Murphy, 2011).

For the Fc region to properly mediate receptor functions such as CDC and ADCC, glycosylation at the asparagine-residue in position 297 is imperative (Boyd, Lines and Patel, 1995). Besides efficacy, correct post-translational modification is vital in preventing immunogenic responses directed towards the therapeutic and prolong the serum half-life (Jefferis, 2005, 2009).

Antibodies specific to a certain antigenic substance were traditionally obtained by immunizing either mice or goats via injection of the respective substance. The host organism would then generate antibodies specific to the antigens on the substance's surface, which could then be extracted and purified for further use. Antibodies generated using this method are termed polyclonal antibodies (Murphy, 2011). Antigenic substances (e.g. cells or virus particles) often carry more than one antigen and the resulting immune response therefore generates a mixture of antibodies specific to an array of antigens. With the development of hybridoma technology, emerging from experiments conducted by Köhler and Milstein (Köhler and Milstein, 1975), it became possible to consistently produce mAbs; antibodies of identical structure, specific to a single antigen. In this method, immunized B-lymphocytes from laboratory animals are fused with myeloma cells to become hybridoma cells. The fusion imparts the newly formed hybridoma qualities of both parent cells, as it is immortal like the myeloma cell and continuously generates antibodies like the B-lymphocyte (Köhler and Milstein, 1975; Kennett, 1981).

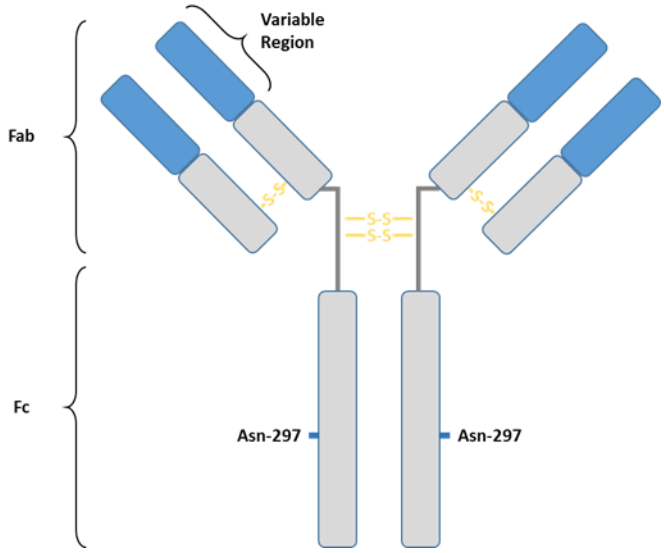

Figure 1.1: Image of an Immunoglobulin G isotope antibody. Two antigen-binding (Fab) regions and one crystallisable fragment (Fc) region form a Y-shaped structure. Fab and Fc regions are connected via a hinge region. The individual chains that make up the fragments are connected through disulfide bonds. The asparagine moiety at position 297 of the Fc region is indicated as it presents a potential site of glycosylation.

Currently, mAbs are the single most important biopharmaceutical product and with new developments in synthetic biology, the focus lies now on designing improved mAbs that trigger fewer immune responses in humans, have a higher efficacy, and a longer serum half-life. Most antibody products to date are murine, chimeric, or humanised. Murine antibodies are derived from mice and as a result are encoded by genes specific to mice. In order to avoid immune responses to these foreign structures in humans, efforts have been made to customise mAbs and make them more human-like (Grilo and Mantalaris, 2019). Chimeric antibodies are encoded by genes from more than one organism and typically have a murine variable region, while the remaining antibody is coded by human genes. Contrastingly, humanised antibodies are murine-based but have a genetically modified protein sequence that closely resembles human structures (Weiner, Surana and Wang, 2010; Chudasama, Maruani and Caddick, 2016). Furthermore, antigens can be screened to create fully human antibodies with the use of, for instance, phage display to present a library of human antigen-binding sites (Baker, 2005; Schirrmann *et al.*, 2011).

1.3 Chinese Hamster Ovary cells

Synthetic biology has not only allowed for the specific design of mAbs, but also made it possible to use more efficient and convenient production systems. The choice of a host cell line is largely dependent on an interplay of productivity, reproducibility of the product characteristics, the time clone development takes, and how important the post-translational modifications of the final product are. Chinese Hamster Ovary (CHO) cells cater to all of these requirements as they exert a comparatively high productivity as well as full post-translational modification of complex proteins (Birch and Racher, 2006). Although they originate from the rodent family and hence produce a slightly different glycosylation pattern when compared to those found in the human body, clinical trials with mAbs produced in CHO cells show that they are not inferior in terms of immunogenicity or serum half-life (Raju, 2003). Furthermore, CHO cells have been adapted to suspended growth in stirred tank reactors (STRs), which facilitates operation and allows for the use of existing technology already extensively described for microbial fermentation. These cell lines are well characterised with robust protocols for transfection, amplification, and clone-screening readily available (Sinacore *et al.*, 1996; Butler, 2005). Although alternatives exist, the vast majority of production processes is based on the use of CHO as production cell line (Dübel and Reichert, 2014; Walsh, 2014; Grilo and Mantalaris, 2019).

1.3.1 Common expression systems

Transfection and amplification of the target gene in CHO cells is typically supported by either the dihydrofolate reductase (DHFR) or the glutamine synthetase (GS) system. Clones deficient for DHFR lack the ability for nucleotide synthesis and as a result, fail to proliferate. The target gene is introduced into the DHFR deficient host cells on a vector containing the DHFR gene. Therefore, the cells will regain their ability to proliferate upon successful transfection. Methotrexate (MTX), a DHFR inhibitor, is subsequently added to the medium in increasing concentrations to amplify the copy number of the target gene (Bebbington *et al.*, 1992; Chartrain and Chu, 2008). The GS system is based on the glutamine synthetase catalysed conversion of glutamate and ammonia to glutamine (Figure 1.2). GS-CHO cells exhibit endogenous activity for glutamine synthetase and are capable of functioning without the addition of glutamine to the growth medium. Transfected

clones can be selected by inhibiting the glutamine synthetase activity through the addition of methionine sulphoximine (MSX), as the GS gene is introduced together with the target sequence. Successive increases of the MSX concentration is then used to amplify the copy number (Burky *et al.*, 2007).

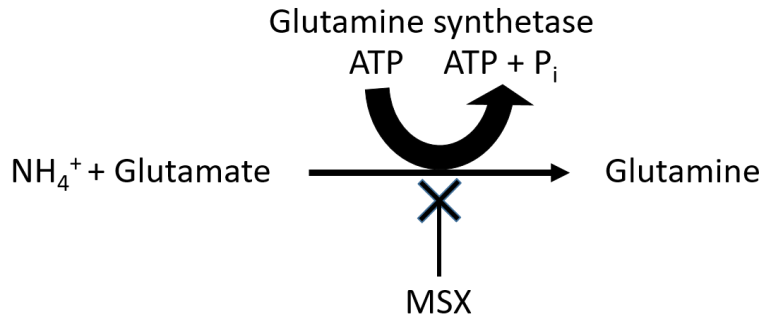

Figure 1.2: Conversion of glutamate and ammonia to glutamine through catalysis with glutamine synthetase. This process can be inhibited with methionine sulphoximine (MSX).

1.3.2 The Warburg Effect

A common characteristic of cancer cells and, by extension, many cancer cell derived production cell lines such as CHO, is their tendency to favour the less profitable anaerobic glycolysis pathway over oxidative phosphorylation even though oxygen is available in sufficient quantities. This alteration of the metabolism is known as the Warburg effect and effectively leads to the acidification of the environment through lactate production (Weinhouse *et al.*, 1956; Gatenby and Gillies, 2004; Hsu and Sabatini, 2008). With regards to the design of a bioprocess, the Warburg effect has two direct ramifications. Firstly, lactate exhibits cytotoxicity at elevated concentrations and requires the concentration levels to remain low (Zhang, 2009). Secondly, the anaerobic reduction of glucose only delivers 2 molecules of ATP per molecule of glucose compared to the 36 molecules of ATP that are generated when one molecule of glucose is degraded via oxidative phosphorylation. As a result, cancer cell derived production clones usually have a high demand for glucose (DeBerardinis *et al.*, 2007; Freshney, 2010). However, when a state of glucose depletion is reached, and the cells approach the static phase, CHO and other mammalian cell lines can undergo a metabolic shift and begin to utilise the accumulated lactate as a carbon

source. This condition is desired in a cell culture process as it coincides with a distinct increase in productivity (Mulukutla, Gramer and Hu, 2012; Zagari *et al.*, 2013; Hartley *et al.*, 2018). One approach aimed at stimulating a metabolic shift to decrease lactate accumulation and increase antibody productivity, uses single inhibitory RNA to down-regulate the enzymes, lactate dehydrogenase A and pyruvate dehydrogenase kinases (Zhou *et al.*, 2011). Similar results were achieved by simply limiting the availability of glucose and glutamine in the culture medium (Ljunggren and Häggström, 1994; Hartley *et al.*, 2018).

1.4 Cell culture

As mammalian production cell lines predominantly originate from cancer tissue where they grow adherently, the complex native microenvironment is laborious to replicate outside of the organism of origin (Freshney, 2010). In suspension culture, however, achievable cell concentrations are independent from the available surface area. This allows for a higher cell concentration and consequently, higher product titres in comparison to sessile cultures (Rodrigues *et al.*, 2010). For this reason, all current mammalian production cell lines have been adapted to growth in suspension (Butler, 2005). Furthermore, mammalian manufacturing processes generally exceed a duration of 12 days, which poses challenges in terms of sterility and the accumulation of toxic metabolites (Chartrain and Chu, 2008). This section will give an overview of the relevant elements of a cell culture process by introducing process conditions, culture methods and the modes of operation currently used in cell culture production processes.

1.4.1 Process conditions

Optimal environmental conditions are key to the design of a profitable process. Parameters like pH, dissolved oxygen concentration (DO), temperature, osmolality, nutrients, and metabolites are routinely measured, easy to control, and have a comparatively high potential for optimisation (Rodrigues *et al.*, 2010). This section will serve as an introduction to the most critical process conditions that must be considered when designing a cell culture process.

1.4.1.1 pH

For the majority of current mammalian production cell lines, a pH higher than 7.7 and lower than 6.5 will negatively affect the growth profile. Likewise, pH levels outside of 7.8 and 6.0 will generally decrease the cell viability (Freshney, 2010). Change in the pH during the cultivation is largely due to the production of lactate, which acidifies the medium over time. In contrast, exogenous pH levels have also been shown to affect the production of lactate; with a lower pH inhibiting the lactate production and an increased level stimulating production (Wu, Ray and Shuler, 1993; Xie *et al.*, 2002). CHO cells are usually cultivated between pH 7.0 - 7.2 for optimal growth conditions. At slightly lower pH values, CHO cells were shown to have a decreased growth rate and reduced metabolic activity, whereas slightly elevated pH values render the cells metabolically more active (Yoon *et al.*, 2005; Trummer *et al.*, 2006). However, an influence on protein expression through changing pH values remains ambiguous (Kaisermayer *et al.*, 2016) and is generally dependent on cell line and mode of operation.

In cell culture processes, the pH is typically downregulated using CO_2 sparging. Conversely, a buffer such as sodium bicarbonate or a strong base like sodium hydroxide can be used for pH upregulation (Doran, 2013). Though ammonia gas can be employed in microbial cultures to increase pH levels, ammonia concentrations, even within the range of a few millimoles, can have a detrimental effect on mammalian cell cultures (McQueen and Bailey, 1990; Wu, Ray and Shuler, 1993).

1.4.1.2 Dissolved oxygen (DO)

If cells use more oxygen than can be supplied by aeration, the concentration of dissolved oxygen will decrease in the medium and eventually reach a point where the oxygen in solution can no longer sustain cell survival (Butler, 2004). The DO is usually given as the percent of air saturation within the culture medium. A 100% air-saturated solution corresponds to 0.22 mM (at 37°C) of oxygen dissolved in the liquid phase. For many mammalian cell lines, the optimal growth is recorded somewhere between 20% and 50% air saturation (Butler, 2004). In order to increase the DO within the medium, compressed air can either be sparged directly into the medium or into the headspace of the bioreactor. As air only contains 21% oxygen, the oxygen transfer rate can

be quintupled by using pure oxygen, which can be particularly desirable when working with high cell densities. However, it is important to note that mammalian cells often proliferate best in environments of lower oxygen concentrations. This is due to the *in vivo* concentrations of dissolved oxygen in mammalian tissues, which typically range from 2 - 9% oxygen-saturation (Bertout, Patel and Simon, 2008; Haque *et al.*, 2013).

In shake flasks or microtitre plates, oxygenation is usually achieved via diffusion of the gas mix provided by the incubator through the filter or seal of the respective culture vessel into the medium. For mammalian cells, this gas mix commonly consists of 95% air and 5% CO_2. This can lead to oxygen limitations and consequently, impaired growth or production kinetics, especially at higher cell concentrations. As the agitation has a direct influence on the rate at which oxygen diffuses into the liquid phase, placing the flasks or microtitre plates on an orbital shaker can increase oxygen transfer. For production processes in STRs, upregulation of the DO is usually done by sparging air or pure oxygen directly into the liquid. Although it improves oxygenation drastically, direct sparging has its own difficulties with cell stress caused by bursting bubbles and excessive foaming (Jöbses, Martens and Tramper, 1991; Butler, 2004). To prevent foaming and hydrodynamic cell damage, the additive Pluronic F-68, a non-ionic surfactant, is commonly used as part of the growth medium (Ma *et al.*, 2004; Gigout, Buschmann and Jolicoeur, 2008).

1.4.1.3 Temperature

The temperature recommended as a good starting point for any mammalian cell line is the temperature found *in vivo* for each respective cell line (37°C for most mammalian cell types). Although the growth is slowed down or even completely inhibited, most cell lines cope well with temperatures below 37°C and therefore, can be refrigerated and frozen for extended periods of time without causing considerable damage to the cells (Freshney, 2010). However, temperatures just a few degrees higher than 37°C will quickly lead to a substantial drop in viability, making accurate temperature regulation crucial. Additionally, the temperature influences the solubility of CO_2 in the medium, which in turn has a direct effect on the pH value (Zhang, 2009).

In recent years, a shift of temperature during the cultivation has gained recognition as a potential way to increase productivity. Keeping the cells at 37°C for both lag-phase and exponential growth phase and subsequently lowering the temperature will slow down growth, yet increase the productivity and viability. This may be due to a partial arrest of the cells in G0/G1 phase at slightly lower temperatures (Moore *et al.*, 1997; Ahn *et al.*, 2008; Kou *et al.*, 2011). For the production of recombinant proteins with CHO cells, this biphasic mode has been shown to successfully increase productivity without affecting the product quality (Bollati-Fogolín *et al.*, 2008).

1.4.1.4 Agitation

In terms of shear stress, high agitation intensities are actually less damaging to mammalian cell lines than previously thought. In a study conducted by Oh et al. (1989), the poor process performance caused by shear stress was shown to be primarily due to bursting bubbles produced by gas sparging. Higher gas flow rates and smaller bubble sizes were ultimately linked to an increase in shear stress. This implies that, if the gas flow is dissipated through agitation resulting in a larger number of small bubbles, agitation indirectly becomes a shear stress increasing factor. However, these effects can be mitigated by adding Pluronic F68, a surfactant that reduces bubble formation, to the medium (Oh *et al.*, 1989, 1992; Nienow, 2006).

1.4.1.5 Growth medium

In general, the growth medium must closely resemble the environment of the cell line's origin and, for mammalian cells in particular, this usually precipitates a complex system. The medium provides the cells with the necessary macro- and micronutrients to stimulate optimal proliferation and product formation (Ljunggren and Häggström, 1994). In addition, growth factors and other supplements with more special functions, like Pluronic F-68 to reduce shear stress, may help to better exploit the cell's potential. Besides growth kinetics and productivity, media components can also have a direct effect on the product quality (Chapman and Calhoun, 1988; Gu and Wang, 1998; Gramer *et al.*, 2011; Rillahan *et al.*, 2012; McCracken, Kowle and Ouyang, 2014; Galleguillos *et al.*, 2017). An optimised product quality leads to a higher efficacy which, in turn, presents an economic incentive as less of the drug has to be administered to achieve the same effect (Konno *et al.*, 2012).

In order to maintain a stable pH, cell culture media commonly contain sodium bicarbonate as a buffer. Even though bicarbonate has a comparatively low buffering capacity at physiological pH when compared to other buffer systems like HEPES, it is still widely used due to its low toxicity, low cost, and nutritional aspect to the cells (Freshney, 2010). The relationship between bicarbonate and carbon dioxide is expressed in the following equation:

$$H_2O + CO_2 \leftrightarrow H_2CO_3 \leftrightarrow H^+ + HCO_3^- \qquad (1.1)$$

Accordingly, the equilibrium can be shifted towards an acidic environment by increasing the concentration of CO_2 in the medium. In order to counteract acidification, sodium bicarbonate can be added as it readily dissociates to a sodium cation and the hydrogen carbonate anion (HCO_3^-).

Mammalian cells typically need a specific amount of serum added to the medium in order to proliferate. Serum is a complex mixture largely consisting of albumin, hormones, growth factors, trace elements, and salts and is recovered from blood plasma. However, due to its route of production, serum is not only subject to batch-to-batch differences, contamination, and high prices, but the use of it also raises ethical concerns (van der Valk *et al.*, 2004, 2010). These reasons present the driving force for the recent trend towards the use of chemically defined media. According to a definition by van der Valk et al., “chemically defined media do not contain proteins, hydrolysates or any other components of unknown composition. Highly purified hormones or growth factors added can be either of animal or plant origin, or are supplemented as recombinant products” (van der Valk *et al.*, 2010). The adaption of cells to serum-free medium is a lengthy process in which the concentration of serum is slowly reduced until it is no longer necessary to be added to the medium (Keen and Steward, 1995; van der Valk *et al.*, 2010).

1.4.1.6 Osmolality

The osmolality is a quantification of the amount of osmolytes in solution and is expressed as the mole of osmolytes per weight of solvent (osmol kg^{-1}). The osmolarity, on the other hand, is given by the moles of osmolytes per volume of liquid (osmol L^{-1}) (Erstad, 2003). Values for typical cell

culture media range from 260 – 420 mOsmol L^{-1}. To put this into perspective, human serum has an osmolality of 307 mOsmol L^{-1} (Waymouth, 1970). Media additions are not alone in affecting osmolality, metabolic waste products like lactate lead to increased levels of osmolytes and in microtitre plates evaporation can additionally lead to considerable fluctuations (Altamirano *et al.*, 2004; Spens and Häggström, 2007).

Although mammalian cells have a repertoire of cellular mechanisms that accumulate H_2O, amino acids, and other osmolytes to counteract increasing levels of extracellular osmolality, these are only effective within a narrow range of osmolalities (Alfieri and Petronini, 2007). However, there is evidence that these mechanisms might be the cause for the increasing productivities that often coincide with higher osmotic environments. The accumulation of amino acids inside the cell is thought to serve as a supply of nutrients that instigates product formation (Chua, Yap and Oh, 1994; Oh, Chua and Choo, 1995). Therefore, changes of osmolality are commonly used to design biphasic cultivation processes. The cells are initially grown in lower, growth-promoting osmolyte concentrations before an elevated osmolality is applied in the production phase in order to increase the productivity (El-Enshasy, 2007; Zhang, 2009; Kaisermayer *et al.*, 2016). Additionally, osmolality has been shown to play an important role in protein folding and post-translational modification, which further substantiates the need to closely monitor this parameter in cell culture processes (Street, Bolen and Rose, 2006; Konno *et al.*, 2012).

1.4.2 Cell culture systems

In order to monitor and control relevant process conditions detailed in section 1.4.1 throughout the cultivation, a suitable cultivation system needs to be considered. Cell culture systems range drastically in working volume and complexity, but also the amount of information they generate per experiment (Figure1.3). Typically, microtitre plates are used for early-stage process development applications such as clone screening, as this format can support high throughputs. However, the lack of monitoring and control capabilities in microtitre plates limit their informative value and scalability. Larger benchtop- or pilot-scale STR systems often offer the same functionalities that can be found at the manufacturing scale, but their footprint, setup time, and operational cost curtails the achievable throughput. Microbioreactors combine monitoring and

control capabilities with a small working volume that allows for a high degree of parallelisation, which helps to generate more process information early on in the development timeline (Hemmerich *et al.*, 2018). This section aims to give an overview of the cell culture systems typically used in upstream process development.

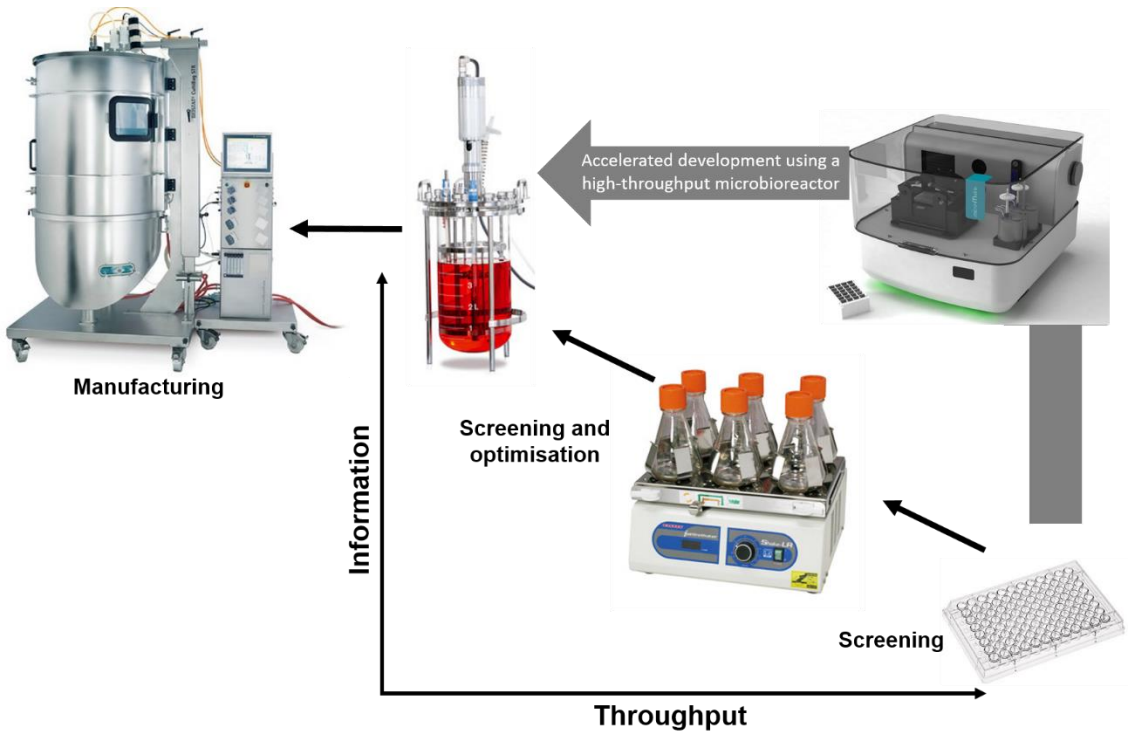

Figure1.3: Process development workflow (adapted from Hemmerich *et al.*, 2018).

1.4.2.1 Microtitre plates

First developed for serological studies in the 1950s (Sever, 1962), microtitre plates were quickly adapted for the use in microbial research and have since been subject to rigorous characterisation in the hope to extend their use as cheap and widely available tools for small-scale cell culture screening approaches. Physiochemical differences to their larger bioreactor counterparts become apparent at this scale. Due to the larger surface-to-volume ratio in microtitre plates, the specific oxygen transfer rates through headspace aeration increase drastically, whereas mixing efficiency can decrease due to surface tension (Hermann, Lehmann and Büchs, 2003; Doig *et al.*, 2005; Duetz, 2007; Wutz *et al.*, 2018; Li, Ducci and Micheletti, 2020).

The 24 standard round well plate (24 SRW) has been established as a suitable format for the cultivation of mammalian cell lines and has been successfully used as a scale-down model for shake flasks (Micheletti and Lye, 2006; Silk *et al.*, 2010). A problem specific to the comparatively long run times of cell culture processes is evaporation from the wells. Evaporation leads to changing concentrations in the culture medium and as a result, higher osmolarities over the course of the cultivation, which has been shown to affect growth and production kinetics (Oh *et al.*, 1989; Silk *et al.*, 2010). The micro-Flask system (Figure 1.4) was developed for the purpose of regulating gas exchange and evaporation in microtitre plates and comprises of an array of well-closure systems based on layered filter materials. The system also prevents cross-contamination, even at higher shaking speeds, by completely sealing each individual well (Duetz, 2007). The specific composition of the lid defines the gas exchange and, by extension, defines liquid evaporation and the application of the lid itself. The micro-Flask lid system consists of: i) silicone seal that provides identical gas exchange per well and prevents well-to-well cross contamination ii) ePTFE and microfiber layers that act as a sterile barrier and limit diffusion and iii) a stainless-steel cover to hold each layer and provide rigidity. The use of such a lid system has been shown to significantly decrease evaporation to volumes below 10 µL per day and well (Duetz *et al.*, 2000).

A) **B)**

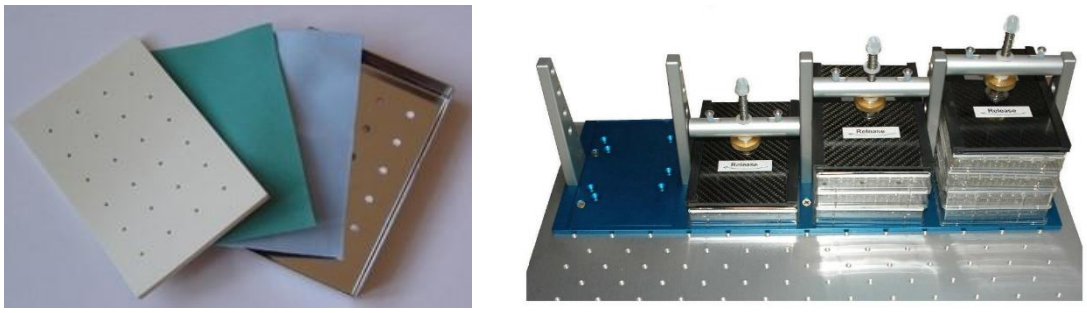

Figure 1.4: A) Composition of the micro-Flask sandwich lid. The depicted materials from front to back are silicone seal, ePTFE, microfiber, and stainless-steel cover. B) The microtitre plates and the lids are mounted onto an orbital shaker and held in place with a clamp system. The system allows stacking of up to 4 plates in one slot. Both images retrieved from *www.Applikon.com*.

Further customisation to the specific needs of an application can be achieved by changing the shape of the well. The geometrical structure of a well can, for instance, be adapted to recreate

the effect of baffles within microtitre plates and promote the transfer of oxygen into the liquid. Using less circular well shapes introduces ripples on the liquid surface, which effectively increase the available surface area for gas exchange and as a result, the oxygen transfer rate (Funke *et al.*, 2009). A promising and commercially available alternative to the round well shape is the square well microtitre plate. Due to the increased oxygen transfer rates, this plate format could prove advantageous for high cell density mammalian cell cultures (Chaturvedi *et al.*, 2014; Markert and Joeris, 2017) or microbial fermentations (Duetz and Witholt, 2001, 2004).

With the development of optical sensor technologies, a growing number of studies investigated online monitoring of pH and DO in microtitre plates in order to gain insight into the process in its early stages of development (Elmahdi *et al.*, 2003; John *et al.*, 2003). Furthermore, the generic format facilitates the setup of automated systems. Researchers at Roche have recently established a system that performs fully automated, microwell-based cell culture and routine analytics. Using the presented setup for media blending and feeding strategy evaluations, the product yield was increased by 22% and the optimised process was successfully scaled up to 1000 L scale. The modular design of the system allows for easy expansion and adaption to the operator's needs (Markert and Joeris, 2017).

The potential for automation and the high degree of parallelisation make microtitre plates a valuable tool for high-throughput screenings, despite their intrinsic differences to larger scale systems (Betts *et al.*, 2006).

1.4.2.2 Microbioreactors

A bioreactor is a reaction vessel used to grow organisms that produce valuable products or convert waste material. By ensuring optimal energy and mass transfer, the bioreactor caters to the needs of the organism and simultaneously maintains a monoseptic environment. Traditionally, over 90% of screening experiments were carried out in 50 mL shake flasks (Büchs, 2001), a system which is far removed from the conventional STR and as a result, limits the conclusions that can be drawn for larger scales on the basis of shake flasks. Additionally, shake flasks lack the control of pivotal process parameters like pH and DO, leaving the operator with a black-box

instrument. Microbioreactors attempt to bridge this gap by providing a fully-controlled environment within defined working volumes between 0.1 and 100 mL (Hewitt and Nienow, 2007). Commercially available microbioreactor systems are typically based on pre-sterilised and disposable materials that reduce the time between experiments from days to just a few hours, as there is no longer a need to clean or autoclave the reaction vessels. A list of currently available commercial options for microbioreactor systems is provided in Table 1.1.

Most microbioreactors are routinely equipped with non-invasive optical sensors for the online monitoring of DO, pH, and temperature adhered to a transparent surface of the culture compartment and offer several gas inlets for control purposes (Hanson *et al.*, 2007; Bareither and Pollard, 2011). The development of these sensors was instrumental in the advancement of microbioreactor systems, as they allow for the measurement and control of conventional process parameters at the small scale (Bareither and Pollard, 2011). The current microbioreactors differ particularly in their approach to agitation and gas transfer, where agitation can be achieved by shaking or stirring and gas transfer by either sparging or headspace aeration (Nienow *et al.*, 2013; Lattermann and Büchs, 2016). The following descriptions will primarily focus on Applikon's micro-Matrix and the ambr15 by Sartorius, as these systems provide a documented record of accomplishment regarding cell culture applications.

Applikon's micro-Matrix (Applikon, Delft, The Netherlands) (Figure 1.5) is a platform that holds 24 individual microbioreactors based on a 24 deep-well microtitre format with 4 independent gas inlets for overhead aeration. The inbuilt orbital shaker operates at shaking speeds between 0 – 400 rpm with an orbital throw of 25 mm. The cassette is placed in a temperature-controlled chamber at a defined setpoint. Additionally, the temperature can be controlled individually for each well, with a maximum difference of 1°C between adjacent wells (De Palma, 2014; Lattermann and Büchs, 2015; Applikon, 2016).

Table 1.1: Commercially available microbioreactor systems (reproduced from Wiegmann, Martinez and Baganz (2020).

Micro-bioreactor	Agitation	Aeration	Working Volume	Vessel Format	Special Features	Vendor
ambr 15	Stirred	Sparger	10 - 15 mL	Disposable micro-bioreactor vessels	Automated liquid handling	Sartorius-Stedim
BioLector‡	Shaken	Overlay	0.8 – 2.4 mL	48 FlowerPlate	Can be combined with liquid handler	m2p-labs
bioREACTOR‡	Stirred	Passive (no control)	8 - 15 mL	Disposable PS vessels	Can be combined with liquid handler	2mag
µ24	Shaken	Sparger / Overlay	3 – 7 mL	24 Deep well plate	Offers two plate designs	Pall
micro-Matrix	Shaken	Overlay	1 – 5 mL	24 Deep Square Well Plate	Automated feeding module	Applikon Biotechnology

‡: Cell culture applications have not yet been documented for this device

Unique to the micro-Matrix is its automated feeding system, which enables pneumatically driven semi-continuous additions of liquid into each well of the cassette. This allows for the testing of more complex feeding strategies, that would otherwise only be feasible at the benchtop scale (Wiegmann *et al.*, 2019). The µ24 (Pall, Port Washington, USA), the BioLector (m2p-labs, Baesweiler, Germany), and the shake flask based RAMOS system (Kuhner AG, Birsfelden, Switzerland) are alternative shaken bioreactors.

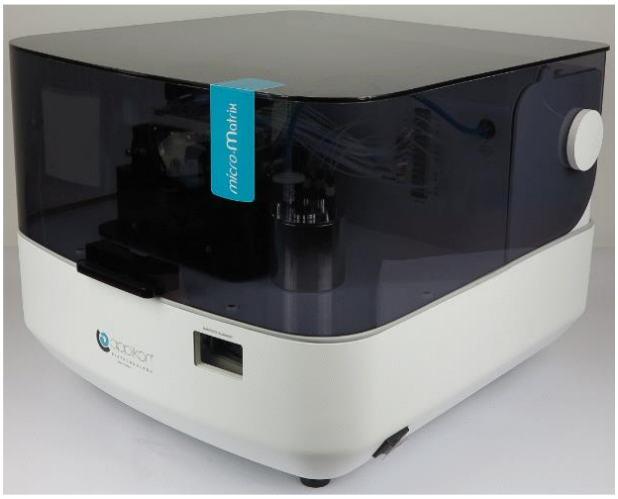

Figure 1.5: micro-Matrix (Applikon Biotechnology BV). Image retrieved from *www.Applikon.com*.

The ambr15 (Sartorius, UK) (Figure 1.6) is based on individual disposable cell culture vessels with a working volume of 10 mL each and an automated liquid handling system performs liquid additions and removals. Each cell culture vessel is equipped with sensors for pH, DO, and temperature, as well as an impeller with two blades set at a 45° angle and a sparge tube for the addition of gases (Hsu *et al.*, 2012; Nienow *et al.*, 2013; Lattermann and Büchs, 2016). An alternative, commercially available stirred microbioreactor system is the bioREACTOR 48 (2mag, Munich, Germany) though this has not been applied for cell culture processes yet.

Figure 1.6: ambr15 (Sartorius). Image retrieved from www.Sartorius.com.

With the high degree of parallelisation and automation as well as the markedly lower working volumes when compared to benchtop systems, process development in microbioreactors has clear economic benefits. Since the cost of drug development has grown exponentially in the last decade, the implementation of scale-down methods for the rapid development and optimisation gain particular importance in marketing new therapies at an affordable price (Collier, 2009; Bareither and Pollard, 2011).

1.4.2.3 Stirred Tank Reactors

The STR remains the most widely used production system as it has been refined and well-characterised through its extended use for microbial fermentations (Chu and Robinson, 2001). This also applies to the methods of sterilisation and scale-up, which are already in place for STRs. A variety of impellers exist that produce different flow patterns depending on the requirements of the application. The implementation of baffles or the use of multiple impellers, particularly in tall vessels, can further improve upon mixing and oxygen transfer, though such configurations are mainly employed in microbial applications due to increased shear rates. For optimal bubble dispersion, the sparger is usually placed underneath the impeller, which increases the surface area of the rising bubbles and therefore, the volumetric mass transfer coefficient. A further increase in oxygen transfer can be achieved by choosing higher aspect ratios to prolong the contact time between bubbles and liquid (Doran, 2013). Problems with insufficiently mixed areas within the bioreactor occur particularly at an increased scale, this leads to the generation of

gradients and consequently, areas that deviate from the optimal culture conditions (Rodrigues *et al.*, 2010). In addition, sparging and mechanical agitation cause cell stress and may adversely affect productivity (Michaels, Mallik and Papoutsakis, 1996).

In recent years, the biotechnology industry shifted towards the use of single-use bioreactors (SUBs). SUBs are typically pre-sterilised polymer bags that are mounted on a metal or plastic frame that holds the bags in place. By nature, SUBs eradicate the need for cleaning, extensive setup, and autoclaving and as a result, save time and eliminate risks of cross contamination and improper reactor setup. However, since the consumable costs for disposable bioreactors are substantial, careful consideration is required to gauge whether the benefits outweigh the financial investment (Chartrain and Chu, 2008; Odeleye *et al.*, 2014).

1.4.3 Cultivation processes

The mode of operation in which a bioprocess is performed, defines whether and how medium enters the running system as well as how spent medium leaves the system. Batch, fed-batch, continuous, and perfusion are the predominant modes of running a bioprocess. The choice of an individual mode, however, is ultimately dependent on the intended application, as well as growth and production kinetics of the cell line (Rodrigues *et al.*, 2010). Independent of the mode of operation, the process parameters may be changed during the process to increase productivity. These so-called “biphasic” processes aim to combine optimal growth conditions with optimal conditions for product formation (Yoon *et al.*, 2005; Trummer *et al.*, 2006). Typically, in the initial growth phase conditions are chosen that favour rapid cell expansion in order to attain high cell densities in a short amount of time. The respective parameter is then shifted to a level where product formation is enhanced and growth is slowed down (Kaisermayer *et al.*, 2016). Parameters that qualify for the design of a biphasic system include but are not limited to pH (see section 1.4.1.1), temperature (see section 1.4.1.3), and osmolality (see section 1.4.1.6).

1.4.3.1 Batch

Batch is the simplest mode of operation and requires few or no interactions with the running system. The cells are provided with a set amount of medium that is initially added to the bioreactor. The cells are then left to grow until the final conditions are reached and the product is harvested. During the cultivation, the concentrations of nutrients gradually decrease with glucose and glutamine being predominantly consumed. At the same time, metabolic waste products like lactate and ammonia accumulate in the medium and may adversely affect cell growth and product expression. Ultimately, the process will halt due to either the depletion of one of the key nutrients or the inhibition through elevated levels of metabolic waste products (Butler, 2004).

Though batch is the simplest mode of operation, it only supports a limited maximum cell density and run time which may impair the product titre (Wurm, 2004). The batch mode might be undesirable as the growth phase only covers a limited period of time in the overall process, particularly if the used cell line exhibits growth-associated product formation (Phillips *et al.*, 1991; Ozturk and Hu, 2005).

1.4.3.2 Fed-Batch

To attain higher cell concentrations, nutrients can be fed over the course of the cultivation in order to avoid cell death due to nutrient depletion. As a result of such feed additions, the working volume increases throughout the run. The influx of feed medium during the fed-batch phase can be either continuous, intermittent, or dynamic. A continuous feeding regime utilises a constant flow rate of feed medium, while intermittent feed additions are performed as single or reoccurring bolus additions. In a dynamic feeding protocol, the feed volumes and flow rates can be linked to process outputs, such as the growth rate or glucose concentration in the cell broth. At the end of the upstream unit operation, the vessel content is either harvested completely or a fraction of the cell broth is used to inoculate a subsequent run (repeated fed-batch) (Lim and Shin, 2013).

Initial research on feeding strategies evaluated further additions of basal medium supplemented with glucose (Bibila and Robinson, 1995). Thereafter, the focus expanded to other media components in the pursuit of more tailored feed media (Luan, Mutharasan and Magee, 1987; Jo

et al., 1990, 1993). Recently, the increasing throughput in upstream process development continues to facilitate the screening of large media libraries, while the improved throughput in spent media analysis generates more granular insights into the cellular demands (Li *et al.*, 2010; Jordan *et al.*, 2013).

Feed media often contain components in high concentrations to minimise the volume required per addition. As a consequence, a more gradual addition of feed medium is often advised to avoid gradients in the cell broth and prevent potential inhibitory effects exerted by components in the feed medium (Bibila and Robinson, 1995). Knowledge of the metabolic footprint for the used cell line is imperative when designing a feed medium and feeding strategy, as the metabolic requirements can differ vastly between cell lines. Yet, even the replacement of nutrients and other media components is not capable of sustaining indefinite growth. Further growth is usually inhibited through the accumulation of one or more metabolic waste products. However, the ease of scale translation and operability, as well as the high productivity compared to cultivations in batch, often renders fed-batch as the preferred mode of operation (Rodrigues *et al.*, 2010).

1.4.3.3 Continuous and Perfusion

In a continuous flow culture, feed medium is continuously added to the system while an equal volume of culture broth simultaneously leaves the system in the effluent. In such a process, the volume and process conditions ideally do not change over time and waste products are perpetually removed from the system (Lim and Shin, 2013). However, viable cells are also flushed out with the effluent which dampens the productivity of the process (Chartrain and Chu, 2008).

A perfused system works in the same way as a continuous system with the difference that the effluent is cell free (Tang, Ohashi and Hamel, 2007). The cells remain inside the bioreactor and the harvested liquid volume is replaced by fresh medium. This mode of operation supports extremely high cell densities and allows for smaller vessels. Additionally, the average residence time of the product in the cultivation broth is drastically reduced when compared with an average batch cell culture process of approximately 14 days. A shorter residence time might be of particular interest in the case of unstable products (Clincke *et al.*, 2013).

On the downside, the high throughput of medium leads to elevated running costs and large volumes for purification in the downstream processing (Chartrain and Chu, 2008). The continuous upstream process would preferably be coupled with an integrated downstream process that also runs continuously, allowing for more compact reaction vessels and by extension, safer processes and lower investment costs (Schaber *et al.*, 2011). Warikoo et al. followed this holistic approach of bioprocess design and combined a perfusion bioprocess running at a quasi-steady state of 50 – 60 x 10^6 cells mL^{-1} with a four-column periodic counter-current chromatography. The fully automated system showed no performance drop even after 30 days of continuous run-time and the product quality remained unchanged in comparison to the batch mode. Additionally, the continuous process enabled the elimination of holding and clarification steps (Warikoo *et al.*, 2012). In another approach, a perfused STR was used as seeding (N-1) reactor to inoculate a continuous-flow STR. This combination facilitated extremely long run times of more than 80 days and, through rejuvenating the cellular composition in the N-1 reactor, it was possible to counteract a loss of specific productivity due to cell line age (Gagnon *et al.*, 2019).

1.5 Process optimisation

With the increasing use of high-throughput cultivation systems and the associated rapid accumulation of process data, unstructured screening and optimisation approaches are not able to exploit the full potential of those technologies (Islam *et al.*, 2007). The one-factor-at-a-time (OFAT) methodology offers a more systematic approach. The optimum for one variable is established through experimentation, before moving on to the next variable, while keeping the optimum of the first variable constant for all subsequent experiments. This methodology, however, neglects interactions between factors and is prone to only capture quasi-optimum parameter combinations, as shown by the exemplary optimisation scenario in Figure 1.7 A (Mandenius, 2016).

Design of Experiment (DoE) is a structured mathematical methodology to overcome the limitations of OFAT experimentation. Using DoE, the effect of multiple factors and their interrelations on the responses can be investigated simultaneously (Guy *et al.*, 2013).

Additionally, the experimental results are used to create a mathematical model, which can then be employed to predict the optimal outcome within the investigated design space. If the optimal condition was not captured in the design space, the model can be used to predict the direction of the ideal parameter combinations and thereby help to define the design space for ensuing iterations of the optimisation (Mandenius, 2016).

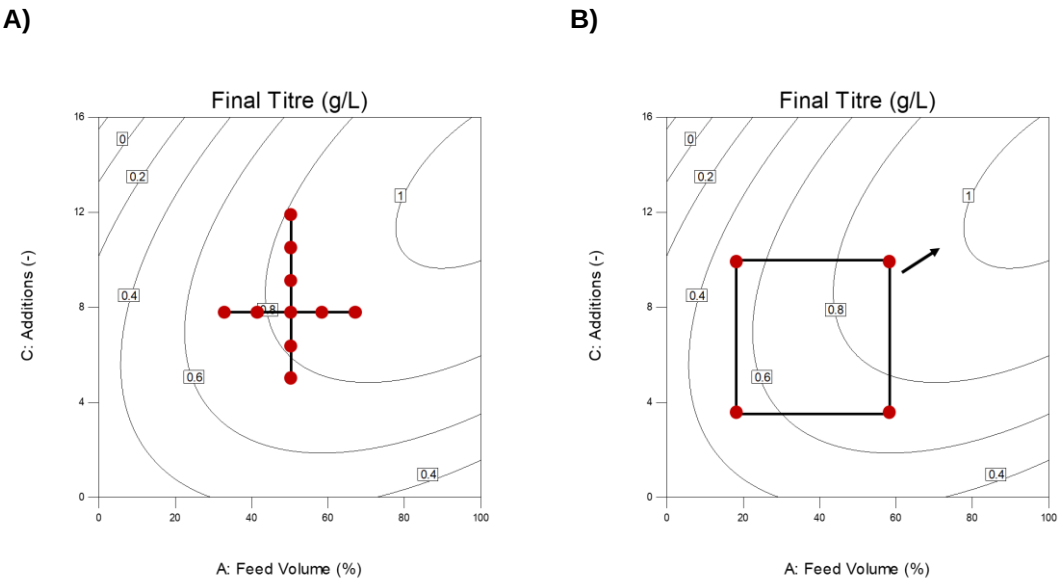

Figure 1.7: Comparison of design space evaluation in OFAT and DoE methodologies. A) In the OFAT approach one factor is varied at a time. This only captures a limited part of the design space and the optimum is likely not captured in the depicted example. B) When multiple parameters are varied at the same time, a larger portion of the design space can be investigated and design of experiment methodology can be employed to estimate the direction of the true optimum (reproduced from Mandenius (2016)).

Cell culture processes are inherently complex and it is therefore often unclear which factors need to be considered during the process optimisation. In such cases, screening designs can be used to quickly exclude factors that have no significant effect on the desired process outcome. Following the Pareto principle, typically only around 3 - 6 variables notably affect a given bioprocess (Snee, 2011). It is therefore important to identify these “vital few variables” early on in the development timeline (Juran, 1992). Screening designs are specifically suited for this purpose, as they allow for the testing of a high number of factors in few experiments through a reduced resolution (Islam *et al.*, 2007). However, some prior process knowledge is needed in

order to make an informed decision on the levels that each factor is tested on. The selection of levels is often based on preliminary experimentation or relevant literature (Mandenius, 2016). In some cases, the outcome of the screening strategy may already meet the expectations of the experimenter (Snee, 2011). In other cases, range adjustments, additional screening runs, or designs with higher resolution may be necessary to optimise a process.

Following the screening and reduction of variables, the remaining variables are investigated in more detail with the aim to determine the optimal combination of values for each factor. Response surface methodology (RSM) is often used for this purpose, as designs of this category are capable of establishing quadratic or higher order relations between the input and output factors. The results are then visualised in contour plots (Figure 1.7) to facilitate the identification of optimal conditions. Popular optimisation designs are for instance circumscribed and face-centred central composite designs (CCF and CCC, respectively) (Mandenius, 2016).

Large data sets with high dimensionality or an unstructured nature can often not be processed through DoE approaches. In such cases, multivariate data analysis (MVDA) methodologies can be used to rapidly identify important process parameters (Goldrick *et al.*, 2019). Tools like principal component analysis (PCA) reduce the dimensionality of complex data sets and visualise the information in a two-dimensional scatter plot. PCA is a well-established technique and has been successfully applied to many areas of bioprocessing, including clone screening, media design, proteomic analysis, and even in sensor technologies like Raman spectroscopy (Darja *et al.*, 2016; Brühlmann *et al.*, 2017; Mora *et al.*, 2018; Rowland-Jones and Jaques, 2019).

Furthermore, changes in the upstream process can affect the outcome of downstream unit operations in an unanticipated fashion. These interactions often go unnoticed until a process is scaled up and the resulting batch is fully processed in subsequent unit operations. Any process change should therefore be considered with the regards to its effect on downstream unit operations as well.

1.6 Engineering characterisation and scale-up

A thorough understanding of a reactor's engineering environment is pivotal in order ensure that a process meets the desired performance and is scalable. Gas transfer, hydrodynamic conditions, and energy dissipation have been shown to exert a significant effect on the performance of bioprocesses and are therefore routinely assessed for bioreactor systems. These tests are usually inexpensive and do not require a sterile environment. The majority of the existing literature in this field focuses on the characterisation of STRs and several mathematical correlations have been developed to predict the magnitude of engineering parameters based on the geometry and operating conditions of the reactor (Bailey and Ollis, 1986; Doran, 2013). Increasingly, *in silico* approaches such as computational fluid dynamics (CFD) are used not only to further reduce the need for laboratory experimentation, but also to facilitate the characterisation of cultivation platforms that are inherently more challenging to study with traditional methods (Wutz *et al.*, 2018).

Gathering process information and ultimately designing the bioprocess on a small scale is not only economically beneficial, but also reduces the required labour and allows for a higher degree of parallelisation. However, in order to design or optimise a bioprocess using a small-scale model, the model must closely resemble the larger scale. Due to the difference in size, it is impossible to keep all the process parameters constant throughout the scales. In practice, the most important process parameter is identified and then kept constant when scaling up. For instance, if the organism in use is shear sensitive, one could consider keeping the impeller tip speed constant. Apart from agitation, a number of parameters have been used as scale-up rules (Shuler and Kargi, 1992), the most common of which are presented in this section.

1.6.1 Mixing time

Mixing is required in order to achieve a state of homogeneity within the liquid and in turn avoid concentration gradients. The homogenous state is reached when the concentration C at all points inside the liquid is equal to the average concentration C_m (Nagata, 1975). The mixing time t_m is defined as the time that is required for the liquid to reach a homogenous state, the degree of

which is chosen arbitrarily (Doran, 2013). The most widely used method to measure mixing times is colorimetry, which is based on the visual observation of the dispersion of a dye within the liquid (Bujalski *et al.*, 1999; Betts *et al.*, 2014; Rodriguez *et al.*, 2014). One major drawback of this method is the potentially poor accuracy rooting in the subjective visual estimation of the mixing time. For this reason, efforts have been made to introduce digital image processing steps towards a more objective way of determining when the desired degree of homogeneity has been reached (François Cabaret *et al.*, 2007; Visuri, Laakkonen and Aittamaa, 2007; Rodriguez *et al.*, 2014). Colorimetry also provides information about mixing patterns and can help to reveal areas of poor mixing (dead zones) (Yao *et al.*, 1998).

Measuring the dispersion of a tracer that can be recorded with a conductivity or pH probe delivers less ambiguous results, but it fails to provide information on the global state of mixing within the vessel. Furthermore, the volume addition must not exceed 0.5% of the reactor volume to avoid alterations of the mixing characteristics (Xing *et al.*, 2009a). A typical response curve oscillates around the final concentration as the bulk of the liquid moves in a circular manner, but is evidently dependent on the location of the pH probe inside the vessel (Doran, 2013). The response is normalised using equation (1.2) and the mixing time is defined as the time it takes for the normalised tracer signal to remain within a range of ± 5% of the final signal (Xing *et al.*, 2009a).

$$H(t) = \left| \frac{pH(t) - pH_i}{pH_f - pH_i} \right| \qquad (1.2)$$

Where *H(t)* is the normalised tracer signal, *pH(t)* is the pH value at time point t, pH_i is the initial pH value at the time point of tracer addition, and pH_f is the final pH value of the fully homogenous solution. Model equations have been developed to predict mixing times. With the assumption that a homogenous state is reached within 5 circulations of the bulk liquid (Voncken, Holmis and Den Hartog, 1964; Khang and Levenspiel, 1976), Nienow et al. proposed the following relationship for vessels with an aspect ratio of 1 (Nienow, 1997):

$$t_m = 5\frac{V}{FlND^3} \qquad (1.3)$$

Where V is the working volume, Fl is the flow number ($Fl = Q_G / ND^3$), N is the impeller speed, and D is the impeller diameter. To date, no universally valid correlations for either shake flasks or microtitre plates have been published.

Though usually limited to the lower range of scales, using the mixing time as a criterion for scale translation is still desirable. For the scale translations between larger volumes, keeping a constant mixing time often results in an excessive power input which is economically unfavourable and physically challenging (Doran, 2013). Typical mixing times for 24 round well plates are below 1 s at shaking speeds above 250 rpm (20 mm orbital diameter) and a working volume around 1 mL (Barrett *et al.*, 2010). In comparison, Pall's µ24 has been shown to produce mixing times of 4 s at a shaking speed of 800 rpm (2.5 mm orbital diameter) for both direct sparging and overhead aeration at 7 mL working volume (Betts *et al.*, 2014). Similarly, for the ambr15™ system mixing times ranging from 4 – 20 s have been reported for impeller speeds of 1500 and 500 rpm, respectively at a working volume of 15 mL without direct sparging (Nienow *et al.*, 2013). In case of larger scale reactors, mixing times can range between 10 – 100 s for impeller speeds between 200 – 50 rpm in a 5 L stirred tank reactor (Barrett *et al.*, 2010).

1.6.2 Volumetric mass transfer coefficient (k_La)

Most cell lines need oxygen to generate the required energy for cell growth, maintenance, and product formation through oxidative phosphorylation. Therefore, it is clear that a certain concentration of dissolved oxygen is essential in the medium (Garcia-Ochoa and Gomez, 2008). The oxygen transfer rate describes how quickly oxygen goes into solution at given process conditions and is limited by the liquid film resistance at the gas-liquid interface (Whitman, 1923). Furthermore, the gas solubility itself is influenced by the type and concentration of electrolytes in solution, as well as the temperature of the liquid and the pressure of the gas phase (Linek and Vacek, 1988; Schumpe, 1993; Weissenborn and Pugh, 1996). For stirred tank reactors a variety of empirical correlations exist that allow for a quick estimation of the k_La in any given system (Shuler and Kargi, 1992).

However, as it is well understood that additions to water considerably distort the volumetric mass transfer coefficient, only measurements in medium containing all additional supplements will provide representative results. For instance, while salts typically cause an increase in k_La, antifoam causes a marked decrease (Nienow, 2015). For shaken systems, the air-liquid interface is the only access point for oxygen into the medium and is subject to changes depending on the shaking conditions and the vessel geometry. Additionally, the liquid film on the vessel wall is saturated with oxygen quicker than the bulk liquid, which makes it challenging to establish a general approximation for the k_La in shaken systems and an experimental determination becomes unavoidable.

As chemical methods (Cooper, Fernstrom and Miller, 1944; Dankckwerts and Litt, 1971) often remove the hydrodynamic properties of the liquid too far from those found in cultivation broths, the volumetric mass transfer is most often determined by measuring the progression of the dissolved oxygen concentration under absorption or desorption conditions (Garcia-Ochoa and Gomez, 2008). Desorption can be achieved by sparging nitrogen gas into an oxygen saturated liquid to remove the oxygen. The change of dissolved oxygen concentration is monitored using a probe and then linearized by applying equation (1.4).

$$\ln\left(\frac{C_0}{C}\right) = k_L a \cdot t \qquad (1.4)$$

Where C_0 is the concentration of dissolved oxygen at t = 0, C is the measured concentration of dissolved oxygen, and k_La is the volumetric mass transfer coefficient.

Conversely, in order to measure the absorption of oxygen into the liquid, oxygen must first be stripped from the liquid by sparging nitrogen. The inlet is then switched to air and the subsequent increase in dissolved oxygen recorded using a probe. Following the linearization of the results according to equation (1.5), the k_La is given by the slope of this correlation (Van't Riet, 1979; Garcia-Ochoa and Gomez, 2008):

$$ln\left(1-\frac{C}{C_1}\right)=-k_L a\cdot t \qquad (1.5)$$

Where C_1 is the dissolved oxygen concentration under saturated conditions.

However, in order to avoid inaccuracies due to lagging probe responses, the k_La has to be corrected for the probe response time (τ_p) using equation (1.6) if $\tau_p \leq k_La^{-1}$.

$$C_p=\frac{1}{t_{mt}-\tau_p}\left[t_{mt}exp\left(\frac{-t}{t_{mt}}\right)-\tau_p exp\left(\frac{-t}{\tau_p}\right)\right] \qquad (1.6)$$

Where C_p is the dissolved oxygen concentration as measured by the probe, t_{mt} is $1/k_La$ and τ_p is the probe response time. τ_p can be determined by measuring the time it takes the probe readings to drop from a DO of 100 % to 33% when first sparging it directly with air and then immediately switching to nitrogen (Dunn and Einsele, 1975; Betts *et al.*, 2014).

For 24 round well microtitre plates shaken at 200 – 900 rpm (3 - 8 mm orbital diameter) in an incubator, k_La values ranging from 18 to 198 h^{-1} have been reported (Doig *et al.*, 2005). With active sparging of the ambr15™ system, k_La values of up to 11.85 h^{-1} could be reached in cell culture medium at an air flow rate of 1 mL min^{-1} and a working volume of 13 mL (Nienow *et al.*, 2013). For Pall's µ24 at a fill volume of 7 mL and shaking speeds between 500 – 800 rpm (2.5 mm orbital diameter) Betts et al. (2014) recorded k_La values ranging between 3 – 22 h^{-1} and 4 – 53 h^{-1} for headspace aeration and active sparging, respectively. In the larger scale, for a 3.5 L stirred tank reactor with a stirrer speed of 150 rpm and 0.1 vvm gas flow rate, Micheletti et al. (2016) reported a value of 61.2 h^{-1} for the k_La (Micheletti *et al.*, 2006).

Besides determining k_La values experimentally, a number of mathematical models have been established to predict this parameter. For STRs, van't Riet and colleagues first proposed a general equation (equation 1.7) to predict k_La (Van't Riet, 1979):

$$k_L a = A\left(\frac{P}{V_L}\right)^{\alpha} \cdot u^{\beta} \qquad (1.7)$$

Where P is the total power input, V_L is the volume of liquid inside the vessel, u is the superficial gas velocity, A is a constant that is dependent on the liquid composition, α and β are constants that are dependent on the system in use (Montes, Catalán and Galán, 1999; Weuster-Botz, Stevens and Hawrylenko, 2002; Nienow, 2006). For shake flasks, a similar correlation (equation 1.8) has been established by Liu, Wu and Ho (2006), which enables accurate predictions for the presented system. However, here too the relationship is not universal and the constants *a* and *b* have to be evaluated for each individual setup.

$$k_L a = k n^a \left(\frac{V_L}{V_0}\right)^b \qquad (1.8)$$

Where n is the shaking frequency, V_L is the working volume, V_0 is the total volume of the shake flask, and k, a, and b are constants that are determined via regression (Liu, Wu and Ho, 2006). Doig *et al.* (2005) and later Islam *et al.* (2008) have created mathematical expressions for the prediction of $k_L a$ values in commonly used microtitre plate formats. Equation (1.9) was developed based on 24, 96, and 384 round well plates (Doig *et al.*, 2005):

$$k_L a = D_i a_i Re^{0.68} Sc^{0.36} Fr^x Bo^y \qquad (1.9)$$

Where D_i is the diffusion coefficient, a_i is the initial specific surface area of the gas phase, *Re* is the Reynolds number ($Re = \rho n d_v^2 / \mu$), *Sc* is the Schmidt number ($Sc = \mu / (\rho D)$), *Fr* is the Froude number ($Fr = (d_t(2\pi n)^2 / 2g$), *Bo* is the Bond number ($Bo = (\rho d_v^2 g) / W$), and x and y are constants that depend on the geometry of the microtitre plate in use. This equation has then been adapted to square deep well microtitre plate formats with either round or pyramidal bottoms (Islam *et al.*, 2008):

$$k_L a = 3.94 \cdot 10^{-4}\left(\frac{D_i}{d_v}\right) a_i Re^{1.91} exp(aFr^b) \qquad (1.10)$$

Where a and b, again, are constants that have to be evaluated for the particular format of the square well microtitre plate format, and d_v and is the inner well diameter. The described correlations offer good predictions (within ± 30% deviation) for the tested well plate formats (Marques, Cabral and Fernandes, 2010) and can be helpful when one of the presented formats is used.

1.6.3 Volumetric power input (*P*/*V*)

The specific power input (*P*/*V)* is regarded as a key parameter used for scale translation of bioprocesses and describes the power that is introduced into the liquid volume. The power source is usually either an electric motor that drives a stirrer (e.g. STRs) or a shaking platform (e.g. shake flasks and microtitre plates). The transfer of power into the liquid occurs at the stirrer or at the wall in contact with the moving liquid. The power input causes the liquid to move and the movement eventually dissipates as heat into the liquid. The power input influences an array of other process parameters such as gas and heat transfer, mixing, and hydromechanical stress on the organism. This emphasizes the concept of keeping a constant power input across scales (Doran, 2013). For non-aerated STRs, the power input has been well characterised and is given by equation (1.11):

$$P = P_0 \rho_L N^3 D^5 \qquad (1.11)$$

Where P_0 is the dimensionless power number ($P_0 = P / \rho\, n^3\, d^5$), ρ_L is the density of the liquid, N is the rotational speed of the impeller, and D is its diameter (Nienow, 2006). Depending on the equipment that is used for stirring and gassing, the power input in an aerated STR is typically given with 30 – 40% of that found in an ungassed system (Oosterhuis and Kossen, 1981). However, for shaken systems it can be harder to determine the power input. Sumino et al. developed a method to estimate the power input in baffled and unbaffled shake flasks by measuring the temperature change of the liquid inside the flasks caused by the rotation (Sumino, Akiyama and Fukuda, 1972). However, the temperature changes are miniscule and may be influenced by unknown heat capacities of the flask material. An alternative setup involving a drive

with an integrated torque sensor connected to a shaking platform was used by Büchs et al. to establish a correlation between the power input and the shaking frequency (Büchs *et al.*, 2000):

$$\frac{P}{V_L} = P_0' \cdot \frac{n^3 \cdot d^4}{V_L^{2/3}} = C_3 \cdot \rho \cdot \frac{n^3 \cdot d^4}{V_L^{2/3}} Re^{-0.2} \qquad (1.12)$$

Where V_L is the fill volume of the flask, P_0' is the modified power number ($P_0' = P / \rho\, n^3\, d^4\, V_L^{1/3}$), n is the shaking frequency, d is the maximum inner diameter of the flask, C_3 is a system specific constant that can be derived through least-square non-linear regression, and Re is the Reynolds number ($Re = n\, d^2 / \eta$, where η is the dynamic viscosity). The discrepancy between the model and the values measured was smaller than 30%. Particularly for shaken microtitre plates, these methods are extremely difficult to implement, which is why researchers started performing such experiments *in silico* (Barrett *et al.*, 2010). Flow simulations using Computational Fluid Dynamics (CFD) have been successfully applied in order to predict parameters such as power input, volumetric mass transfer coefficient, and shear rate in both shake flasks (Zhang *et al.*, 2005) and microtitre plates (Zhang *et al.*, 2008; Barrett *et al.*, 2010).

1.6.4 Computational fluid dynamics (CFD)

With the processing power of computers steadily increasing, computational work has become an attractive alternative to lab-based experimentation. CFD, in particular, has the potential to quickly generate detailed insights into the engineering environment not only of existing systems, but also of design concepts that have not yet been realised. Furthermore, small-scale systems that are difficult to characterise with conventional methods can be made accessible using computational methods (Zhang *et al.*, 2005; Wutz *et al.*, 2018).

Fluid flow can be described either as continuum or atomistic. The continuum method describes flow variables as a moving macroscopic fields, whereas an atomistic description relies on the prediction of particle movement. Solving of the Navier-Stokes equations is a continuum approach to the computational prediction of macroscopic flow variables. These equations comprise expressions for the conservation of mass, momentum, and energy (Sharma, Malhotra and

Rathore, 2011). Particle movement in a single-phase environment is simulated through simultaneous solving of the continuity equation and the Navier-Stokes equation. Solving of the Lattice-Boltzmann equation (LBE) is an atomistic approach to the simulation of fluid movement, where the fluid is viewed as a collection of particles. The particles' location is described by the LBE as molecular probability and the evolution of such particle distributions defines the flow.

Such models are valuable in describing the fluid flow patterns in cultivation systems and have for example been used to explore flow conditions in shake flasks (Zhang *et al.*, 2005), microtitre plates (Barrett *et al.*, 2010; Wutz *et al.*, 2018), microbioreactors (Nienow *et al.*, 2013), and STRs (Ahmed *et al.*, 2010). As most cultivation processes require some form of gas input, a second phase needs to be considered in order to estimate parameters such as the k_La (Kerdouss *et al.*, 2008; Sarkar *et al.*, 2016). These multi-phase simulations are more complex and therefore demand greater processing power (Rathore, Kanwar Shekhawat and Loomba, 2016).

The continued interest in CFD has led to the development of several software packages (e.g. Fluent, CFX, OpenFOAM, M-Star) that facilitate the setup of fluid flow simulations and the analysis of their results (Sharma, Malhotra and Rathore, 2011). Initially, the reactor geometry needs to be designed using computer-aided design (CAD) software. The geometry is then divided into a finite number of cells as part of the meshing. Meshing is necessary to create a discrete representation of the model, which is numerically solvable. A finer mesh increases the number of cells and returns solutions that are more accurate. However, a finer mesh also increases the computational time. It is therefore necessary to strike a balance between accuracy and computational cost.

This balance is established through mesh-independence testing. In a number of preliminary simulations, the mesh size is gradually reduced until the solution remains unaffected by any further reduction of the mesh size. At this point, the solution is considered independent of the mesh (Rathore, Kanwar Shekhawat and Loomba, 2016). Following the mesh-independence testing, the software is used to solve the specified conservation equations for the desired conditions. This process generates data which can be visualised within the software interface (Sharma, Malhotra and Rathore, 2011).

1.7 Novel applications: CAR-T cell manufacturing

With its encouraging clinical results in treating systemic cancers that are otherwise only treated on a palliative basis, chimeric antigen receptor (CAR) T cell therapy has emerged as an exciting and rapidly moving area of research (Maude *et al.*, 2014; Porter *et al.*, 2015; Vormittag *et al.*, 2018). The two CAR T cell therapies Kymeriah™ (Novartis) and Yescarta™ (Gilead/Kite) are currently commercially available and more than 800 clinical trials are ongoing (clinicaltrials.gov, accessed 06/03/20). Yet, little published research exists on upstream process development of such therapies. In a collaborative project, the micro-Matrix was used to investigate the effect of cultivation conditions on the expansion and differentiation of primary T cells (Chapter 6).

The commercially available therapies are autologous, which means that the administered cells are derived from the patient. Leukapheresis is used to isolate the white blood cells from the patient before they are activated and transduced with the CAR transgene. For the delivery of the CAR transgene, lentiviral, retroviral and non-viral (such as transposon / transposase) methods exist (Vormittag *et al.*, 2018). The CAR is a synthetic membrane protein that consists of an internal and an external domain. The external domain is designed to recognise tumour-associated cell surface antigens and consists of an immunoglobulin-derived single chain variable fragment (scFv) (Gross, Waks and Eshhar, 1989). The scFv is linked to an internal signalling domain, which prompts a signalling cascade upon recognition of the antigen. This signalling process not only results in the expansion of the T cell, but also causes it to produce cytokines and cytotoxic compounds that help eliminate the cancer cell. Yet, the specific composition of the CAR is still matter of ongoing research and efforts are made to further improve upon it (Brown and Mackall, 2019).

After successful gene delivery, the CAR T cells need to be expanded *ex vivo* in order to reach the cell number of 10^6 – 10^7 cells kg^{-1} that is deemed an efficacious dose (Vormittag *et al.*, 2018). A standardised process for the expansion of CAR T cells has not yet been established. Expansion platforms currently used include WAVE bioreactors (GE Healthcare Life Sciences), CliniMACS prodigy (Miltenyi Biotec Inc.), G-Rex cell culture flasks (Wilson Wolf), and VueLife® Bags (Cell Genix) (Iyer *et al.*, 2018). From other areas, such as mAb manufacturing, it is understood how

important the tight control of the key process parameters DO and pH is in order to produce sufficient quantities of a safe and efficacious product (Yoon *et al.*, 2005; Trummer *et al.*, 2006; Bertout, Patel and Simon, 2008; Freshney, 2010; Haque *et al.*, 2013). Yet, many of the currently used production platforms lack active control capabilities for these parameters and little is known about the ramifications on the CAR T cell expansion. Furthermore, reproducibility and robustness remain challenging in the manufacturing of CAR T cell products, which curtails the commercial success of these therapies and emphasises the need for process development in this field (Costariol *et al.*, 2019).

Initially, the expansion of T cells has been considered optimal under static incubator conditions in T-Flasks, microtitre plates (Vormittag *et al.*, 2018) or bespoke cell culture flasks such as G-Rex (Zhan *et al.*, 2013; Bajgain *et al.*, 2014; Mock *et al.*, 2016). Under non-agitated conditions, however, the direct environment of the cells is difficult to control and heterogeneities in the medium are likely to occur throughout the process (Costariol *et al.*, 2019). To implement active control strategies while maintaining a low-shear environment, rocking motion bioreactors have been employed by several research groups (Kalos *et al.*, 2011; Brentjens *et al.*, 2013; Janas *et al.*, 2015). Costariol *et al.* (2019) examined the use of the ambr250 system for the cultivation of human primary T cells under varying vessel configurations and stirrer speeds with overlay aeration. The research shows that primary T cells can be grown under stirred conditions without affecting the phenotypic distribution. In fact, higher stirrer speeds resulted in an improved fold expansion.

In contrast to allogeneic products such as mAbs, the working volumes in CAR T cell manufacturing are small. However, research into “off-the-shelf” allogeneic CAR T cell therapies is underway and has the potential to tackle the bottlenecks characteristic for autologous products (Depil *et al.*, 2020). In light of emerging allogeneic therapies (Gouble *et al.*, 2014), process scalability becomes critical. To meet the demand of allogeneic T cell therapies, a shift from overlay aeration to sparging is necessary to prevent mass transfer limitations at larger scales. However, previous studies with hybridoma cells have shown that bursting bubbles are the main source of

shear stress in conventional STR systems (Oh *et al.*, 1989, 1992), which calls for a more in depth investigation of T cell behaviour under sparged conditions.

1.8 Aims and objectives

This project seeks to evaluate the micro-Matrix for its capability to serve as a tool for cell culture process optimisation and scale-translation using a model CHO cell line. Furthermore, it aims to provide a framework for the rapid process optimisation using the micro-Matrix system and then test this framework for the optimisation of a CHO fed-batch process and the expansion of primary T cells. The following objectives present specific objectives in concluding this project:

- Perform a thorough engineering characterisation of the micro-Matrix. An experimental determination of the parameters mixing time (t_m), volumetric mass transfer coefficient (k_La), and volumetric power input (P/V) will be underpinned by computational fluid dynamics (CFD) approaches.
- Establish a robust and reproducible cell culture protocol for a GS-CHO cell line in the micro-Matrix.
- Examine scale-up strategies to translate a model fed-batch process from a benchtop scale STR to the micro-Matrix via the engineering characteristics of the respective systems.
- Using the micro-Matrix and Design of Experiment to rapidly optimise the fed-batch protocol at the small-scale and validate the optimised protocol at the benchtop scale.
- Investigate the suitability of the micro-Matrix as process development tool for the optimisation of primary T cell expansion.

1.9 Thesis structure

While, Chapter 2 introduces the materials and methods employed for this work, Chapter 3 focuses on the engineering characterisation of the micro-Matrix microbioreactor and details initial cell cultivations. Evaporation and well-to-well variabilities were identified as characteristic challenges of the micro-Matrix system and addressed through the repeated replacement of evaporated liquid. Chapter 4 establishes a scaling strategy between a 5 L STR and the micro-Matrix based on the

engineering characterisation of Chapter 3. In Chapter 5 a bolus feeding strategy is optimised in the micro-Matrix using response surface methodologies and the optimised protocol is then scaled up to the 5 L STR using the scaling strategy outlined in Chapter 4. Chapter 6 focuses on the expansion of primary T cells in the micro-Matrix by investigating the effect of varying operating conditions on T cell growth and differentiation.

Chapter 2. Material and methods

Content of this chapter is published in Wiegmann, Martinez and Baganz (2020)

2.1. Cell culture

2.1.1. Cell line and revival

The IgG4 expressing GS-CHO cell line GS-CY01 (Lonza, UK) was used for most of this work. The cells were thawed and diluted with 49 mL of warmed CD-CHO medium (Life-Technologies, UK) containing 25 µM MSX (Sigma-Aldrich, UK). The cells were then expanded in a shake flask with a vent cap (250 mL nominal volume, Corning Life Sciences, USA), which was placed onto an orbital shaker with an orbital throw of 25 mm (Certomat MO II, Sartorius Stedim, Aubagne, France) and incubated at 160 rpm, 37°C, 5% CO_2, and 70% humidity.

2.1.2. Preparation of the working cell bank

Prior to cell banking, the cells were expanded for at least two passages according to the subculture protocol (section 2.1.3). The viable cell concentration was then measured, and the required volume with a 10% overage was calculated following equation 2.1. This volume was then centrifuged at 450 g for 5 minutes in a benchtop centrifuge (5810 R, Eppendorf, Hamburg, Germany). The pellet was re-suspended in fresh medium to a viable cell concentration of 30 x 10^6 cells mL^{-1}. A suitable number of cryo-vials were filled with 500 µL of CD-CHO containing 20% Hybri-Max dimethyl sulfoxide (DMSO) (Sigma-Aldrich, USA) and pre-chilled in a Mr. Frosty™ freezing container (Thermo Scientific, UK) before 500 µL of the concentrated cell suspension were added to each cryo-vial. The resulting cryo-vials contained 1 mL of cell suspension with a viable cell concentration of 1.5 x 10^6 cells mL^{-1}. The cryo-vials were cooled down in the freezing containers for 24 hours at -80°C before they were transferred to liquid nitrogen for long-term storage. All GS-CHO experiments presented in this work were executed with cells from the same cell bank.

$$Cell\ broth\ (mL) = \frac{1.5 \cdot 10^6 \frac{VC}{mL} \cdot number\ of\ vials}{VCC\ of\ subculture} \cdot 1.1 \qquad (2.1)$$

2.1.3. Subculture and inoculum preparation

After revival (section 2.1.1), cells were passaged every 3 – 4 days by splitting them into vented shake flasks (250 mL nominal volume, 50 mL working volume, Corning Life Sciences, USA) at a density of 3 x 10^5 cells mL^{-1}. The shake flasks were mounted on an orbital shaker with an orbital throw of 25 mm (Certomat MO II, Sartorius Stedim, Aubagne, France) and incubated at 160 rpm, 37°C, 5% CO_2, and 70% humidity. The inoculum was prepared after 12 – 14 days of expansion from cells in the exponential growth phase. For experiments in the 5 L STR, a larger volume of cell broth was required for the inoculum. The cells were therefore transferred to shake flasks with a nominal volume of 1000 mL (Corning Life Sciences, USA) which were cultivated with a working volume of 200 mL in the above combination of shaker and incubator.

2.1.4. 24 standard round well (24 SRW) culture

The previously described 24 SRW "sandwich" cover lids (see section 1.4.2.1) (Applikon-Biotechnology, The Netherlands) were used for all experiments in 24 SRW microtitre plates. 24 hours prior to inoculation, the lids were autoclaved and left inside the laminar flow cabinet to cool and dry. A suspension with a final concentration of 3 x 10^6 cells mL^{-1} was prepared from the preculture using the appropriate amount of CD-CHO medium. This suspension was then used to fill the wells of the 24-SRW (Corning Life Sciences, USA) to a working volume of 0.8 mL. Two different lids (regular and low-evaporation, Table 2.1) were used in the 24-SRW, thus creating two systems with different gas exchange rates (1.1 vvm and 0.25 vvm, respectively).

Table 2.1: Description of the micro-Flask lids used in the experiments. Data for evaporation rates were obtained from the manufacturer (Enzyscreen, 1999).

Name	Description	Evaporation Rate [µL/well/day]
CR1524	Sandwich lid for 24-SRW	30
CR1524a	Low-evaporation sandwich lid for 24-SRW	6

The lid was placed on top of the 24 SRW and a micro-Flask cover clamp (Applikon-Biotechnology, The Netherlands) was used to fixate the assembled plate on an orbital shaker (Certomat MO II, Sartorius Stedim, Aubagne, France) with an orbital diameter of 25 mm and a shaking speed set to 220 rpm. Cultivations were performed at 37°C, 5% CO_2, and 70% humidity. Samples were first taken daily and later every second day on a sacrificial basis. As a result of the irregular evaporation across microtitre plates (Martuza et al., 1976), corner wells were sampled first, then wells positioned on the side of the 24 SRW, and lastly wells with a central location on the plate. Upon sampling, the cell suspension inside the wells was extracted and weighed in order to determine the volume of the evaporated liquid. All volume-dependent parameters were corrected for loss of volume.

2.1.5. micro-Matrix culture

2.1.5.1. Description of the micro-Matrix system

The micro-Matrix is a microbioreactor based on a 24 deep square well microtitre plate (cassette) format. Each well of the cassette has a total volume of 10 mL and a recommended working volume of 2 - 5 mL. The cassette is placed onto an orbital shaker inbuilt into the micro-Matrix, which operates at shaking speeds between 0 – 400 rpm with an orbital throw of 25 mm.

Clamps hold the cassette in place when the system is in operation. The clamps also reinforce the contact between the pH and DO optodes underneath the cassette to the LEDs and detectors of the sensor module, thus allowing for stable measurements. An overview of the micro-Matrix system is given in Figure 2.1.

As shown in Figure 2.2, an additional pair of clamps fixes the top plate to the cassette. The top plate functions as a sterile barrier and enables the delivery of gases and liquids into the wells. Each row is equipped with a single-use gas filter bar, which holds hydrophobic membranes of 0.2 μm pore size for the sterile filtration of in- and outflowing gases. Up to four different gases can be supplied to each well through overlay aeration. For mammalian cell culture, these typically

include compressed air (cAir), oxygen (O_2), and nitrogen (N_2), to regulate the DO and carbon dioxide (CO_2) for the down-control of the pH.

Figure 2.1: The fully assembled micro-Matrix microbioreactor. Image retrieved from *www.Applikon.com.*

A manifold of microvalves installed on the top plate controls the pneumatically driven liquid additions. The manifold is connected to an autoclavable liquid addition feed bottle (LAFB), which is pressurised by a gas supply next to the inbuilt shaker. The key process parameters pH, DO, and temperature can be controlled for each well individually, with the limitation that temperature differences between neighbouring wells must not exceed 1°C.

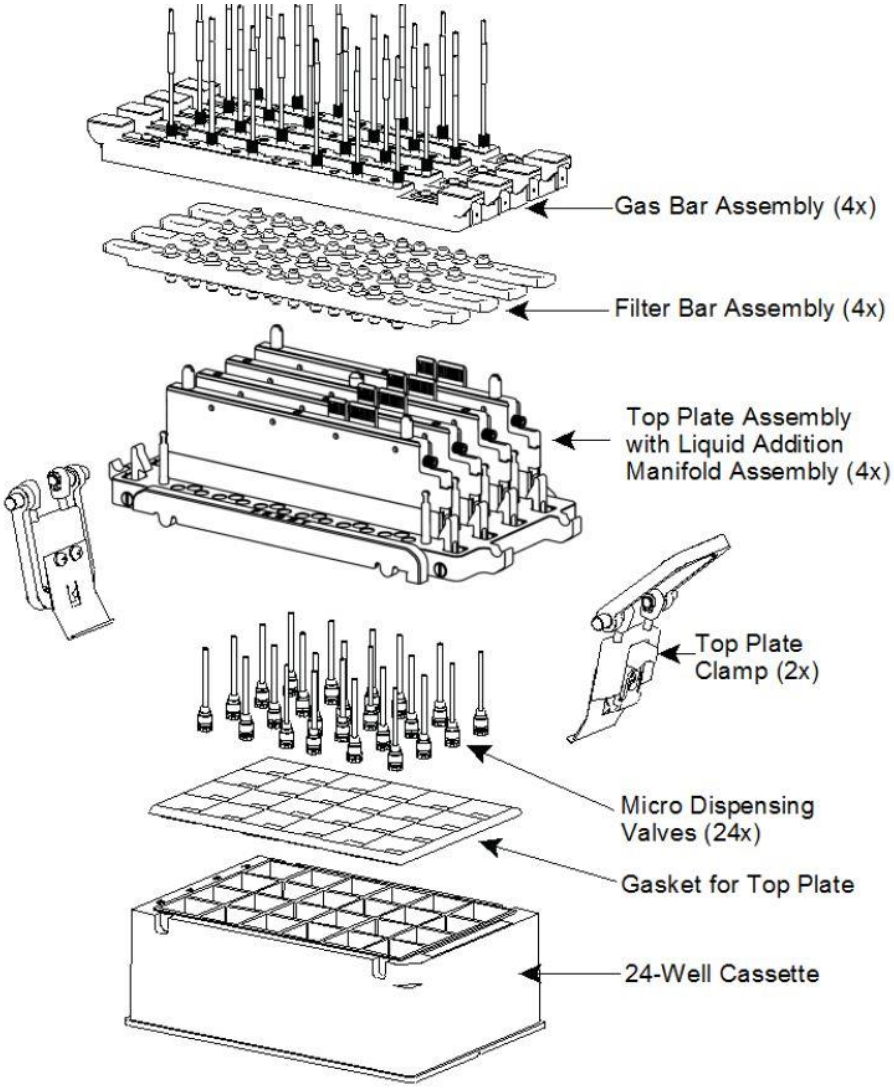

Figure 2.2: Exploded view of the micro-Matrix cassette assembly. Image retrieved from *www.Applikon.com.*

2.1.5.2. Setup and operation

For the initial setup, all relevant gasses were connected to the main gas inlets of the micro-Matrix. Gases used for cell cultivations were either pure cAir, O_2, N_2, and CO_2 (all BOC, UK) or blends of these gases with 5% CO_2 (all BOC, UK). Next, the liquid feeding module was calibrated by filling 200 mL of the liquid to be used in the experiment into the LAFB and initiating a sequence of 1000 pulses of feed additions into pre-weighed sample tubes. The volume of the delivered liquid was determined gravimetrically and used to calibrate the feed volume per pulse specific to each microvalve. The top plate was then autoclaved together with the LAFB before aseptically filling the LAFB with feed medium or base and priming the feed lines.

To calibrate the pH sensors, a new micro-Matrix cassette (Applikon-Biotechnology, The Netherlands) was filled with 2 mL of sterile PBS (Life-Technologies, UK) per well. The cassette was then closed with the previously autoclaved top plate and mounted onto the micro-Matrix. The pH was monitored for at least 1 hour or until a stable reading was obtained. During this time, no gases were connected and temperature control as well as shaking were disabled in order to avoid changes of the pH levels caused by the environmental conditions. Subsequently, 1 mL of PBS was extracted from three wells and analysed using an offline pH meter (Mettler Toledo, Switzerland). The measured values were then adjusted to match the average of the three offline measurements. Finally, the PBS was removed from each well using serological pipettes.

A suspension with a final concentration of 3 x 10^6 viable cells mL^{-1} was prepared using the appropriate amount of CD-CHO medium. A volume between 2 and 5 mL of this suspension was used to fill each well of the micro-Matrix cassette. The micro-Matrix cassette was covered with the top plate, connected to the gas supply lines and clamped onto the micro-Matrix. The software was then used to specify the set points of pH, DO, and temperature for each well. Down-control of the pH was achieved through the automated overlay of CO_2, whereas up-control was achieved through either bolus or automated additions of 0.75 M NaOH or 0.25 mM bicarbonate buffer (0.25 mM $NaHCO_3$ and 0.25 mM Na_2CO_3). The DO was controlled through the addition of cAir / O_2 and N_2. The maximum gas flow rate was set to between 1.4 and 11.1 mL min^1. Both pH and DO were measured in 10 s interval and the time-averaged values were fed into the PID control loop. The temperature was controlled at 37°C. The cabinet temperature was initially set to 1°C below the cell culture setpoint and later increased to 1°C above the setpoint to reduce evaporation and condensation. Sampling was either done sacrificially or based on the feed volumes.

2.1.6. Stirred tank reactor (STR) culture

For cultivations at the benchtop scale, a BIOSTAT B-DCU (B.Braun Biotech, Sartorius, Surrey, UK) with a nominal volume of 5 L was used. The reactor was run under standard configuration as previously described by Silk (2014). Briefly, the unbaffled vessel had a diameter of 160 mm and a round bottom. A single, down-pumping, 45° pitched blade impeller was used and set to a

rotational speed of 260 rpm. Gases were either pure cAir, O_2, N_2, or CO_2 (all BOC, UK) or blends of these gases with 5% CO_2 (all BOC, UK). Submerged aeration was achieved using a ring sparger located underneath the impeller, which was set to a continuous gas flow of 200 mL min^{-1}.

Prior to autoclaving, the pH probe (Mettler Toledo, Switzerland) was calibrated using pH 4.01 and 7.0 standard buffers (Mettler Toledo, Switzerland). The two-point calibration (0% and 100% air saturation) of the VisiFerm DO ECS 325 H2 DO probe (Hamilton, Switzerland) was performed in deionised water at 37°C after autoclaving. The vessel was then emptied and filled with 2 L of CD-CHO medium (Life-Technologies, UK) and left to equilibrate at the cell culture setpoints for at least two hours. The inoculum was prepared in a sterile 1 L bottle and added to the vessel through an overlay port via pressure differential. The seeding density was 3 x 10^5 cells mL^{-1} and the working volume at the beginning of each run was 2.75 L. In fed-batch experiments, the working volume increased to up to 4.1 L. The DO was controlled at 30%, the pH at 7.2, and the temperature at 37°C. Up-control of the pH was achieved through automated additions of 1 M NaOH. Bolus additions of 10 mL 1% Antifoam C Emulsion (Sigma-Aldrich, UK) were added daily to the culture. 10 mL of sample were taken daily or twice a day when feed was added. Following each experiment, the reactor was first cleaned with 5 L of NaOH at 50°C and later rinsed with deionised water.

2.1.7. Feeding strategy and its scale translation

For all cultivations with GS-CHO cells, the basal medium was CD-CHO (Life Technologies, UK) without MSX and the feed medium was Efficient Feed B (Life Technologies, UK). The standard fed-batch protocol for the 5 L STR was based on recommendations made by the manufacturer of the medium (Invitrogen, 2007). Feeding commenced on day 3 of the cultivation when 10% of the initial working volume was added to the culture in the form of bolus additions. Feeding was repeated every two days until 50% of the initial working volume worth of feed medium were added to the culture.

As the sample volume relative to the working volume was substantially larger in the micro-Matrix than it was in the 5 L STR (roughly 10% of the working volume per sample), simply applying

above protocol to the smaller scale would lead to overfeeding. For the small scale, the feed volume was therefore based on the current working volume rather than the initial working volume. In the scaled down version of the protocol, bolus feeding commenced after 3 days of cultivation (10% of the working volume) and was repeated on day 5 (9.1%), day 7 (8.3%), day 9 (7.7%), and day 11 (7.1%).

2.1.8. Isolation and cultivation of primary T Cells

Initially, the T Cells needed to be isolated from fresh blood of healthy donors (Cambridge Bioscience, UK). The blood was collected under comprehensive informed consent, which allows the use of this blood for research purposes. Furthermore, permission of the Research Ethics Committee (REC) was obtained (REC reference: 17/SW/0189) ahead of the experiments.

In the first step, Lymphoprep density gradient medium (Stemcell Technologies, Canada or Norway) was used to separate peripheral blood mononuclear cells (PBMCs) from the donor blood. Then, CD3+ T Cells were separated using the Pan T Cell Negative Isolation Kit (Miltenyi Biotec, Germany). Pan T Cells of each individual donor were aliquoted in CryoStor CS10 (STEMCELL Technologies UK Ltd, UK) and stored in liquid nitrogen. For the micro-Matrix experiments, cells were thawed and resuspended in basal medium consisting of RPMI1640 (Gibco, UK), supplemented with 10% FBS (Gibco, UK), 2 mM Glutamine (Gibco, UK), and 1 mM sodium pyruvate (Gibco, USA). The cells were kept under static incubator conditions for 12 – 24 hours before they were seeded at a concentration of 4×10^5 cells mL^{-1} in 2 mL of the basal medium in each well of the micro-Matrix. Under experimental conditions, the basal medium was further supplemented with 25 ng mL^{-1} Interleukin 7 (IL-7, Miltenyi Biotec, Germany), 10 ng mL^{-1} Interleukin 15 (IL-15, Miltenyi Biotec, Germany), and washed anti-CD3 / CD28 Dynabeads (Life Technologies, Norway) at a Dynabead to cell ratio of 3:1.

2.2. Engineering characterisation of the micro-Matrix

2.2.1. Mixing time

As shown in Figure 2.3, the mixing time experiments were performed in a custom-built mock-up well replicating the geometry and dimensions of the micro-Matrix wells. The mock-up well had a square shape with a length and width of 16 mm and a height of 40 mm. To facilitate recordings of the fluid, the mock-up well was made from transparent acrylic, whereas the micro-Matrix cassette was made from opaque polystyrene. Based on previous reports (Rodriguez *et al.*, 2014; Li, Ducci and Micheletti, 2020), the mixing time was assumed to be unaffected by the material differences. The mock-up well was mounted on an orbital shaker with an orbital throw of 25 mm (Certomat MO II, Sartorius Stedim, Aubagne, France). An LED panel was installed behind the well to generate consistent background lighting.

The Dual Indicator System for Mixing Time (DISMT) was used to determine mixing times and visualise flow patterns inside the well (Melton *et al.*, 2002; Li, Ducci and Micheletti, 2020). The DISMT solution consisted of 64.4 µg L^{-1} Thymol Blue (Fisher Scientific, UK) and 64.8 µg L^{-1} Methyl Red (Fisher Scientific, UK) dissolved in Milli-Q water. The coloration of the DISMT solution is pH-dependent and can assume either a red (pH < 6.3), yellow (pH 6.3 - 8), or green (pH > 8) hue. Prior to the experiments, the DISMT solution was adjusted to a neutral pH (yellow coloration) and a volume between 2 – 5 mL was filled into the mock-up well. All additions of acid (0.75 M HCl, Fluka, Germany) and base (0.75 M NaOH, Acros, Belgium) were done in increments of 10 µL, using two PHD ULTRA syringe pumps (Harvard Apparatus, USA). First, the solution was acidified through the addition of 10 µL acid under shaken conditions. Once the liquid adopted a homogeneous red colour, the shaking speed was set to the experimental conditions and 10 µL of base was added. The colour transition from red to yellow was recorded using an iCube high-speed camera (NET New Electronic Technology GmbH, Germany). The time necessary for the solution to reach a homogenous yellow colour was reported as the mixing time.

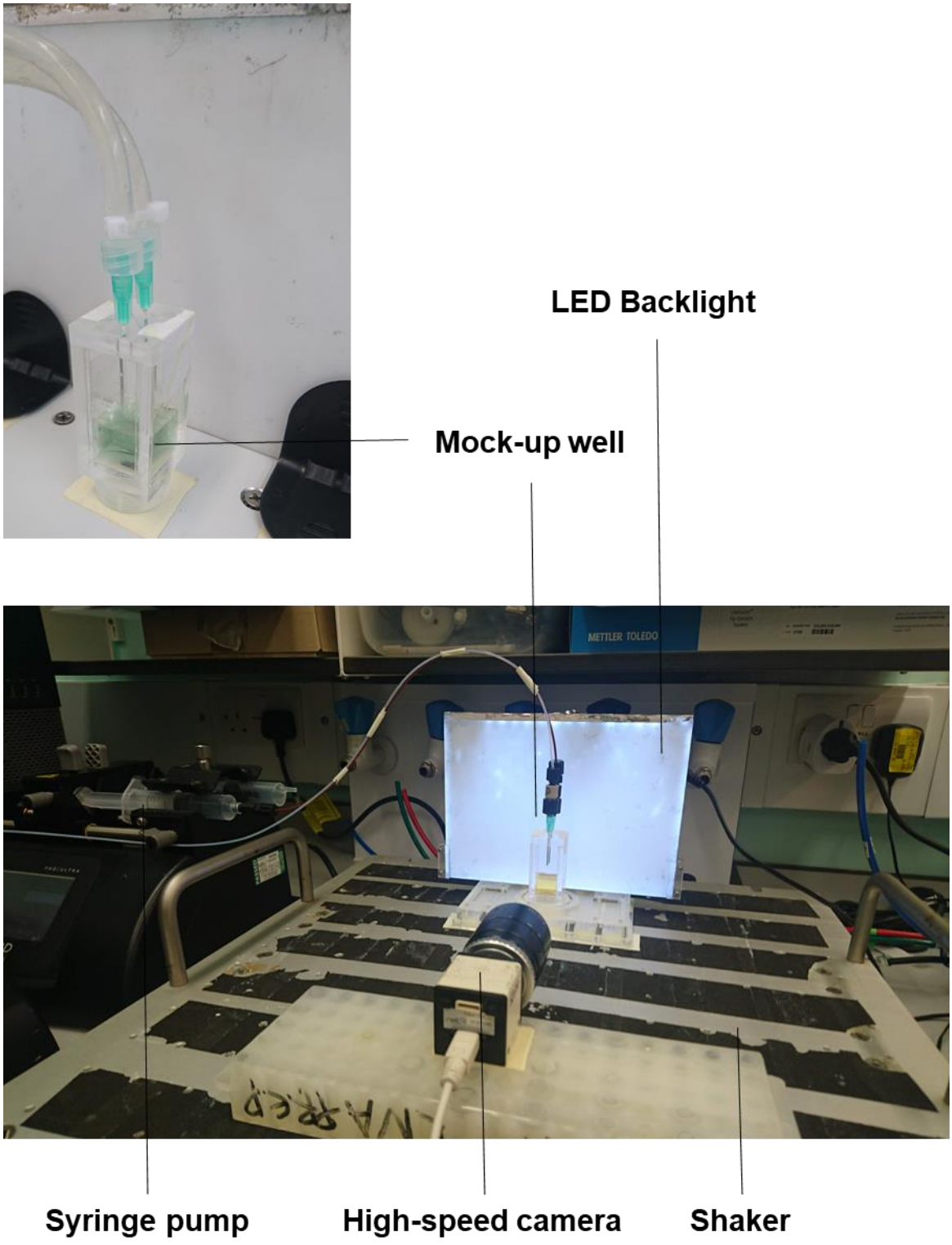

Figure 2.3: Experimental setup of the mixing time experiments in a mock-up deep square well. The mock-up well was mounted onto an orbital shaker in front of an LED backlight. Syringe pumps controlled additions of acid and base while the shaker was in operation. Colour changes and fluid motion were recorded using a high-speed camera.

2.2.2. Volumetric mass transfer coefficient (k_La)

The static gassing out method was used to determine the k_La in the micro-Martrix wells (Van't Riet, 1979). As the probe response time (τ_p) of the micro-Matrix optodes was roughly 1 min and the measurements were averaged by the software, an alternative sensor was used for the k_La measurements. The Needle-Type Oxygen Microsensor with 80 mm length (PreSens, Germany) performed measurements with a frequency of 1 Hz and provided a sufficiently short probe response time (τ_p < 3 s). As the probe response time of the microsensor was $\tau_p < 1/k_La$, it did not have to be accounted for in calculating the k_La (Van't Riet, 1979). As illustrated in Figure 2.4, to submerge the sensor in the liquid, it was inserted into the well through the off-gas filter of the micro-Matrix filter bar. A stand and clamp were used to stabilise the sensor while the shaker was in motion. Additionally, a spacer above the off-gas filter ensured that the sensor tip was no closer than 3 mm to the bottom of the well, to prevent damage to the sensor's internal glass fibre.

Before the measurement, oxygen was first removed from the liquid through overlay with nitrogen and continuous shaking at 300 rpm. When the DO reached 0%, shaking was stopped; a syringe with air was inserted through the off-gas filter to flush the headspace with five times its volume of air. Then, the microsensor was inserted through the off-gas filter and the experimental conditions (shaking speed, gas flow rate) were applied. Recording of the DO commenced once shaking was initiated. Measurements were taken for DO values between 0 and 80% and the k_La was calculated according to equation 2.2 (Doran, 2013):

$$k_L a = \frac{ln\left(\frac{C_{max} - C_{t1}}{C_{max} - C_{t2}}\right)}{t_2 - t_1} \qquad (2.2)$$

Where C_{max} is the steady-state concentration of dissolved oxygen when the liquid is saturated with air, $C_{t1}$and C_{t2} are the concentrations of dissolved oxygen at times t_1 andt_2, respectively. All measurements were performed in PBS (Life Technologies, UK) to facilitate comparability to other devices.

A)

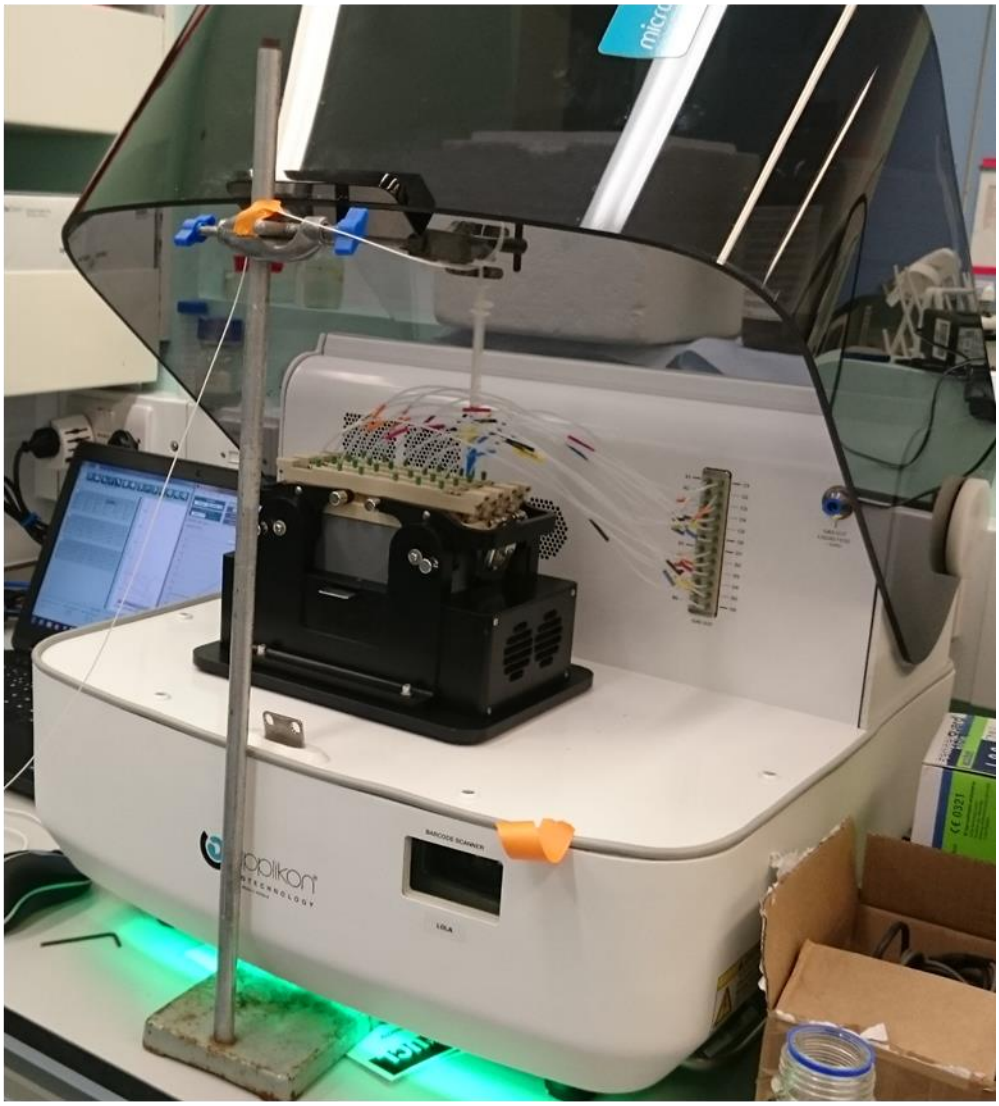

B)

Figure 2.4: Experimental setup for k_La measurements in the micro-Matrix (A). A needle-type microsensor (B) was inserted into the well through the off-gas filter and stabilised using a stand. The hood of the micro-Matrix was partially closed to help maintain a temperature of 37°C inside the wells.

2.2.3. Computational fluid dynamics

The commercial software package M-Star (M-Star Simulations, USA) was used for all fluid flow simulations within the micro-Matrix well. The 3D model had a length and width of 16 mm and a height of 40 mm, which is dimensionally equivalent to the micro-Matrix well (Figure 2.5).

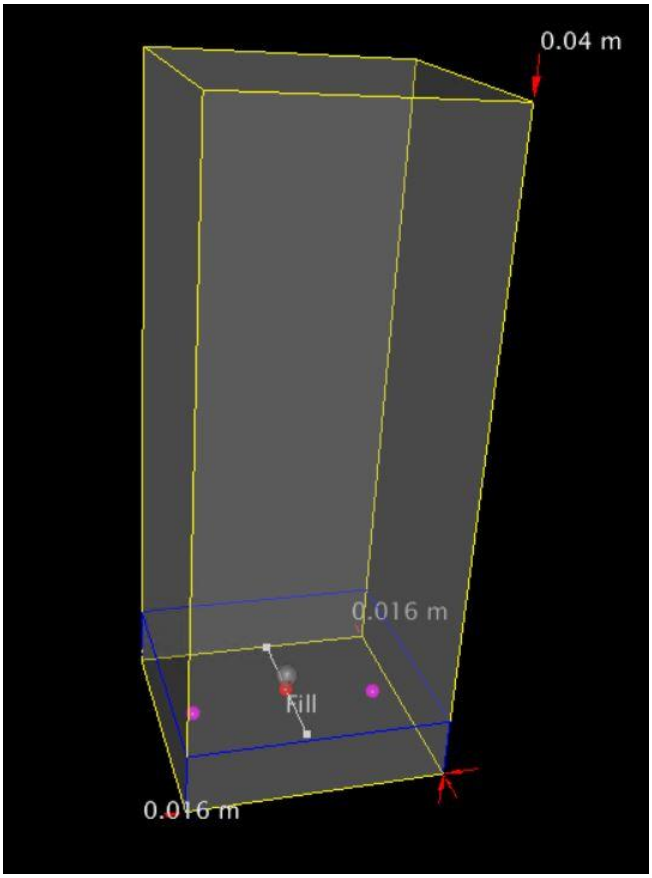

Figure 2.5: Design of the deep-square micro-Matrix well in M-Star. The blue line indicates the liquid body, which has a volume of 1 mL in this example. Probes were arranged at the bottom of the well, analogous to the micro-Matrix well. A grey sphere just above the liquid level represents a bolus addition of base, which was intended for mixing time experiments.

A free surface model of a single Newtonian fluid with the density (1 g mL^{-1}) and kinematic viscosity (1 x 10^{-6} m^2 s^{-1}) of water was used for all simulations. The lower portion of the well was filled with the fluid according to the working volume that was tested as part of the simulation. Direct Numerical Simulation (DNS) and Large Eddy Simulation (LES) were tested as turbulence models. As both models yielded similar results, the fluid flow was later exclusively computed using LES with a Smagorinsky coefficient of 0.1. The influence of the surface tension was tested and later

set to 0.072 N m^{-1}, which is the surface tension of water (Li, Ducci and Micheletti, 2020). The rotation of the well was defined by the accelerations in X, Y, and Z directions and given by equation 2.3.

$$\alpha_X = r\omega^2 \cos(\omega t)$$
$$\alpha_Y = -9.81 \frac{m}{s^2} \qquad (2.3)$$
$$\alpha_Z = r\omega^2 \sin(\omega t)$$

Where r is the radius of the orbital throw (0.0125 m) and ω is the angular velocity (rad s^{-1}). As Y is the rotational axis, the acceleration needs to antagonise gravitation. The shaking speed of the well model was defined by modulating the value of ω.

The mesh resolution was determined analogously to the mesh-independence testing described in section 1.6.4. The fluid velocity along a predefined output line within the working volume was compared for the same condition at increasing mesh resolutions. The solution was considered independent of the mesh resolution once the velocity profile seized to change with further increases of the resolution. Similarly, the minimum rotations of the well required for the simulation to reach a steady state was determined by comparing the velocity profile along an output line after each rotation. Steady-state was assumed once the velocity profile did not indicate further changes with additional rotations.

2.3. Analytical techniques

2.3.1. Viable cell concentration

The Vi-CELL XR (Beckman Coulter, UK) works based on the trypan blue dye exclusion test. For each measurement 500 µL sample volume were filled into a Vi-Cell sample cup and placed into the sample carousel. The system automatically mixes sample and trypan blue dye and pumps the mixture through a flow cell that is equipped with an imager. The device analyses 50 images per sample and automatically averages the generated data for viable cell concentration, total cell concentration, and viability. In addition, the image analysis also provides distributions of cell size

and circularity. To provide accurate measurements, the samples were diluted when the cell concentration exceeded 10^6 cells mL^{-1}.

2.3.2. At-line determination of nutrients, metabolites, and pCO_2

The Bioprofile FLEX (Nova Biomedical, USA) was used to determine the levels of all relevant nutrients, metabolites, and electrolytes. The system is divided into the modules nutrients / metabolites and gas / electrolytes. In case of the nutrient and metabolite module, membrane-bound enzymes catalyse reactions of the respective metabolites (glucose, lactate, glutamine, and glutamate), the concentration of which can then be measured potentiometrically. The concentration of gases and electrolytes (NH^{4+}, pH, pCO_2, pO_2, Na^+, K^+, and Ca^{2+}) is determined through ion selective electrodes, except for the pO_2, which is measured using a Clarke electrode. For each module and sample, 500 µL of sample volume were filled into an Eppendorf tube and clamped onto the tray. For smaller sample volumes, the samples were diluted with Milli-Q water. PBS was used as diluent for higher dilutions (1:5 and higher). When the pCO_2 was measured, the sample was taken up with a syringe to avoid gas exchange and measured using the system's syringe function.

2.3.3. Antibody titre

IgG4 quantification was conducted using an Agilent 1200 (Agilent Technologies, UK) high-performance liquid chromatograph (HPLC) with a 1 mL HiTrap Protein G HP column (GE Healthcare, UK). Buffer A was prepared from 10 mM NaH_2PO_4 (Fluka, Cat No. 71642-1KG) and 10 mM $NaH_2PO_4 \cdot H_2O$ (Sigma-Aldrich, Cat No. 71507-1KG) and adjusted to pH 7; Buffer B was prepared from 20 mM glycine (VWR, Cat No. 101196X) and adjusted to pH 2.8. A 96 well plate was loaded with 75 µL of sample volume per well and covered with a pierceable cap mat (Nunc, Denmark). Table 2.2 shows the method used for the analysis in which the maximum pressure was set to 80 bar. The elution peak was recorded via UV absorption at 260 nm and a dilution series of a purified IgG4 standard was used to correlate the resulting peaks with the concentration of IgG4. The analytical results were corrected for evaporation where applicable.

Table 2.2: Protein G HPLC timeline for the analysis of IgG4 content in the cell culture supernatant.

Time [min]	Component of Buffer A [%]	Component of Buffer B [%]	Flow [ml/min]
0.00	100	0	1
4.00	100	0	2
4.01	0	100	2
11.50	0	100	2
11.51	100	0	2
14.00	100	0	2

2.3.4. Osmolality

Osmotic pressure was measured using an Osmomat 3000 (gonotec, Germany). 50 µL of cell culture supernatant was transferred into a 0.5 mL centrifuge tube, which was then mounted so that the electrode was fully immersed in the liquid. The device cooled down the sample to its freezing point and then correlated the freezing point depression to the concentration of osmolytes in solution.

2.3.5. Antibody purification

The purification of IgG4 from the crude supernatant was done manually using an Econo-Pac Chromatography Column (Bio-Rad, UK) loosely packed with 1 mL of MabSelect Sure resin (GE Healthcare, UK). Buffer A (Equilibration) was prepared from 12.2 mM NaH_2PO_4 (Fluka, Cat No. 71642-1KG), 7.8 mM $NaH_2PO_4 \cdot H_2O$ (Sigma-Aldrich, Cat No. 71507-1KG), and 150 mM NaCl (Sigma-Aldrich, Cat No. S7653-1KG) and adjusted to pH 7.2. Buffer B (Elution) was prepared from 40.1 mM citric acid (Sigma-Aldrich, Cat No. C1909-1KG) and 58.6 mM sodium citrate (Sigma-Aldrich, Cat No. S4641-1KGG) and adjusted to pH 3.5. Buffer C (Neutralisation) was prepared from 1 M Tris-HCl (Fisher Scientific, BP152-1).

The resin was first washed with 10 column volumes (CVs) of Buffer A. 1 mL of the crude supernatant was then diluted in 2 mL of Buffer A and slowly dispensed into the column. The eluate was captured and again cycled through the column; this was repeated five times. The resin inside the column was then washed with 10 CVs of Buffer A. For the elution, the column was first emptied to the fill level of the resin, before 1 mL of Buffer B was added. The column was then closed to prevent any of the liquid flowing out and left to incubate for 30 s. The column was then opened

and 1 mL of the eluate was collected in a sample tube and immediately neutralised with 100 µL of Buffer C. The elution step was repeated five times. The IgG4 content of every fraction was determined via UV at 260 nm using a NanoDrop 1000 Spectrophotometer (Thermo Fisher Scientific, UK). Fractions were pooled when appropriate and frozen immediately until further analysis.

2.3.6. Glycoprofiling

The analysis of the IgG4 glycan structures was performed by Ludger Ltd (Oxfordshire, UK). The samples were analysed using a HILIC-UHPLC using a Dionex Ultimate 3000 UHPLC (Thermo Fisher Scientific, UK) together with an Acquity BEH-Glycan 1.7 µm, 2.1 x 150 mm column (Waters Corporation, USA) at 40°C on a Dionex UltiMate 3000 instrument (Thermo Fisher Scientific, UK) with a fluorescence detector, controlled by Bruker HyStar 3.2 software (Bruker, USA).

Buffer A was 50 mM ammonium formate made from LudgerSep N Buffer stock solution, pH4.4 (Ludger Ltd, Cat No. LS-N-BUFFX40). Buffer B was acetonitrile (Acetonitrile 190 far UV/gradient quality; Romil #H049). Samples were injected in 24% aqueous / 76% acetonitrile at an injection volume of 25 µL. Chromeleon data software version 7.2 (Thermo Fisher Scientific, USA) with a cubic spline fit was used to allocate Glucose Unit (GU) values to peaks. Procainamide labelled glucose homopolymer was used as a system suitability standard as well as an external calibration standard for GU allocation for the system.

2.3.7. Immunophenotypic analysis of T Cells

At the end of each T Cell cultivation, cells were labelled with the primary antibodies CD3-BUV305, CD4-BUV805, CD8-BUV737, CCR7-BV421, and CD45RO-PE-Cy7 (all BD Biosciences, USA). A 5-laser LSRF Fortessa-X20 flow cytometer (BD Biosciences, USA) was then used to measure the florescence. The resulting data was analysed with FlowJo version 10 (FlowJo LLC, USA).

2.4. Design of Experiment (DoE)

Design Expert v10 (Stat-Ease, Inc., Minnesota, USA) was used for the conception of DoE designs and the evaluation of their results. Centre points were replicated five times to ensure sufficient statistical power of the lack of fit test. Replicating the centre point less than five times in a central composite design, risks leaving significant lack of fit unnoticed. Furthermore, high centre point replication also decreases the standard error in the middle of the design space, adding to the predictive power of the resulting model. A centre point replication of five to six replicates is therefore recommended. When it was necessary to approximate normal distribution through transformation of the data, a suitable transformation was selected as suggested by the software (Guy *et al.*, 2013). Significant effects were computed through backwards elimination with a cut-off *p*-value of 0.1. The resulting model was then analysed using ANOVA to ensure significance of each term and non-significant lack of fit. Models were only accepted if the F-values indicated a sufficiently high effect to noise ratio. Furthermore, it was checked that the Pred R-Squared value was no more than 0.2 lower than the Adj R-Squared value.

The model was analysed with Design Expert's diagnostics function to ensure that the assumptions made in the ANOVA were correct. Normal plots were checked for linearity of the data points, the residuals vs predicted plot was checked for random scattering, and the residuals vs run plot was checked for lack of trending. The Box-Cox plot was used to decide whether a power law transformation was necessary to create the model and the residuals vs factor plot was checked for random scattering at both ends.

If all diagnostic plots confirmed the quality of the model, it was used for process optimisation. The model was first visualised either in line plots or, if multiple factors had an effect on a response, in contour plots. Subsequently, the numerical optimisation tool was used to find the optimal parameter combination for a given response.

All DoE experiments were performed in the micro-Matrix microbioreactor platform. Details of the design matrices and the experimental background are provided in the respective chapters.

2.5. Determination of derived growth parameters

2.5.1. Specific growth rate

The specific growth rate (μ) (h^{-1}) was calculated between two time points using equation 2.4.

$$\mu = \frac{ln(VCC_i) - ln(VCC_{i-1})}{t_i - t_{i-1}} \quad (2.4)$$

Where VCC_{i-1} and VCC_i (cells mL^{-1}) are the viable cell concentrations at times t_{i-1} and t_i (hour), respectively. The resulting values in the exponential growth phase were averaged to calculate μ_{max}.

2.5.2. Integral viable cell concentration (IVCC)

The integral viable cell concentration (IVCC) (cells d mL^{-1}) is a measure for cell growth and was calculated using the trapezoid method (equation 2.5).

$$IVCC_i = \frac{VCC_i + VCC_{i-1}}{2} \cdot (t_i - t_{i-1}) \quad (2.5)$$

Where VCC_{i-1} and VCC_i (cells mL^{-1}) are the viable cell concentrations at times t_{i-1} and t_i (day), respectively. The cumulative integral viable cell concentration (cIVCC) was calculated by summing up the IVCC values of each time point over the course of the cultivation (equation 2.6).

$$cIVCC = \sum IVCC_i \quad (2.6)$$

2.5.3. Specific antibody productivity

The cell specific productivity (q_{mAb}) (pg $cell^{-1}$ d^{-1}) describes the amount of antibody produced per cell in a given time interval and was calculated by dividing the change in antibody concentration by the IVCC between two time points (equation 2.7).

$$q_{mAb} = \frac{[IgG]_i - [IgG]_{i-1}}{IVCC_i} \quad (2.7)$$

Where $[IgG]_i$ and $[IgG]_{i-1}$ (pg mL^{-1}) are the concentrations of antibody at times t_i and t_{i-1} and $IVCC_i$ (cells d mL^{-1}) is the integral viable cell concentration at time point t_i. The maximum specific productivity ($q_{mAb,max}$) (pg cells^{-1} d^{-1}) was given by the highest value of q_{mAb} achieved during a cultivation. The specific lactate production rate (q_{Lac}) (pg cells^{-1} d^{-1}) was calculated analogously.

2.5.4. Specific metabolite consumption rate

The specific nutrient consumption rate (q_{Nut}) (pg cells^{-1} mL^{-1}) describes the specific consumption of a nutrient per cell in a given time interval and gives information on the metabolic activity of the cell population. q_{Nut} was calculated according to equation 2.8.

$$q_{Nut} = \frac{[Nut]_{i-1} - [Nut]_i}{IVCC_i} \quad (2.8)$$

Where $[Nut]_i$ and $[Nut]_{i-1}$ (pg mL^{-1}) are the concentrations of a specific nutrient (e.g. Glucose) in the cell broth at times t_i and t_{i-1} and $IVCC_i$ (cells d mL^{-1}) is the integral viable cell concentration at time point t_i. In cases where nutrients and metabolites could not be measured before and after feeding, the concentration of nutrients after the addition of feed was calculated based on the dilution and the concentrations of the nutrient in the feed and the cell broth. In perfusion experiments, $q_{Nut,Perf}$ was calculated as described by Sewell *et al.* (2019) (equation 2.9).

$$q_{Nut,Perf} = \frac{(([Nut]_{i-1} \cdot (1 - D) + ([Nut]_{Media} \cdot D)) - [Nut]_i}{IVCC_i} \quad (2.9)$$

Where $[Nut]_{Media}$ (pg mL^{-1}) is the concentration of a specific nutrient in the perfusion medium and D (-) is the dilution rate.

2.5.5. Lactate yield

The lactate yield $Y_{Lac/Gluc}$ is a measure for the amount of lactate generated per glucose consumed and gives information about the metabolic activity of the cells. The lactate yield was calculated according to equation 2.10.

$$Y_{Lac/Gluc} = \frac{q_{Lac}}{q_{Gluc}} \quad (2.10)$$

Where q_{Lac} and q_{Gluc} are the specific rates of lactate production and glucose consumption, respectively.

2.6. Statistical tests

To compare the mean of two conditions, a two-sided student's t-test was performed using an α of 0.05. For the comparison of multiple mean values, a post-hoc Tukey test was performed.

Chapter 3. Engineering characterisation of the micro-Matrix system and initial cell culture performance

Content of this chapter is published in Wiegmann, Martinez and Baganz (2018)

3.1. Introduction and aim

A well-characterised engineering environment of the cultivation system constitutes the foundation of knowledge-based process development. Cultivation processes often have unique requirements and challenges, which are only met in a timely manner if the cultivation system is adequately described. Increasingly, early stage process development takes place in miniaturised bioreactor systems that can cut down development timelines through parallelisation, automation and utilisation of single-use materials (Markert and Joeris, 2017; Markert *et al.*, 2019). Once suitable operating conditions have been established, the process needs to be translated to larger scales in order to manufacture an economically viable product. However, to recreate similar conditions in the larger scale is rarely straightforward and requires a sound understanding of the engineering environment (Rameez *et al.*, 2014). Therefore, a thorough characterisation of the equipment must precede any efforts made in cell culture process development.

The physical characterisation of bioreactor systems is largely captured by their properties regarding mass transfer, fluid flow, and power input. These parameters can be established with relatively little experimental effort and sometimes even *in silico* through computational approaches. Many system characterisations have already been performed and made available to the scientific community (Betts, Doig and Baganz, 2006; Xing *et al.*, 2009b; Barrett *et al.*, 2010; Nienow *et al.*, 2013; Betts *et al.*, 2014; Wutz *et al.*, 2018). However, for Applikon's micro-Matrix microbioreactor no such characterisation is available in the literature. This chapter therefore seeks to establish a thorough engineering characterisation of the micro-Matrix to form the foundation for cell culture process development using this device. The methodologies used encompass wet-lab experimentation to determine mixing and mass transfer properties, but also computational fluid dynamics to gain a more in-depth understanding of the energy dissipation within the device. Furthermore, evaporation and reproducibility were addressed in this chapter, as they are common issues in small-scale cell culture.

Chapter aims and objectives:

- Experimentally measure liquid phase mixing time in the microbioreactor format using the DISMT method for a range of shaking speeds and working volumes.
- Determine the volumetric mass transfer coefficient in the microbioreactor format for a range of shaking speeds, working volumes, and gas flow rates.
- Use computational fluid dynamics to simulate the fluid flow within the microbioreactor wells and derive the energy dissipation rates for varying shaking speeds and working volumes.
- Establish an initial cell culture protocol for GS-CHO cells and address excessive evaporation as well as lack of well-to-well reproducibility.

3.2. Engineering characterisation

3.2.1. Liquid phase mixing time

As described in section 2.2.1, the DISMT method was used to determine the mixing times at varying shaking speeds and working volumes in the micro-Matrix microbioreactor under dynamic conditions. Due to the colorimetric nature of this method, it was also possible to evaluate fluid flow patterns in the well. Figure 3.1 A shows an exemplary mixing time experiment within the micro-Matrix well mimic. In the first frame, the shaker was operating at 240 rpm and 10 µL of base just detached from the needle that was connected to a syringe pump. Once the drop of base entered the liquid phase, the mixing time experiment was started. The two subsequent frames show how the colour transition of the DISMT solution progressed. Visual analysis of this transitional phase provided a more detailed understanding of the fluid flow within the well and facilitated the identification of poorly mixed zones. Well-mixed areas quickly assumed a yellow (neutral) colouration, whereas dead zones remained either red (acidic) or green (basic) for extended periods.

A) **240 rpm**

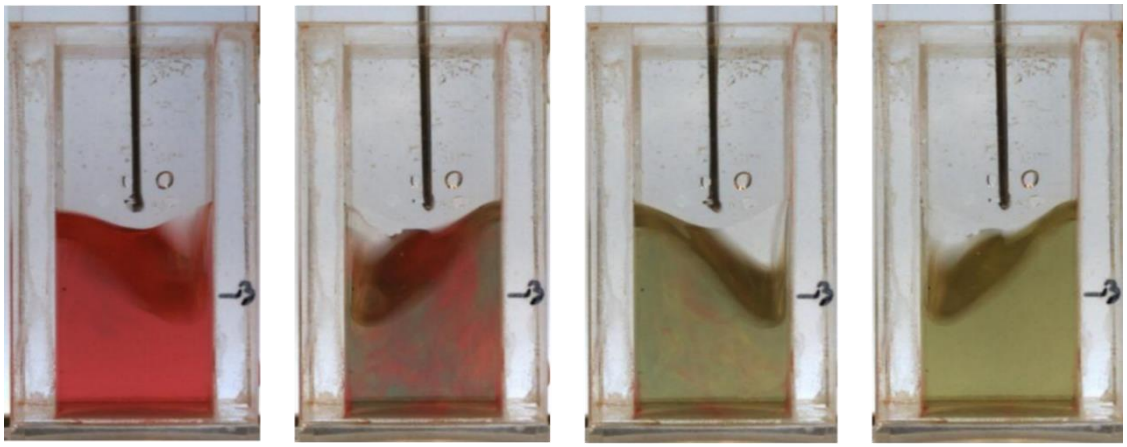

B) **100 rpm**

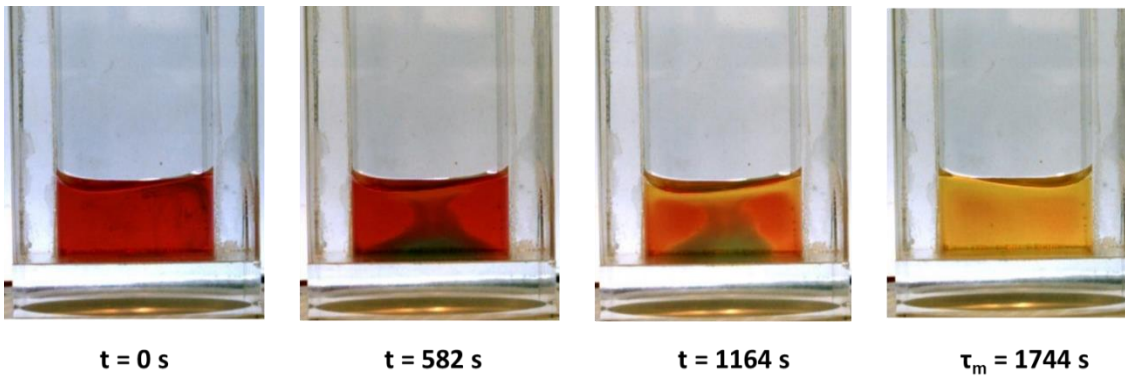

Figure 3.1: Fluid flow in the micro-Matrix. A) Liquid phase mixing time experiment at a shaking speed of 240 rpm and a working volume of 4 mL. At t_0, base entered the liquid phase, which marked the beginning of the colour transition and therefore the mixing time experiment. The images of the following time points illustrate fluid flow patterns and zones of varying homogeneity. A uniform yellow colouration indicated a homogenous neutral pH of the DISMT solution and consequently the endpoint of the mixing time experiment at τ_m. B) Mixing time experiment at a shaking speed of 100 rpm and a working volume of 2 mL.

Observation of the liquid motion revealed that a minimum shaking speed was required for the liquid surface to show deformation. This behaviour has been documented previously by other research groups (Hermann, Lehmann and Büchs, 2003; Doig *et al.*, 2005), who argued that the inertia incurred by the surface tension needs to be overcome before the surface can deform and the liquid starts to move in phase with the shaking motion. For cylindrical well formats, the shaking speed at which the surface tension of the liquid is overcome can even be predicted by calculating the phase number (Büchs, Lotter and Milbradt, 2001). Efficient mixing was only achieved above

this critical shaking speed, which was exceeded at 200 rpm for all tested working volumes. An example for a shaking speed that was too low to set the liquid body in motion is given in Figure 3.1 B. In addition to this global effect on the motion of the liquid, some shaking speeds also caused localised mixing inefficiencies. At speeds of 200 and 220 rpm, the surface showed deformation and the liquid moved in unison with the shaker, yet the lower half of the liquid body remained poorly mixed causing a surge in mixing times for these conditions. This effect has been previously documented by Tissot *et al.* (2010), who used a shaken cylindrical bioreactor with a nominal volume of 30 L for mixing time studies. Lower shaking speeds were reported to stunt mixing at the bottom of the vessel and create an area where mixing was mainly governed by diffusion.

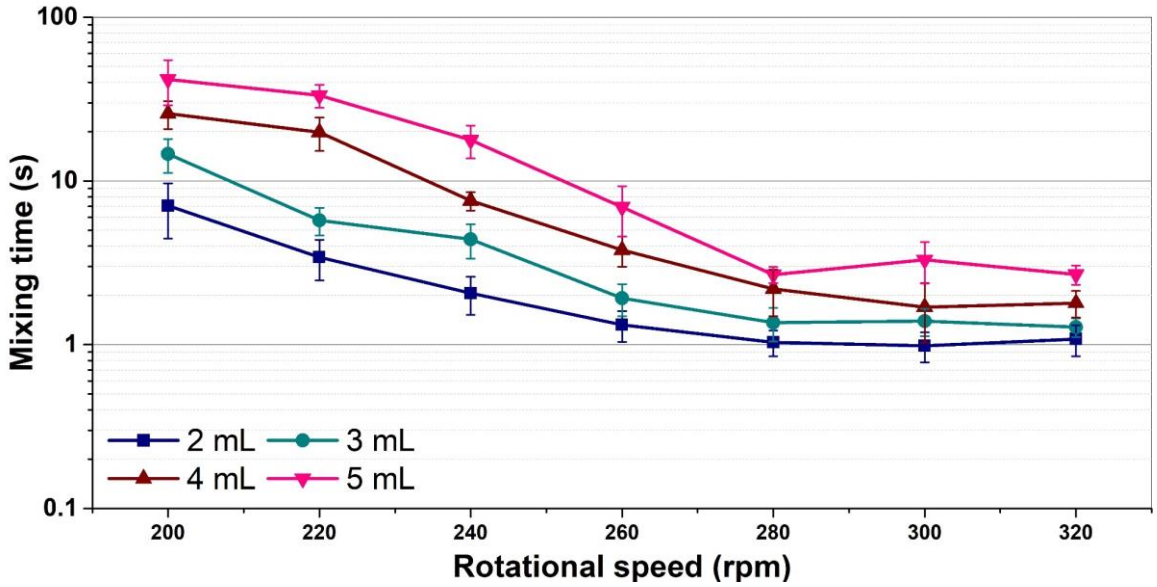

Figure 3.2: Liquid phase mixing time in the micro-Matrix well mimic at shaking speeds between 200 and 320 rpm and working volumes between 2 and 5 mL. The data is presented in a logarithmic scale and data points represent the mean ± standard deviation of 3 to 10 replicates per condition.

The mixing times recorded from the dynamic DISMT experiments, as shown in Figure 3.2, ranged between 1 – 42 s. A shaking speed of 100 rpm was only tested for a working volume of 2 mL and resulted in a mixing time of 1129 s (data not shown in graph). An increased working volume led to longer mixing times, though the trend was similar. With an increasing shaking speed, the mixing times shortened and remained largely stagnant for shaking speeds above 280 rpm. Higher

shaking speeds were not tested, as further changes of the mixing time were not expected and more vigorous shaking caused the well content to splash onto the lid, which could compromise sterility during cell cultivations. Particularly for a working volume of 5 mL, an unexpected, small, but significant increase of the mixing time was observed for a shaking speed of 300 rpm compared to the mixing time at 280 rpm (p = 0.047, t-test) and 320 rpm (p = 0.048, t-test). Sudden increases of the mixing time at higher shaking speeds have previously also been reported for deep-square wells with conical bottoms shaken with an orbital throw of d_O = 3 mm (Li, Ducci and Micheletti, 2020). Li and colleagues related this unexpected behaviour to the small orbital shaking diameter and confirmed this hypothesis by showing that the same effect could not be demonstrated with an orbital throw of d_O = 15 mm. As for the micro-Matrix d_O = 25 mm, an analogous explanation may therefore not be valid. Closer inspection of the images relating to a shaking speed of 300 rpm revealed however that base is occasionally dispensed at the upper end of the extended liquid body, which caused homogeneity to be reached later compared to when base was dispensed into the bulk liquid (Figure 3.3). The stochastic nature of this event is also reflected by the increased standard deviation for this condition.

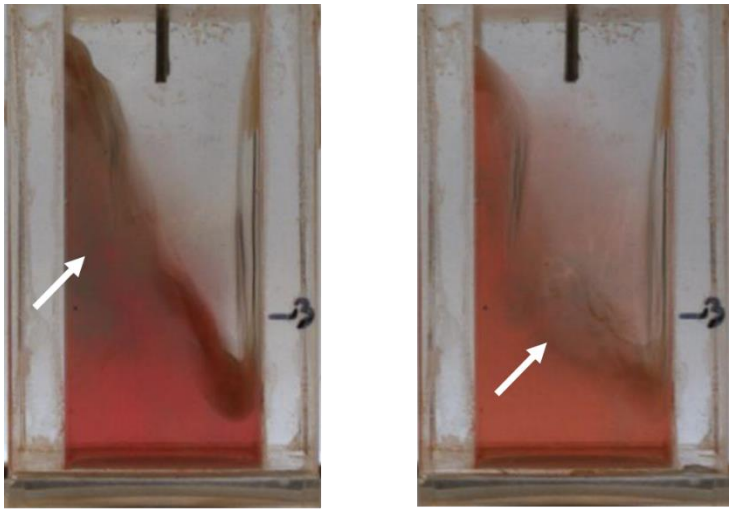

Figure 3.3: Liquid phase mixing time experiments at a working volume of 5 mL and a shaking speed of 300 rpm. Occasionally, base was dispensed into the upper portion of the liquid (left), instead of the bulk of the liquid (right). The former caused slightly extended mixing times. Arrows indicate the location of the base additions.

Compared to other microbioreactor and benchtop bioreactor systems, the micro-Matrix delivered similar mixing times. A characterisation of the µ24 bioreactor established mixing times of 1 – 13 s with working volumes of 5 and 7 mL (Betts *et al.*, 2014), whereas Barrett et al. (2010) reported

mixing times ranging from 1.7 s to 12,900 s for the 24 SRW format and 10 – 100 s for a 5 L STR. The ambr® 15 was reported to reach mixing times as low as 5 s (Nienow *et al.*, 2013).

3.2.2. Oxygen mass transfer - k_La

For all measurements of the k_La in the micro-Matrix microbioreactor, the static gassing out method was used as described in section 2.2.2. To facilitate system-to-system comparability, the measurements were performed in PBS. As cultivation media, particularly in mammalian cell culture, are inherently more complex in nature, the k_La levels during the cultivation are likely to differ to some extent (Betts *et al.*, 2014). Prior to testing all other conditions, it was first investigated whether each well yields a similar oxygen mass transfer under the same operating condition (200 rpm, 3 mL working volume, and 11 mL min^{-1} gas flow rate).

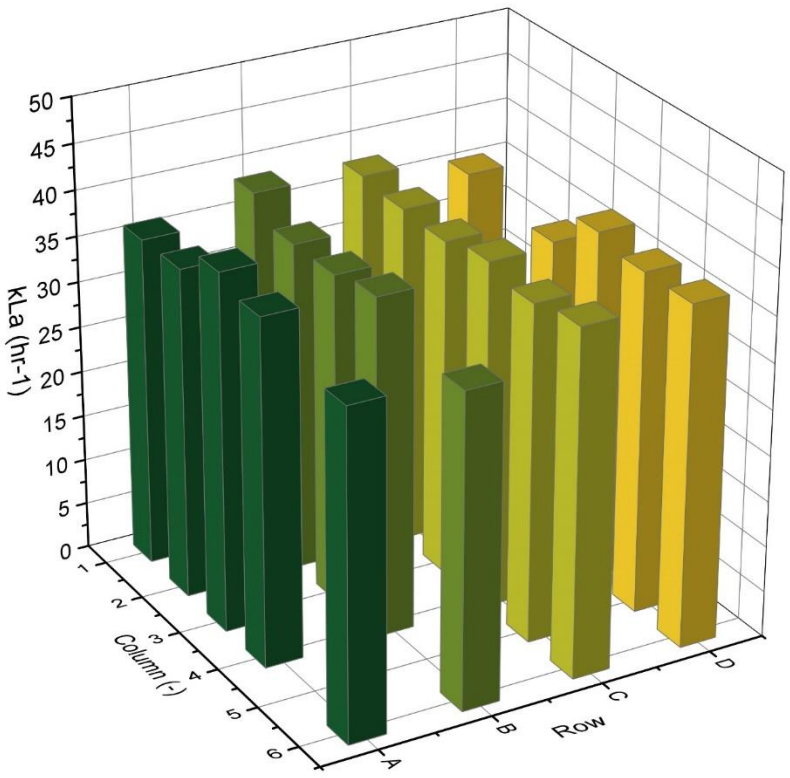

Figure 3.4: Test of the variability of the measured k_La value between wells under the same operating condition of 200 rpm shaking speed, 5 mL working volume of PBS, and 11.1 mL L^{-1} air flow rate.

Figure 3.4 shows that the determined k_La value was similar in all tested wells. The k_La for the tested parameter combination ranged between 34.1 – 39.2 h^{-1} with an average of 36.9 ± 1.6 h^{-1} (mean ± 1σ). A low coefficient of variance of 3.7% proves that the variability between wells is low and the measurement in one well can be considered representative for the remaining wells. All following measurements can therefore be performed in a few select well positions. No measurements were possible in wells A5 and B5 due to blocked off-gas filters and in well D2 due to a leaking gas valve.

As illustrated in Figure 3.5, the k_La ranged between 2.4 and 240.8 h^{-1} depending on the shaking speed and working volume tested. As expected, the k_La increased with an increasing shaking speed and decreased with an increase of the working volume. The ratio of surface area to liquid volume is a major driving force for the gas transfer in shaken systems (Hermann, Lehmann and Büchs, 2003; Doig *et al.*, 2005). As described in section 3.2.1, the liquid surface progressively deforms with an increase of the shaking speed. With increasing deformation of the liquid surface topology, in turn the surface area of the liquid increases, leading to a rise in k_La levels. Additionally, the inclination of the liquid surface grows, which further adds to this effect.

In contrast to other microbioreactor systems (Nienow *et al.*, 2013; Betts *et al.*, 2014), the gas flow rate did not affect the observed k_La values in the micro-Matrix to a significant degree for any of the tested conditions ($p > 0.05$). An important difference to most other bioreactor systems is that the micro-Matrix is restricted to surface aeration. In sparged systems, the gas flow rate directly affects the k_La as it governs the area of the gas-liquid interface through the number and size of the rising gas bubbles. In exclusively surface aerated systems, however, the gas-liquid interface is restricted to the liquid surface. The independence of the k_La from the gas flow rate indicates that the amount of air present in the headspace at the beginning of the experiment was adequate to increase the DO to a sufficient level so that further overlay with air had no effect on the mass transfer into the liquid.

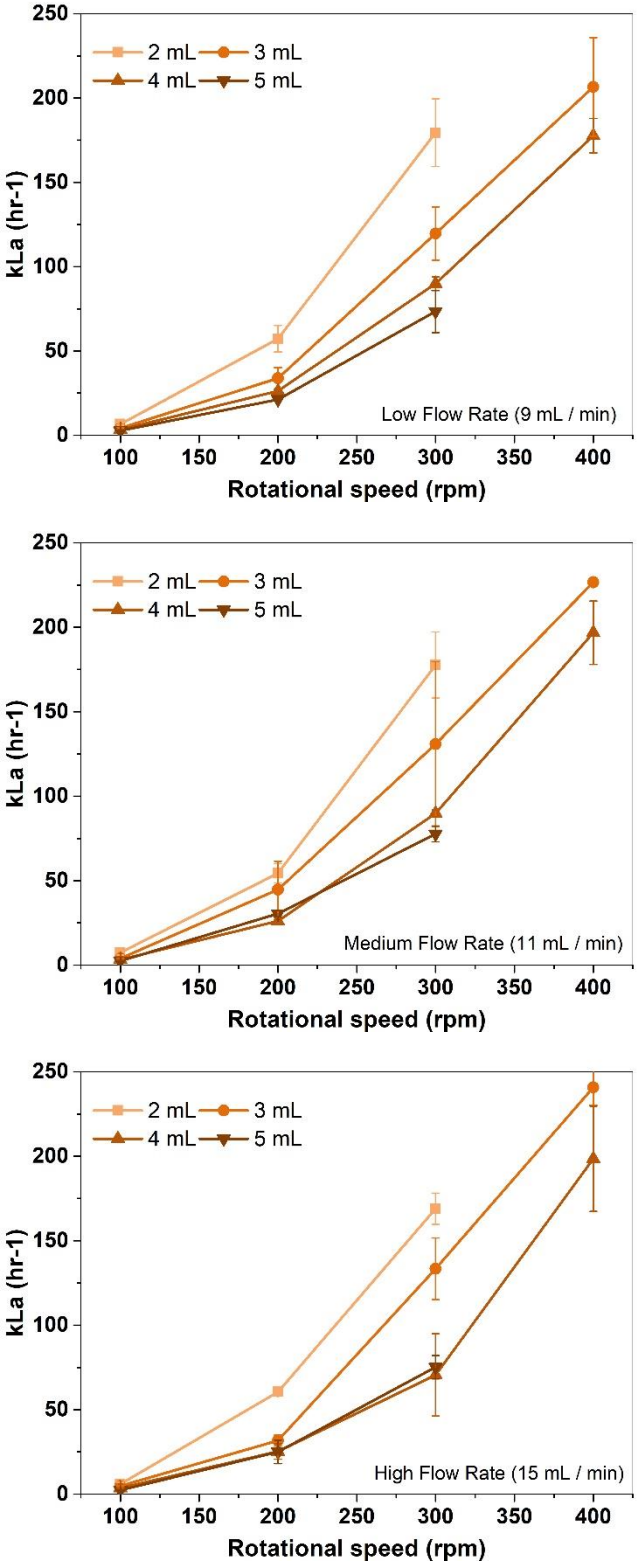

Figure 3.5: Volumetric mass transfer coefficient (k_La) measured in the micro-Matrix using the static gassing out method in PBS. Measurements were performed in working volumes between 2 and 5 mL, shaking speeds between 100 and 400 rpm, and gas flow rates between 9 and 15 mL min^{-1}. Data points represent the mean ± standard deviation (n = 3).

Figure 3.5 shows that some data points are missing for each gas flow rate at the high end of the shaking speed. As mentioned in section 3.2.1, a combination of high shaking speed and high working volume lead to splashing. At a working volume of 5 mL and a shaking speed of 400 rpm, liquid droplets wetted the underside of the top plate and caused some of the liquid to be forced through the off-gas filter. Ensuing filter blockages and sterility concerns, therefore, render this operating condition not suitable in a cultivation process and no measurements were performed for this parameter combination. Although splashing was minimal for a working volume of 2 mL and a shaking speed of 400 rpm, measurements of the DO could not be sustained for the duration of the experiment. This was due to the high surface inclination of the liquid for this condition. Most of the liquid was spread as a thin layer across the walls of the well so that the DO probe was not continuously immersed in the liquid, which caused considerable fluctuations of the resulting measurements.

The k_La values obtained in the micro-Matrix cover a wide range and are comparable to other small-scale cell culture formats such as 24 SRWs (Hermann, Lehmann and Büchs, 2003; Doig *et al.*, 2005), the µ24 microbioreactor (Isett *et al.*, 2007; Betts *et al.*, 2014), or the ambr15 (Nienow *et al.*, 2013). The broad range of k_La values provides flexibility in how the micro-Matrix can be used, which for instance opens potential applications in the area of microbial fermentation, where gas transfer is a key factor. However, standard STR configurations in mammalian cell culture typically yield k_La values between 1 – 15 h^{-1} (Nienow, 2006). To recreate those mass transfer conditions in the micro-Matrix would require the shaking speed to be set below 200 rpm, which would inevitably cause mixing inefficiencies as shown in section 3.2.1. In cases where a matched k_La is an important component of the scaling strategy, the use of gas blends could be considered to lower the mass transfer while at the same time maintaining the desired mixing conditions.

3.2.3. Computational characterisation using CFD

3.2.3.1. Model setup and validation

Fluid flow simulations were performed using M-Star CFD version 2.7 (M-Star Simulations, Maryland, USA). In contrast to other CFD tools that solve the Navier-Stokes equations directly, this software package uses lattice-Boltzmann algorithms instead. In principle, the lattice-

Boltzmann approach can solve the Navier-Stokes equations without a turbulence model. However, for the simulation of low viscosity and high Reynolds number conditions, solutions quickly become unstable. To avoid impractical timesteps and resolutions, the LES filter was introduced, which superimposes eddy viscosity onto the fluid viscosity.

Initially, simulations were run for a working volume of 4 mL and a shaking speed of 200 rpm and visually compared to images of the fluid flow that were recorded within the context of the liquid phase mixing time experiments (section 3.2.1). Surface inclination was used to determine whether the simulations generated a similar fluid flow compared to the experimental conditions. Initially, it was unclear whether the surface tension of the liquid had to be considered as part of the simulations. Therefore, three simulations were performed in which the surface tension was defined to be either 0.0, 0.072, or 0.08 N m^{-1}. Simulations and experimental conditions were compared at a shaking speed of 200 rpm and a working volume of 4 mL. The maximum liquid height was then compared to the experimental findings using equation 3.1:

$$Normalised\ liquid\ height\ difference = \frac{h_{CFD}}{h_{CFD,well}} - \frac{h_{Exp}}{h_{Exp,well}} \quad (3.1)$$

Where h_{CFD} was the maximum liquid height (cm) reached once the simulation had reached a steady-state, $h_{CFD,well}$ was the height (cm) of the simulated deep square well, h_{Exp} was the maximum liquid height (cm) reached under experimental conditions, and $h_{Exp,well}$ was the height (cm) of the simulated deep square well. The maximum liquid height was normalised to allow for a more accurate comparison of photos and exported images obtained from the experiments and simulations, respectively.

Figure 3.6 shows that the surface tension plays an important role in the simulation of the free surface. Repeating the same simulation for several surface tensions revealed that only a surface tension of 0.072 N m^{-1} resulted in a comparable surface inclination. As this is the surface tension of water at room temperature (Li, Ducci and Micheletti, 2020), the findings are in agreement with the expectations. The pronounced influence of the surface tension on the liquid surface inclination

also suggests that any characterisation should ideally be performed with the cultivation medium, as media additives affect the surface tension considerably (Nienow, 2006).

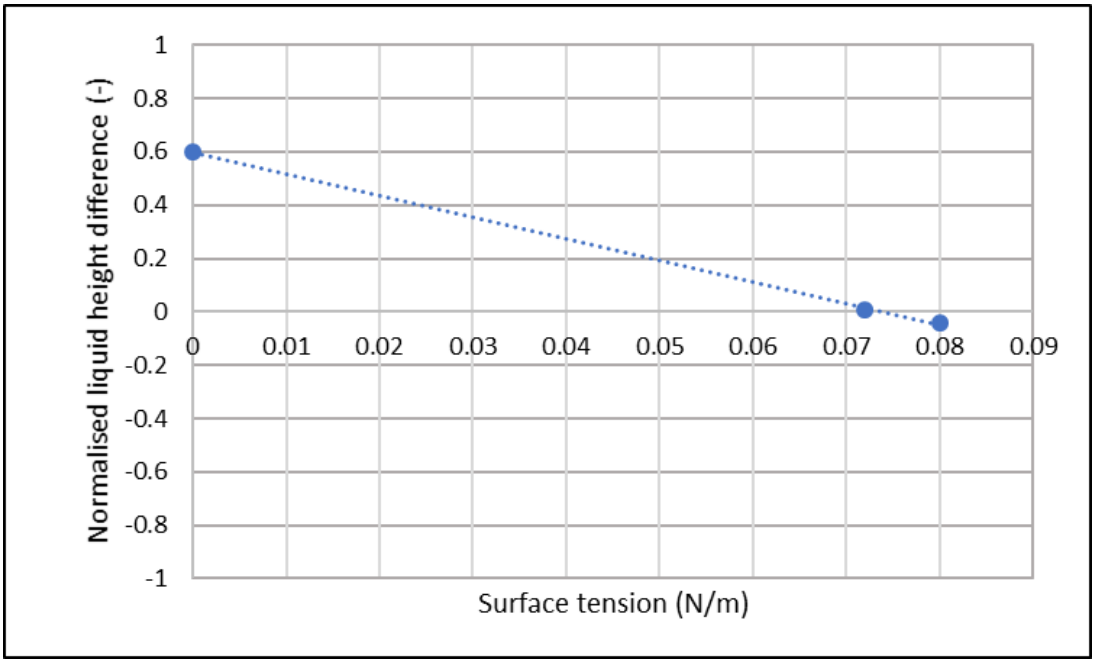

Figure 3.6: Difference of the simulated and experimental liquid height at a shaking speed of 200 rpm, a working volume of 4 mL and various surface tensions. Comparability of the liquid height was used as marker for the validity of the fluid flow model.

To simulate the fluid flow, the software breaks the fluid body up into discrete cells rather than solving the Navier-Stoke equation for the entire body of fluid. The number of cells any given fluid body is divided into defines the resolution of the simulation. A high resolution, meaning a high number of discrete cells, yields more accurate simulations, but also a higher computational cost and hence longer simulation runtimes. It is therefore desired to decrease the resolution as much as possible without affecting the accuracy of the simulation. In M-Star the resolution is defined by rx, the “Resolution on Reference Length” parameter, which defines the number of cells along the x-direction. The software generates a uniform grid of cells, which is why the number of cells in y- and z-direction can also be calculated using rx. In order to compare the simulations at varying resolutions, an output line along the x-direction at a height of 8 mm was defined within the deep well model. Throughout the simulation, the software collected data of the fluid velocity along the output line. After five well rotations, the fluid velocity was compared between the tested resolutions (Figure 3.7). It was found that the fluid velocity was highly comparable for resolutions

of 150 and 180 rx, while velocities diverged more readily with decreasing resolution. For future simulations, the resolution was therefore decreased to 150 rx.

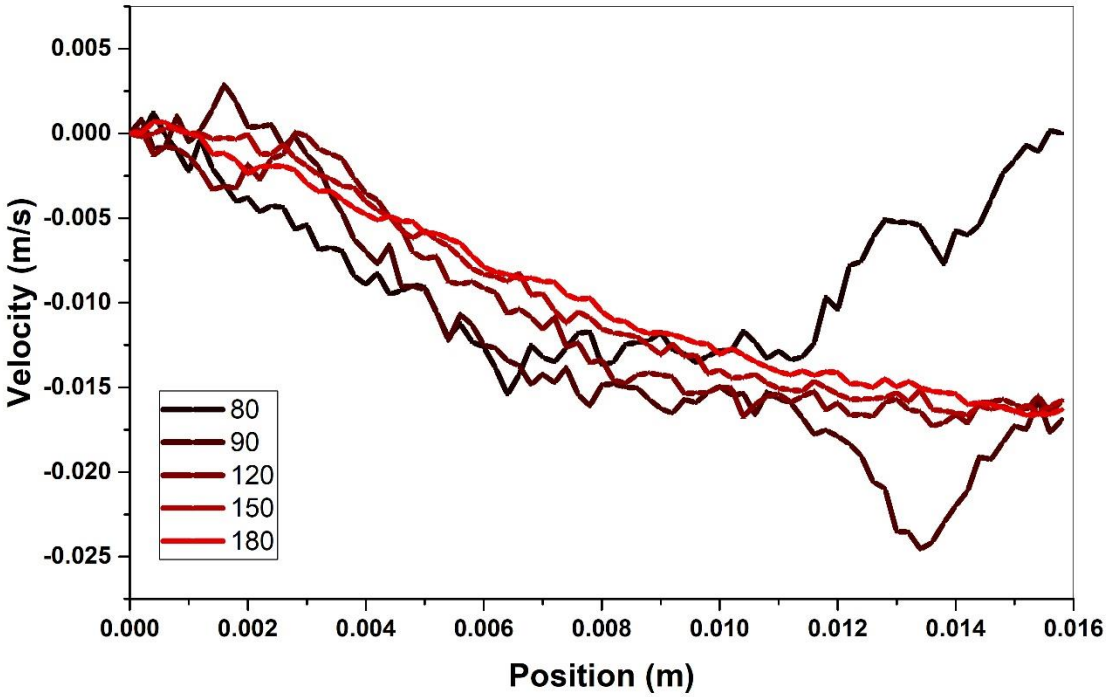

Figure 3.7: Comparison of the simulated liquid velocity along a line within the model deep square well at different resolution of 80, 90, 120, 150, and 180 rx.

Figure 3.8 shows a comparison of the simulated and the experimental fluid flow after the surface tension and resolution parameters were adjusted. Simulated surface inclination and deformation were found to be in agreement with the experimental fluid flow. The experimental fluid flow, however, appeared to show a higher degree of wall adhesion compared to the simulations. Although this difference is unlikely to affect mixing or power input to a significant degree, wall adhesion has previously been shown to affect mass transfer in shake flasks (Maier and Büchs, 2001). However, disposable materials, such as the micro-Matrix cassette, often have hydrophobic surface properties and therefore do not encourage the formation of a liquid film (Klöckner and Büchs, 2012). Consequently, the implementation of a wall adhesion model to match the observations from the Perspex mock-up well was not considered as part of the CFD simulations.

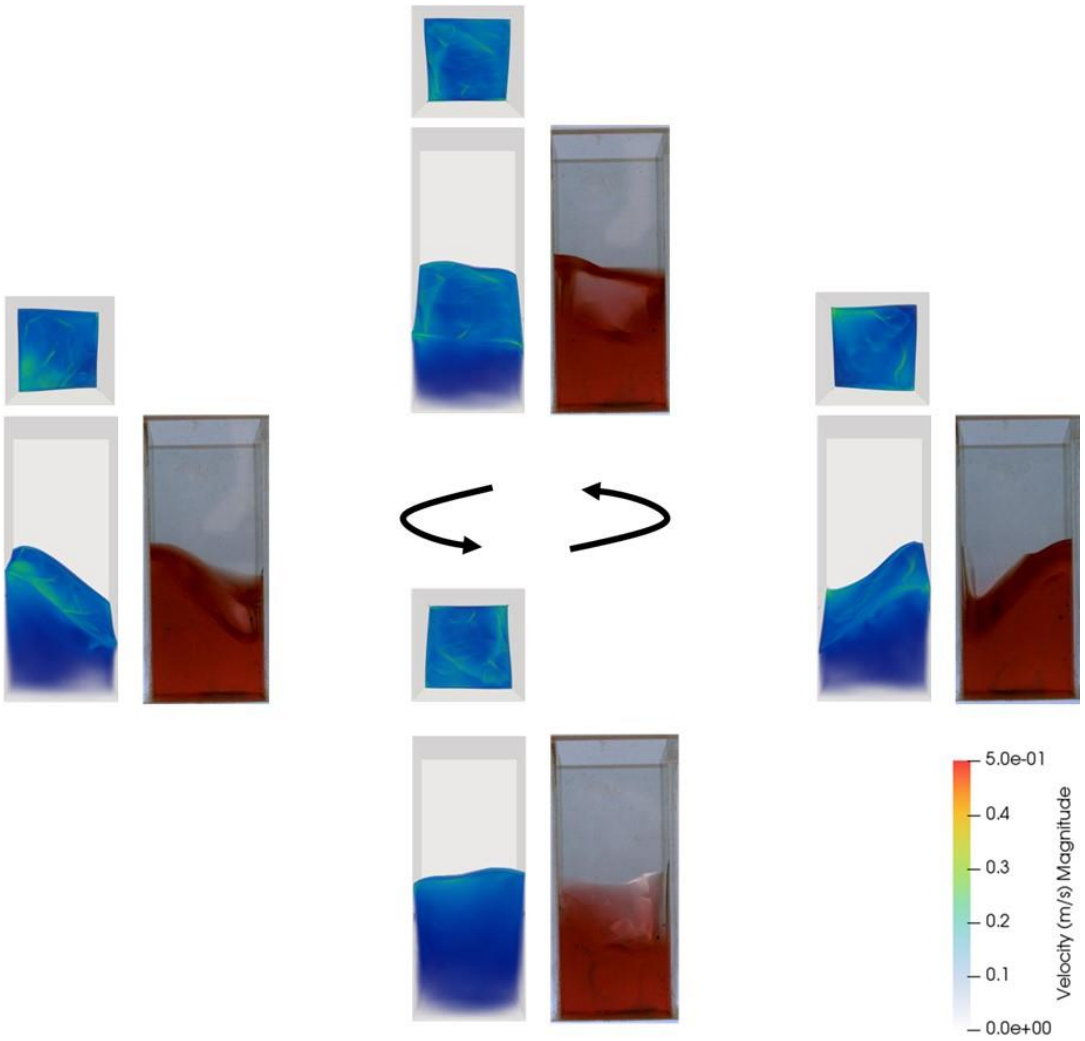

Figure 3.8: Comparison of simulated (blue) and experimental (red) fluid flow in a micro-Matrix well for a shaking speed of 250 rpm and a working volume of 4 mL. The colour map in the simulated wells represents the velocity magnitude (m s^{1}) of the fluid.

3.2.3.2. Simulating power input (P/V) and mass transfer (k_La)

Based on the model setup and validation outlined in section 3.2.3.1, the simulations were used to derive the engineering parameters P/V and k_La for the micro-Matrix cassette. As outlined by Wutz *et al.* (2018), the global strain rate together with the surface area of the liquid can be derived from CFD simulations and used to calculate the k_La using equation 3.2:

$$k_L a = \frac{A}{V_L}\sqrt{D_{O2}}(C_1 S^B + C_2) \qquad (3.2)$$

Where A is the surface area of the liquid (m^2), V_L is the liquid volume (mL), D_{O2} is the diffusion coefficient of oxygen in water (1.97 x 10^{-9} m^2 s^{-1}), S is the strain rate (s^{-1}), and C_1, C_2, and B are constants established through calibration of the formula with experimental values. The calibration was achieved using the Levenberg Marquardt multiple regression algorithm with the corresponding k_La values previously determined in section Chapter 2:

$$k_L a = \frac{A}{V_L}\sqrt{D_{O2}}\left(5.3 \cdot 10^5 \cdot S^{-1.5 \cdot 10^5} + 6.2 \cdot 10^9\right) \quad (3.3)$$

The global P/V was derived directly from the software output. Values of the k_La and the P/V were fitted using equation 3.3:

$$\Phi = a + b \cdot V_L^c \cdot n^d \quad (3.3)$$

Where Φ is the fitted engineering parameter, V_L is the working volume (mL), n is the rotational speed and a, b, c, and d are fitting constants. Using the Levenberg Marquardt algorithm, the constants of equation 3.3 were fitted (Table 3.1). The fitted functions together with the data points derived from simulations and experiments are illustrated in Figure 3.9.

Table 3.1: Parameters derived from CFD simulations for the fit of P/V and k_La using equation 3.3.

Φ	**a**	**b**	**c**	**d**
P/V	0	8.56 x 10^{-7}	-0.60	3.45
k_La	0	5.01 x 10^{-4}	-0.71	2.31

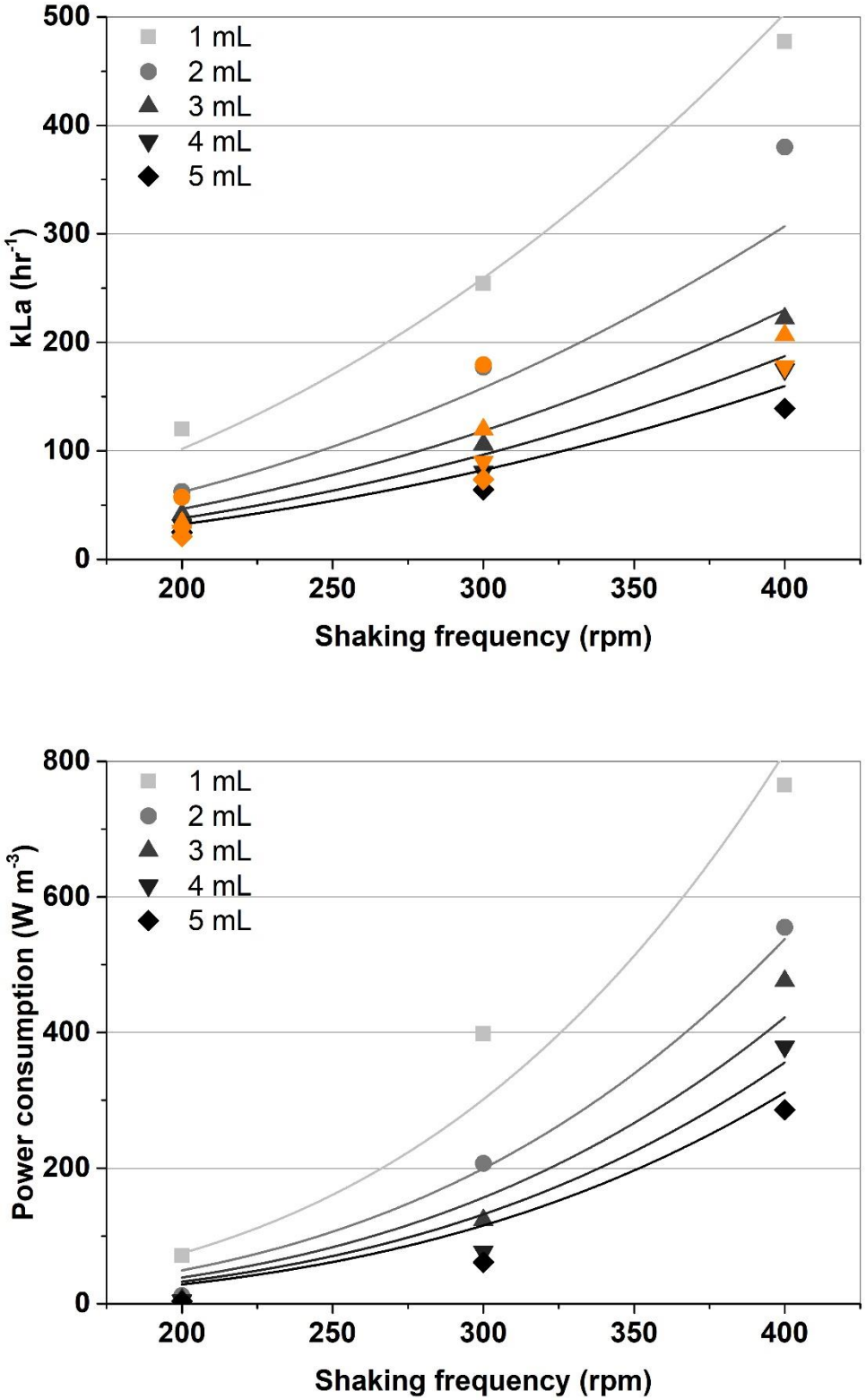

Figure 3.9: Volumetric mass transfer coefficient (k_La) (top) and volumetric power input (P/V) (bottom) in the micro-Matrix determined using CFD simulations. Lines represent curve fits based on equation 3.3. Grey symbols represent data points obtained through CFD simulations. Orange symbols represent experimental data.

As illustrated in Figure 3.9, the simulated k_La values agree well with the experimental data. Conditions that were not considered experimentally due to limitations of the experimental setup could be investigated using CFD. Particularly, the lower working volumes of 1 and 2 mL in combination with shaking speeds above 300 rpm achieved high k_La values, which may therefore present a suitable window of operating conditions for microbial fermentations (Islam *et al.*, 2008).

Although values for the power input have been determined for other shaken systems experimentally in the past (Büchs *et al.*, 2000; Büchs, Lotter and Milbradt, 2001; Dürauer *et al.*, 2016), this parameter has frequently been derived successfully from CFD simulations (Barrett *et al.*, 2010; Markert and Joeris, 2017; Wutz *et al.*, 2018). Here, the P/V ranged from 4 W m^{-3} (200 rpm, 5 mL) to 765 W m^{-3} (400 rpm, 1 mL) W m^{-3}, which is comparable to P/V values reported for the ambr15 (Nienow *et al.*, 2013), microtitre plates (Zhang *et al.*, 2008; Barrett *et al.*, 2010; Dürauer *et al.*, 2016), and STR systems used for animal cell culture (Lavery and Nienow, 1987). The fitted function (Table 3.1) describes the obtained values reasonably well, particularly for the lower working volumes.

3.3. Initial cell cultivation

3.3.1. Batch cultivation and evaporation

To assess whether the micro-Matrix is a suitable device for the cultivation of GS-CHO cells, an initial batch was performed and compared to published data that were obtained using the same cell line. The experiment was also conducted to uncover potential issues that arise when using the system. A list of the cell culture conditions is given in Table 3.2.

Table 3.2: Experimental conditions for an initial batch experiment in the micro-Matrix.

	micro-Matrix
Mode of operation	Batch
Working volume	3.5 mL
Shaking speed	220 rpm (25 mm orbit)
Temperature	37°C
DO	30% (air ↑, N_2 ↓)
pH	7.2 (CO_2 ↓)

As shown in Figure 3.10 A and B, the cells grew and maintained a high viability for the first 6 days of the cultivation. Thereafter, the viability slowly decreased and the VCC remained stagnant before reaching a maximum VCC of 4 x 10^6 cells mL^{-1} after 10 days of cultivation. As the samples were taken sacrificially, this slight increase of the VCC could have been caused by well-to-well variability. The cultivation finished when the viability dropped to approximately 53% on day 13. The titre (Figure 3.10 C) initially showed a steady increase but fluctuated considerably on day 11. Again, this was likely caused by well-to-well variability and may not reflect the typical production kinetics of GS-CHO cells. A final titre of 0.22 g L^{-1} was reached on day 13. Overall, the growth and production kinetics are comparable to GS-CHO cells grown in 24 SWR microtitre plates as reported by Silk *et al.* (2010). The low titre is likely due to the early decrease of cell viability as no feed medium was added throughout the experiment.

Conversely, the amount of evaporated liquid (Figure 3.10 D) quickly exceeded any acceptable limits and reached a final value of 32.9 ± 3.4% on day 13. Furthermore, evaporation was subject to a high degree of variability as indicated by the large errors of the biological replicates. Such extreme liquid loss can have considerable ramifications for the stability and reproducibility of a cultivation process. A changing working volume not only alters process conditions such as mixing and mass transfer, it can also lead to elevated concentrations of waste metabolites and high osmotic pressures (Silk *et al.*, 2010; Bareither and Pollard, 2011; Lattermann and Büchs, 2016).

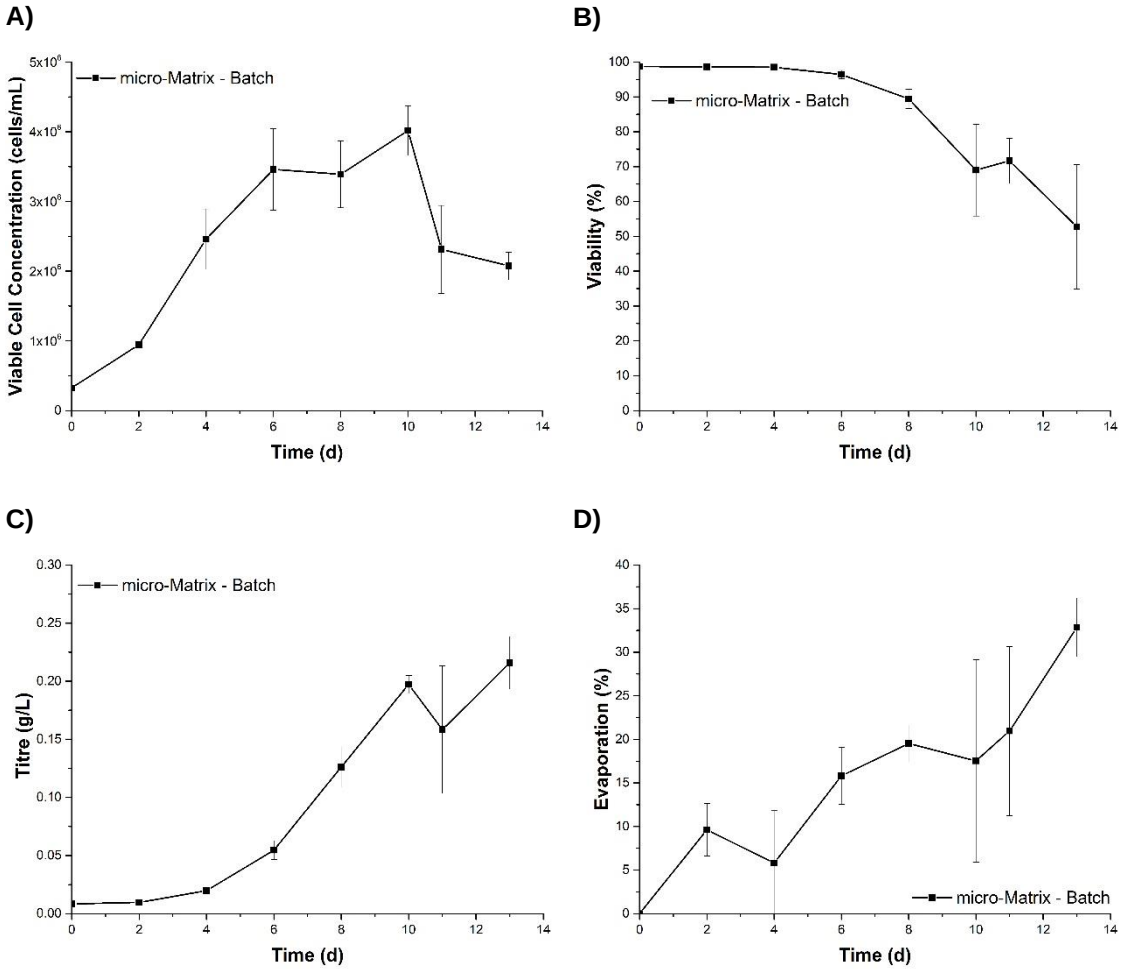

Figure 3.10: Growth kinetics (A), viability (B), production kinetics (C), and liquid loss through evaporation (D) during a batch cultivation of GS-CHO in the micro-Matrix at a shaking speed of 220 rpm and a working volume of 3.5 mL. Temperature was controlled at 37°C, pH at 7.2, and DO at 30%. Samples were taken sacrificially, and error bars represent one standard deviation about the mean of three sacrificed wells.

Minimising evaporation rates without negatively affecting gas exchange rates remains one of the main issues for microscale cultivations (Kumar, Wittmann and Heinzle, 2004). Though the simplest solution is the periodic corrective addition of distilled water to counteract the liquid loss, this requires the knowledge of the exact volume that has evaporated. Extracting and weighing the content of each individual well of a microtitre plate is time-consuming and introduces risks of contamination. Furthermore, most microtitre plates are either opaque or impervious to light and as a result, visual assessment of the fill level becomes infeasible. Measuring a concentrating

effect of one or more media components can be a viable alternative that is less invasive and easily conducted alongside the sample analysis. The samples of this initial batch experiment were therefore analysed for ions in the supernatant to evaluate whether their concentration can be used as a way to indirectly determine evaporation.

Figure 3.11 shows the percentage of evaporated liquid in relation to the concentration of the respective ions measured with the bioanalyser at various time points during the cultivation. The linearity of the correlation for sodium and potassium ions suggests that their concentration remains largely unaffected by the cellular activity. The linear regression for sodium ions is marginally better (R^2 = 0.95) than for potassium ions (R^2 = 0.92). For calcium ions the prediction is less accurate (R^2 = 0.45), which suggests that their concentration is either affected by the cells or too close to the lower boundary of the bioanalyser's detection limit (0.1 mmol L^{-1}). Because of their good correlation and favourable concentration range in the cultivation medium, which falls well within the range of the bioanalyser's range of detection (40 – 220 mmol L^{-1}, with a resolution of 0.1 mmol L^{-1}), the concentration of sodium ions was considered a suitable marker for evaporation.

Based on these findings, a correlation between the amount of evaporated liquid and the concentration of sodium ions in solution was established (equation 3.4).

$$V_{Evap} = V_0 - \frac{V_0 \cdot [Na]_0}{[Na]_t} \qquad (3.4)$$

Where V_{Evap} is the volume of evaporated liquid, V_0 is the initial liquid volume, $[Na]_0$ is the initial concentration of sodium ions, and $[Na]_t$ is the concentration of sodium at time t.

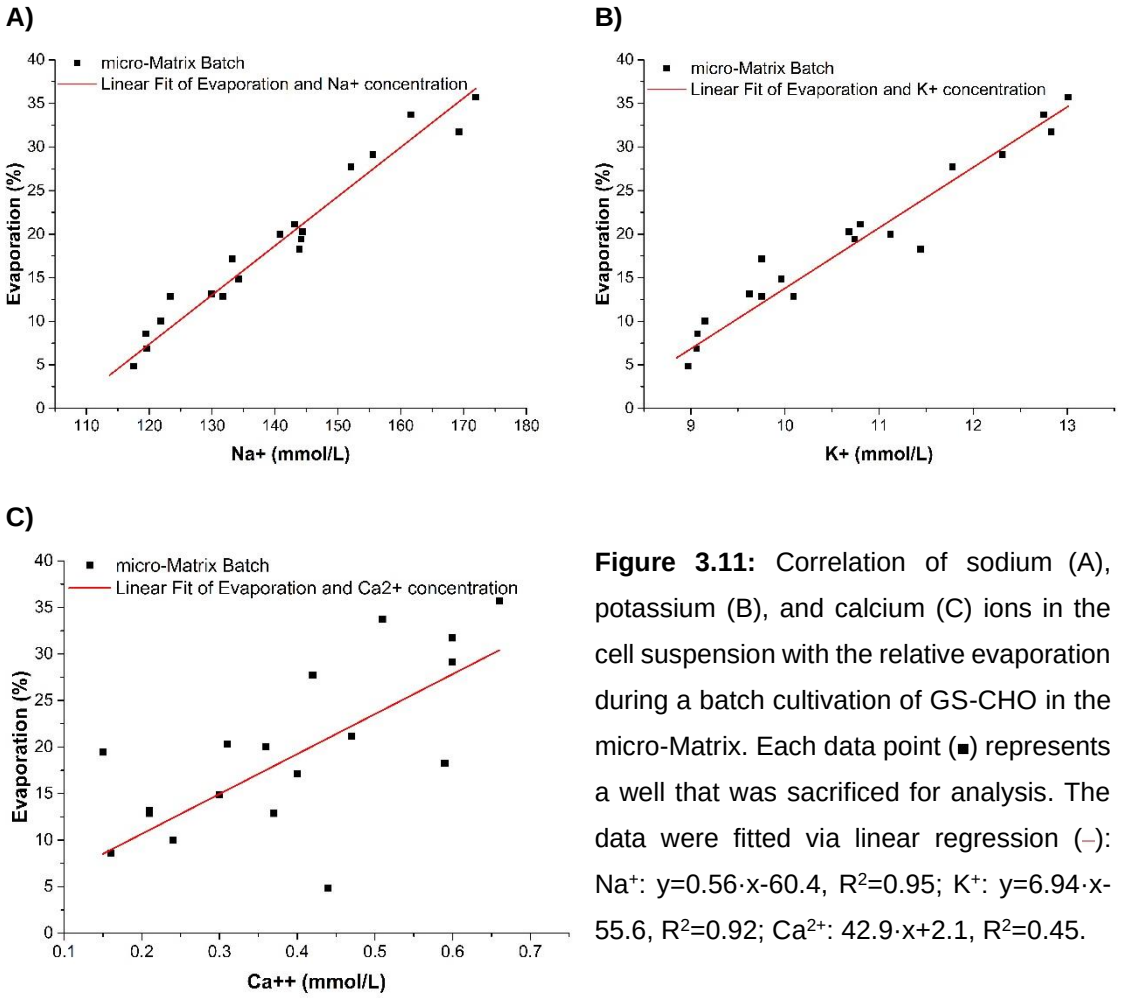

Figure 3.11: Correlation of sodium (A), potassium (B), and calcium (C) ions in the cell suspension with the relative evaporation during a batch cultivation of GS-CHO in the micro-Matrix. Each data point (■) represents a well that was sacrificed for analysis. The data were fitted via linear regression (–): Na^+: y=0.56·x-60.4, R^2=0.95; K^+: y=6.94·x-55.6, R^2=0.92; Ca^{2+}: 42.9·x+2.1, R^2=0.45.

In case of a fed-batch cultivation or the addition of other fluids like acid or base, the desired concentration of sodium in the liquid has to be corrected based on the concentration of sodium in the feed medium and the volume of feed medium that is added to the cell suspension. For a system of the three components basal medium, buffer, and feed medium, the correlation above can be modified according to equation 3.5.

$$V_{Evap} = V_{total} - \frac{[Na]_{medium} \cdot V_{medium} + [Na]_{buffer} \cdot V_{buffer} + [Na]_{feed} \cdot V_{feed}}{[Na]_{measured}} \qquad (3.5)$$

Where V_{total} is the theoretical volume inside the cultivation vessel at time t. The practicability of this method to counteract evaporation in small-scale cultivation systems was investigated in the following section.

3.3.2. Preventing and counteracting evaporation in a fed-batch cultivation

In this experiment, the method described in section 3.3.1 to counteract evaporation in small-scale bioreactors was tested as part of a fed-batch cultivation. By nature, feeding prolongs the duration of the cultivation run and due to the higher cell densities, higher gas flow rates are required to control the concentration of dissolved oxygen at the desired setpoint. It has been shown in the previous experiment that towards later stages of the cultivation, a substantial amount of liquid is lost through evaporation and the exact amount is highly variable for each well. For this reason, the proposed correlation with sodium ions was used to determine the amount of evaporated liquid. Additionally, it was tested whether the use of pure oxygen (O_2) instead of compressed air (cAir) for the control of the DO level could further decrease evaporation.

The experiment also served as a first step towards a benchmark feeding regime that is based on recommendations by the manufacturer of the feed medium (Invitrogen, 2007). The addition of feed medium is a common way of prolonging and intensifying a bioprocess. With high concentrations of glucose, vitamins, and amino acids, feed medium is specifically designed to replenish certain components and support the cells from the exponential growth phase onwards. The simplest mode of feeding is the periodic addition of bolus shots with a set volume of feed medium. As this form of feeding has been successfully implemented in other small-scale systems (Silk *et al.*, 2010), the initial feeding strategy for cultivations in the micro-Matrix was also based on bolus additions. Because of the increasing working volume, it was possible to move away from sacrificial sampling and instead consider each well individually and assess well-to-well variability over the course of the cultivation.

Here, feeding commenced after 5 days of cultivation with an addition every two days and was set to 10% of the initial working volume. On day 7 of the cultivation, the sodium concentration was measured for each individual well, which was used to determine the amount of distilled water

needed to compensate for the evaporated liquid. All experimental conditions are summarised in Table 3.3.

Table 3.3: Experimental conditions for an initial fed-batch experiment in the micro-Matrix.

	micro-Matrix
Mode of operation	Fed-batch
Working volume	3.5 mL
Shaking speed	280 rpm (25 mm orbit)
Temperature	37°C
DO	Columns 1-3: 30% (air ↑, N_2 ↓)
	Columns 4-6: 30% (O_2 ↑, N_2 ↓)
pH	7.2 (CO_2 ↓, 250 mM bicarbonate buffer↑)

Figure 3.12 shows the growth and production kinetics of the fed-batch experiment. In the beginning of the cultivation, the viable cell concentration increased in a similar fashion for all wells. On day 5, the well-to-well variability increased considerably for the wells that were DO controlled with cAir. For the wells that were DO controlled using O_2, the variability increased on day 7, but to a lesser extent. In both cases, the average maximum VCC was reached on day 11 and was $9.4 \times 10^6 \pm 1.6 \times 10^6$ cells mL^{-1} for cells cultured with cAir and $1.0 \times 10^7 \pm 1.2 \times 10^6$ cells mL^{-1} for cells cultured with O_2. The coefficient of variance (CV) of the VCC averaged over the course of the cultivation was 17.1% and 12.1% for cells cultured with cAir and O_2, respectively. The viability progressed similarly for all wells and was maintained above 80% for the duration of the experiment.

The titre remained stagnant in all wells for the first 5 days of the cultivation and then increased to values ranging from 0.61 g L^{-1} (well D3) to 0.81 g L^{-1} (B6) on day 15. The average final titre was 0.75 ± 0.06 g L^{-1} for cells cultured with cAir and 0.76 ± 0.05 g L^{-1} for cells cultured with O_2. In contrast to the VCC, the titre progressed with evidently less variability in between the micro-Matrix wells. The CV of the titre averaged over the course of the cultivation was 11.6% and 6.7% for cells cultured with cAir and O_2, respectively.

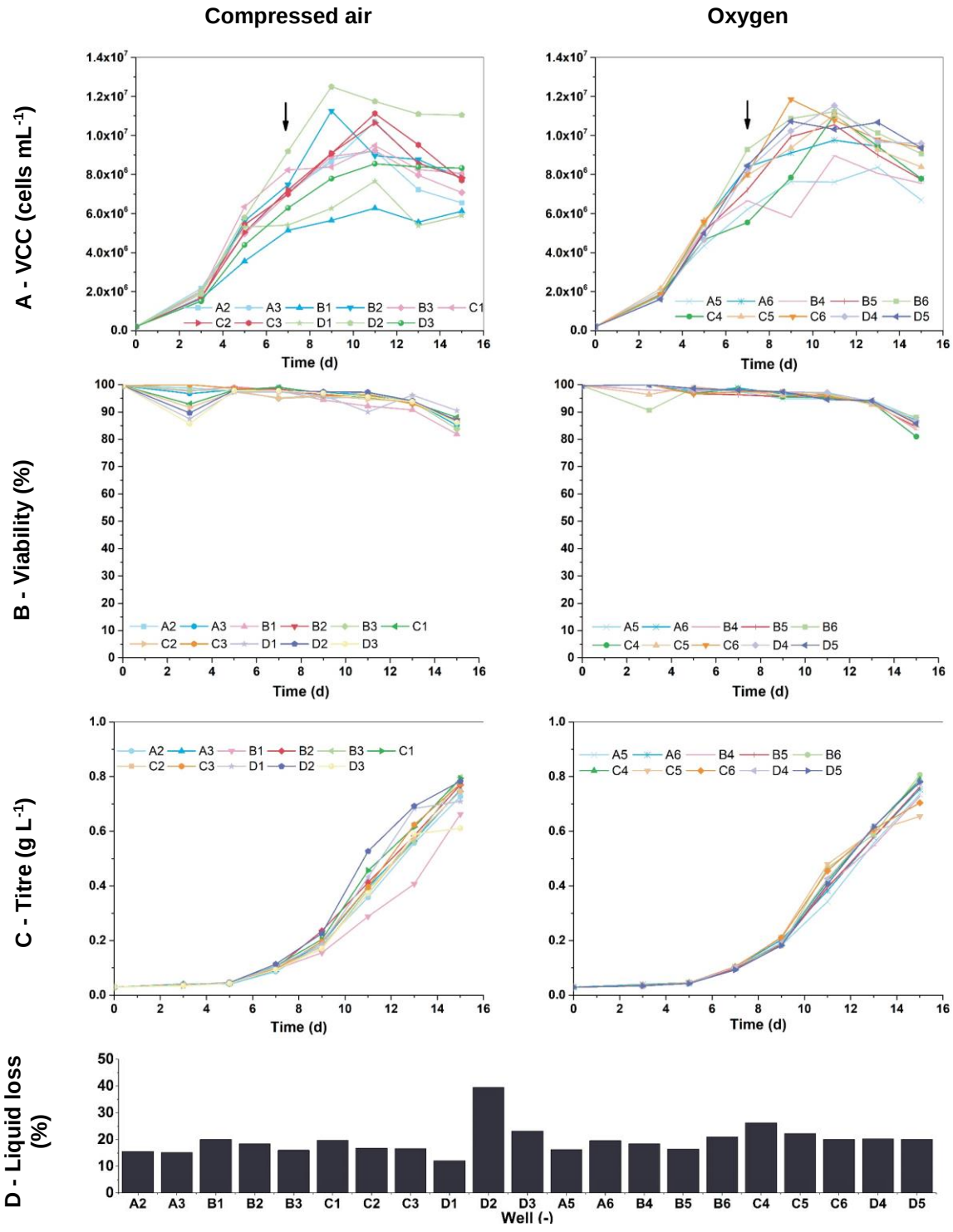

Figure 3.12: Growth kinetics, production kinetics and liquid loss on day 15 of GS-CHO cells grown under fed-batch conditions in the micro-Matrix at a shaking speed of 280 rpm and a working volume of 3.5 mL. Temperature was controlled at 37°C, pH at 7.2, and DO at 30%. Up-control of the DO was achieved either using compressed air or pure oxygen. Cultures were fed with 5 bolus additions of Feed B on days 5, 7, 9, 11, and 13. Each line represents the results obtained from an individual well. Arrows indicate the time points of dH_2O additions to counteract evaporation based on the sodium level measured.

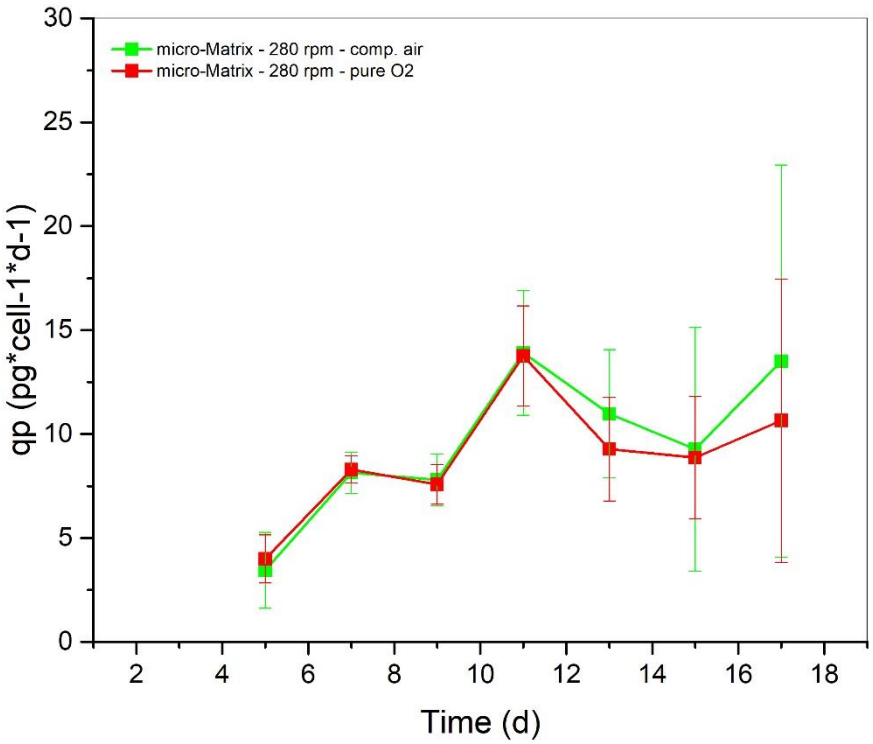

Figure 3.13: Specific productivity of GS-CHO cells grown under fed-batch conditions in the micro-Matrix at a shaking speed of 280 rpm and a working volume of 3.5 mL. Temperature was controlled at 37°C, pH at 7.2, and DO at 30%.

The lack of variability in the titre suggests that the specific productivity is higher for those wells that show lower cell counts, which could indicate differing metabolic fluxes within the cells. Cells that predominately channel their resources towards growth will grow to a higher density, though each individual cell secretes less product when compared to a metabolic state where most resources are channelled towards product formation (Kumar, Gammell and Clynes, 2007). A difference between the specific productivity for both control strategies, however, could not be observed (Figure 3.13).

Figure 3.12 D shows the liquid loss due to evaporation after 15 days of cultivation based on the liquid volume that remained in each well. Liquid loss was periodically counteracted through additions of dH_2O following the method established in section 3.3.1. Although evaporation was reduced compared to the initial batch experiment, an average liquid loss of 20% at the end of the run. A concentration of the cultivation broth to that extent can give rise to variability and may prove

problematic with regards to scalability. The spread around the mean value, however, is relatively narrow (cAir: 19.3 ± 7.3% and O_2: 20.0 ± 2.9%). As demonstrated in Figure 3.14, an effect of the evaporation on the final product yield could not be observed. To further reduce the liquid loss and its variability, future experiments will include more frequent compensation for evaporation of each individual well. Furthermore, these results reveal that contrary to the initial assumption, the use of pure oxygen does not significantly decrease evaporation (p = 0.77, t-Test).

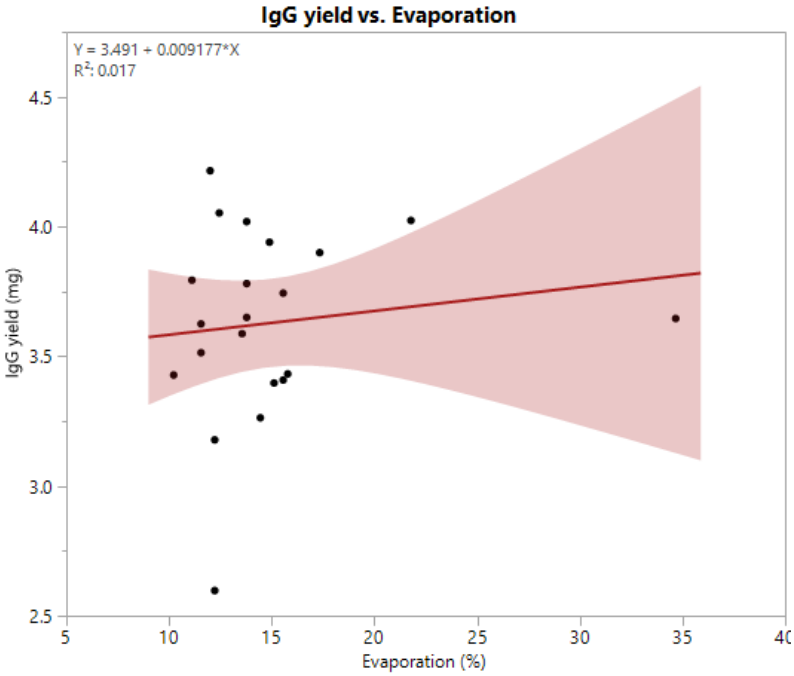

Figure 3.14: Final IgG yield over relative evaporation at harvest.

Overall, by introducing a bolus feeding strategy, the VCC could be increased and maintained for a longer duration compared to the batch cultivation (section 3.3.1). The additional nutrients and increased run time also had a positive effect on the final titre, which increased by roughly 5-fold. The maximum VCC achieved in the micro-Matrix even outperformed fed-batch cell growth reported in 24 SRW plates using the same cell line (Silk *et al.*, 2010). The improved growth performance could be a result of the active pH control in the micro-Matrix. Silk *et al.* (2010) reported the pH to drop to 6.7 during cultivations in the 24 SRW plates, whereas the pH was continuously controlled at 7.2 in the micro-Matrix. The influence of the pH on growth kinetics and

the metabolism of CHO cells has been well-documented in the literature (Yoon *et al.*, 2005; Trummer *et al.*, 2006; Toussaint, Henry and Durocher, 2016).

By applying the previously described method to compensate for evaporated liquid, the liquid loss was to some extent diminished, although a more frequent use should be considered to further reduce the impact of evaporation. Interestingly, although the use of O_2 for the control of the DO did not significantly affect evaporation, the well-to-well variability was reduced to a considerable extent. A possible cause of the lower variability when pure oxygen is used for the upregulation of DO could be the lower volume of gas needed to achieve the same concentration of dissolved oxygen. It is anticipated that the gas pressure across the gas delivery module is not homogenous, which leads to differing gas volumes delivered to the well. If the total amount of gas needed for the control of dissolved oxygen concentrations is higher, as it is in the case of compressed air, the error caused by differing gas pressures propagates more readily.

3.2.3. Improvement of well-to-well reproducibility during fed-batch cultivation

The final experiment of this chapter sought to combine all the outcomes of the preceding cell cultivations in order to create a protocol that generates reliable results in the micro-Matrix. The previously described and tested method to counteract evaporation (sections 3.3.1 and 3.3.2) was repeated every second day following day 5 and O_2 was used for DO control instead of cAir. To elucidate the effects that evaporation has on the variability of the process, this protocol was compared to a cultivation in which evaporation was not counteracted. A full list of the conditions is given in Table 3.4.

Table 3.4: Experimental conditions for the improved fed-batch protocol in the micro-Matrix.

	micro-Matrix
Mode of operation	Fed-batch
Working volume	3.5 mL
Shaking speed	280 rpm (25 mm orbit)
Temperature	37°C
DO	30% (O_2 ↑, N_2 ↓)
pH	7.2 (CO_2 ↓, 250 mM bicarbonate buffer↑)

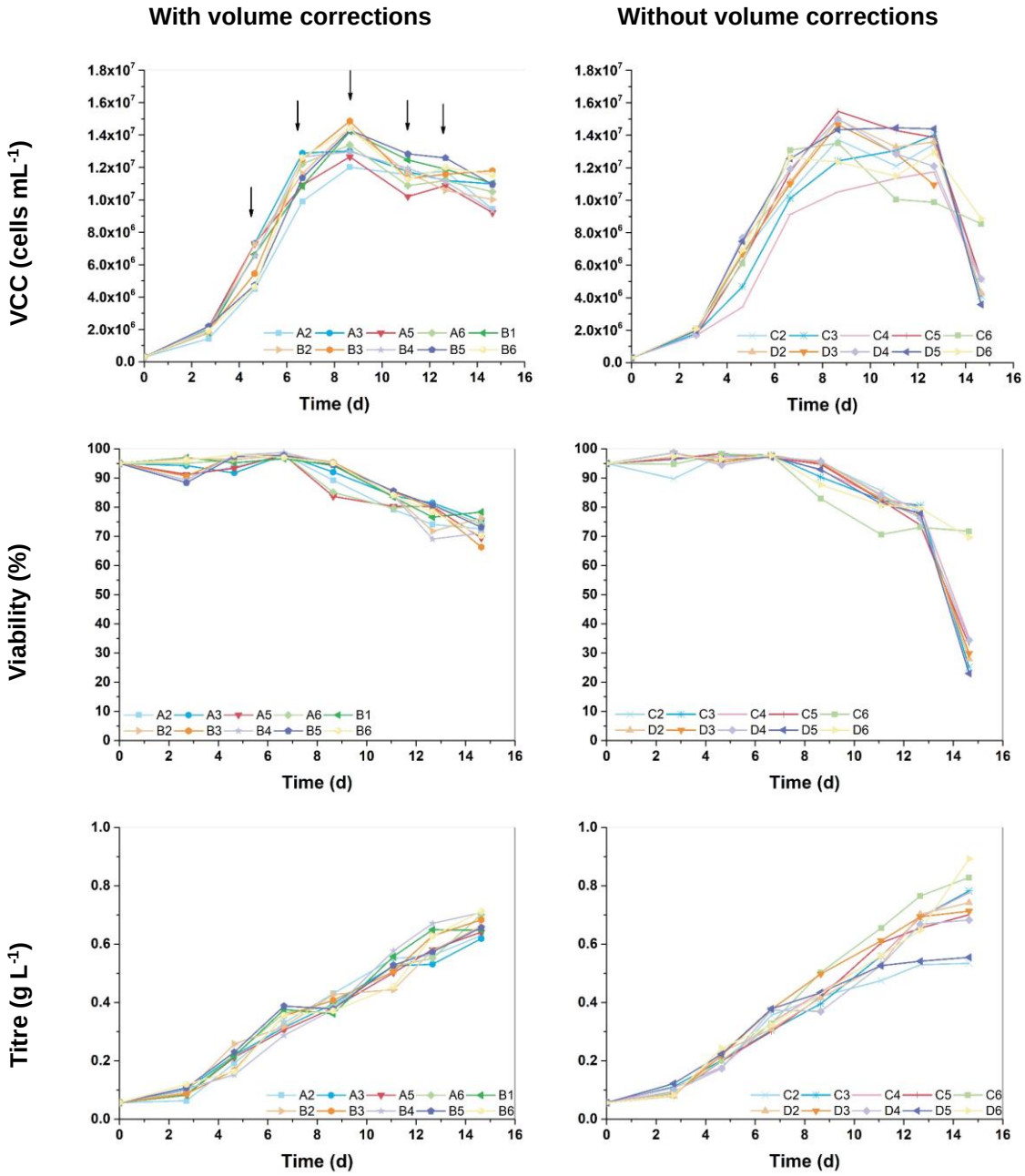

Figure 3.15: Growth and production kinetics of GS-CHO cells grown under fed-batch conditions in the micro-Matrix at a shaking speed of 280 rpm and a working volume of 3.5 mL. Temperature was controlled at 37°C, pH at 7.2, and DO at 30%. Up-control of the DO was achieved either using compressed air or pure oxygen. Cultures were fed with 5 bolus additions of Feed B on days 5, 7, 9, 11, and 13. Each line represents the results obtained from an individual well. Arrows indicate the time points of dH_2O additions to counteract evaporation based on the sodium level measured.

Setpoints of DO, pH, and temperature were well-maintained throughout the cultivation (Appendix II. Figure A 1 – 3). Figure 3.15 summarises the growth and production kinetics of two fed-batch experiments performed in the micro-Matrix. In one condition, the working volume was corrected for liquid loss five times throughout the cultivation, whereas in the other no such corrections were performed. Until day 7, the VCC progressed similarly for both conditions. Thereafter, the variability started to increase notably for the wells in which no volume corrections were performed. The CV of the viable cell density averaged over the course of the cultivation was 9.5% and 15.5% with and without volume corrections, respectively. The average peak VCC was reached on day 9 in both cases and was $1.4 \times 10^7 \pm 9.4 \times 10^5$ cells mL^{-1} and $1.4 \times 10^7 \pm 1.7 \times 10^6$ cells mL^{-1} with and without volume corrections, respectively. It is important to note, that the VCC and the viability experienced a sharp decrease on day 15 when no volume corrections were performed, whereas the viability could be maintained above 70% for most of the wells when the liquid loss was counteracted.

The titre showed a similar spread without volume corrections, which was particularly pronounced towards the final stages of the cultivation. The average final titre on day 15 was 0.67 ± 0.03 g L^{-1} and 0.72 ± 0.11 g L^{-1} for cells cultured with and without volume corrections, respectively. The slightly higher final titre in the latter condition is likely caused by concentrating effects due to evaporation.

Figure 3.16 shows the relative liquid loss and osmolality for each well on day 15. Through frequent repetition of the volume corrections, the evaporation could be decreased considerably from $36.7 \pm 6.7\%$ to $6.9 \pm 6.5\%$. As a result, the improved cultivation protocol was able to maintain volume losses within an acceptable range. In the case of well B1, evaporation was slightly overcompensated, leading to a negative liquid loss. The differences in evaporation also affected the osmolality. With volume corrections, the average final osmolality was 273.8 ± 13.1 mOsmol, whereas without liquid additions this value was considerably higher with 430.4 ± 31.2 mOsmol.

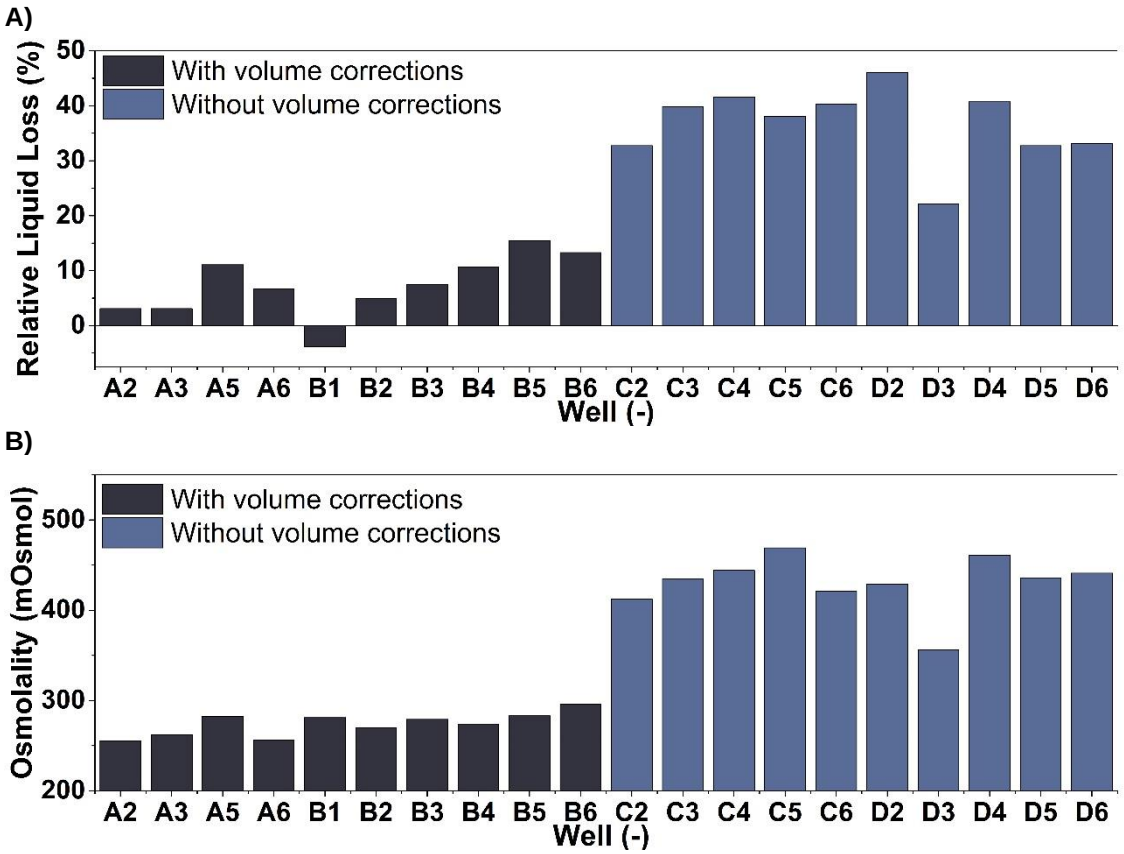

Figure 3.16: Relative liquid loss (A) and osmolality (B) after 15 days of two fed-batch cultivations with GS-CHO in the micro-Matrix. The liquid volume was corrected five times throughout the cultivation (black) or no volume corrections were performed (grey). The shaking speed for both runs was set to 280 rpm, the working volume was 3.5 mL, temperature was controlled at 37°C, DO at 30%, and pH at 7.2.

The periodic additions of distilled water to counteract evaporation successfully lowered the liquid loss to an acceptable level. This also had an impact on the variability of the VCC and titre results. Without volume corrections, the average CV of the VCC was 15.5% and therefore above variabilities generally reported as acceptable in the literature (10 – 15%) (Chaturvedi *et al.*, 2014). Thus, counteracting evaporation in conjunction with the use of O_2 for DO control appears critical in order to generate reproducible results in the micro-Matrix.

Furthermore, by performing volume corrections the duration of the process was increased. The sudden drop of cellular viability in the condition without volume corrections could have been

caused by the high osmolality, as it has been previously reported that increased osmolalities can adversely affect cell growth (Takagi, Hayashi and Yoshida, 2000). However, increasing osmolalities are often documented in cell culture processes (Altamirano *et al.*, 2004; Spens and Häggström, 2007; Silk *et al.*, 2010) and are sometimes associated with increased specific productivities (El-Enshasy, 2007; Zhang, 2009; Kaisermayer *et al.*, 2016). Yet, this effect could not be observed for the experimental conditions tested here (Figure 3.17). Additionally, evaporation causes changes in the working volume, which also affect environmental conditions such as mixing and mass transfer. This is of particular importance considering scale translations, where the tight control of these engineering parameters is critical. It is evident that such fundamental fluctuations caused by evaporation need to be avoided to generate high quality screening data using the micro-Matrix.

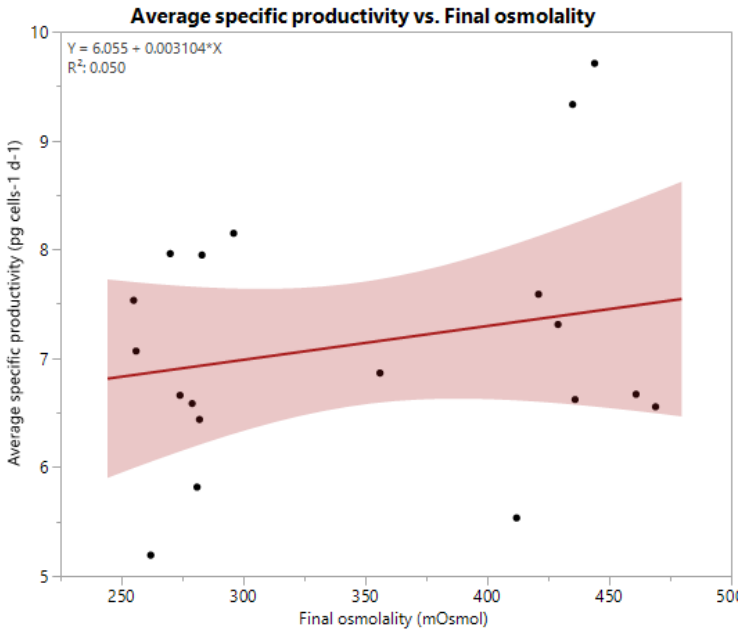

Figure 3.17: Average specific productivity over harvest osmolality.

The cultivation protocol outlined in this section successfully addressed the initial problems that were encountered regarding evaporation and well-to-well variability.

3.4. Conclusion

The cultivation environment inside the micro-Matrix was investigated using experimental and computational techniques. The DISMT method revealed micro-Matrix mixing times similar to conditions found in conventional STRs used for cell culture. The oxygen mass transfer on the other hand was generally substantially higher compared to reference STRs and was therefore ruled out as a suitable scaling criterion. The P/V, which is typically challenging to determine experimentally for shaken systems, was derived through CFD simulations and found to be comparable to other bioreactor systems.

In initial cell cultivations, the concentration of sodium ions in solution was shown to correlate with the volume of evaporated liquid, which enabled the calculation and replacement of the evaporated liquid throughout the experiment. This procedure successfully addressed two of the key challenges of small-scale cell culture: excessive evaporation and lack of well-to-well reproducibility.

The cell cultivation protocol together with the engineering characterisation form the backbone of the following chapters, which focus on establishing the micro-Matrix as a scale-down model for a benchtop scale STR and finally using the micro-Matrix as a tool for process optimisation.

Chapter 4. Scale-down from a 5 L STR to shaken small-scale cultivation systems

Content of this chapter is published in Arndt *et al.* (2021)

4.1. Introduction and aim

As a result of their high degree of parallelisation, quick turnover time, and low running costs compared to benchtop scale STRs, microbioreactors increasingly gain importance in today's bioprocessing landscape (Rao, Moreira and Brorson, 2009; Hemmerich *et al.*, 2018). They are quick in generating an in-depth understanding of the bioprocess, especially in conjunction with statistical tools such as DoE or MVDA (Goldrick *et al.*, 2019; Sandner *et al.*, 2019).

Yet, small-scale process optimisation is only valuable if the information is transferable to larger scale systems. Conventionally, screening and optimisation experiments were performed in shake flasks (Büchs, 2001). However, the lack of control impedes transferability of the results obtained in shake flasks to controlled cultivation systems. Recently developed microbioreactor systems are equipped with disposable sensor technology so that the key process parameters DO and pH can be actively controlled (Bareither and Pollard, 2011). Yet, matched pH and DO setpoints may not be sufficient to translate a cultivation process from one scale to another effectively. It is often necessary to create similar hydrodynamic and mass transfer conditions in both scales as well (Lattermann and Büchs, 2015). Therefore, one or more engineering parameters are maintained constant across the scales, which reiterates the importance of a thorough engineering characterisation of all cultivation systems involved.

The choice of engineering parameter, however, is not always obvious and depends on the cultivation systems as well as the requirements of the process. Whether the scale translation was successful, is evaluated based on process performance markers. These should include matched growth and product formation throughout the process and a comparable metabolic activity of the cells. Furthermore, in mAb manufacturing product quality attributes such as glycosylation, aggregation, and charge variants are pivotal for a safe and efficacious product and should therefore be maintained across scales as well.

This chapter sought to leverage the engineering characterisation of Chapter 3 with the aim to establish a scale-down strategy from a 5 L benchtop STR to the micro-Matrix. The scale-down strategy was tested in a batch and a fed-batch scenario and its success was evaluated through comparison of cell growth, product formation, product glycosylation, and metabolic footprint.

Chapter aims and objectives:

- Establish a engineering parameter to maintain constant across the bioreactor scales.
- Test the scale-down strategy with GS-CHO cells in a batch and fed-batch scenario.
- Evaluate the success of the scaling strategy by comparing growth, production, mAb glycoprofile, and metabolism.

4.2. Choice of scaling parameter

In microbial and cell culture process development, the P/V is often chosen to remain constant between scales, because it captures mixing as well as mass transfer behaviours (Raval, Kato and Büchs, 2007; Hsu *et al.*, 2012; Xu *et al.*, 2017; Velez-Suberbie *et al.*, 2018). Particularly for shaken systems like the micro-Matrix, measurements of the P/V are not straightforward and although several cultivation formats have been characterised already (Büchs *et al.*, 2000; Raval, Kato and Büchs, 2007; Klöckner *et al.*, 2012; Dürauer *et al.*, 2016), many have not yet received literary attention. To derive the P/V in shaken systems in a time-effective and economic manner, CFD analysis can be employed (Zhang *et al.*, 2008; Markert and Joeris, 2017; Wutz *et al.*, 2018).

Particularly for microbial processes, the k_La is often used as an engineering basis for scale translation. The oxygen requirements to sustain microbial growth are far higher compared to mammalian cells. Therefore, the k_La is more likely to be the limiting factor in a cultivation process. Using a matched k_La, microbial cultivation processes have been translated successfully from microtitre plate formats (Micheletti *et al.*, 2006; Islam *et al.*, 2008; Zhang *et al.*, 2008) and microbioreactors (Kensy, Engelbrecht and Büchs, 2009; Zoro, 2016) to benchtop scale STRs. However, in mammalian batch and fed-batch cultivation processes the maximum cell densities

are often too low for the k_La to become a limiting factor (Lavery and Nienow, 1987). A relatively low k_La of 1 h^{-1} is generally considered sufficient to support cell densities of 1 x 10^7 cells mL^{-1} (Fenge *et al.*, 1993). Therefore, the mass transfer is rarely considered as a scaling parameter for mammalian cultivation processes.

The third scaling criterion is a matched fluid phase mixing time, which ensures that the hydrodynamic conditions between scales are comparable. However, a matched mixing time is only practical at the lower range of bioreactor scales. As the reactor scale increases, mixing times tend to increase drastically (Tissot *et al.*, 2010) and therefore an alternative parameter should be considered for the scale-up from benchtop to pilot- and manufacturing scale (Xing *et al.*, 2009a). A matched mixing time has been used successfully for the scale translation of cell culture processes from a microbioreactor to shake flasks (Betts *et al.*, 2014) and from microtitre plates to an STR (Silk, 2014).

Table 4.1: Comparison of operating, hydrodynamic, and mass transfer conditions between benchtop, microbioreactor, and microtitre plate formats at a matched mixing time of ~6 s. Data for 5 L STR and micro-Matrix systems were determined experimentally, whereas parameters for the 24 SRW were derived from literature.

Parameter	**5 L STR**	**micro-Matrix**	**24 SRW**
Agitation	260 rpm	250 rpm (ø 25 mm)	220 rpm (ø 25 mm)
k_La (h^{-1})	~ 5-6	~ 50	> 20 (Silk, 2014)
Mixing time (s)	~ 6	~ 6	~ 4 (Silk, 2014)
pH	7.2	7.2	-
DO (% air sat.)	30	30	-
Temperature (°C)	37	37	37
CO_2 fraction (%)	min. 0 or 5	min. 0 or 5	5
Working volume (mL)	3500	4	0.8

Here, a matched mixing time was chosen as scaling criterion, because of its documented success in realising a transition from shaken to stirred small scale systems (Silk, 2014). Furthermore, the

mixing time was easily established for all employed systems and the scales were small enough for the mixing time to be a viable criterion (Xing *et al.*, 2009a; Tissot *et al.*, 2010). Later experiments revealed that the concentration of dissolved CO_2 also played a key role in the successful scale translation of GS-CHO processes.

Table 4.1 summarises the operating conditions that were used for the scale-down of a reference cell culture protocol previously established by Silk (2014) in a 5 L STR to the micro-Matrix and 24 SRW microtitre plates. In the micro-Matrix and the 5 L STR, the parameters pH, DO, and temperature were actively controlled, whereas the 24 SRW cultures were conducted under incubator conditions (5% CO_2, 37°C, and 70% humidity) without active control of pH and DO. The k_La values for the small-scale cultivation formats are up to an order of magnitude higher than in the 5 L STR. As mentioned in section 3.2.2, the mass transfer in the micro-Matrix is already very effective at lower shaking speeds so that a matched k_La of 6 h^{-1} would result in a shaking speed at which the cells would not be suspended. However, the k_La achieved in the 5 L STR is evidently sufficient to sustain the cell densities expected in batch and fed-batch cultivations (Fenge *et al.*, 1993). The large difference in mass transfer between scales is therefore not expected to affect scalability.

4.3. Batch scale-down at matched mixing time

Figure 4.1 shows the growth and viability profile for the scale translation of the GS-CHO batch process, which was performed based on the operating conditions outlined in Table 4.1. The growth progressed similarly in the micro-Matrix and the 5 L STR during the first five days of the cultivation and the maximum viable cell concentration (see Table 4.2) was roughly reached at the same time point and showed no significant differences ($p > 0.05$). However, while the VCC plateaued in the 5 L STR culture, in the micro-Matrix it started to decline following day 5. This difference was also reflected by the divergent progression of the viability in both formats. The 24 SRW culture showed comparatively rapid cellular expansion in the initial growth period, which thereafter slowed down and reached the maximum VCC on day 7. Though the maximum VCC was reached roughly two days later than in the STR, there were no significant differences in its

magnitude ($p > 0.05$). In the 24 SRW, the viability was maintained above 80% until day 9, which was followed by a sharp drop.

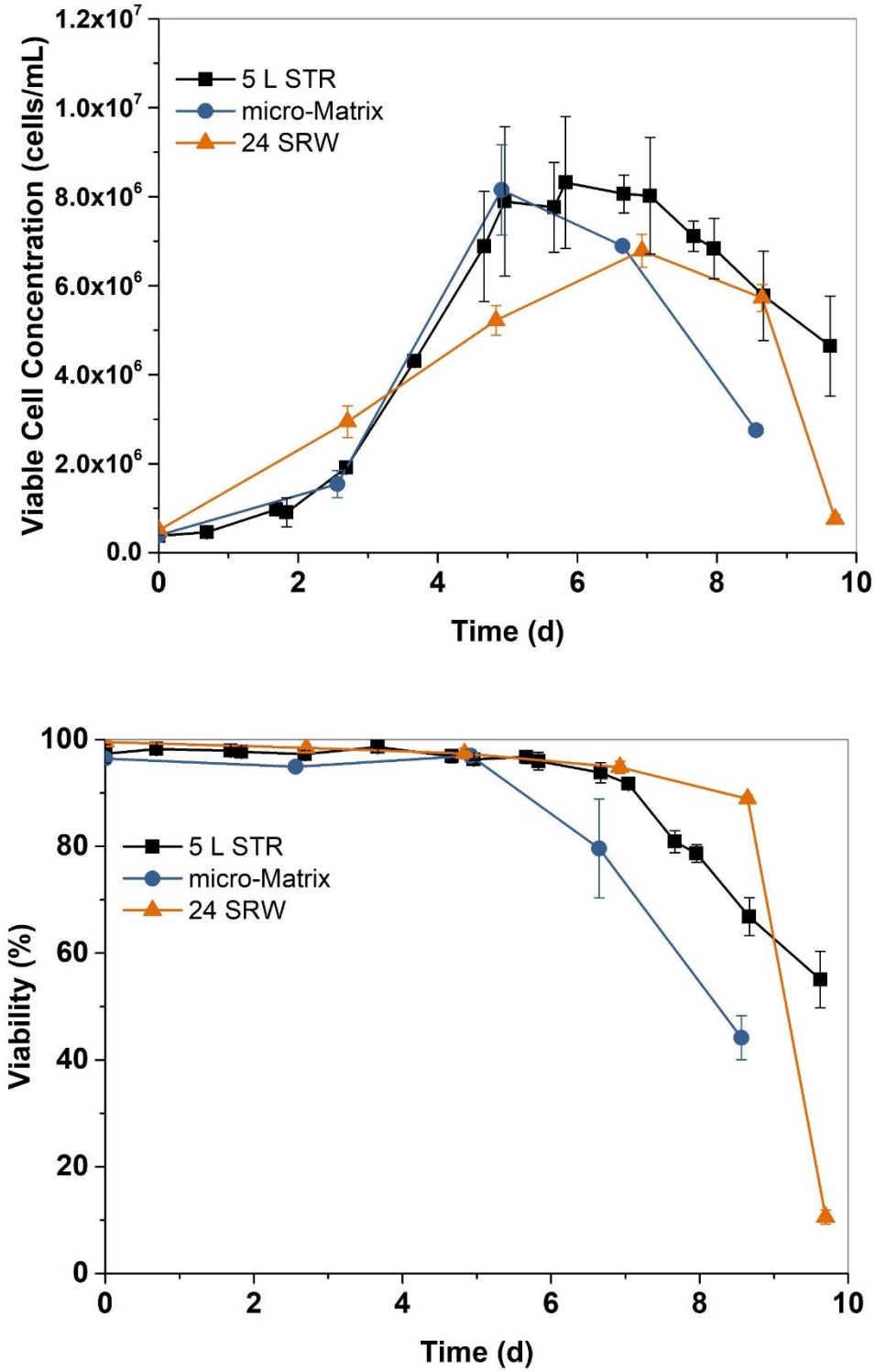

Figure 4.1: Growth kinetics of GS-CHO cells grown in a 5 L STR (■), the micro-Matrix (●), and 24 SRW microtitre plates (▲) at a matched mixing time of ~6 s. Data points represent the mean ± standard deviation (5 L STR: n = 2; micro-Matrix: n = 3; 24 SRW: n = 3).

The growth differences between the micro-Matrix and the 5 L STR could have been caused by the high sample volume of ~4% v/v relative to the working volume of the micro-Matrix. The steadily decreasing working volume within the micro-Matrix wells inevitably altered the environmental conditions related to mixing and mass transfer, which in turn is likely to have taken effect on the growth kinetics (Lattermann and Büchs, 2016). For example, the decreasing working volume could have led to an increase of the shear forces in the deep square well plate, which in turn caused the early onset of cell death.

Although high relative to the working volume of the micro-Matrix, the sample volume of 140 µL per well was limiting in terms of analytics. Dilutions had to be performed for all analyses, which likely resulted in titre fluctuations in the initial phases of the experiment. Furthermore, the low working volume did not permit the measurements of the Na^+ concentration to derive and correct for the liquid volume lost to evaporation. Therefore, evaporation had to be estimated and counteracted based on the average evaporation rates of previous cultivations.

Nonetheless, the relative liquid loss at the end of the cultivation was found to be 18.8 ± 5.0% in the micro-Matrix, which was too high to dismiss any adverse effects caused by evaporation (Silk *et al.*, 2010). As the average evaporation upon sampling was around 9.4 ± 5.5% for the 24 SRW, liquid loss could account for some of the differences observed compared to the 5 L STR.

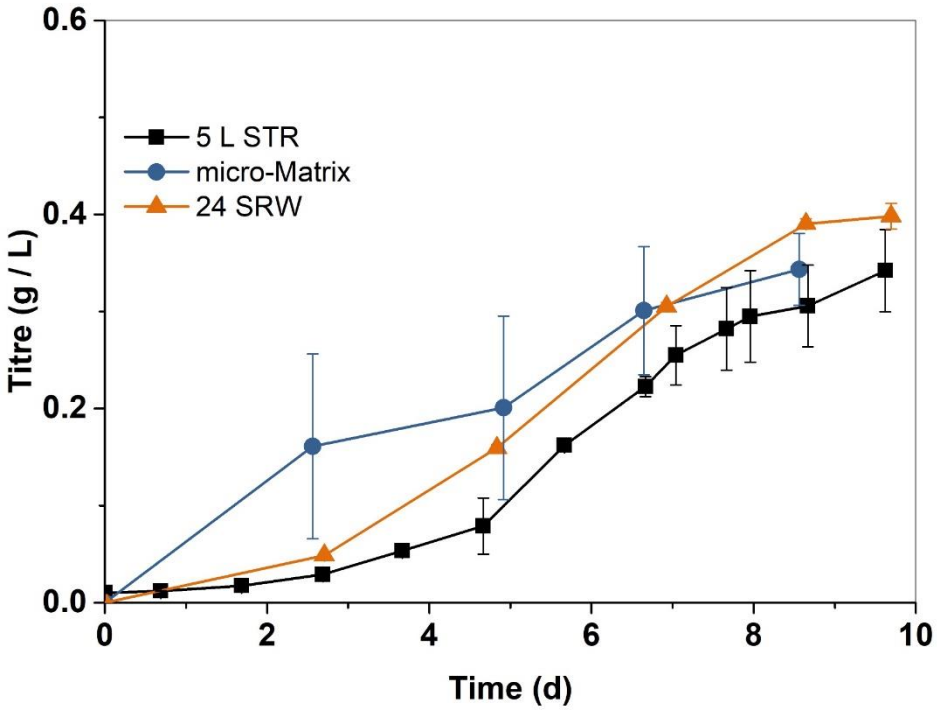

Figure 4.2: Production kinetics of GS-CHO cells grown in a 5 L STR (■), the micro-Matrix (●), and 24 SRW microtitre plates (▲) at a matched mixing time of ~6 s. Data points represent the mean ± standard deviation (5 L STR: n = 2; micro-Matrix: n = 3; 24 SRW: n = 3).

Following an initial lag period, the titre (Figure 4.2) increased steadily in the 5 L STR and reached its maximum value (see Table 4.2) on the final day of the cultivation. The cultivation in the micro-Matrix appeared to show a higher productivity in the beginning of the cultivation only to reach a similar final titre as the STR with no significant difference ($p > 0.05$). The progression of the titre in the 24 SRW followed the expected trend and started to plateau around day 9. The final titre in the 24 SRW was slightly, but not significantly ($p > 0.05$), above the final titre found in the STR. For both, the micro-Matrix and the 24 SRW, the elevated titre potentially reflects a concentrating effect caused by evaporation.

For all three cultivation formats, the concentration of glucose (Figure 4.3 A) steadily decreased in the beginning of the cultivation. In the micro-Matrix, glucose depletion was reached on day 5, in the 5 L STR on day 6, and in the 24 SRW on day 7. In the 24 SRW and the STR, the concentration of glucose increased slightly towards the end of the cultivation. This could have been caused by

concentrating effects, but also by measurement inaccuracies of the bioanalyser, as the raw values were close to the lower detection limit of the device.

The concentration of lactate (Figure 4.3 B) showed considerable differences between the systems. In the STR, lactate was produced until day 5 and reached a maximum concentration of 3.43 ± 0.16 g L^{-1}. Afterwards, lactate was partially consumed by the cells. A similar trend, but on a lower level was observed for the micro-Matrix, where a maximum lactate concentration of 2.57 ± 0.11 g L^{-1} (day 5) was reached, before the cells started to partially consume lactate. In the 24 SRW, the maximum concentration of 1.61 ± 0.06 g L^{-1} was also reached on day 5, but lactate was fully consumed thereafter. Previous studies that employed pH monitoring during cultivations in 24 SRW microtitre plates reported dropping pH values (Naciri, Kuystermans and Al-Rubeai, 2008; Toussaint, Henry and Durocher, 2016). A more acidic culture environment has been associated with a slower and extended growth phase as well as lower lactate production in mammalian cells (Wu, Ray and Shuler, 1993; Xie *et al.*, 2002), all of which could be observed for the cultivation in the 24 SRW. The lower glucose consumption and simultaneously lower lactate production in the 24 SRW suggests that the cells show less glycolytic activity and instead channel more of the glucose towards oxidative phosphorylation.

Table 4.2: Growth and production parameters of GS-CHO cells grown at different scales at a matched mixing time of ~6 s. Data represent the mean ± standard deviation (5 L STR: n = 2, micro-Matrix: n = 3, 24 SRW: n = 3).

Culture parameter	**5 L STR**	**micro-Matrix**	**24 SRW**
Max. VCC (x 10^6 cells mL^{-1} d^{-1})	8.3 ± 1.5	8.2 ± 1.0	6.8 ± 0.4
Cumulative IVCC (x 10^6 cells mL^{-1} d^{-1})	46.1 ± 0.6	36.1 ± 2.5	39.8 ± 0.4
μ_{max} (d^{-1})	0.57 ± 0.01	0.71 ± 0.03	0.49 ± 0.01
Final titre (g L^{-1})	0.34 ± 0.04	0.34 ± 0.05	0.40 ± 0.01
average q_{mAb} (pg $cells^{-1}$ d^{-1})	7.5 ± 1.8	13.7 ± 0.3	10.1 ± 0.2

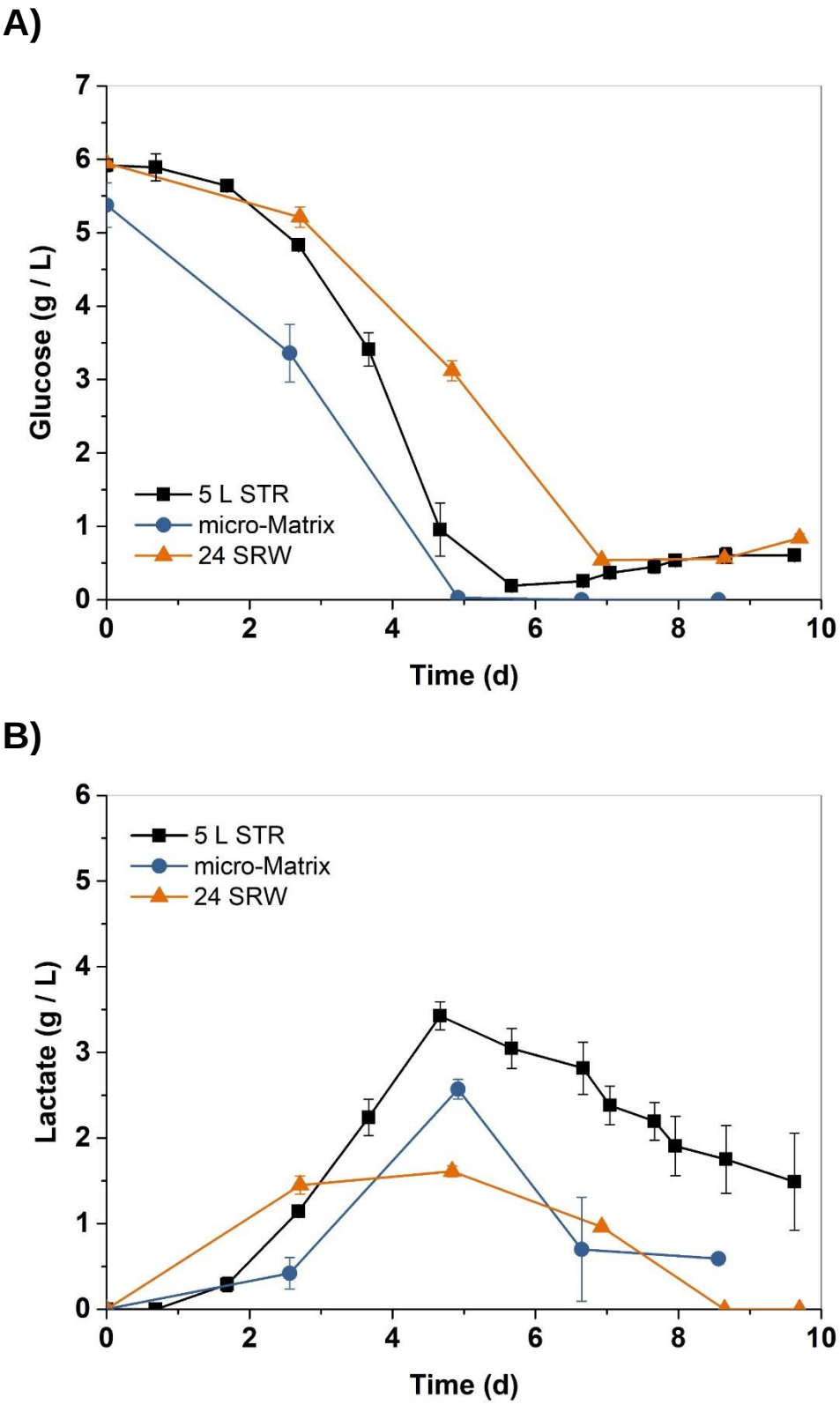

Figure 4.3: Glucose (A) and lactate (B) metabolism of GS-CHO cells grown in a 5 L STR (■), the micro-Matrix (●), and 24 SRW microtitre plates (▲) at a matched mixing time of ~6 s. Data points represent the mean ± standard deviation (5 L STR: n = 2; micro-Matrix: n = 3; 24 SRW: n = 3).

In summary, the scale-down of the GS-CHO batch process yielded mixed results across the cultivation formats. Most of the differences between the STR and the 24 SRW could be traced back to a lack of pH control in the microtitre plate culture. This is an inherent limitation to this format, which has to be condoned when microtitre plates are used for process development. Most of the differences between the STR and the micro-Matrix, however, were presumed to arise from high evaporation rates and large sample volumes. Both of these factors are easier to control under fed-batch conditions, as the volume increase can be used for more frequent and less diluted analyses. The following scale-down experiments, therefore, focus on the translation of a fed-batch protocol.

4.4. Fed-batch scale-down at matched mixing time

The scale-down of the fed-batch process was conducted following the operating conditions outlined in Table 4.1. The fed-batch protocol was performed and scaled down as described in section 2.1.7. Figure 4.4 A illustrates the resulting growth and viability profiles of GS-CHO cells grown in the 5 L STR and the micro-Matrix. In the first three days of the cultivation, the cells grew similarly in both systems. Thereafter, the growth profiles diverged considerably. The micro-Matrix reached its maximum VCC (Table 4.3) on day 7, whereas the VCC in the STR steadily increased and only plateaued towards the end of the experiment. The magnitude of the maximum VCC in both systems showed a significant (p = 0.042, t-test) difference. The viability largely reflected the progression of the VCC. In the STR, the viability slowly decreased over the course of the cultivation and was maintained above 80% for most of the run. In the micro-Matrix, the viability remained high until day 5, when the maximum VCC was reached, and then quickly decreased to 62.5% on day 13. Notably, the viability showed marked fluctuations towards the end of the experiment.

The trend lines of the titre (Figure 4.4 B) were almost congruent and the final titre values (Table 4.3) showed no significant differences (p > 0.05). Although this was surprising considering the stark differences seen in the growth kinetics, previous experiments have shown that the titre is less affected by changes in the cultivation environment (sections 4.3 and 3.3). If the cultivation

environment encourages proliferation, fewer resources appear to be channelled towards product generation and the specific productivity decreases (Table 4.3).

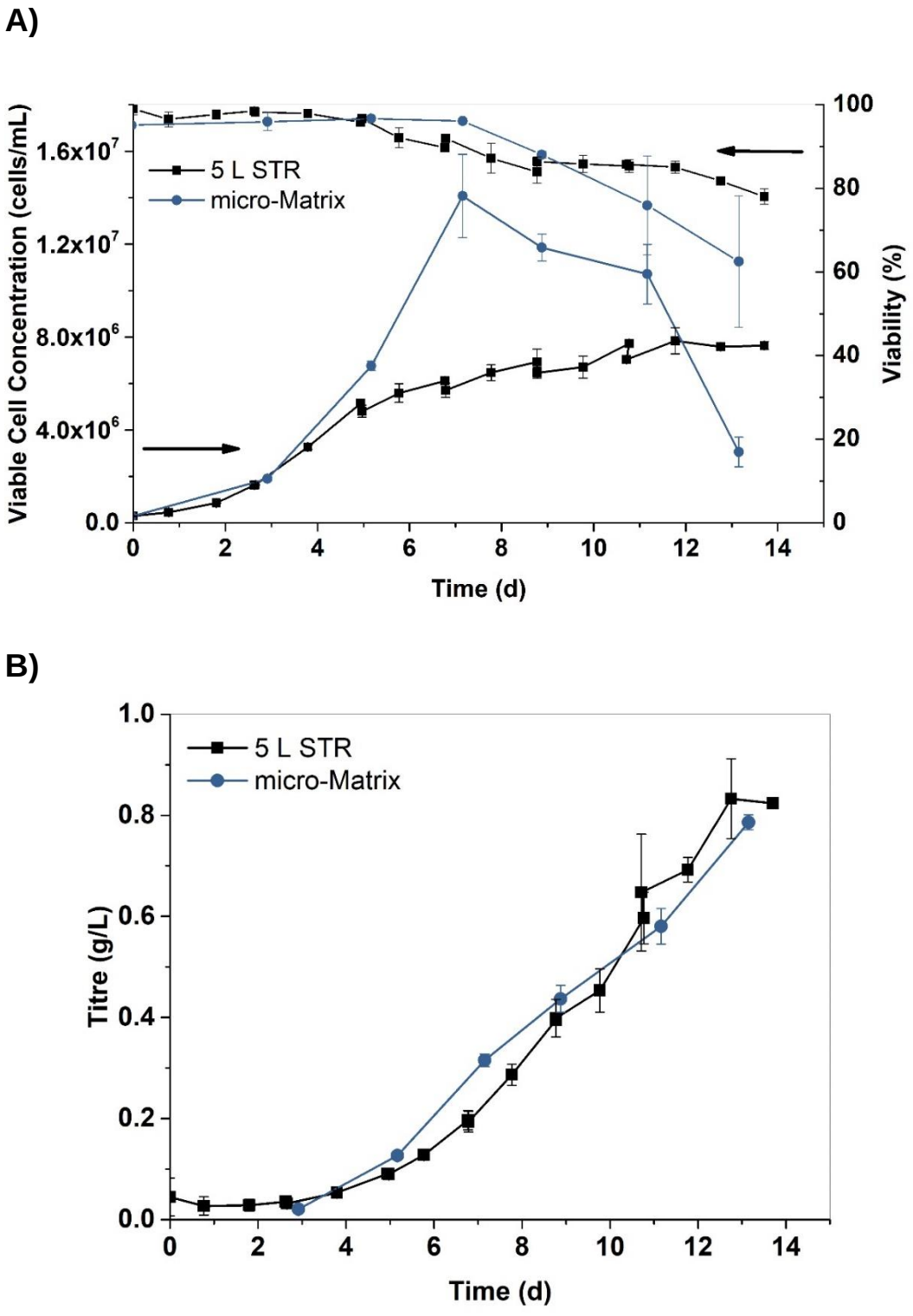

Figure 4.4: Growth (A) and production (B) kinetics of GS-CHO cells grown under fed-batch conditions in a 5 L STR (■) and the micro-Matrix (●) at a matched mixing time of ~6 s. Data points represent the mean ± standard deviation (5 L STR: n = 2; micro-Matrix: n = 3).

Table 4.3: Growth and production parameters of GS-CHO cells grown under fed-batch conditions at different scales at a matched mixing time of ~6 s. Data represent the mean ± standard deviation (5 L STR: n = 2, micro-Matrix: n = 3).

Culture parameter	**5 L STR**	**micro-Matrix**
Max. VCC (x 10^6 cells mL^{-1} d^{-1})	7.8 ± 0.6	14.1 ± 1.8
Cumulative IVCC (x 10^6 cells mL^{-1} d^{-1})	68.6 ± 2.5	82.4 ± 0.8
μ_{max} (d^{-1})	0.54 ± 0.03	0.64 ± 0.03
Final titre (g L^{-1})	0.83 ± 0.08	0.79 ± 0.01
average q_{mAb} (pg $cells^{-1}$ d^{-1})	12.5 ± 1.1	8.2 ± 0.2

The glucose and lactate metabolism of the fed-batch process in the small and benchtop scale is shown in Figure 4.5. Because of the larger working volume in the STR, samples were taken before and after the addition of feed medium. In the micro-Matrix, the samples were merely taken post-feed addition; the measured glucose concentration therefore did not show the same oscillations as in the STR. Cells cultured in the micro-Matrix consumed glucose faster compared to cells grown in the STR, as higher cell numbers had to be sustained in this cultivation system. At the same time, less lactate was produced in the micro-Matrix, indicating a metabolism that is less glycolytic compared to the STR. In both scales, the lactate shift occurred, but lactate was only consumed partially. A high degree of variability was seen for the concentration of lactate in the micro-Matrix on the last three days of the cultivation. In two out of the three replicate wells, lactate was partially consumed by the cells, whereas the other well showed a complete consumption of lactate. The complete consumption coincided with a higher final viability. The variability of the metabolism is therefore also reflected by the spread in the growth kinetics. However, an effect of the lactate consumption on the productivity, as it is often reported in the literature (Mulukutla, Gramer and Hu, 2012; Zagari *et al.*, 2013; Hartley *et al.*, 2018), could not be observed here. Nevertheless, the glucose and lactate analyses have to be considered with some caution, as the micro-Matrix samples had to be diluted by a factor of three. After dilution, some of the glucose

and lactate concentrations were close to the bioanalyser's lower detection limit (glucose: 0.2 g L^{-1}; lactate: 0.2 g L^{-1}), which can cause the analyses to deliver inaccurate results.

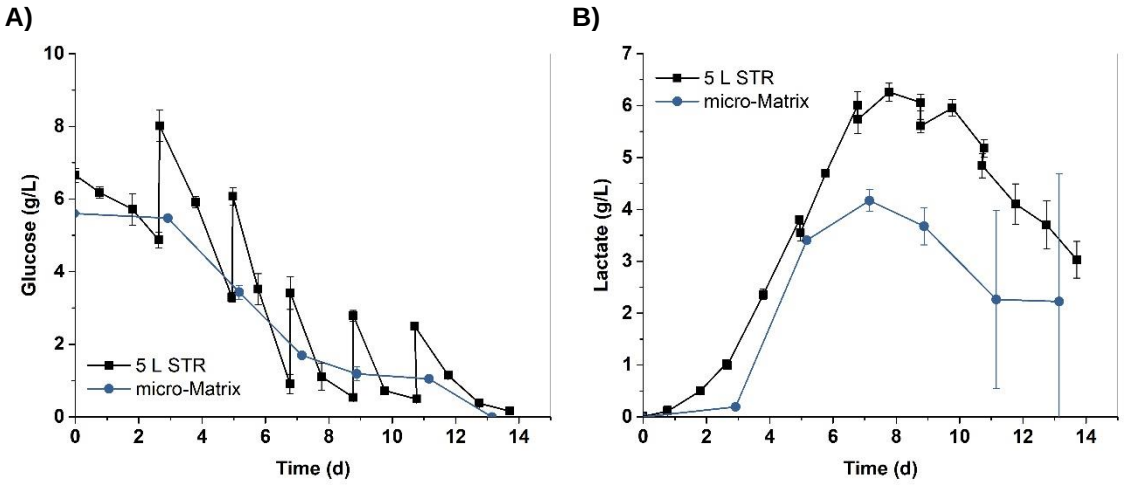

Figure 4.5: Progression of the glucose (A) and lactate (B) concentration of GS-CHO cells grown under fed-batch conditions in a 5 L STR (■) and the micro-Matrix (●) at a matched mixing time of ~6 s. Data points represent the mean ± standard deviation (5 L STR: n = 2; micro-Matrix: n = 3).

In summary, the scale-down of the fed-batch protocol from the 5 L STR to the micro-Matrix via a matched mixing time has resulted in significantly different cell growth. The cellular expansion in the micro-Matrix was faster and reached higher cell densities compared to the STR. Yet, the production kinetics appeared to be scalable. The progression of the titre was similar in both devices and the final concentration of IgG4 did not show significant variation. Although the metabolism showed some differences, the trends were similar and some variability may have been introduced by the high dilution rates of the micro-Matrix samples.

In order to find an explanation for the striking differences in growth between the scales, other process parameters were investigated for potential dissimilarities. Figure 4.6 shows the CO_2 addition profile of the micro-Matrix and the STR throughout the cultivation. The values were normalised to the final value reached in the respective system. In the micro-Matrix, CO_2 was added continuously, although the rate of CO_2 addition slowed slightly after the third day of the cultivation. In contrast, the CO_2 addition in the STR stopped around the 3-day mark. Between days 3 to 10, almost no CO_2 was added and its addition only increased in the final stages of the

experiment. Mid-culture, no CO_2 was necessary to control the pH, because the medium was sufficiently acidified through the generation of lactate and the acidification beyond the setpoint was counteracted through automated base additions. Only once the cells underwent a metabolic shift and started consuming lactate towards the end of the run, CO_2 additions were required to control the pH. In the micro-Matrix, on the other hand, manual bolus additions of base were used to upregulate the pH. Following each bolus addition, the pH increased past the setpoint and had to be downregulated by the micro-Matrix control through the addition of CO_2.

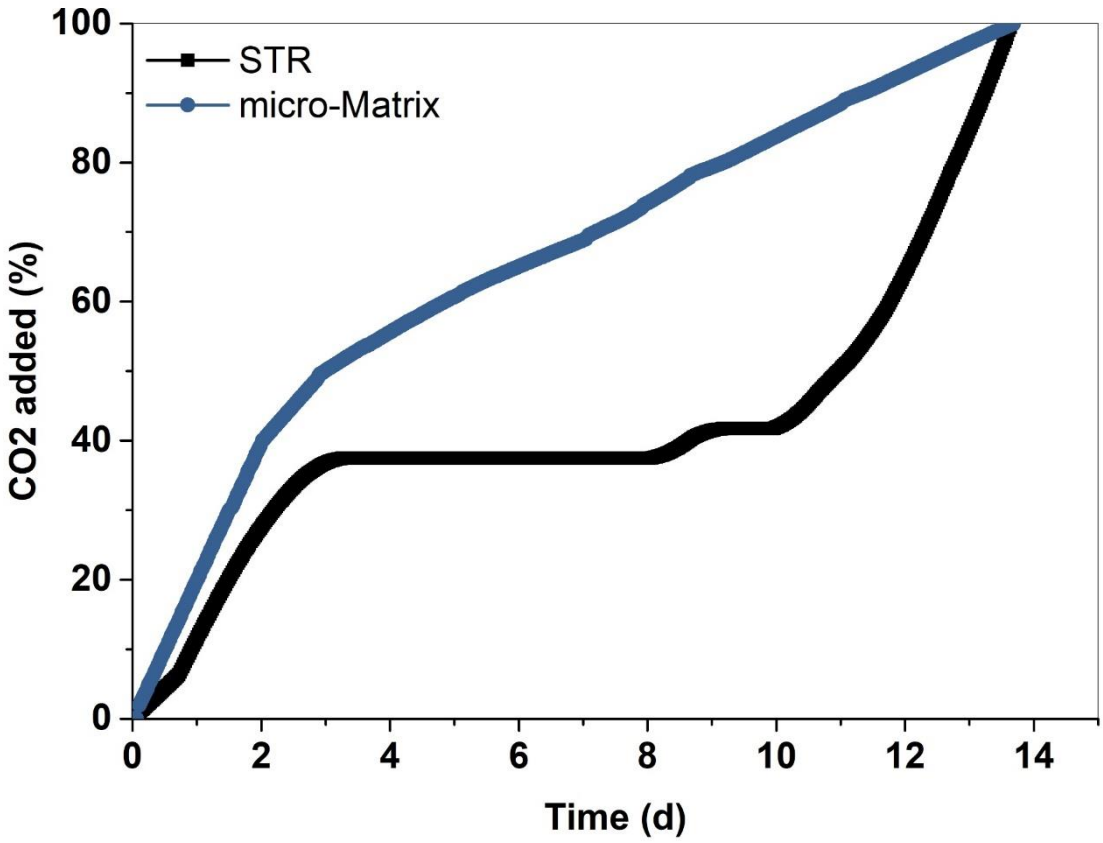

Figure 4.6: CO_2 addition profile of GS-CHO cells grown under fed-batch conditions in a 5 L STR (■) and the micro-Matrix (●) at a matched mixing time of ~6 s.

The next iteration of the fed-batch scale-down will seek to emulate the CO_2 addition profile of the STR in the micro-Matrix by using the automated feeding module instead of manual additions of base. Furthermore, it will be investigated, whether an increased addition of CO_2 has a similarly stimulating effect on the cell growth in the 5 L STR.

4.5. Fed-batch scale-down at matched mixing time and matched CO_2 addition profile

As the results of the previous experiment (section 4.4) suggested that the growth of GS-CHO cells is affected considerably by the addition of CO_2, this experiment combined the matched mixing time approach with a matched CO_2 addition profile in the micro-Matrix and the 5 L STR. The CO_2 addition profile of the STR (Figure 4.6) was recreated in the micro-Matrix by using the automated feeding module for base additions. Additionally, the CO_2 supply to the system was disconnected between days 3 – 10 to prevent any accidental influx of CO_2 caused for instance by imprecise feedback control of the pH. This condition was hereafter called "Low CO_2".

In a second condition ("High CO_2"), elevated concentrations of CO_2 in the inflowing gases were tested. Instead of the main gas supplies, in this condition both systems were connected to gas cylinders containing blends of 5% CO_2 balanced with either cAir, O_2, or N_2. The scale-down of the fed-batch process was conducted following the operating conditions outlined in Table 4.1. The fed-batch protocol was performed and scaled down as described in section 2.1.7. The resulting pCO_2 profiles from both conditions were tracked for the cultivations in the STR. The scaling strategies were evaluated through comparison of growth, production, metabolism, and product quality. Additionally, the fed-batch protocol was translated to the 24 SRW microtitre plate format to evaluate the influence of an uncontrolled pH and DO environment on the scalability.

Figure 4.7 shows the growth and production kinetics of GS-CHO cells grown at three different scales under either high CO_2 or low CO_2 conditions. The data showed a clear dependence of the growth kinetics on the concentration of CO_2 in the inflowing gas. For the high CO_2 condition, the maximum VCCs (Table 4.4) in the controlled systems (STR and micro-Matrix) were about 60% higher compared to the low CO_2 condition. The growth profiles were similar to previous cultivations (sections 4.4 and 3.3), wherein the VCC either increased rapidly in the beginning of the culture, or the cell growth was dragged out over the course of the cultivation and the maximum VCC was reached in the final days of the experiment. Within each condition, the growth profiles generated in the micro-Matrix and the STR were highly comparable and the maximum VCCs did not show significant differences ($p > 0.05$). The growth kinetics observed in the 24 SRW format showed trends that resembled an intermediate of both CO_2 conditions in the controlled systems.

Although the maximum VCC was not significantly different ($p > 0.05$) to the ones found in the micro-Matrix and the STR for the high CO_2 condition, the cell growth was prolonged, similar to what could be observed for cells grown in the controlled systems at low CO_2. A difference between the 24 SRW and the controlled systems was also apparent for the viability, which was considerably higher throughout the cultivation.

The final titre (Figure 4.7 and Table 4.4) was not found to be significantly different ($p > 0.05$) in any of the formats or conditions tested. The similar final titre however indicates differences in the cell specific productivity (Table 4.4) depending on the CO_2 condition. This confirms observations made in previous experiments (section 4.4) where cell populations with better growth characteristics showed a consistently lower specific productivity.

As the concentration of CO_2 in the inflowing gas gives little information on the concentration of dissolved CO_2 in the medium, the pCO_2 was measured for both CO_2 conditions throughout the STR cultivation. This was not possible for cultivations in the micro-Matrix or the 24 SRW, because of the high sample volume (1 mL) necessary to perform the gas measurements. Figure 4.8 shows that the pCO_2 behaved similarly in both conditions until day 3. In the high CO_2 condition, the pCO_2 subsequently continued to rise and reached a final concentration of 93.9 ± 8.1 mmHg. In the low CO_2 condition, the pCO_2 plummeted to 0 mmHg around day 4, only slowly increased thereafter, and reached a final value of 52.3 ± 5.4 mmHg on day 12.

A varying pCO_2 environment is often reported to affect the osmolality of the cultivation broth (Darja *et al.*, 2016; Xu *et al.*, 2018). The progression of the osmolality was therefore measured throughout the cultivation in the 5 L STR for both CO_2 conditions. Figure 4.8 illustrates that the difference in pCO_2 levels did not affect the osmolality. The highest osmolality reached was 374 ± 6.8 mOsmol L^{-1}, which is well below the value reported as critical for suspension cultures (450 mOsmol L^{-1}) (Takagi, Hayashi and Yoshida, 2000). As no differences of the osmolality could be observed between high and low CO_2 conditions, it is plausible to assume that the effects of these conditions on cell growth are caused by the varying pCO_2 levels.

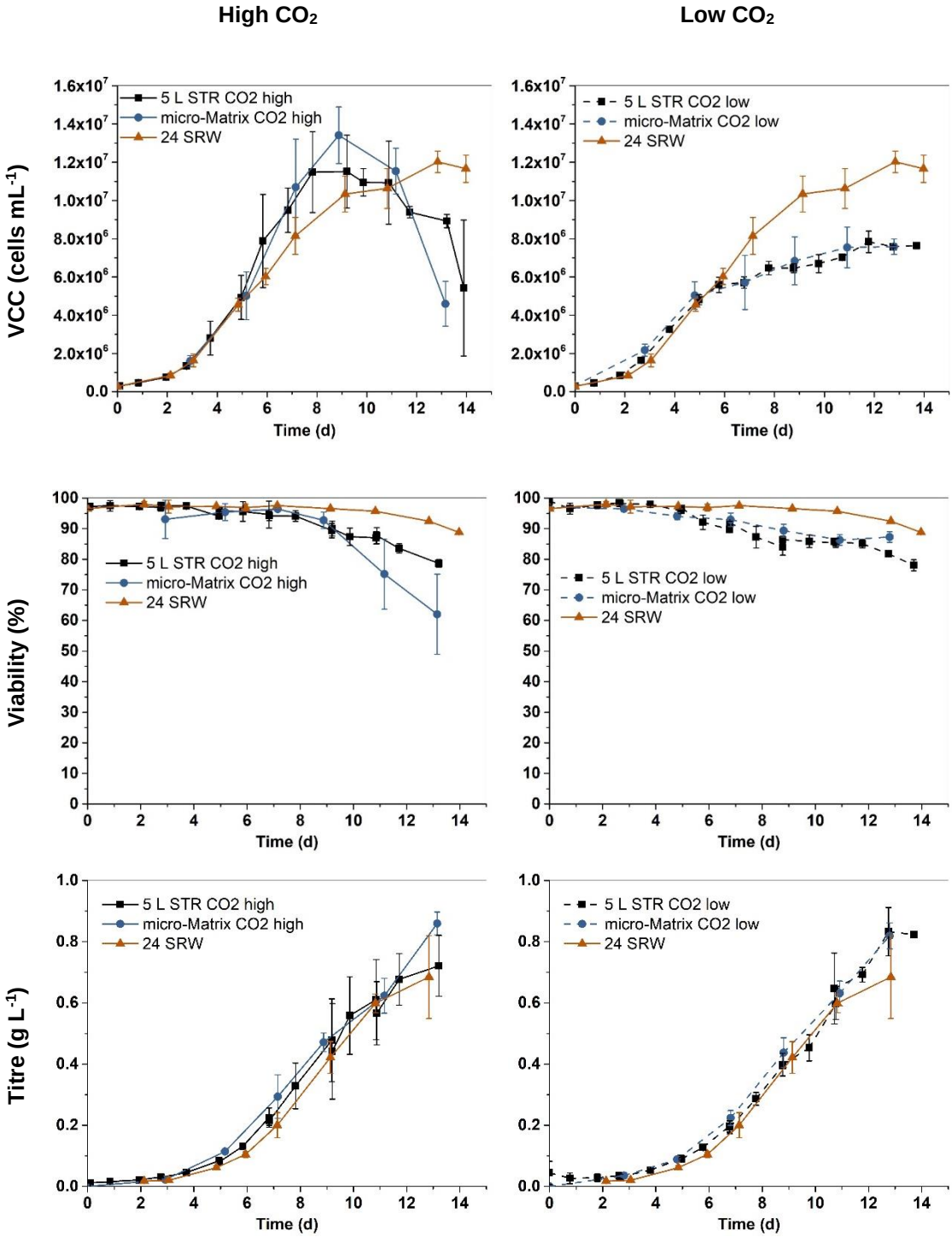

Figure 4.7: Growth and production kinetics of GS-CHO cells grown in a 5 L STR (■), the micro-Matrix (●), and 24 SRW microtitre plates (▲) at a matched mixing time of ~6 s. In the controlled systems (STR and micro-Matrix), the cultivation was performed with pure gases (continuous line) or gas blends contiaing 5% CO_2 (broken lines). Data points represent the mean ± standard deviation (5 L STR: n = 2; micro-Matrix: n = 4; 24 SRW: n = 6).

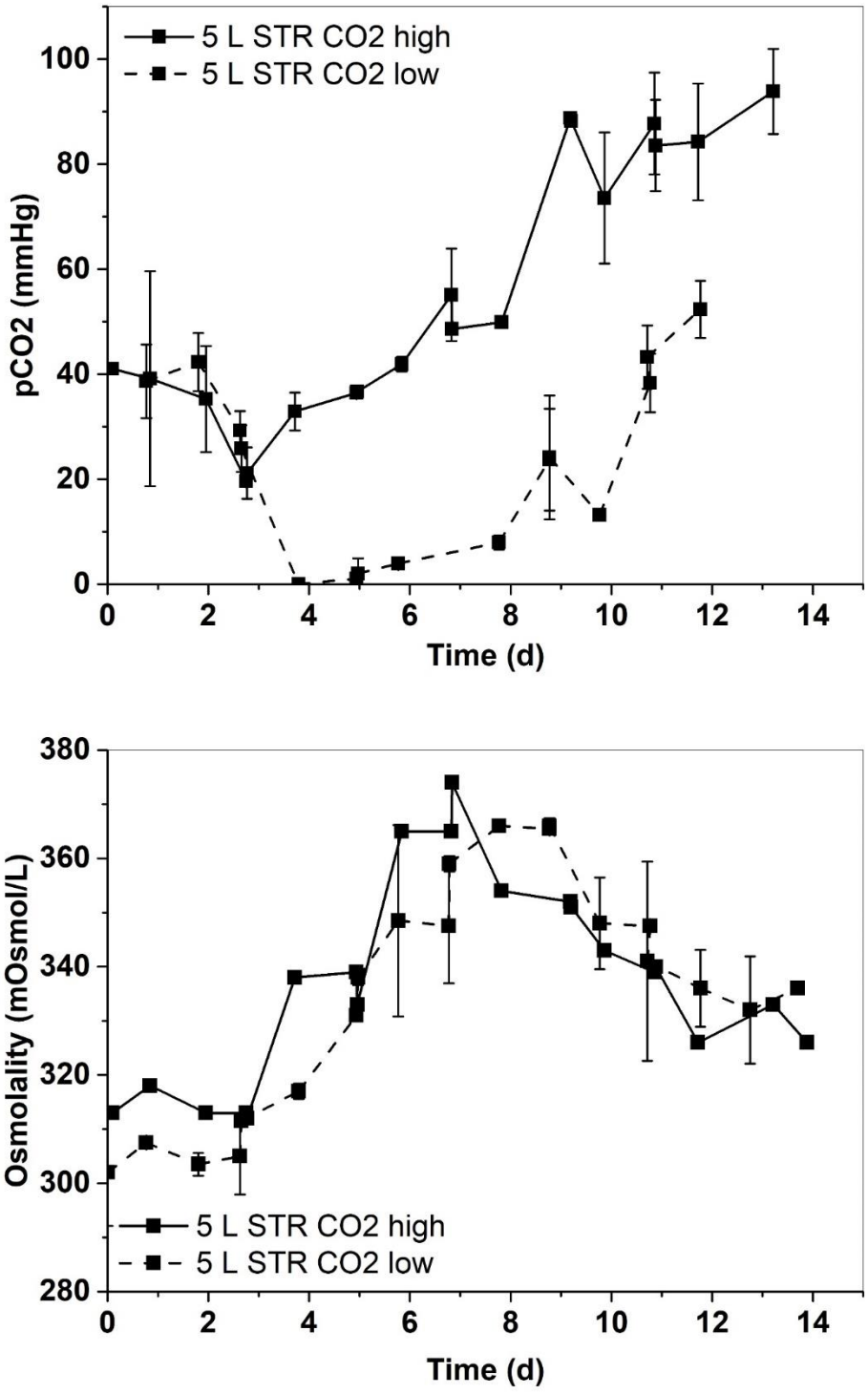

Figure 4.8: The progression of the pCO_2 (top) and the osmolality (bottom) during a fed-batch cultivation of GS-CHO in a 5 L STR. The cultivation was performed with pure gases (continuous line) or gas blends containinng 5% CO_2 (broken lines). Data points represent the mean ± standard deviation (n = 2).

The negative effect of elevated concentrations of dissolved CO_2 on the growth and production kinetics of mammalian cells is often discussed in the literature (Darja *et al.*, 2016; Brunner *et al.*, 2018; Nguyen Dang *et al.*, 2019). Here, however, a negative effect on the cell proliferation of GS-CHO cells was found for conditions of CO_2 depletion. In the standard benchtop scale cultivation protocol, the acidification of the medium through the production of lactate halted further addition of CO_2 mid-culture. Because the removal of CO_2 from solution is very effective at this scale, the pCO_2 dropped to 0 mmHg. With increasing scale, CO_2 removal becomes inherently less effective (Mostafa and Gu, 2003; Xing *et al.*, 2017; Xu *et al.*, 2017). Recreating conditions of complete CO_2 removal at the pilot- and manufacturing scale is therefore challenging, which renders the low CO_2 condition potentially unsuitable as predictive model for cell growth at the larger scales. To avoid discrepancies between scales, a preferred strategy is therefore to increase the pCO_2 levels in the scale-down models to mimic the conditions found at the large scale.

Table 4.4: Growth and production parameters of GS-CHO cells grown under fed-batch conditions at different scales at a matched mixing time of ~6 s. Data represent the mean ± standard deviation (5 L STR: n = 2, micro-Matrix: n = 4, 24 SRW: n = 6).

	5 L STR		**micro-Matrix**		**24 SRW**
Culture parameter	min. 0% CO_2	min. 5% CO_2	min. 0% CO_2	min. 5% CO_2	
Max. VCC (x 10^6 cells mL^{-1} d^{-1})	7.8 ± 0.6	11.5 ± 1.9	7.6 ± 0.4	13.4 ± 1.5	12.0 ± 0.6
Cumulative IVCC (x 10^6 cells mL^{-1} d^{-1})	68.6 ± 2.5	96.5 ± 9.0	63.4 ± 8.2	91.1 ± 9.3	82.0 ± 2.7
μ_{max} (d^{-1})	0.54 ± 0.03	0.45 ± 0.04	0.47 ± 0.08	0.45 ± 0.03	0.40 ± 0.03
Final titre (g L^{-1})	0.83 ± 0.08	0.72 ± 0.1	0.82 ± 0.04	0.86 ± 0.04	0.68 ± 0.14
average q_{mAb} (pg $cells^{-1}$ d^{-1})	12.5 ± 1.1	7.7 ± 1.3	11.1 ± 1.2	9.5 ± 0.9	10.6 ± 0.5

Similarly, the negative impact of elevated pCO_2 levels on the production kinetics is often focus of the literature (Goudar *et al.*, 2007; Becker *et al.*, 2019). However, low CO_2 concentrations are rarely considered as part of these studies. Yoon et al. (2001) explored the impact of varying CO_2 concentrations on the production of EPO in CHO cells under incubator conditions. At an

environmental CO_2 concentration of 0%, the cells were also reported to show an increased cell specific productivity. Yet, as the cultivations were performed without active control of pH and DO, a direct comparison is not feasible.

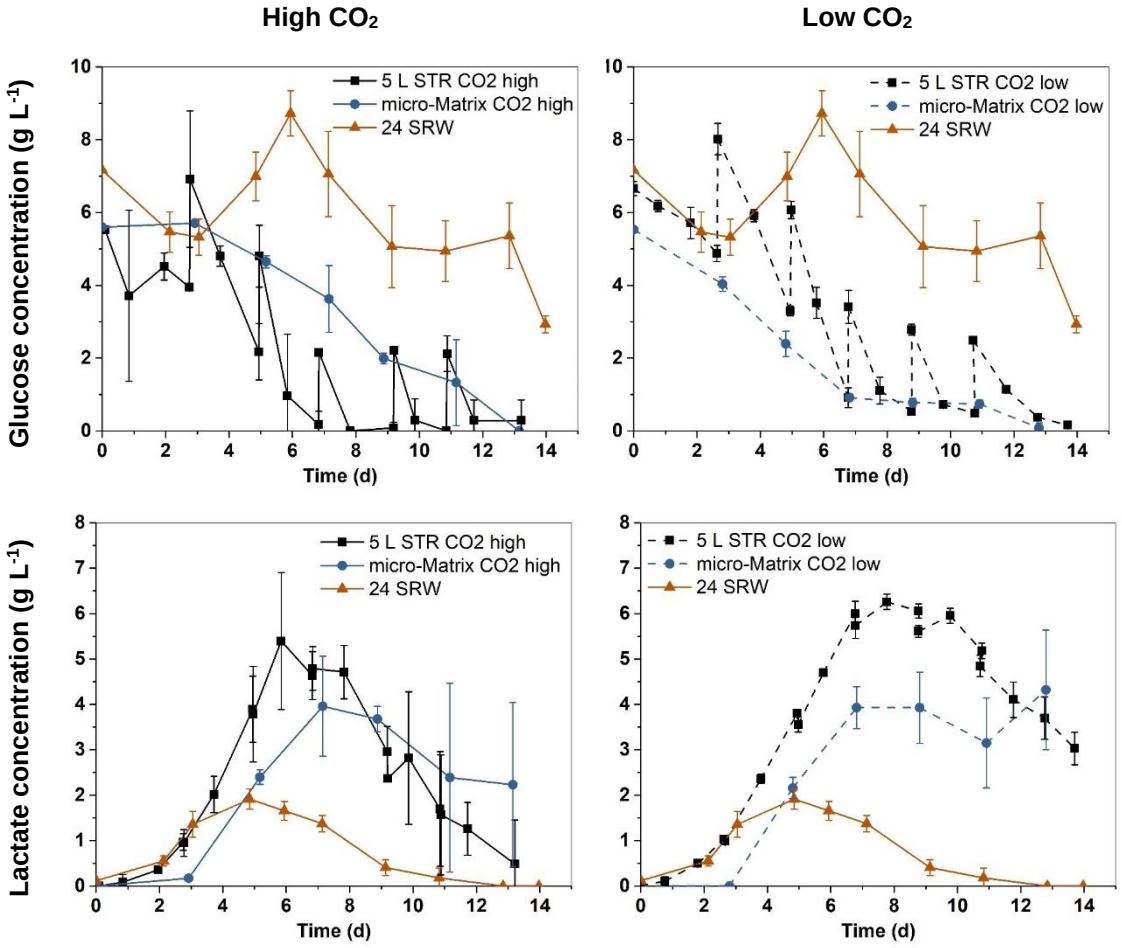

Figure 4.9: Glucose and lactate metabolism of GS-CHO cells grown in a 5 L STR (■), the micro-Matrix (●), and 24 SRW microtitre plates (▲) at a matched mixing time of ~6 s. In the controlled systems (STR and micro-Matrix), the cultivation was performed with pure gases (continuous line) or gas blends contiaing 5% CO_2 (broken lines). Data points represent the mean ± standard deviation (5 L STR: n = 2; micro-Matrix: n = 4; 24 SRW: n = 6).

Figure 4.9 shows the glucose and lactate metabolism. Because of the larger working volume in the STR, samples were taken before and after the addition of feed medium. In the micro-Matrix and the 24 SRW, the samples were only taken post-feed addition; the measured glucose concentration therefore did not show the same oscillations as in the STR. The progression of the glucose and lactate profiles appeared more scalable between micro-Matrix and STR in case of

the high CO_2 condition. In the low CO_2 condition, cells grown in the micro-Matrix seemed to consume glucose quicker, while producing less lactate compared to the STR, which indicates a less glycolytic metabolism. Interestingly, a higher pCO_2 seemed to encourage the consumption of lactate to some degree. A reduced lactate production and increased lactate consumption have previously been linked to elevated concentrations of CO_2 (Darja *et al.*, 2016; Xu *et al.*, 2018), although the opposite effect has also been reported for a pCO_2 of 20% (Brunner *et al.*, 2018). In comparison to the controlled systems, the 24 SRW showed less glucose consumption, lower lactate production, and an earlier onset of lactate consumption, which led to the depletion of lactate at the end of the experiment. This metabolic behaviour is similar to what was reported in section 4.3 and probably caused by a drop of the pH during the cultivation (Naciri, Kuystermans and Al-Rubeai, 2008; Toussaint, Henry and Durocher, 2016), which then led to a slower growth and a lower lactate production (Wu, Ray and Shuler, 1993; Xie *et al.*, 2002). Consequently, cells grown in the 24 SRW use the available glucose more efficiently, which also resulted in a comparatively high viability even after 14 days of cultivation.

To evaluate whether the quality of the produced IgG4 was scalable, the N-linked glycosylation was investigated for each condition. Due to a limited analytical capacity, the purified samples of the replicates of each condition were pooled and the glycoanalysis was performed on the pooled sample. The data presented in Figure 4.10, therefore show the average glycoprofile of the biological replicates but does not inform about the magnitude of error between them.

More than 95% of the antibodies were fucosylated in all scales and conditions, which was similar to values previously reported for IgG4 produced by the same cell line (Tait *et al.*, 2013; VelezSuberbie *et al.*, 2013). A bisecting N-acetylglucosamine moiety was only found for 1.3 – 3.0% of the antibodies with little difference between the scales. Sialylation was comparable (4.2 – 5.7%) for the controlled systems, but found to be reduced (1.9%) for the 24 SRW format. A similar discrepancy was seen for the galactosylation. While the fraction of galactosylated antibodies was similar for the controlled systems (36.1 - 40.6%), it was substantially reduced for antibodies produced in the 24 SRW (21.4%). The difference between the controlled and the uncontrolled systems regarding the glycoprofile was likely another effect of the variation in pH.

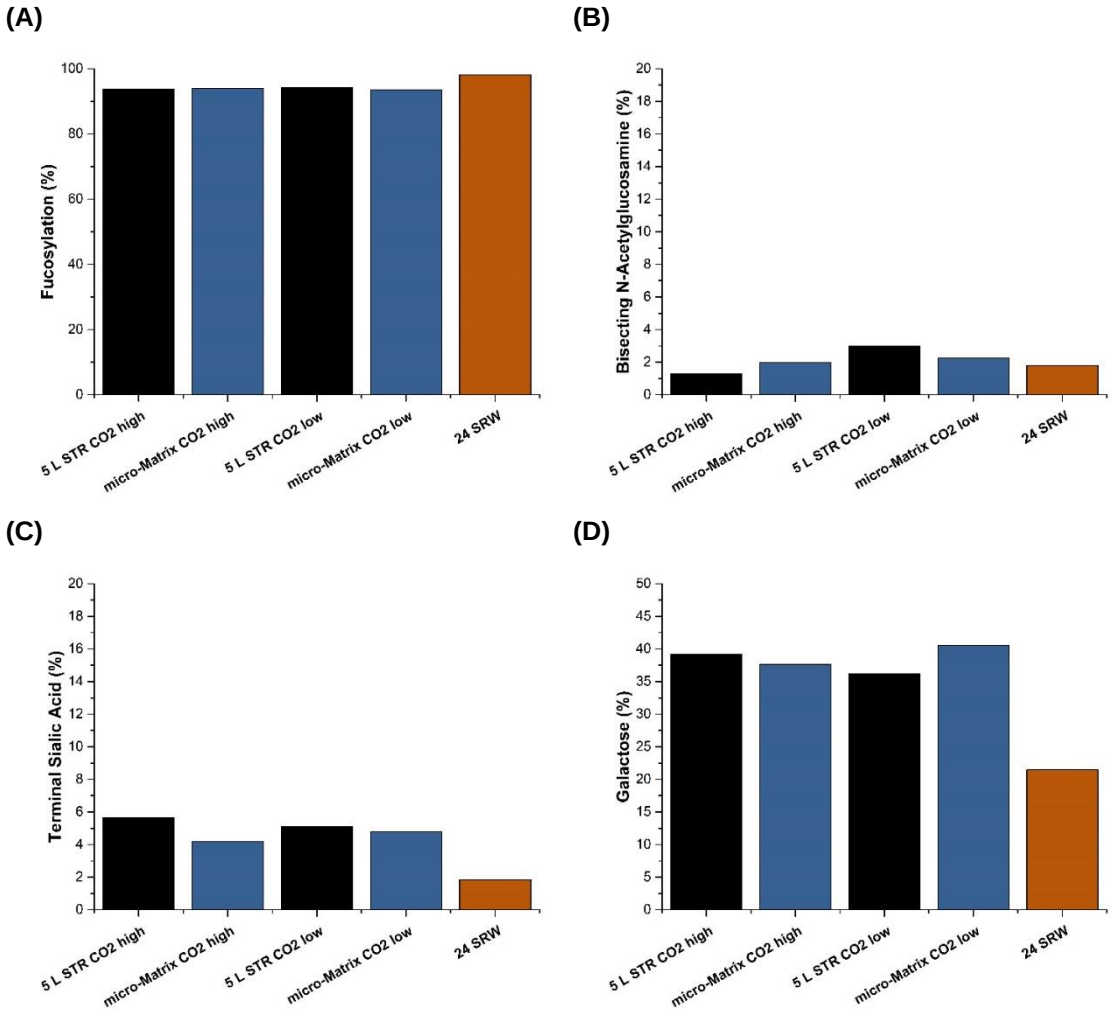

Figure 4.10: Percentage of N-linked glycans of the IgG4 produced at different scales that contain fucose (A), bisecting N-acetylglucosamine (B), sialic acid (C), and galactose (D). The IgG4 was either produced in a 5 L STR, the micro-Matrix, or 24 SRW microtitre plates. In the controlled systems (STR and micro-Matrix), the cultivation was performed with pure gases (CO_2 high) or gas blends containing 5% CO_2 (low CO_2). Glyconalaysis was performed on pooled samples of each replicate.

An effect of culture pH on the glycoprofile has been reported frequently in the literature, but proved highly dependent on the cell line and the glycoprotein. For instance, Müthing *et al.* (2003) observed increased galactosylation of an IgG3 produced by hybridoma cells with increasing culture pH, whereas Seo *et al.* (2013) and Ivarsson *et al.* (2014) reported the opposite effect for a human antibody produced in a human cell line and an IgG1 produced in hybridoma cells, respectively. In a comprehensive study by Jiang, Chen and Xu (2018) on the effect of pH variability on galactosylation in several CHO cell lines, it was found that pH related effects are

highly specific to the cell line in use. Yet, fucosylation has been reported to be affected by a changing pCO_2 environment (Nguyen Dang *et al.*, 2019). Interestingly, here the difference in pCO_2 did not affect the glycoprofile in either of the scales.

In summary, the matched mixing time approach in conjunction with a matched CO_2 addition profile was successful in translating a fed-batch process from the 5 L STR to the micro-Matrix bioreactor. Similar growth and production kinetics were achieved in both scales and the glycosylation of the produced IgG4 was found to be comparable. The metabolic profiles showed some differences between cells grown in the micro-Matrix and cells grown in the STR, which could have been caused by the high dilutions that were necessary in order to measure the residual glucose and lactate in the micro-Matrix samples. Future experiments will use the same dilutions for samples of both scales. The fed-batch process was less scalable to the 24 SRW. Growth and metabolism in particular showed considerable differences to the controlled systems, which was probably caused by the lack of pH control in this cultivation format. While the final concentration of IgG4 produced in the 24 SRW was comparable, its glycoprofile lacked sialic acid and galactose moieties compared to IgG4 produced in the controlled systems.

4.6. Conclusion

Based on the engineering characterisation of the micro-Matrix described in Chapter 3, a matched mixing time was selected as suitable scaling criterion. The initial scale-down experiments revealed that the cell line's growth kinetics are highly dependent on the pCO_2. The CO_2 addition profile was therefore also matched between the microbioreactor and the STR. Using this augmented scaling strategy, growth, production, and product quality were shown to progress analogously in the micro-Matrix and the STR for a scaled down fed-batch process. Further scale-down to 24 SRW microtitre plates proved challenging and evoked major differences in growth, metabolism, and product quality compared to the controlled systems. A possible cause for these deviations was given by the lack of active pH control in the 24 SRW format.

This chapter has established the micro-Matrix as scale-down model for a conventional benchtop STR. In the following chapter, this knowledge will be applied to optimise the fed-batch process at

the small-scale before scaling up the optimised process again via the scaling strategy outlined in this chapter.

Chapter 5. Optimisation of a CHO feeding strategy

Content of this chapter is published in Wiegmann *et al.* (2019)

5.1. Introduction and aim

The addition of feed medium throughout a cultivation is a well-established method of enhancing growth and productivity in mammalian cell cultivations. Compared to the batch mode, fed-batch yields can improve substantially, while the technical complexity of the process is maintained low compared to more advanced modes such as perfusion. As a result, fed-batch remains the preferred mode of operation in biomanufacturing (Wlaschin and Hu, 2006; Rodrigues *et al.*, 2010; Vallée, Durocher and Henry, 2014).

Feeding provides additional nutrients to support cellular growth and product generation. At the same time, the concentration of ions is usually lowered to counteract rising osmolalities. As the components of feed media are often concentrated, the feeding regime has to be considered carefully to prevent inhibitory effects. Therefore, more gradual or continuous additions of feed medium can be preferable in some cases (Bibila and Robinson, 1995). Additionally, feeding can be coupled to queues in the cultivation, such as glucose or glutamine consumption (Zhou, Rehm and Hu, 1995; Chee Furng Wong *et al.*, 2005) or the cell concentration (Lu *et al.*, 2013).

In benchtop scale reactors, a continuous addition of feed medium can be achieved using peristaltic pumps. The pneumatically driven feeding module of the micro-Matrix can realise such additions at the small scale, which facilitates the screening of continuous feeding regimes (Wiegmann *et al.*, 2019). Working with scale-down models of larger scale reactors also facilitates the use of statistical tools such as DoE, which can help to greatly decrease the number of experiments compared to traditionally used one-factor-at-a-time (OFAT) approaches for optimisation (Mandenius, 2016; Sandner *et al.*, 2019).

Chapter aims and objectives:

- Test whether process performance is improved through semi-continuous feeding in the micro-Matrix compared to bolus feeding.

- Conception and execution of a response surface DoE design for the optimisation of the feeding regime.
- Validation of the results obtained for the optimised process at the small scale.
- Scale-up of the optimised feeding regime to the benchtop scale.

5.2. Testing of bolus and semi-continuous feeding strategies

This experiment investigated the effect of six different feeding strategies on the growth and IgG4 production kinetics of GS-CHO cells using the scaled-down cultivation conditions established in Chapter 4. However, since the feeding module was utilised for the additions of medium, base additions had to be performed manually to maintain the pH at the setpoint. The CO_2 addition could therefore not be controlled as accurately as in the previous experiments. Feed medium was added either gradually or as bolus additions. The feed rates were either fixed or determined dynamically based on cell culture parameters. For all feeding strategies, feeding commenced after three days of cultivation and the total feed volume was set to 1200 µL. The following list outlines each feeding strategy in detail:

5.2.1. Design of feeding strategies

FB1 Manual bolus feed addition:

The total feed volume of 1200 µL was split into five additions of 240 µL of feed medium that were added to the cultivation manually as bolus additions. Feeding commenced on day 3 and was thereafter repeated every second day until day 11. FB1 serves as a reference, as it approximates the feeding regime used in previous cultivations.

FB2 Automated bolus feed additions:

This feeding strategy mimicked FB1, but additions were done automatically using the micro-Matrix software in conjunction with the feeding module. Prior to the experiment, the feeding module was calibrated with Efficient Feed B to minimise volume deviations to FB1. The bolus additions were scheduled just before the cassette was taken out of the micro-Matrix for the manual bolus additions (FB1), to minimise differences caused by time-delay.

FB3 Constant flow rate:

The total feed volume was added gradually with a constant flow rate of 109 µL d^{-1}. Feeding was initiated on day 3 and the total volume of 1200 µL feed was reached on day 14.

FB4 Feeding based on the cumulative integral viable cell density (cIVCC):

This feeding strategy attempted to relate the feed volume to the cell concentration. The cIVCC typically achieved in previous fed-batch cultivations with GS-CHO was used to scale the additions of feed medium under the assumption that the glucose consumption rate would remain the same. A final $cIVCC_{max}$ of 12 x 10^7 cells d^{-1} mL^{-1} was assumed and the feed volume was calculated based on equation 5.1.

$$V_{FeedB} = \frac{V_{max}}{cIVCC_{max}} \cdot (cIVCC_i - cIVCC_{i-1}) \qquad (5.1)$$

Where V_{FeedB} is the new cut-off value of Feed B to be added, V_{max} is the maximum amount of feed added throughout the cultivation (1200 µL), $cIVCC_i$ is the value calculated based on the current cell count, and $cIVCC_{i-1}$ is the value calculated based on the cell count of the previous sample. The calculated feed volume was then added to each well as a bolus addition.

FB5 Feeding based on the concentration of glucose:

Upon sampling, the glucose concentration was measured in each well. The measured concentration was then used to calculate the volume of feed medium that was necessary to increase the glucose concentration of the cultivation broth to 6 g L^{-1}, which is roughly the concentration of glucose in CD CHO, the basal medium. The calculated volume of feed medium was added gradually at a constant flow rate over the course of two days. Feeding was stopped once the total feed volume of 1200 µL was reached.

FB6 Feeding based on the consumption rate of glucose:

Upon sampling, the glucose concentration was measured in each well. The measured concentration was then used to calculate the glucose consumption rate according to equation 5.2.

$$r_S = \frac{[Gluc]_i - [Gluc]_{i-1}}{t_i - t_{i-1}} \quad (5.2)$$

Where r_S is the consumption rate of glucose between t_{i-1} and t_i, $[Gluc]_i$ is the current concentration of glucose in the cultivation broth, and $[Gluc]_{i-1}$ is the concentration of glucose in the cultivation broth of the previous sample. The continuous feed addition was then matched to the calculated glucose consumption rate in each well. Feeding was stopped once the maximum feed volume was reached.

5.2.2. Process performance under varying feeding strategies

The feed additions of FB2 – FB6 were performed by the micro-Matrix feeding module; the cumulative volume of added feed could therefore be tracked over the course of the cultivation as shown in Figure 5.1. Feeding was done manually in the case of FB1 and therefore not logged by the software. A step-wise addition indicated bolus feeding strategies (FB2 and FB3), whereas gradual increases of the liquid dosage represented the semi-continuous strategies (FB4 – FB6). The selected feeding strategies generated a broad range of feeding time points and rates, where some instances reached the maximum feed volume as early as on day 8. The feeding strategies that were based on maintaining a constant glucose concentration or matching the glucose consumption rate (FB5 and FB6, respectively), led to particularly rapid additions of feed medium in the early stages of the cultivation. However, in one case (FB4) the calculated feed volumes led to a comparatively slow addition of feed medium, which failed to reach the intended maximum cumulative feed volume on day 14.

Figure 5.2 shows the growth kinetics of all tested feeding strategies. Both, VCC and viability were comparable for most feeding strategies with a maximum VCC of up to 1.9 x 10^7 cells mL^{-1}. Only FB4 yielded a lower maximum VCC, likely caused by the reduced feed rate and amount of total feed added compared to the other feeding strategies. The maximum VCC of FB4 was 1.2 x 10^7 cells mL^{-1}, which was significantly lower compared to the reference feeding strategy FB1 (p = 0.017, t-test). The viability could be maintained above 70% for all feeding strategies during

the cultivation. Compared to the maximum VCCs of previous experiments (see section 3.3), the cell densities reached here are considerably higher. This was most likely caused by the manual additions of buffer that were required to maintain a steady pH value and the resulting fluctuations in the CO_2 addition profile, while the feeding module was utilised for the automated additions of feed medium.

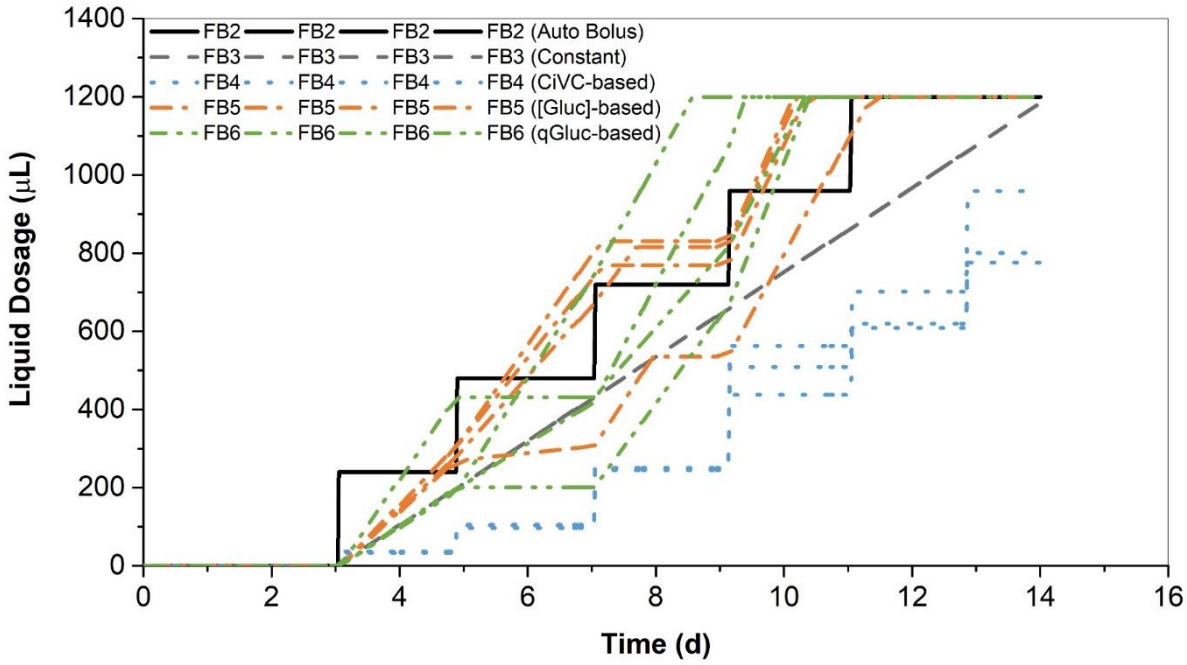

Figure 5.1: Cumulative feed volume added to each micro-Matrix well throughout the cultivation of GS-CHO cells grown under six different feeding strategies. Each feeding condition was performed with n = 4. FB1 does not appear on the graph, as feed additions were done manually and were therefore not logged by the software.

The final titre progressed similarly for all tested strategies and ranged between 0.98 g L^{-1} (FB4) and 1.13 g L^{-1} (FB3). The difference between the highest and lowest final titre, however, was not significant (p = 0.38, t-test). Interestingly, although FB4 had received less feed in total, the final titre was similar to the other feeding strategies. This finding suggests that it may be possible to reduce the amount of feed without forfeiting product yield. The total feed volume was therefore included in following rounds (see section 5.3) of process optimisation.

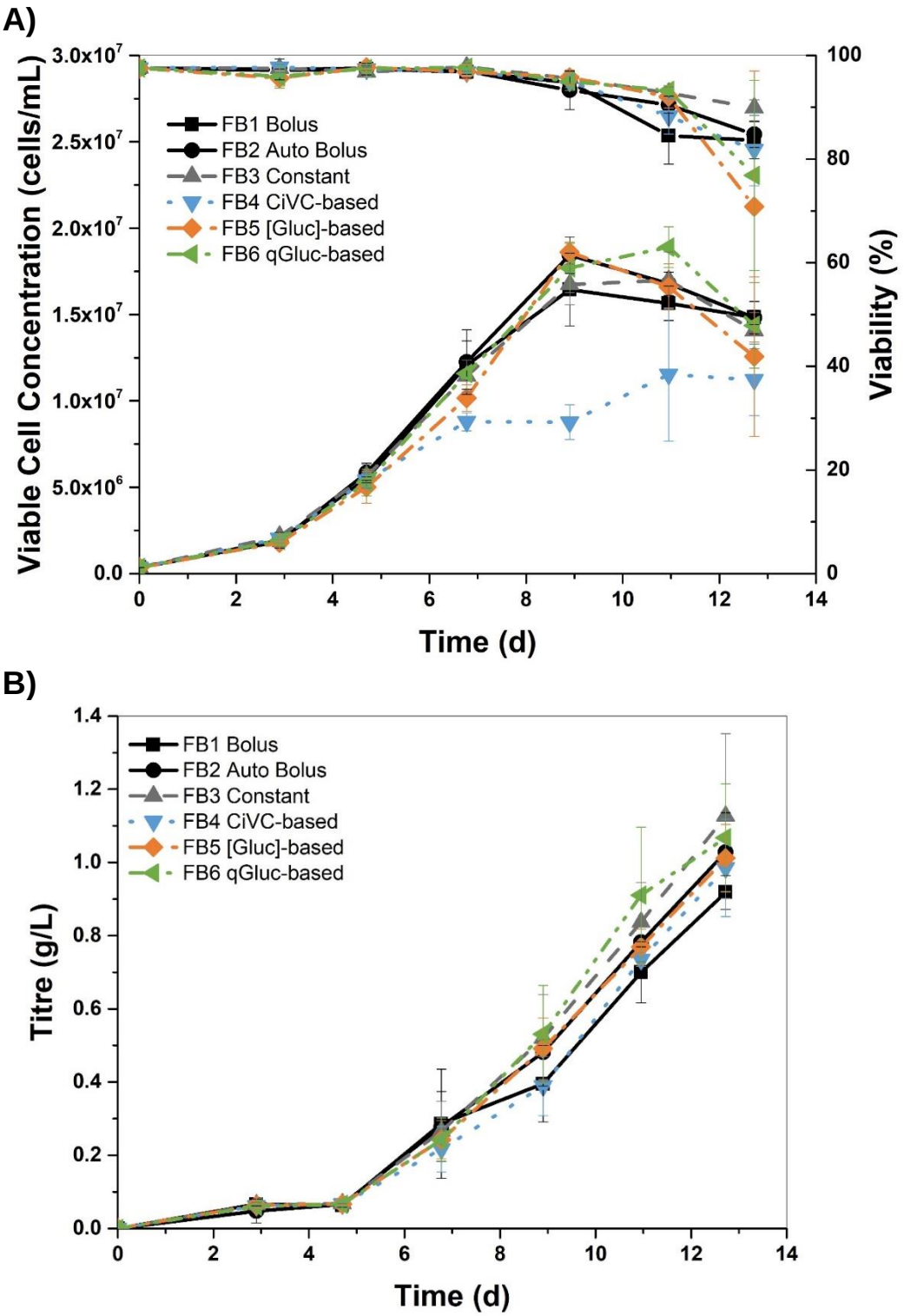

Figure 5.2: Viable cell concentration and viability (A) and titre (B) of GS-CHO cells grown using different feeding strategies. The micro-Matrix was operated at a shaking speed of 250 rpm, 4 mL working volume, and active control of pH (7.2), DO (30%), and temperature (37°C). Error bars represent one standard deviation about the mean (n ≥ 4).

The metabolic footprint for each feeding strategy is shown in Figure 5.3. The trend of glucose consumption followed a similar trajectory for all feeding strategies. Glucose depletion was reached quickest for FB4 on day 6, because of the comparatively small volume of feed added. This appeared to promote an early onset of lactate consumption for this condition, which was documented to take place on day 5 at which point the lactate concentration had reached 3.4 g L^{-1}. Low-level lactate production and early metabolic shifts are often related to improved productivities, which could explain the similar final titre of FB4 (Altamirano *et al.*, 2004, 2006). For all other feeding strategies, the lactate shift occurred after day 7, whereupon the lactate concentration had reached between 4.3 g L^{-1} (FB5) and 4.9 g L^{-1} (FB3). A complete consumption of lactate ensued for all feeding strategies except FB1 in which two out of four replicates showed residual lactate at the end of the experiment.

The nutrient-based feeding strategies FB5 and FB6 were particularly successful at maintaining glucose levels of 1 g L^{-1} and above for the majority of the cultivation. As described earlier, FB6 was designed to match the cells' glucose consumption and was therefore expected to maintain a stable glucose concentration. However, the concentration of glucose was found to drop in unison with the other feeding strategies. As the calculation of the glucose consumption rate was based on the preceding time interval, the actual rate was probably underestimated during the growth phase, which caused the concentration of glucose to drop.

The consumption of glutamate followed a similar trend for all tested feeding strategies. Glutamate reached depletion level after 7 days in FB1, FB2, and FB4, and after 9 days of cultivation in FB3, FB5, and FB6.

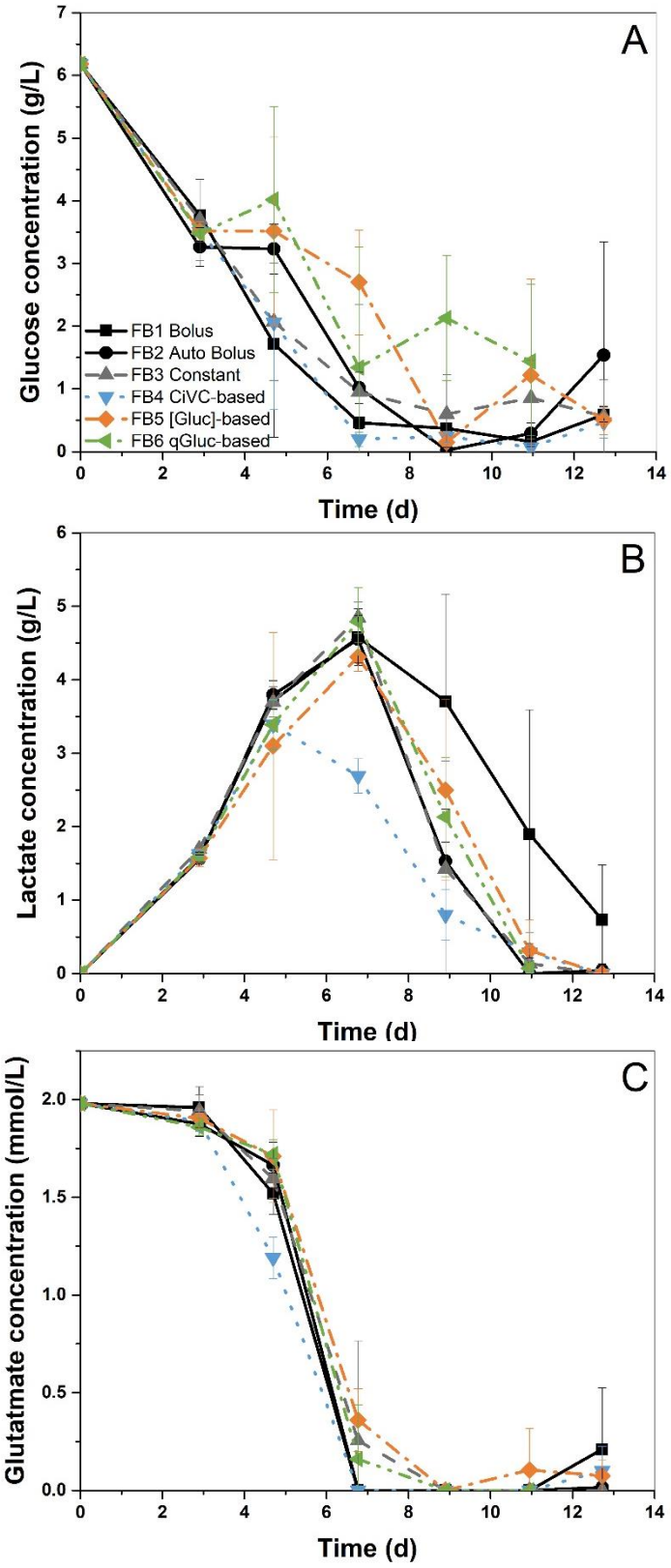

Figure 5.3: The concentration of glucose (A), lactate (B), and glutamate (C) over the course of the cultivation of GS-CHO cells grown using different feeding strategies. The micro-Matrix was operated at a shaking speed of 250 rpm, 4 mL working volume, and active control of pH (7.2), DO (30%), and temperature (37°C). Error bars represent one standard deviation about the mean ($n \geq 4$).

This study demonstrated that growth and productivity of GS-CHO cells are comparable for bolus and semi-continuous feeding. The feeding strategies covered a broad range of addition profiles, but the cells largely maintained the same VCC and titre profiles. Within a certain range of glucose concentrations, this cell line appears to behave remarkably robust. The growth profile was only affected when glucose was limited, as it was the case for FB4. How a process is affected by the feeding strategy is highly dependent on the cell line. Lu *et al.* (2013), for instance, compared bolus additions to continuous feeding of two IgG expressing CHO cell lines grown in a 3 L STR and found that the feeding regime only had an effect on growth and antibody production of one of the investigated cell lines.

Although a reduction in the total amount of feed medium decreased the cell growth, the productivity was maintained and a more favourable lactate metabolism was observed. Ensuing optimisations will therefore also take varying feed volumes into account. As nutrient- or cell-based feeding strategies failed to show improvement over bolus feeding, subsequent experiments focused on optimising the bolus feeding strategy. Not only are bolus additions inherently less complex compared to dynamic feeding strategies, but they can also be performed manually, which means that the micro-Matrix feeding module can be used for base additions instead. Controlled additions of base have been proven instrumental for a successful scale translation in previous sections (see sections 4.4 and 4.5).

5.3. Optimisation using response surface methodology

In the previous section (5.2), bolus was established as the preferred mode of feeding for the GS-CHO cell line. In this section, the bolus feeding strategy will be optimised in the micro-Matrix under scale-down cultivation conditions (Table 4.1), using response surface methodology due to its proven track record in bioprocess development (Islam *et al.*, 2007; Muntari *et al.*, 2012).

5.3.1. Optimisation design

The focus of the optimisation was the feeding regime in which the choice of feed medium was restricted to Efficient Feed B in order to facilitate comparability to previous fed-batch experiments.

The tested feeding regimes were composed of three factors: feed start, feed rate, and feed volume. To allow for the investigation of curvature in the results, the factors were tested in a response surface framework. A circumscribed central composite design (CCD) was employed, as the star points lead to an expanded design space, while their circumscribed spacing results in rotatable predictability as shown in Figure 5.4. For this design a list of the tested parameters and their levels is shown in Table 5.1.

The feed volume was varied around 50% (coded value: 0) of the initial working volume, which was the feed volume used in the original feeding strategy. As it was shown in section 5.2 that underfeeding could yield potential benefits, total feed volumes as low as 8% (-1.68) were included in the design space. At the other end of the spectrum, the working volume was almost doubled through the addition of 92% (+1.68) feed medium, which was aimed to maintain a consistently elevated level of glucose in the cultivation broth.

Table 5.1: Factors and levels of the circumscribed central composite design for the optimisation of the bolus fed-batch strategy.

		Levels				
Factor	**Type**	**-1.682**	**-1**	**0**	**+1**	**+1.682**
A: Feed volume (%)	Numeric, Continuous	8	25	50	75	92
B: Feed start (d)	Numeric, Continuous	0.6	2	4	6	7.4
C: Number of additions (-)	Numeric, Continuous	1	4	8	12	15

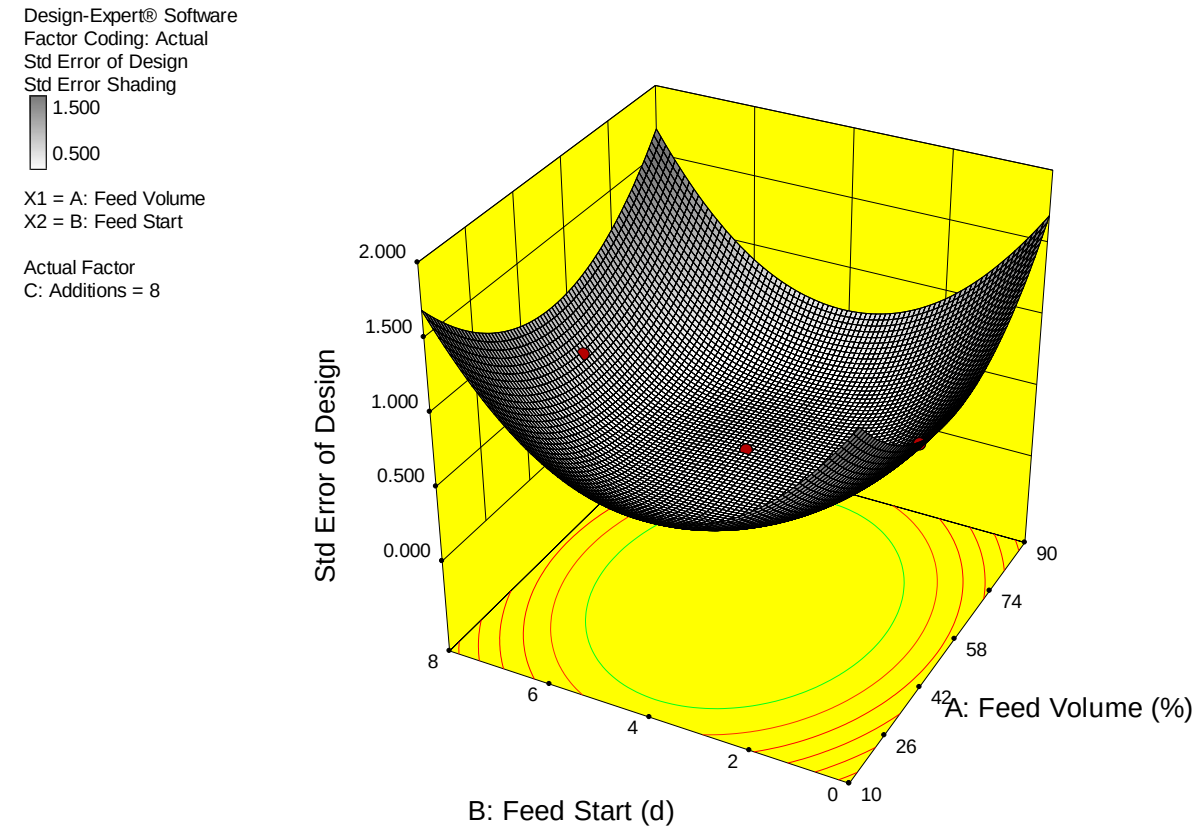

Figure 5.4: Standard error for the factors feed start and feed volume of the circumscribed central composite design for the optimisation of the GS-CHO bolus fed-batch strategy. As the design is rotatable, the distribution of the error is equivalent for other parameter combinations.

The feed start of the centre point was chosen to be on day 4 (0), which was one day later compared to the fed-batch strategy of previous experiments. This was done to expand the design space, while maintaining the circumscribed nature of the CCD. The positive factorial cube point was chosen to be a feed start after 6 days (+1), whereupon glucose was expected to have reached depletion level based on previous experiments (see section 4.3). The positive star point was given for a feed start after 7.4 days (+1.68) of cultivation, which coincides with the onset of the death phase in a batch process. The early feed starts after 0.5 (-1.68) and 2 days (-1) were aimed to support cellular growth in the exponential phase.

The total feed volume was divided into equal bolus additions of feed medium that were added daily. In the previous bolus feeding regime, additions were made every two days. To allow for more nuance, the CCD was based on daily bolus additions instead. In the extreme cases, the

whole volume of feed was either added at once (-1.68), or over 15 (+1.68) consecutive additions. For the centre point condition, the feed volume was spread over 8 consecutive additions (0), whereas in the reference feeding protocol, feed additions were spread over 9 days. The centre point was reduced by one addition, to avoid extended cultivation processes, particularly with respect to the positive star point.

As shown in Table 5.2, the 3-factor CCD with 6 replicates of the centre point resulted in a design matrix of 20 runs. As the micro-Matrix cassette comprises of 24 wells, all experiments could be performed in a single run and no blocking was necessary. The conditions were distributed randomly across the cassette.

The response parameters final titre, final product yield, and space-time-yield (STY) were chosen because these parameters focus on measures of the process productivity. Measures of the cell growth, such as the maximum VCC or the growth rate, were not included in the optimisation, because such responses are not necessarily indicative of a more cost-efficient process.

5.3.2. Data processing and analysis

Table 5.2 shows the parameter combinations of the CCD design matrix based on the previously discussed input factors and levels together with the obtained raw data for each response. Each of the tested conditions was monitored over the course of the cultivation for the progression of cell growth and product formation to gain a more in-depth understanding of the influence that the feeding regime has on the behaviour of the cells (Figure 5.5 and Figure 5.6).

Overall, a broad spectrum of growth and antibody production kinetics was found for the different parameter combinations. The feeding strategies with early additions of feed medium promoted a rapid initial growth phase followed by short stationary phases, whereas a later feed start and slower feed rates encouraged extended stationary phases and as a result prolonged process durations.

Table 5.2: CCD design matrix and response raw data.

	Factors			Responses		
Well	**Feed volume (%)**	**Feed start (d)**	**Additions (-)**	**Final Titre (g L^{-1})**	**Yield (mg)**	**STY (mg d^{-1} L^{-1})**
A2	50	4	1	0.60	3.93	51.52
A3	25	2	12	0.57	3.87	51.35
A4	25	6	12	0.49	2.96	42.04
A5	50	4	8	0.92	5.52	72.23
A6	50	0.6	8	0.63	3.48	53.95
B1	8	4	8	0.42	2.73	38.11
B2	75	2	4	0.60	3.58	54.17
B3	50	4	8	0.84	5.01	65.55
B4	50	4	15	0.65	3.93	55.77
B5	50	7.4	8	0.92	5.07	58.99
B6	75	6	4	0.90	5.41	64.17
C1	75	2	12	0.89	4.89	60.17
C2	92	4	8	0.93	6.07	66.50
C3	50	4	8	0.82	4.23	64.28
C4	50	4	8	0.92	5.51	72.02
C5	50	4	8	0.92	5.50	71.94
C6	75	6	12	1.14	7.05	54.78
D1	25	6	4	0.77	4.62	65.70
D2	50	4	8	0.83	5.00	65.40
D3	25	2	4	0.38	2.08	39.00

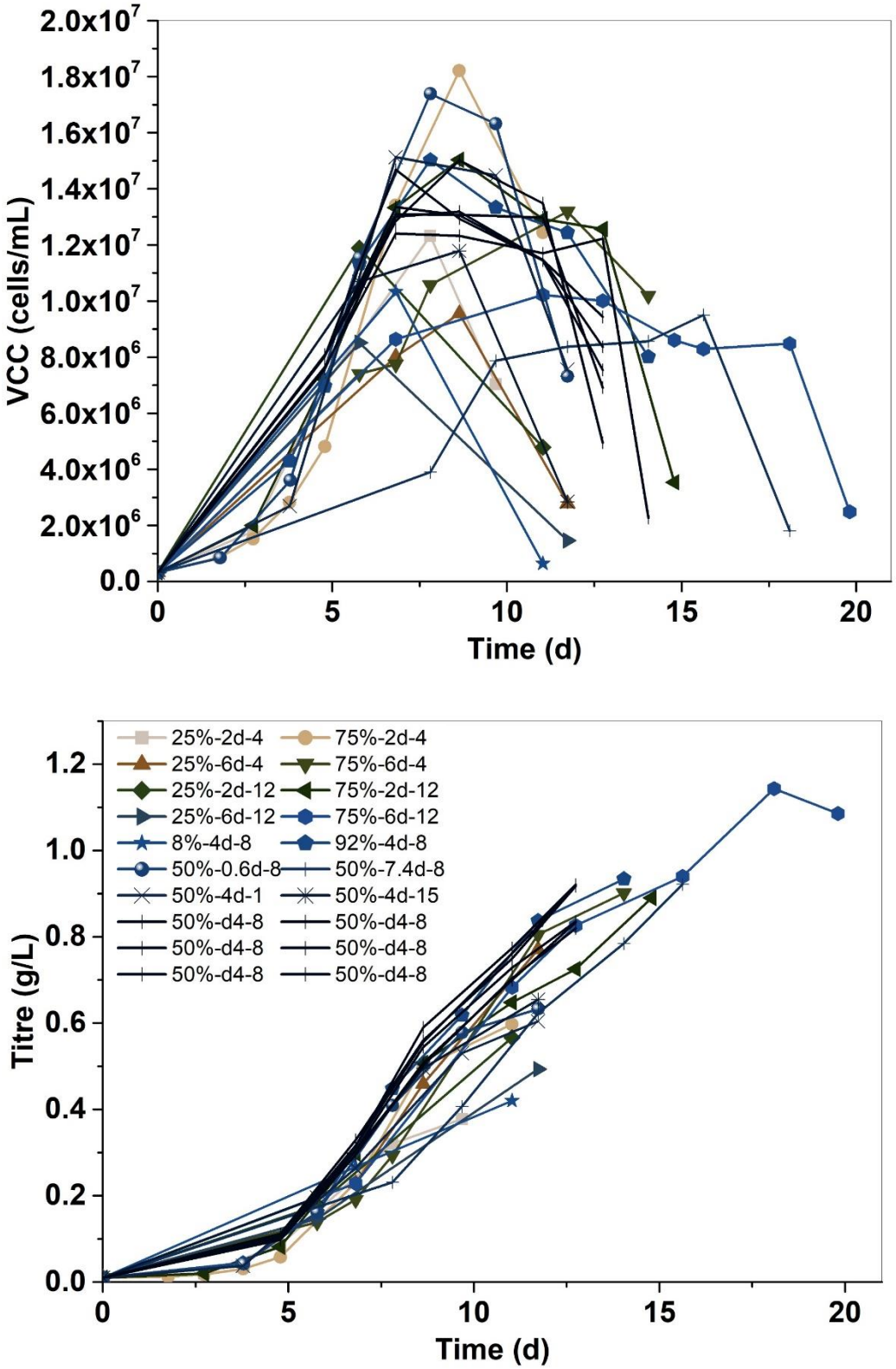

Figure 5.5: Growth (top) and IgG4 production (bottom) of GS-CHO cells grown in the micro-Matrix as part of the DoE-assisted optimisation of the bolus fed-batch strategy. The micro-Matrix was operated at a shaking speed of 250 rpm, 4 mL working volume, and active control of pH (7.2), DO (30%), and temperature (37°C).

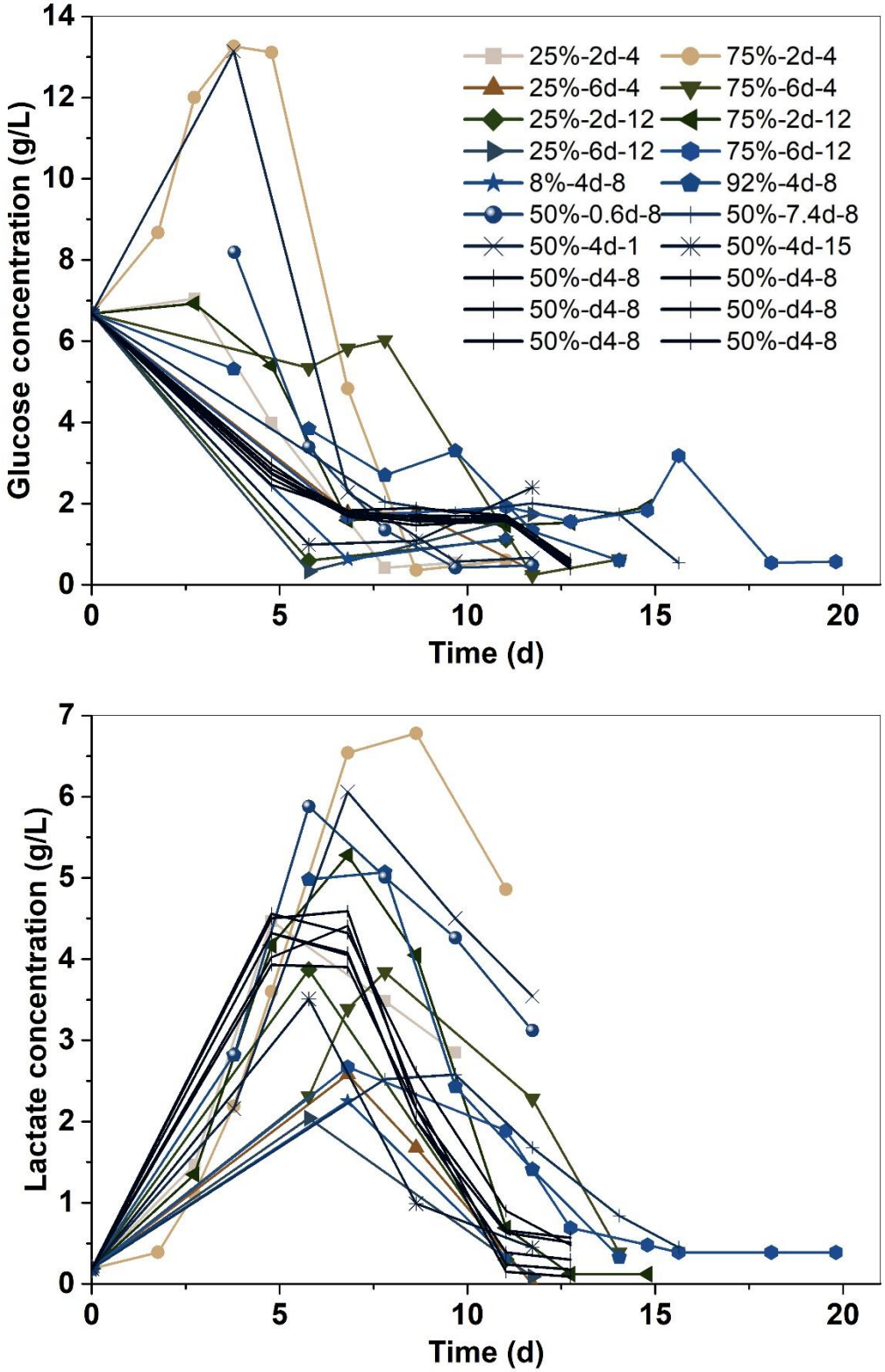

Figure 5.6: Progression of the glucose (top) and lactate concentration (bottom) of GS-CHO cells grown in the micro-Matrix as part of the DoE-assisted optimisation of the bolus fed-batch strategy. The micro-Matrix was operated at a shaking speed of 250 rpm, 4 mL working volume, and active control of pH (7.2), DO (30%), and temperature (37°C).

The final titre was highest for slow feed rates, when feeding was started on day 4 or later. Notably, a feed start on day 6 with a feed addition of 75% of the initial working volume divided into 12 consecutive bolus additions yielded a considerably higher titre of 1.14 g L^{-1} compared to the other conditions. This condition also showed the longest process duration of around 19 days. Nevertheless, the centre point condition also reached a comparatively high titre of 0.87 ± 0.05 g L^{-1} (n = 6), but in merely 13 days of cultivation.

An early feed start as well as the addition of large feed volumes appeared to increase the production of lactate. Lactate concentrations as high as 6.8 g L^{-1} were recorded for a feed start after 2 days of cultivation. Such feeding regimes supported rapid proliferation in the initial stages of the process and very high maximum VCCs. However, after the exponential growth phase, the cell number was often unsustainable and the cell count quickly decreased. A later feed start distinctly suppressed the generation of lactate and instead promoted its consumption. Interestingly however, a state of lactate depletion was often reached later for those conditions compared to feeding regimes with an early feed start.

The results of Table 5.2 were used to create predictive models around the responses as described in section 2.4. As indicated by the ANOVA tables of each response model (Figure 5.7, Figure 5.8, and Figure 5.9), the models of all responses were significant and showed insignificant lack of fit. The data did not require transformation for any of the responses and the diagnostics did not imply systematic errors. Figure A 6 in Appendix II provides further detail on the correlations of input and output factors.

Figure 5.7 summarises the predictive model for the final concentration of antibody, which had an adjusted R^2 value of 0.87. The feed start and the feed volume affected the final titre significantly, while the number of feed additions and the feed volume also showed a quadratic relationship to the response. An interaction between the number of feed additions and the feed volume was found. While a higher feed volume was generally expedient for a higher titre, this was only the case if it is split into a sufficient number of bolus additions. If a high volume of feed was added to the culture in only one or few additions, the titre did not necessarily increase. This could be caused

by inhibitory effects of media components or by an increased lactate formation due to high levels of glucose. Yet, if a low volume of feed was divided into too many bolus additions, the feed additions may not have contained enough nutrients to sustain further cell growth and product generation. Another interaction was found between the feed start and the number of feed additions, in which a late feed start favours fewer feed additions, whereas an early feed start reverses this relationship. Early on in the process, the cells do not require excessive amounts of feed medium, while later on glucose is already close to depletion and a more rapid addition of feed is required to sustain cellular function. The maximum final titre was found for a late feed start in combination with a high feed volume that was divided into a large number of bolus additions. The contour plot of Figure 5.7 illustrates that the optimal final titre was not fully captured by the investigated design space. Further optimisation of the titre would therefore require additional experiments to expand the design space. However, it is debatable whether a further increase of the feed volume would be desirable in a manufacturing process.

The antibody yield at the end of the process (Figure 5.8) was only significantly affected by the feed volume and the feed start. No quadratic terms or interactions were found for this response. However, the model for this response only had an adjusted R^2 value of 0.57, which indicates weak predictive power. With an increase of the feed volume, the mass of antibody increased in a linear fashion, probably caused by the higher final working volume with a reasonably similar final product concentration. Correspondingly, with a later feed start, the antibody yield also increased linearly, which could be a result of a more favourable lactate metabolism through initial glucose starvation and a resulting titre increase.

The model of the STY (Figure 5.9) showed a satisfactory adjusted R^2 value of 0.81. The feed volume and the feed start were significant model terms, while all tested factors were found to have a significant quadratic relationship with the STY. An interaction effect was found between the feed start and the number of feed additions, with an analogous causal relationship as explained above. The optimum STY was captured by the investigated design space for a feed start after 5 days and a feed volume of 64% that was divided into 6 bolus additions to be added

on consecutive days. The predicted optimum STY for this parameter combination was 71.0 mg d^{-1} L^{-1}.

Response 1 Final Titre

ANOVA for Response Surface Reduced Quadratic model

Analysis of variance table [Partial sum of squares - Type III]

Source	Sum of Squares	df	Mean Square	F Value	p-value Prob > F	
Model	0.71	7	0.10	18.97	< 0.0001	significant
A-Feed Volur	*0.35*	*1*	*0.35*	*64.77*	*< 0.0001*	
B-Feed Start	*0.13*	*1*	*0.13*	*24.81*	*0.0003*	
C-Additions	*0.020*	*1*	*0.020*	*3.75*	*0.0767*	
AC	*0.048*	*1*	*0.048*	*8.96*	*0.0112*	
BC	*0.034*	*1*	*0.034*	*6.30*	*0.0274*	
A^2	*0.053*	*1*	*0.053*	*9.83*	*0.0086*	
C^2	*0.088*	*1*	*0.088*	*16.45*	*0.0016*	
Residual	0.064	12	5.361E-003			
Lack of Fit	*0.052*	*7*	*7.427E-003*	*3.01*	*0.1218*	*not significant*
Pure Error	*0.012*	*5*	*2.470E-003*			
Cor Total	0.78	19				

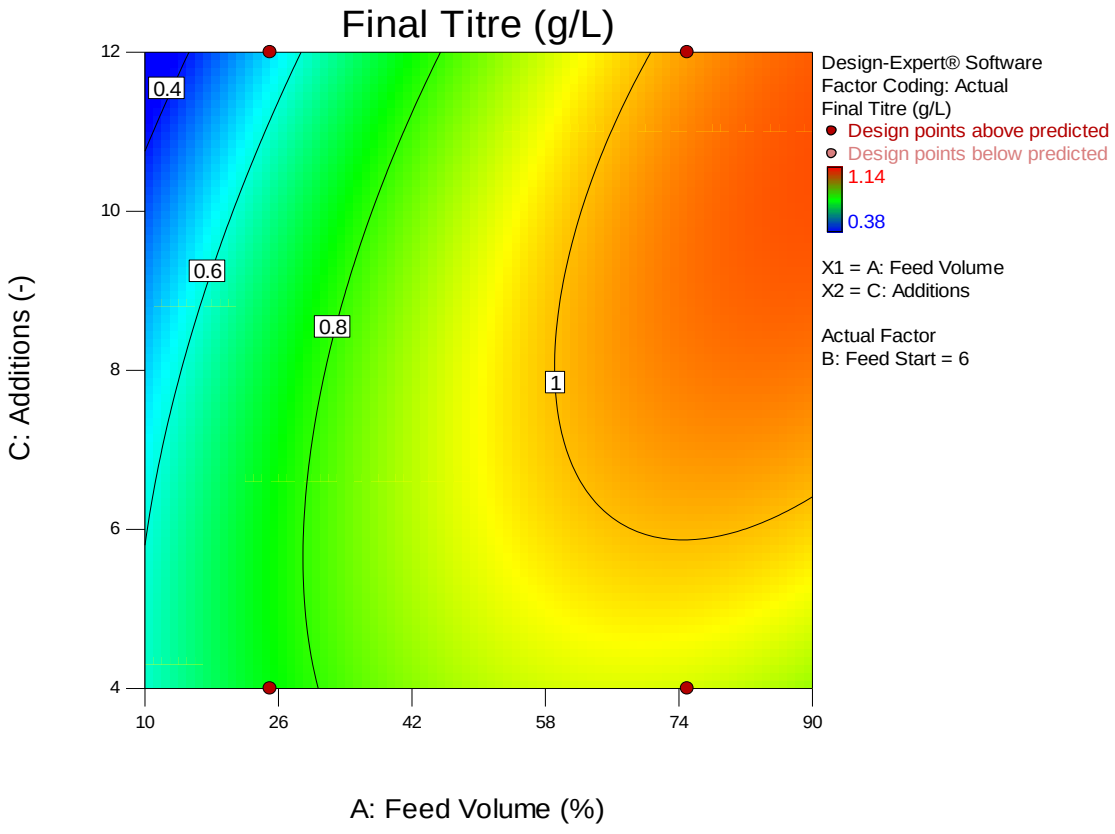

Figure 5.7: ANOVA table (top) and contour plot (bottom) of the response model for the final titre. For the contour plot, the feed start was set to the predicted optimum of 6 days.

Response 2 Yield

ANOVA for Response Surface Reduced Linear model

Analysis of variance table [Partial sum of squares - Type III]

Source	Sum of Squares	df	Mean Square	F Value	p-value Prob > F	
Model	17.44	2	8.72	13.77	0.0003	significant
A-Feed Volur	*12.41*	*1*	*12.41*	*19.58*	*0.0004*	
B-Feed Start	*5.04*	*1*	*5.04*	*7.95*	*0.0118*	
Residual	10.77	17	0.63			
Lack of Fit	*9.50*	*12*	*0.79*	*3.10*	*0.1099*	*not significant*
Pure Error	*1.27*	*5*	*0.25*			
Cor Total	28.22	19				

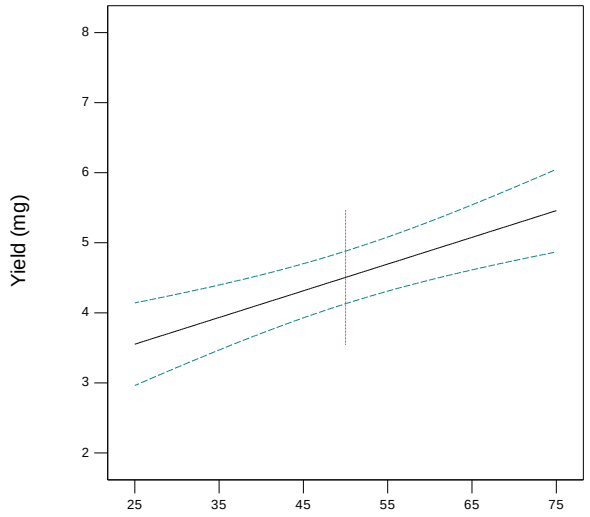

Design-Expert® Software
Factor Coding: Actual
Yield (mg)
---- 95% CI Bands

Actual Factors
A: Feed Volume = 50
B: Feed Start = 3.94595
C: Additions = 7.89189

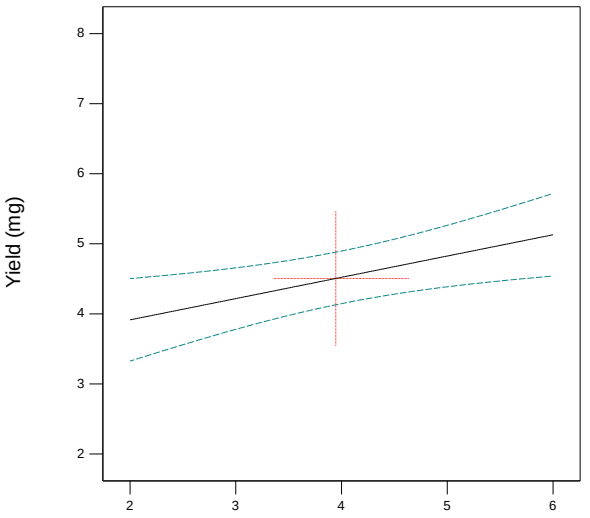

Figure 5.8: ANOVA table (top) and line plots for the feed volume (middle) and the feed start (bottom) of the response model for the final product yield.

Response 4 STY

ANOVA for Response Surface Reduced Quadratic model

Analysis of variance table [Partial sum of squares - Type III]

Source	Sum of Squares	df	Mean Square	F Value	p-value Prob > F	
Model	1812.75	7	258.96	12.52	0.0001	significant
A-Feed Volur	*503.78*	*1*	*503.78*	*24.36*	*0.0003*	
B-Feed Start	*68.01*	*1*	*68.01*	*3.29*	*0.0948*	
C-Additions	*4.18*	*1*	*4.18*	*0.20*	*0.6612*	
BC	*330.24*	*1*	*330.24*	*15.97*	*0.0018*	
A^2	*453.83*	*1*	*453.83*	*21.94*	*0.0005*	
B^2	*246.91*	*1*	*246.91*	*11.94*	*0.0048*	
C^2	*380.44*	*1*	*380.44*	*18.40*	*0.0011*	
Residual	248.17	12	20.68			
Lack of Fit	*173.94*	*7*	*24.85*	*1.67*	*0.2951*	*not significant*
Pure Error	*74.23*	*5*	*14.85*			
Cor Total	2060.92	19				

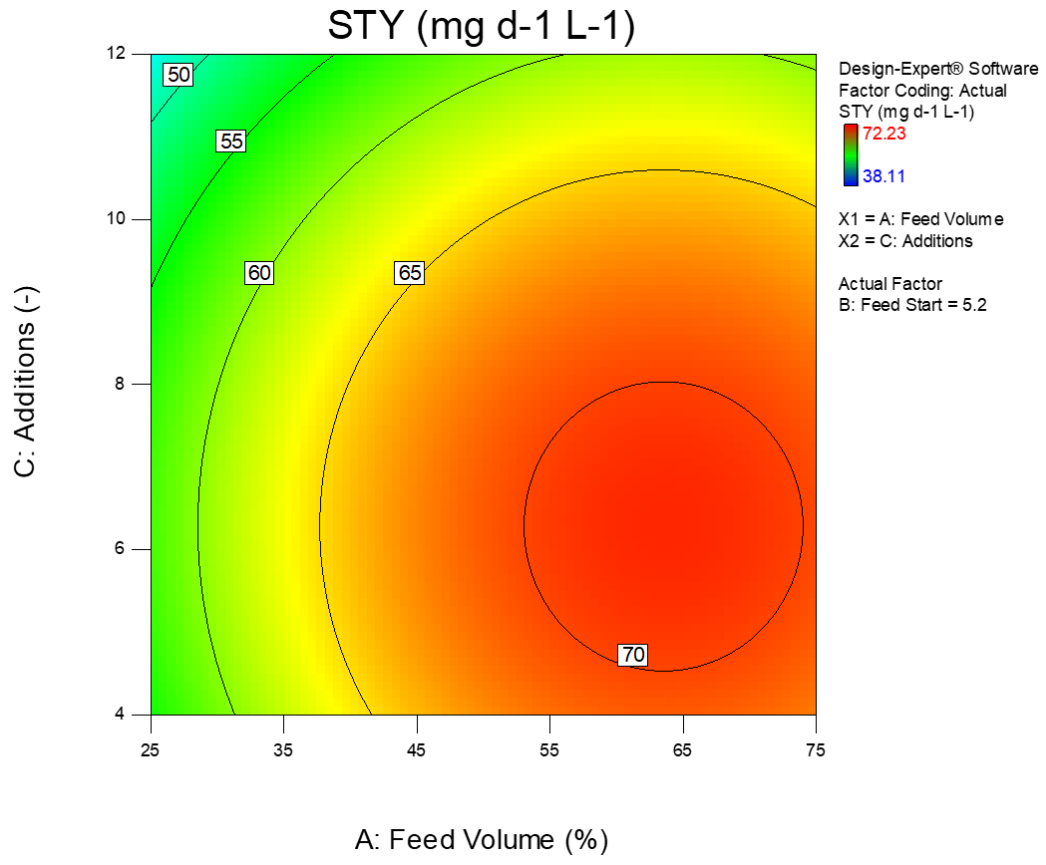

Figure 5.9: ANOVA table (top) and contour plot (bottom) of the response model for the final space-time-yield. For the contour plot, the feed start was set to the predicted optimum of 5.2 days.

After evaluating the response models, an optimisation of the STY was deemed most suitable. The model for the antibody yield lacked in predictive power and the optimal final titre was not captured by the investigated design space. More importantly, a maximum final titre was predicted for long-running processes with high volumes of feed. In a manufacturing setting, a long process duration may not be desirable, if the final product concentration is not substantially higher. A shorter running process with a slightly lower final titre may be more profitable per annum, because the number of batches can be increased if the bioreactor turnaround allows. By considering the timeframe in which the product was generated, the STY helps to identify the feeding regime that generates the highest amount of product in the shortest amount of time (Bausch, Schultheiss and Sieck, 2019). The bolus fed-batch protocol was therefore optimised for the maximum STY. The following section investigated whether the prediction of the model holds true by running the predicted optimum condition in the micro-Matrix.

5.4. Validation of the optimised feeding strategy at the small-scale

Prior to scale-up, the STY-optimised feeding strategy was repeated at the small scale to confirm the validity of the predictive model. To increase confidence in the results, a high replication (n = 11) was chosen.

As shown in Figure 5.10, the cells entered the stationary phase around day 8 with a maximum VCC of 1.45 ± 0.08 x 10^7 cells mL^{-1}. The stationary phase was maintained for roughly 4 days, before the cell count and viability declined and the process came to a halt on day 13. Before that, the viability was sustained above 80% throughout the cultivation. The titre showed the steepest increase during the exponential growth phase and reached a final value of 0.88 ± 0.06 g L^{-1} after 13 days of cultivation. The final product yield together with the process duration achieved an STY of 67.7 ± 4.6 mg d^{-1} L^{-1}, which is in good agreement with the predicted STY of 71.0 mg d^{-1} L^{-1}.

Figure 5.11 shows the metabolic footprint of GS-CHO cells grown with the optimised feeding regime. The concentration of glucose was seemingly maintained above 1 g L^{-1} for the majority of the cultivation. However, samples were taken after each feed addition; the concentration of glucose prior to feeding is estimated to be substantially lower. Glucose reached depletion levels

around day 12 of the cultivation, two days after the final addition of feed medium. The lactate concentration reached its peak value of 2.52 ± 0.20 g L^{-1} on day 7 of the cultivation. Subsequently, lactate was consumed and fully depleted by day 13. Glutamate was consumed steadily and reached depletion on day 8 of the cultivation.

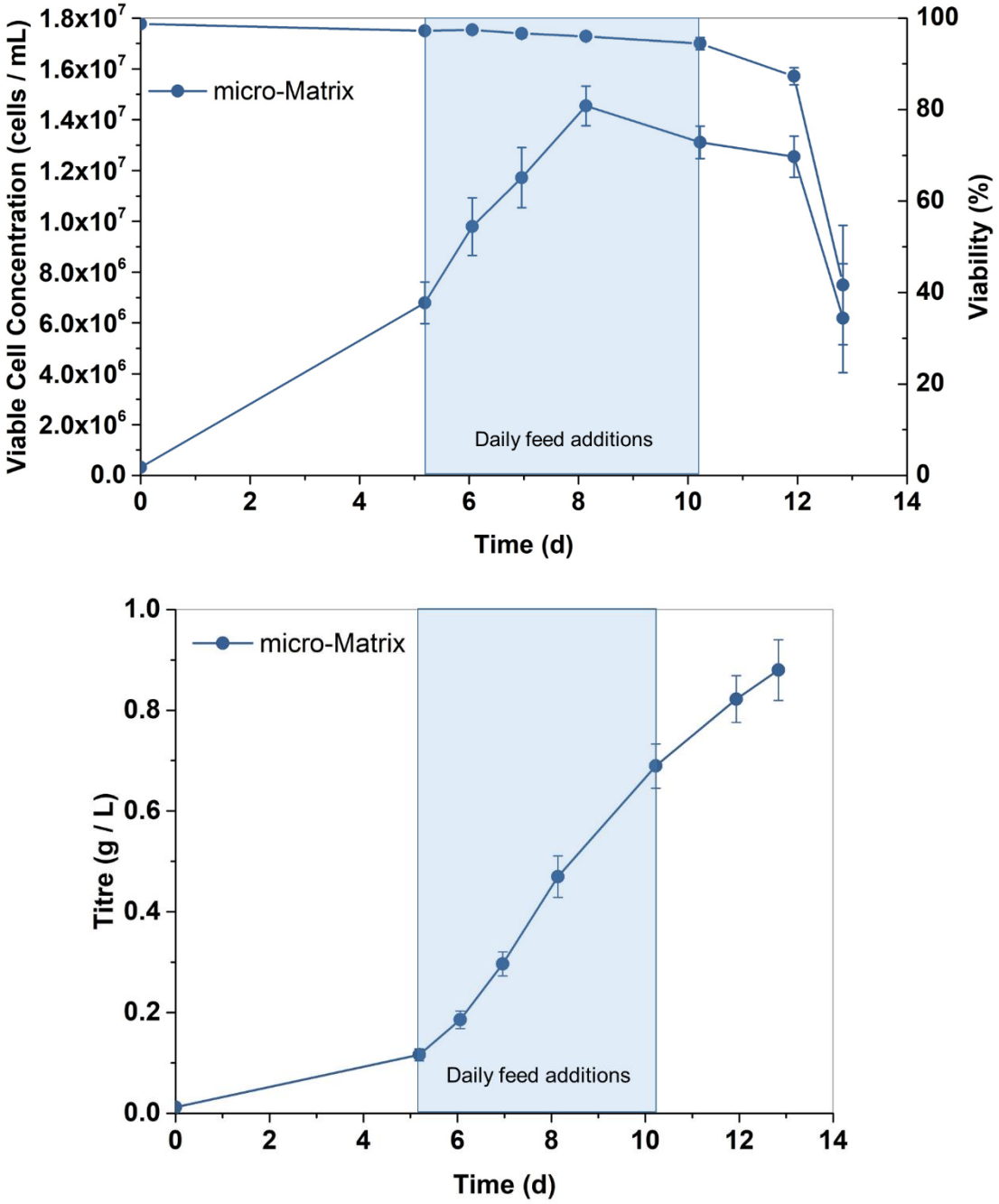

Figure 5.10: Growth (top) and IgG4 production (bottom) kinetics of the optimised bolus fed-batch strategy for GS-CHO cells grown in the micro-Matrix at a shaking speed of 250 rpm, 4 mL working volume, and active control of pH (7.2), DO (30%), and temperature (37°C). Error bars represent one standard deviation about the mean (n = 11).

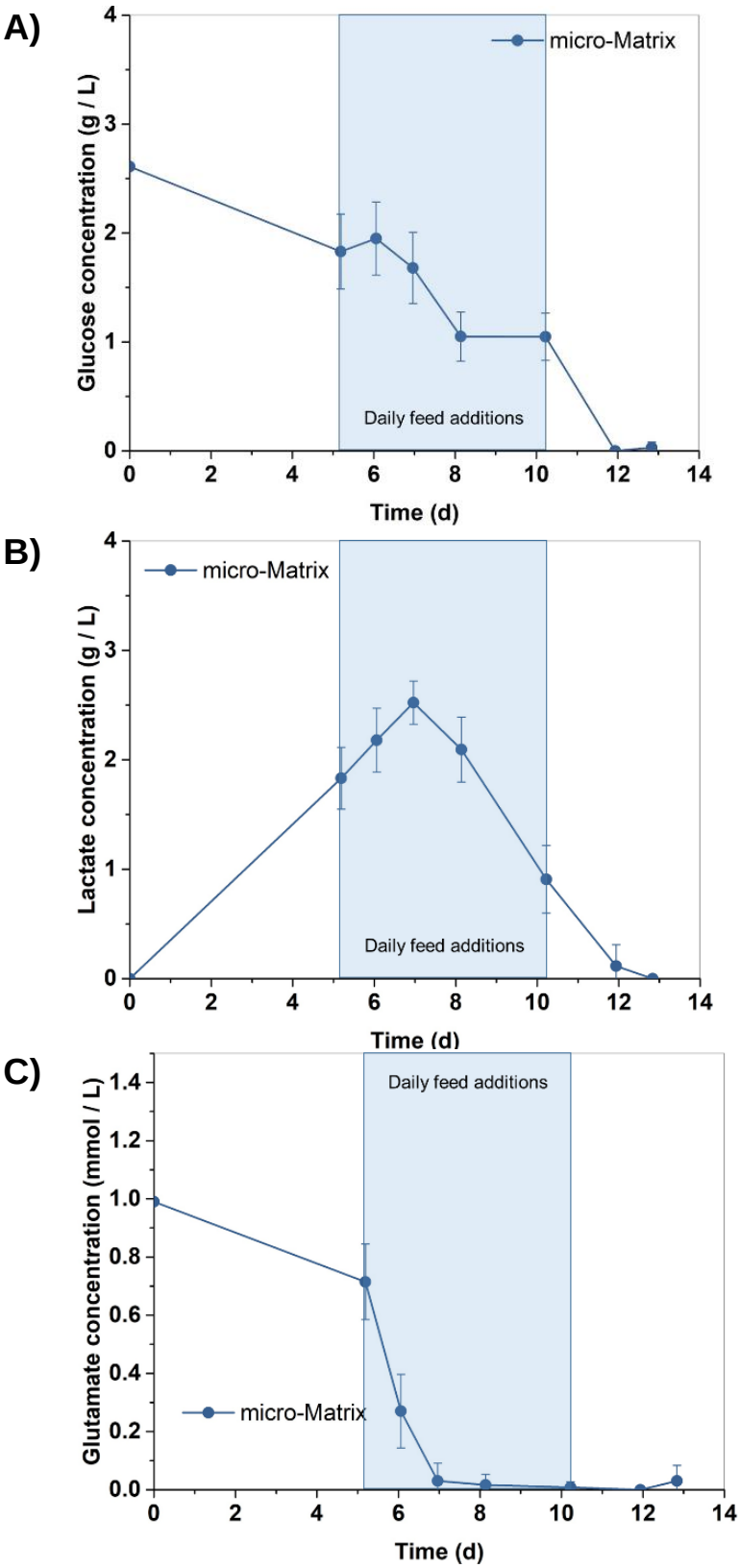

Figure 5.11: Progression of the glucose (A), lactate (B), and glutamate (C) concentration under optimised bolus fed-batch conditions for GS-CHO cells grown in the micro-Matrix at a shaking speed of 250 rpm, 4 mL working volume, and active control of pH (7.2), DO (30%), and temperature (37°C). Samples were taken after the feed addition. Error bars represent one standard deviation about the mean (n = 11).

Running the optimised bolus fed-batch strategy at the small-scale confirmed the model predictions. The optimised feeding regime was therefore scaled to the 5 L STR in the next section, using the scaling strategy established in Chapter 4.

5.5. Scale-up of the optimised feeding strategy

In this experiment, the optimised feeding strategy was scaled up to the benchtop STR using the previously established scaling strategy in the high CO_2 configuration. To assess the success of the scale translation, the growth, IgG4 production, and metabolism were compared to the results obtained at the small scale. The results were also compared to the original fed-batch strategy, to evaluate the success of the optimisation.

Figure 5.12 shows the growth kinetics of the optimised feeding strategy in comparison to the standard feeding regime. Overall, the growth and viability profiles were scalable from the micro-Matrix to the 5 L STR and only showed very minimal differences, such as a slightly earlier onset of cell death in the micro-Matrix. The optimised feeding regime achieved a moderate increase of the maximum VCC and was able to maintain a longer stationary phase, which resulted in an increased cIVCC (Table 5.3) compared to the standard fed-batch protocol.

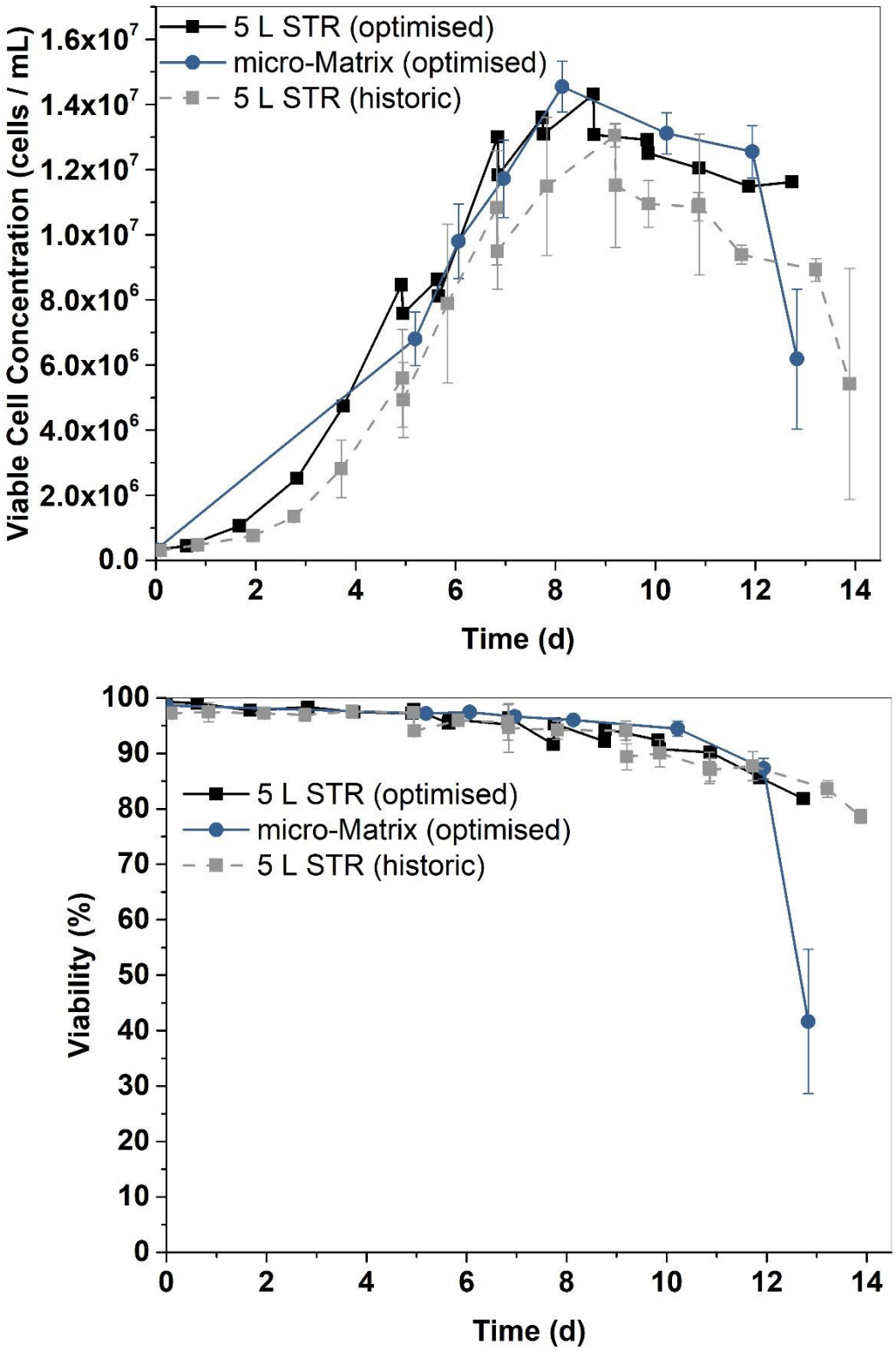

Figure 5.12: Growth (top) and viability (bottom) of GS-CHO cells grown with the optimised feeding regime in the micro-Matrix (●) and the 5 L STR (■), in comparison to historic data of the cells grown with the original feeding regime in the 5 L STR (■). Data points represent the mean ± standard deviation (5 L STR optimised: n = 1; micro-Matrix optimised: n = 11; 5 L STR historic: n = 2).

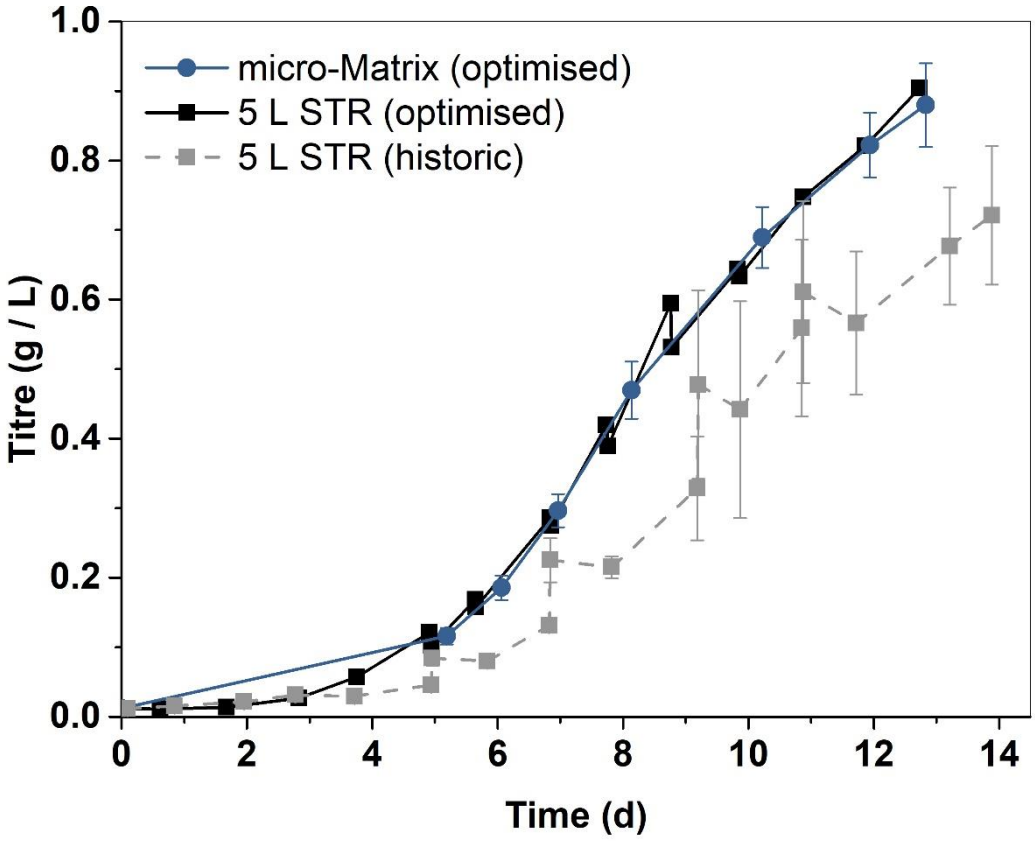

Figure 5.13: Progression of the titre for GS-CHO cells grown with the optimised feeding regime in the micro-Matrix (●) and the 5 L STR (■), in comparison to historic data of the cells grown with the original feeding regime in the 5 L STR (■). Data points represent the mean ± standard deviation (5 L STR optimised: n = 1; micro-Matrix optimised: n = 11; 5 L STR historic: n = 2).

The titre (Figure 5.13) showed analogous behaviour between the scales and was found to be improved substantially compared to the standard fed-batch protocol. By optimising the schedule of bolus feed additions, it was possible to generate 25.0% more mAb product, while reducing the process duration by one day. The final product yield together with the process duration achieved an STY of 69.6 mg d^{-1} L^{-1}, which is in excellent agreement with the predicted STY of 71 mg d^{-1} L^{-1} and 25.4% higher compared the standard protocol with an STY of 55.4 mg d^{-1} L^{-1}.

The progression of the glucose concentration (Figure 5.14) was largely comparable between the scales. It is important to note that for the 5 L STR, samples were taken before and after feed additions, resulting in oscillations of the glucose profile on feeding days. For the micro-Matrix,

samples were only taken after feeding, causing a steadier profile of the glucose concentration. In earlier scale comparisons (see section 4.5), dissimilarities of the metabolic profiles were thought to be caused by differences in the sample dilutions. For this experiment, all samples of the 5 L STR and the micro-Matrix were diluted 3 times prior to measurement in the bioanalyser. Although the readings were comparable between the scales, they may not reflect the actual concentrations in the cell broth. The initial glucose concentration after inoculation should approximate the concentration of the basal medium CD CHO (~6 g L^{-1}). However, for the 5 L STR and the micro-Matrix readings of only 3.24 g L^{-1} and 2.61 g L^{-1} were obtained, respectively. An underestimation of the actual concentrations should therefore be expected and the direct comparison to the historic fed-batch strategy treated with caution.

Table 5.3: Growth and production parameters of GS-CHO cells grown under optimised and non-optimised feeding regimes at different scales. Data represent the mean ± standard deviation (5 L STR optimised: n = 1; micro-Matrix optimised: n = 11; 5 L STR historic: n = 2).

	5 L STR (optimised)	**micro-Matrix (optimised)**	**5 L STR (historic)**
Max. VCC (x 10^6 cells mL^{-1} d^{-1})	14.3	14.5 ± 0.1	11.5 ± 1.9
Cumulative IVCC (x 10^6 cells mL^{-1} d^{-1})	106.5	110.1 ± 0.1	96.5 ± 9.0
μ_{max} (d^{-1})	0.46	0.47 ± 0.01	0.45 ± 0.04
Final titre (g L^{-1})	0.90	0.88 ± 0.06	0.72 ± 0.1
average q_{mAb} (pg $cells^{-1}$ d^{-1})	8.5	8.0 ± 0.6	7.7 ± 1.3
STY (mg d^{-1} L^{-1})	69.6	67.7 ± 4.6	55.4 ± 4.5

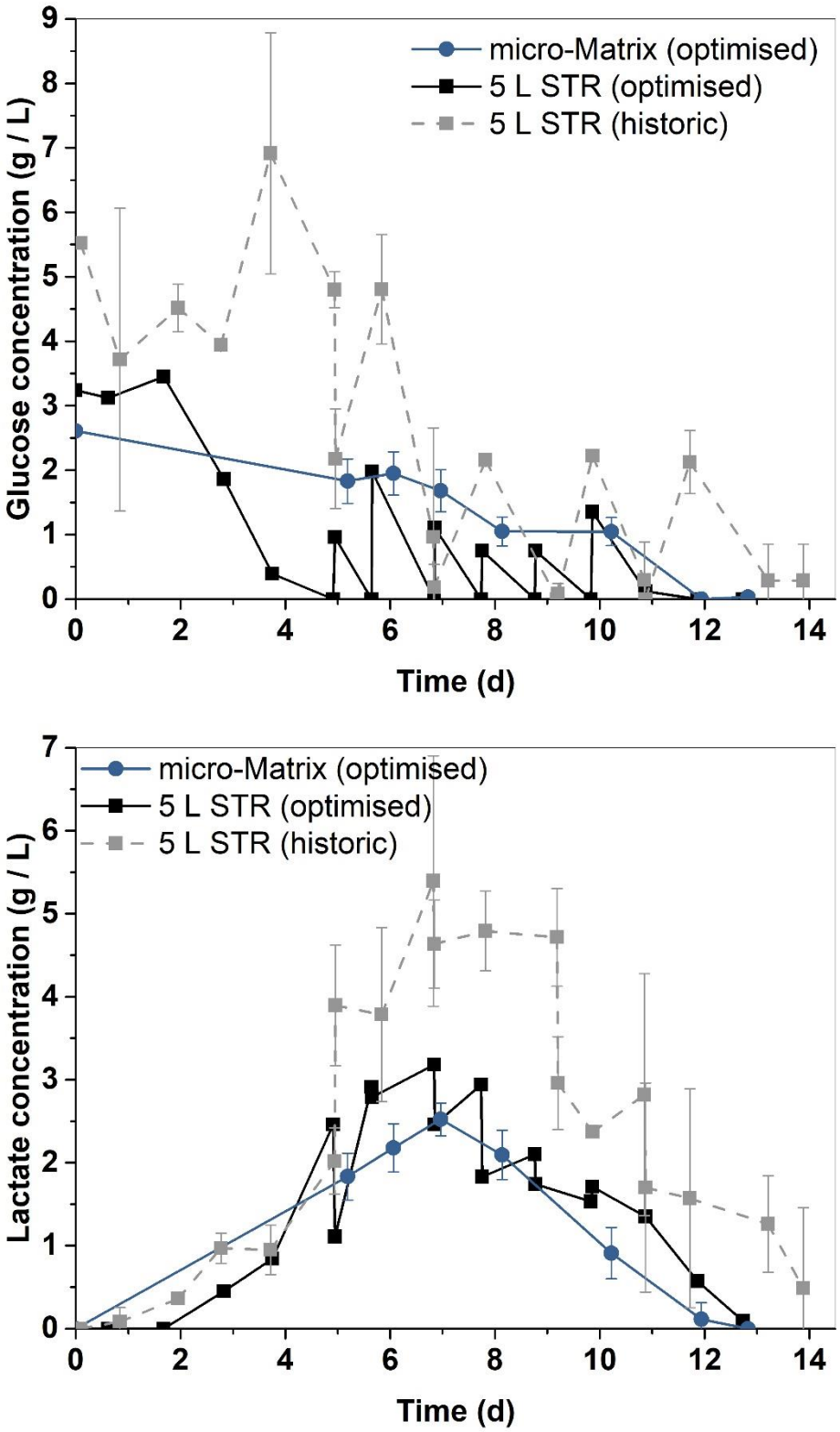

Figure 5.14: Progression of the glucose (top) and lactate (bottom) concentration GS-CHO cells grown with the optimised feeding regime in the micro-Matrix (●) and the 5 L STR (■), in comparison to historic data of GS-CHO cells grown with the original feeding regime in the 5 L STR (■). Data points represent the mean ± standard deviation (5 L STR optimised: n = 1; micro-Matrix optimised: n = 11; 5 L STR historic: n = 2).

Similarity was also found for the concentration of lactate between the micro-Matrix and 5 L STR. In both bioreactors, the highest concentration of lactate (5 L STR: 3.18 g L^{-1}; micro-Matrix: 2.5 g L^{-1}) was reached after 7 days of the cultivation and lactate was thereafter fully consumed. In contrast, the standard fed-batch strategy yielded a substantially higher maximum concentration of lactate (5.4 g L^{-1}) and an ensuing incomplete lactate consumption. These results may indicate a more favourable lactate metabolism for the optimised feeding strategy, although the differences in sample dilutions present a limitation to the direct comparison as discussed above.

In summary, the optimised bolus fed-batch strategy was successfully scaled up from the micro-Matrix to the 5 L STR. Growth, antibody production, and metabolism were found to be highly comparable between the scales. Furthermore, the optimised feeding regime achieved a 25.0% increase of the final titre and a 25.4% increase of the STY. However, to gain further confidence in the outcome of the optimisation, the process should be replicated in the 5 L STR. Additionally, the glycoprofile of the resulting antibodies could be investigated to assess whether the glycosylation was also comparable.

5.6. Conclusion

In this chapter, the feeding strategy of Chapter 3 was optimised using a combination of high-throughput scale-down cell culture technology and DoE methodology. First, several modes of bolus and semi-continuous feed additions were compared with the help of the micro-Matrix feeding module, which allowed for the automated addition of feed. As no improvements were found for gradual additions over bolus feeding, further optimisation was based on the manual addition of bolus shots of feed medium. As a result, the feeding module could be used for automated base additions instead, which permitted tighter control of the CO_2 addition profile and in turn improved scalability.

The bolus feeding strategy was optimised within the framework of a circumscribed CCD in which the factors feed start, feed volume, and feed rate were investigated on five levels in 20 runs, including 6 centre point replicates. The different design points yielded a diverse spectrum of process run times and final titres. To prevent a bias towards excessive process durations, the

feeding regime was optimised for the STY. The optimum STY was captured within the design space and predicted for a feed start after 5 days and a feed volume of 64% of the initial working volume, divided into 6 additions on consecutive days. The prediction was affirmed by a highly replicated scale-down experiment and then successfully scaled up to the 5 L STR. Compared to the standard feeding regime, the optimised variation achieved a 25.0% higher final titre, a 25.4% increase of the STY, and a reduction of the run time by 1 day.

Future studies could explore whether alternative feed media or media blending can further improve upon the process productivity or product quality (Fletcher, 2005; Jordan *et al.*, 2013). The high-throughput capability of the micro-Matrix also lends itself to the screening of large libraries of media supplements to assist cellular functions in a more targeted way (Allen *et al.*, 2008; Gramer *et al.*, 2011)

Chapter 6. Investigation of the influence of environmental conditions on T cell expansion and differentiation

Content of this chapter is published in Amini *et al.* (2020)

6.1. Introduction and aim

The clinical success of the recently FDA-approved CAR-T cell therapies Yescarta (Kite-Gilead) and Kymriah (Novartis) for the treatment of B-cell acute lymphoblastic leukaemia (ALL) have led to a sharp increase of research interest in this area (Kalos *et al.*, 2011; Maude *et al.*, 2014; Porter *et al.*, 2015). These products are extremely high in value and their complex manufacturing has to adhere to strict timelines to guarantee a safe and efficacious product. The autologous nature of CAR-T cell therapies invokes a multitude of challenges such as patient-to-patient variability of the starting material's quality and quantity. An efficient and dependable manufacturing process is therefore essential.

However, the available literature often reports T cell expansion under static incubator conditions (Zhan *et al.*, 2013; Bajgain *et al.*, 2014; Mock *et al.*, 2016; Vormittag *et al.*, 2018), which consequently lacks monitoring and control of key parameters such as DO and pH. Furthermore, the influence of these parameters on growth and differentiation of T cells is not comprehensively documented in the literature, while their importance for the process performance of other mammalian cell types has long been recognised (Link *et al.*, 2004; Trummer *et al.*, 2006; Ivarsson *et al.*, 2014, 2015). Emerging allogeneic therapies (Gouble *et al.*, 2014) also necessitate further research into the expansion of T cells under agitated conditions to facilitate scalability.

In this chapter, the expansion of T cells is investigated using microtitre plates and the micro-Matrix system. A 24 deep square well microtitre plate (24 DSW) was employed initially, to explore the effect of agitation on T cell proliferation under incubator conditions. Subsequently, the effect of varying pH, DO, and agitation conditions was examined in more detail as part of a full-factorial design executed in the micro-Matrix.

Chapter aims and objectives:

- Compare agitation and static cultivation of Jurkat T cells under incubator conditions to gain process understanding and aid process design.
- Investigate the impact of pH, DO, and agitation on the proliferation, metabolism, and differentiation of primary T cells grown under controlled conditions within the framework of a full-factorial design.
- Create a predictive model for growth and differentiation and propose optimal cultivation conditions.

6.2. Initial process design

6.2.1. Comparison of static and shaken T cell expansion in microtitre plates

As little published information is available on the expansion of T cells under agitated conditions, an initial study was performed to examine the growth behaviour of an immortalised T lymphocyte cell line, called Jurkat, under static and shaken conditions. The discovery of Jurkat cells was first published by Schneider, Schwenk and Bornkamm (1977) and the cell line was thereafter used extensively to explore T cell signalling (Abraham and Weiss, 2004). The advantages of using an immortal cell line instead of primary T cells are given by the lack of patient-to-patient variability and the elimination of T cell isolation steps prior to the experiment, which drives down the cost of initial experimentation. However, the lack of patient-to-patient variability also presents a disadvantage because the observations made for Jurkat cells may not be transferable to primary T cells and should only be treated as vague indications that require confirmation with primary cells of at least three different donors.

The initial experiment was performed with 24 DSW microtitre plates of the same dimensions as the micro-Matrix cassette, which were cultivated under incubator conditions. To investigate the effect of agitation on the growth kinetics and metabolism of Jurkat cells, one 24 DSW plate was mounted onto an orbital shaker with 25 mm throw, while the other one was placed adjacent to the shaker. As T cells are reportedly shear sensitive (Chen *et al.*, 2019), a variation of the working volume (either 2 mL or 4 mL) was used to create different shear environments. Additionally, some

of the shaken conditions were supplemented with 1% Pluronic F68, which is employed regularly as shear protectant for other mammalian cell types (Oh *et al.*, 1989, 1992; Nienow, 2006). Jurkat cells were seeded at 4 x 10^5 cells mL^{-1} and half of the working volume was replaced with fresh medium after 2, 4, and 5 days of cultivation. Cell counts and metabolite analyses were performed on the cell broth that was extracted as part of the media exchange.

Figure 6.1 shows the growth and viability profiles of the cells under the tested conditions. A lag phase of two days was observed for all tested conditions. Thereafter, static cultivation resulted in the slowest growth with maximum cell densities of 2.7 x 10^6 cells mL^{-1} and 2.2 x 10^6 cells mL^{-1} reached on day 5 for a working volume of 2 mL and 4 mL, respectively. Subsequently, both cell density and viability decreased. For the shaken conditions with a working volume of 2 mL, the growth profile progressed similarly, but on a higher level with maximum cell densities of 3.1 x 10^6 cells mL^{-1} and 3.3 x 10^6 cells mL^{-1} reached on day 5 for cultivations without and with supplementation of Pluronic, respectively. The supplementation with Pluronic did not cause a significantly different maximum cell density ($p < 0.05$). For shaken conditions with a working volume of 4 mL, growth continued after day 5 and resulted in a virtually identical maximum cell density of 3.9 x 10^6 cells mL^{-1} on day 7, while the viability was maintained just above 80%.

Figure 6.2 shows the metabolic profiles of Jurkat cells grown under the tested conditions. Under static and shaken conditions in conjunction with a working volume of 4 mL, glucose was consumed slowest and only reached depletion level on day 5. For shaken cultures with a working volume of 2 mL, glucose depletion was reached earlier on day 4. These differences become more apparent, though not significant ($p > 0.05$), when considering the maximum specific glucose consumption rate (Figure 6.3), which suggests an increase of the glucose consumption with increasing hydrodynamic turbulence. The slow consumption of glucose for shaken cultures with a working volume of 4 mL led to a prolonged availability of glucose, which in turn may explain the extended growth period. At a working volume of 2 mL, on the other hand, early glucose depletion may have limited cell growth, which suggests that more frequent media exchanges could prolong the growth phase for this condition. The lactate production profiles indicate similar trends, but in an inverse fashion and the maximum lactate concentration for all conditions was roughly 1.5 g L^{-1}.

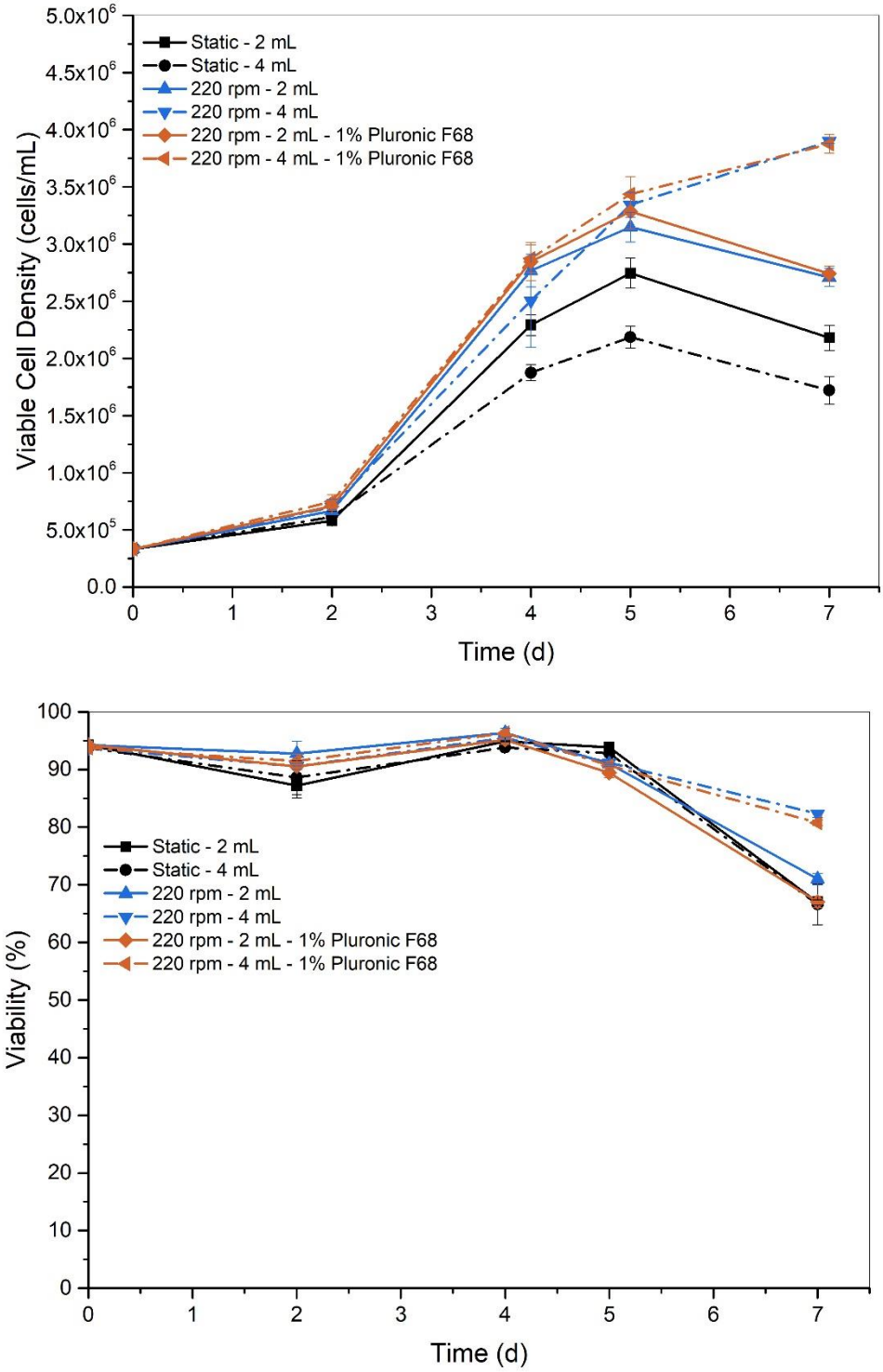

Figure 6.1: Growth (top) and viability (bottom) profiles of Jurkat cells grown under incubator conditions in 24 DSW microtitre plates. The working volume was either 2 mL (continuous lines) or 4 mL (broken lines) and the microtitre plates were either shaken (220 rpm, 25 mm orbital throw) or static. Shaken cultures were either performed with or without supplementation of 1% Pluronic F68. Data points represent one standard deviation about the mean (n = 3).

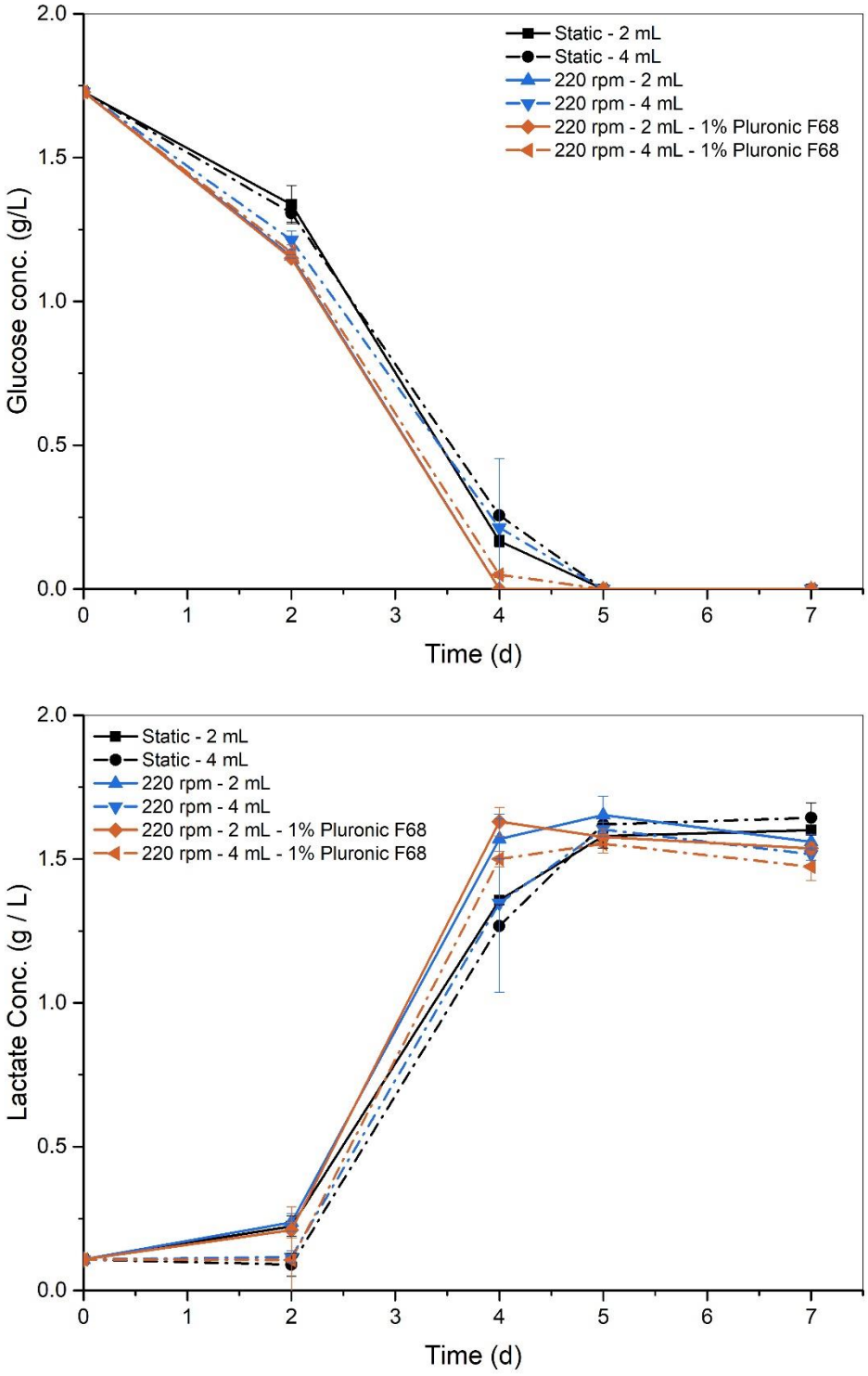

Figure 6.2: Progression of the glucose (top) and lactate (bottom) concentrations of Jurkat cells grown under incubator conditions in 24 DSW microtitre plates. The working volume was either 2 mL (continuous lines) or 4 mL (broken lines) and the microtitre plates were either shaken (220 rpm, 25 mm orbital throw) or static. Shaken cultures were either performed with or without supplementation of 1% Pluronic F68. Data points represent one standard deviation about the mean (n = 3).

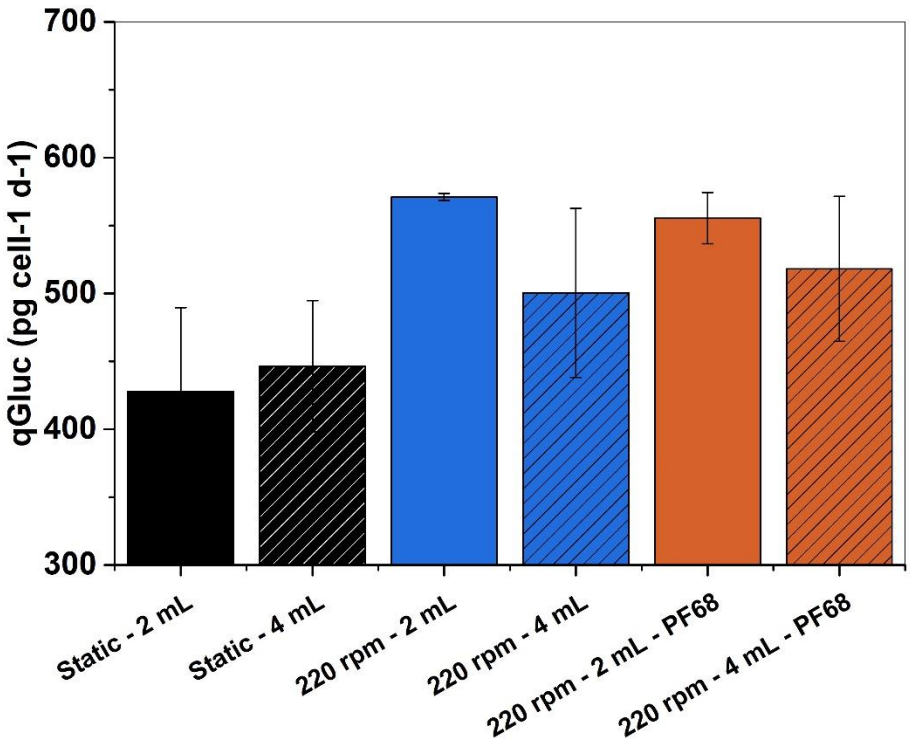

Figure 6.3: Maximum specific glucose consumption rate of Jurkat cells grown under incubator conditions in 24 DSW microtitre plates.

This experiment demonstrates that Jurkat cells can be grown in 24 DSW microtitre plates under shaken conditions. Furthermore, agitation appears to promote cell proliferation and glucose consumption compared to static conditions. The addition of the shear protectant Pluronic F68 did not affect growth or metabolism of the cells, indicating that the shear forces created through agitation were low enough to leave the cells unimpaired. Under shaken conditions, a low working volume led to an increased consumption of glucose and in turn early glucose depletion, which may have caused a premature decline of the VCC. However, these results can only serve as an indication for the expansion of primary T cells. The following experiments will investigate whether primary T cells of healthy donors show a similar preference to a shaken culture environment. Furthermore, the micro-Matrix will be used to monitor and control environmental pH and DO conditions.

6.2.2. Cultivation of primary T cells under controlled conditions

The experiment of section 6.2.1 suggested that agitation could be a useful tool to improve the expansion of T cells if sufficient nutrients are supplied throughout the process to sustain further proliferation. In the experiment of this section, those findings were applied to the expansion of primary T cells from a single healthy donor. As primary cells were expected to be more shear sensitive than Jurkat cells, the shaking speed of the agitated conditions was lowered from 220 rpm to 200 rpm and a working volume of 2 mL was chosen for all conditions. Primary T cells were expanded in 24 DSW microtitre plates under incubator conditions and in the micro-Matrix under controlled pH and DO conditions. In micro-Matrix cultures, the pH was controlled at 6.9, which complies with the pH level found in the tumour microenvironment (Corbet and Feron, 2017) and which was roughly the pH value that cells were cultured at in a comparable study by Costariol *et al.* (2019). The DO was controlled at 25%, which corresponds to the oxygen tension found in lymph nodes (Caldwell *et al.*, 2001).

The primary T cells were revived from liquid nitrogen shortly before the start of the experiment and therefore an extended lag phase compared to the one observed in the Jurkat cultures was expected. Consequently, only one media exchange was performed for cultivations in the 24 DSW plates. However, as the previous experiment revealed potential glucose limitations, alternative media exchange strategies were tested in the micro-Matrix. For the standard protocol, half of the cell broth was exchanged with fresh medium after 4 days of the cultivation. In the enhanced protocol, the media exchange was performed twice, on day 3 and day 5. In the perfusion-mimic protocol, the cells were sedimented through centrifugation and half of the supernatant was exchanged with fresh medium either daily (on day 3 and 4) or twice a day (on day 5 and 6), which was equivalent to a perfusion rate of 0.5 VVD and 1.0 VVD, respectively. This sedimentation-based type of perfusion-mimic approach has been successfully applied to other cell types and cultivation formats (Tregidgo, Micheletti and Pollard, 2017; Kreye *et al.*, 2019; Sewell *et al.*, 2019; Wolf *et al.*, 2019). Table 6.1 outlines the process flow sheets for each condition.

As illustrated in Figure 6.4, the growth of primary T cells in the 24 DSW was slightly, but not significantly ($p > 0.05$), improved through agitation and the cells continued to proliferate at a slow

rate until the final day of the cultivation. The maximum VCC on day 7 was 1.73 x 10^6 cells mL^{-1} and 1.90 x 10^6 cells mL^{-1} for static and dynamic 24 DSW cultures, respectively. The introduction of pH and DO control in the micro-Matrix, led to an initial improvement of the cell growth, but the final density of 1.86 x 10^6 cells mL^{-1} was not significantly improved compared to the uncontrolled 24 DSW cultures ($p > 0.05$). An additional media exchange caused the final VCC to increase to 2.44 x 10^6 cells mL^{-1}; the increase, however, was not found to be significant compared to the micro-Matrix cultivation with a single media exchange ($p > 0.05$). In contrast, the perfusion-mimic process achieved a considerably improved final VCC of 5.50 x 10^6 cells mL^{-1}, which was significantly higher compared to the micro-Matrix cultivation with two media exchanges ($p = 0.004$, t-test). The favourable cultivation environment for this condition was also reflected by the high viability, which was maintained above 90% for the duration of the experiment.

The glucose profiles (Figure 6.5) indicated a similarly rapid consumption of glucose as previously shown for Jurkat cells (section 6.2.1). With one or two media exchanges, glucose was either depleted or close to depletion levels early in the process. With a perfusion-mimic approach, glucose could be maintained above depletion level for the duration of the experiment. These findings suggest that further proliferation for the other conditions was suppressed due to glucose limitation and a more frequent media exchange is pivotal to improve upon the final cell density.

Table 6.1: Process flow of primary T cell cultures with one or two media exchanges or a perfusion-mimic approach. Cells were not retained in the media exchange conditions, while for the perfusion-mimic process cell retention was achieved via centrifugation. Basal and feed medium was RPMI 1640 supplemented with IL-7, IL-15, and Dynabeads at a bead-to-cell ratio of 3:1. VVD: vessel volume per day; wv: working volume.

Day	**0**	**1**	**2**	**3**	**4**	**5**	**6**	**7**
1 Exchange					0.5 wv change			
2 Exchanges				0.5 wv change		0.5 wv change		
Perfusion-mimic	Batch phase			0.5 VVD		1.0 VVD		

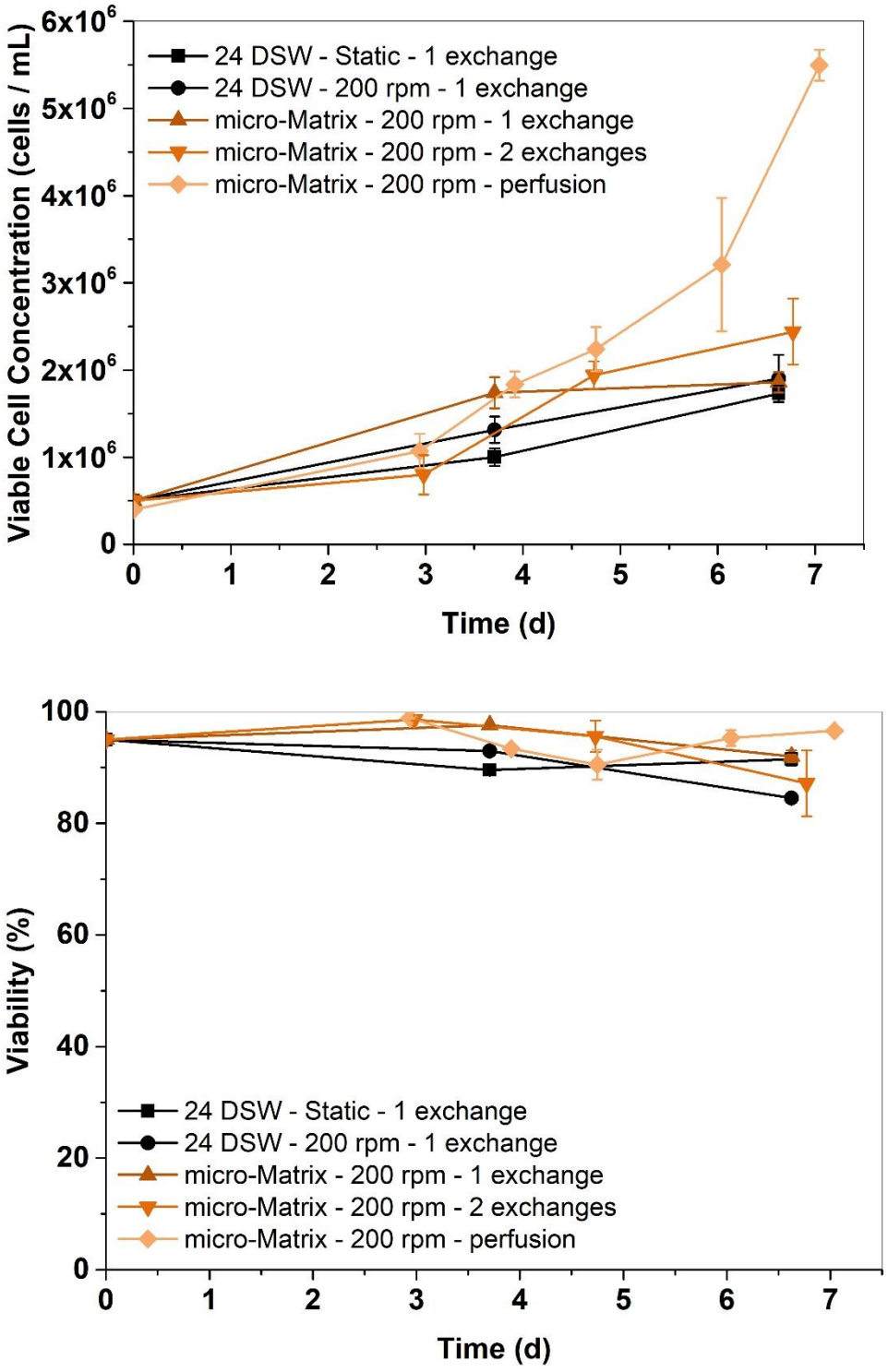

Figure 6.4: Growth (top) and viability (bottom) profiles of primary T cells of the same donor grown under incubator conditions in 24 DSW microtitre plates and the micro-Matrix. The working volume was 2 mL and the cultivation was either done under static or shaken conditions. In the micro-Matrix, different frequencies of media exchanges were tested and the pH was controlled at 6.9, the DO at 25%, and the temperature at 37°C. Data points represent one standard deviation about the mean ($n \geq 2$).

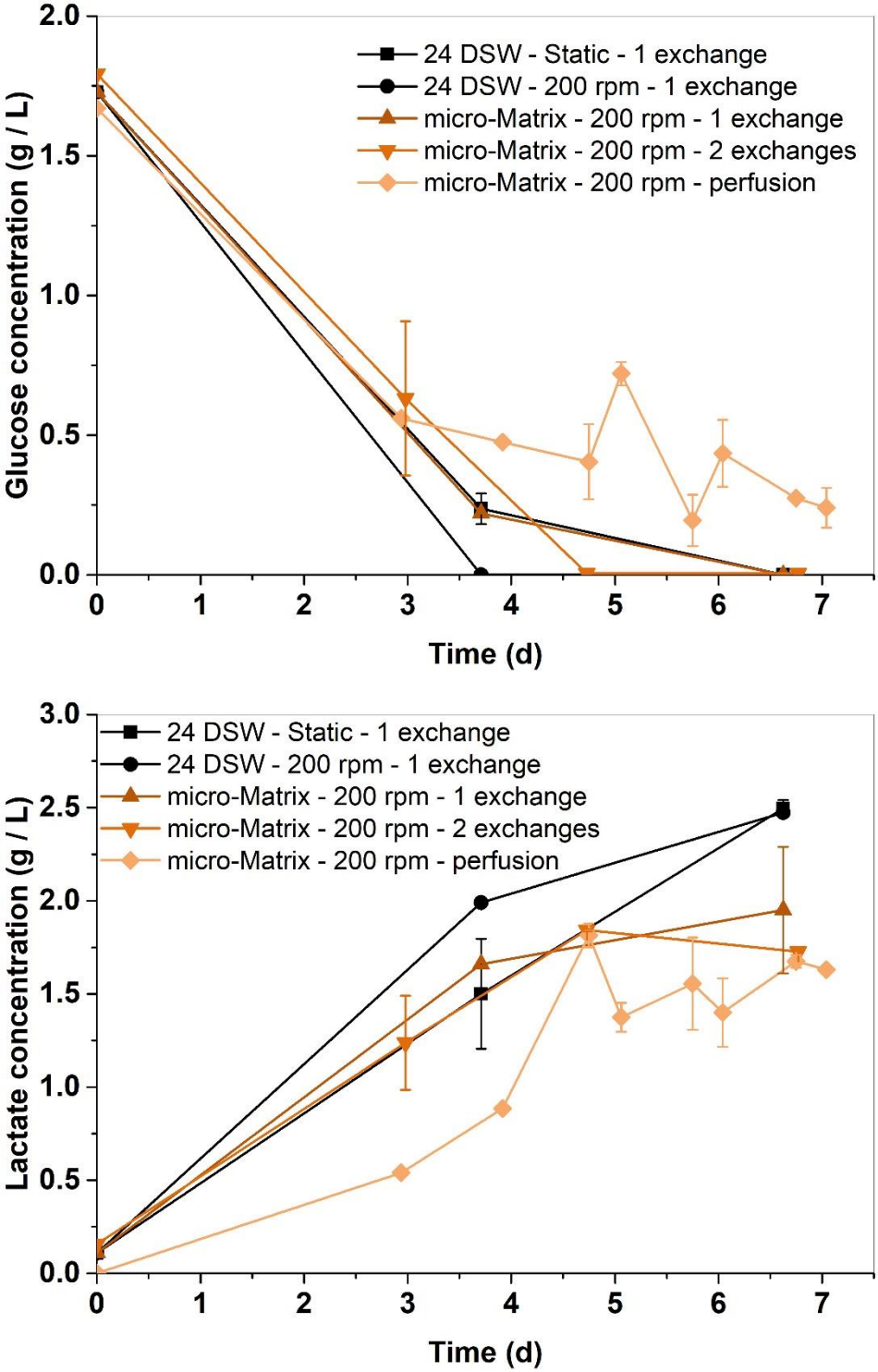

Figure 6.5: Progression of the glucose (top) and lactate (bottom) concentrations of primary T cells of the same donor grown under incubator conditions in 24 DSW microtitre plates and the micro-Matrix. The working volume was 2 mL and the cultivation was either done under static or shaken conditions. In the micro-Matrix, different frequencies of media exchanges were tested and the pH was controlled at 6.9, the DO at 25%, and the temperature at 37°C. Data points represent one standard deviation about the mean (n ≥ 2).

The maximum concentration of lactate for both uncontrolled conditions in the 24 DSW plates was with about 2.50 g L^{-1} slightly, but not significantly ($p > 0.05$), higher compared to the 1.95 g L^{-1} reached in the micro-Matrix cultivation with one media exchange. The lactate concentration was further decreased to a final value of 1.73 g L^{-1} and 1.63 g L^{-1} for micro-Matrix cultures with two media exchanges and the perfusion-mimic approach, respectively. Media exchanges are not only necessary to replenish nutrients in the cultivation broth, but are also needed to reduce the concentration of waste metabolites such as lactate (Kaiser *et al.*, 2015; Costariol *et al.*, 2019). The perfusion-mimic approach has proven successful in providing enough nutrients to sustain comparatively high cell densities and at the same time efficiently removing the accumulated lactate.

The perfusion process was clearly identified as the most favourable mode for the expansion of primary T cells, as it provided enough glucose to sustain growth over the duration of the experiment. The concentration of glucose in RPMI 1640 medium (2.0 g L^{-1}) is low when compared to CD CHO (~6.0 g L^{-1}), for instance. A potential solution to the glucose limitation could be an increase of the glucose concentration in the basal medium. However, without sufficient removal of spent medium, the lactate concentration could reach cytotoxic levels and impair cellular functions. A controlled limitation of the available glucose may therefore be effective at reducing the formation of lactate, which has also often been the focus of process design for other mammalian cell types (Gagnon *et al.*, 2011; Hegde *et al.*, 2012).

The final VCCs of the perfusion process and the static cultures were found to be comparable to similar studies. Costariol *et al.* (2019) reported a maximum final VCC of $4.65 \pm 0.24 \times 10^6$ cells mL^{-1} in a miniature STR under agitated conditions without pH control, while the cell density in static T-flasks under incubator conditions was reported to reach $2.38 \pm 0.25 \times 10^6$ cells mL^{-1}. Those findings highlight the beneficial effect of agitation on the expansion of T cells, which goes contrary to the prevalent assumption that this cell type is particularly sensitive to shear. A key element of successful T cell proliferation is their activation with anti-CD3 / CD28 coated Dynabeads. Costariol *et al.* (2019) found that static cultures achieved higher T cell expansion than agitated cultures at low stirrer speeds, because at low

stirrer speeds the beads may not have been suspended sufficiently, which resulted in a decreased interaction between cells and beads. Judging by the high final VCC achieved in the micro-Matrix, the Dynabeads were in fact suspended together with the cells to a sufficient degree. However, in this experiment only the cells of one donor were tested. Whether the outcome is transferable to other sets of donor cells will be subject of further experimentation.

As the concentration of glucose was limiting in most conditions, the effect of active pH and DO control on the cell growth could not be investigated clearly. In the following experiment, varying setpoints of pH, DO, and shaking speed were assessed using the perfusion-mimic process in the micro-Matrix as part of a full-factorial experimental design.

6.3. The effect of pH, DO, and agitation on the growth and differentiation of T Cells

Previous experiments reiterated the potential benefit of agitation for the expansion of primary T cells. To date, few T cell studies have considered a pH and DO controlled culture environment in bioreactor systems and described its effect on proliferation and differentiation in a systematic fashion (Klarer *et al.*, 2018). Here, the micro-Matrix was employed for the cultivation of primary T cells under varying environmental conditions and the results were used to create predictive models for the identification of ideal culture conditions. For an efficacious T cell product, the phenotype of the cells also needs to be considered (Klarer *et al.*, 2018; Thitilertdecha *et al.*, 2018; Costariol *et al.*, 2019). Therefore, the optimisation also included the phenotypic distribution of the harvested T cell population. Furthermore, growth and differentiation can differ grossly between sets of donor cells (Klarer *et al.*, 2018). To include patient-to-patient variability, cells of three healthy donors were subjected to each condition in this experiment. The experimental procedure followed the protocol outlined in section 2.1.8.

6.3.1. Full-factorial design

To investigate the influence of environmental conditions on the expansion and differentiation of primary T cells, a full-factorial design was used in which the factors pH, DO, and shaking speed were varied over two levels. Five centre point replicates were included to assess quadratic

relationships between the factors and the responses. Each parameter combination was repeated with three sets of different donor cells to include patient-to-patient variability within the model. Each of those replicates was repeated three times to assess biological variability for each set of donor cells throughout the cultivation. Consequently, each design point occupied nine wells in the micro-Matrix cassette. An overview of the full-factorial design is given in Table 6.2 and Table 6.3.

Table 6.2: Three-factor, two-level full-factorial design of the pH, DO, and shaking speed set points.

Factor	Name	Units	Low level (-)	High level (+)
A	pH	pH unit	6.9	7.4
B	DO	%	25	90
C	Shaking speed	rpm	100	200

The pH was varied between 6.9 (-1) and 7.4 (+1). At the low level, the pH was similar to the microenvironment found in the proximity of tumour cells and therefore the environment of the therapeutic target of CAR-T cells (Corbet and Feron, 2017). Furthermore, a pH of ~6.9 also approximates the level around which the pH oscillates in an uncontrolled cultivation environment (Costariol *et al.*, 2019). The high setting of 7.4 was chosen to reflect the pH environment found in healthy tissue (Mordon *et al.*, 1992; Gerweck and Seetharaman, 1996; Erra Díaz, Dantas and Geffner, 2018).

A DO setpoint of 25% (in %air saturation) (-1) was chosen for the low setting, as it complies with the oxygen tension of 0.5 – 4.5% (in %oxygen saturation) in lymphoid tissue (Caldwell *et al.*, 2001), which is a major route of T cell trafficking *in vivo* (Hunter, Teijeira and Halin, 2016). At the other end of the spectrum, a DO of 90% (+1) was representative for the “normoxic” environment that is commonly found for *in vitro* cell cultivations in 5% CO_2 incubators (Wenger *et al.*, 2015) and therefore reflects the cultivation conditions under which primary T cells are frequently expanded.

A low shaking speed of 100 rpm (-1) was chosen to create a low shear environment, while providing sufficient agitation to avoid gradients. An increased shaking speed of 200 rpm (+1),

resulted in a more shear-intensive cultivation environment, which was, as demonstrated previously, still tolerable by the cells. At a working of 2 mL, a shaking speed of 100 and 200 rpm resulted mixing times of 1129 s and 7 s, respectively.

Shaking speed, DO, and pH were mostly well-controlled throughout the experiments (see exemplary data in Appendix II Figure A 4 and Figure A 5). However, pH and DO drifted during sampling and perfusion mimic operations, which is represented by spiking online data once the cultivation had been continued.

Table 6.3: Full-factorial design matrix of three factors investigated on two levels with an additional centre point. Each design point was replicated with cells of three healthy donors.

Pattern	A: pH	B: DO	C: Shaking speed
---	6.9	25	100
+--	7.4	25	100
-+-	6.9	90	100
--+	6.9	25	200
++-	7.4	90	100
+-+	7.4	25	200
-++	6.9	90	200
+++	7.4	90	200
ooo	7.15	57.5	150

The final cell density and the percentage of CD8+ T central memory cells (T_{CM}) were selected as relevant responses for the process optimisation. To quickly reach the therapeutic dose, which can vary between 0.5 – 20 x 10^6 cells kg^{-1} depending on the clinical study (Hay and Turtle, 2017), an efficient expansion process is pivotal. Optimisation of the T cell growth can potentially shorten process timelines and in turn reduce the time between T cell isolation from the patient and the administration of CAR-T cells back into the patient. However, aside from the cell quantity, their quality or phenotypic distribution is of importance as well. Particularly, a high percentage of T_{CM} is often documented to be a good indicator for a positive treatment outcome (Gattinoni *et al.*, 2011; Biasco *et al.*, 2015; Wang *et al.*, 2016).

Significant model effects were selected based on backwards elimination with a *p*-value cut-off of 0.1 (Guy *et al.*, 2013). When necessary, the data sets were transformed based on the

suggestion by the Design Expert software. Throughout the experiments, growth kinetics and metabolism were tracked to evaluate in more detail how each parameter combination influenced the cellular behaviour. In the following section, growth, metabolism, and differentiation are first discussed separately, thereafter predictive DoE models were used to propose ideal culture conditions within the investigated design space.

6.3.2. Growth and metabolism

Initially, primary T cells of all conditions underwent an extended lag phase of about 72 hours (Figure 6.7) as consequence of their recent revival from liquid nitrogen. Following the lag phase, the exponential growth phase ensued, which for most conditions continued until the final day of the cultivation. This suggests that higher harvest VCCs may be possible if the process was carried forward in a similar fashion. However, in a CAR-T cell manufacturing environment, it would not be necessary to prolong a process past the point at which the dose requirement was met. Final cell densities ranged between 1.26 x 10^6 cells mL^{-1} (100 rpm, DO 90%, pH 6.9) and 9.22 x 10^6 cells mL^{-1} (200 rpm, DO 25%, pH 6.9). Lower shaking speeds generally led to a lower final cell density and an earlier onset of the stationary phase. This behaviour was also reflected in the viability, which was maintained above 90% throughout the experiments for a shaking speed of 200 rpm and dropped to 80 - 90% when a shaking speed of 100 rpm was used.

The fold expansion (Figure 6.7) clearly illustrates the separation between agitation conditions. Within the high shaking speed setting, a low pH and low DO as well as a high pH and high DO set point yielded the best fold expansion over the course of the cultivation, which indicates an interaction effect between DO and pH. With a shaking speed of 100 rpm, an increase of the pH appeared to improve the fold expansion significantly.

For other mammalian cell types, the positive effect of mixing on cell proliferation has been documented extensively and largely attributed to improved mixing and oxygen transfer characteristics (Barrett *et al.*, 2010; Betts *et al.*, 2014; Wutz *et al.*, 2018). As discussed previously, this was also shown to be true for the expansion of primary T cells in miniature STRs (Costariol *et al.*, 2019).

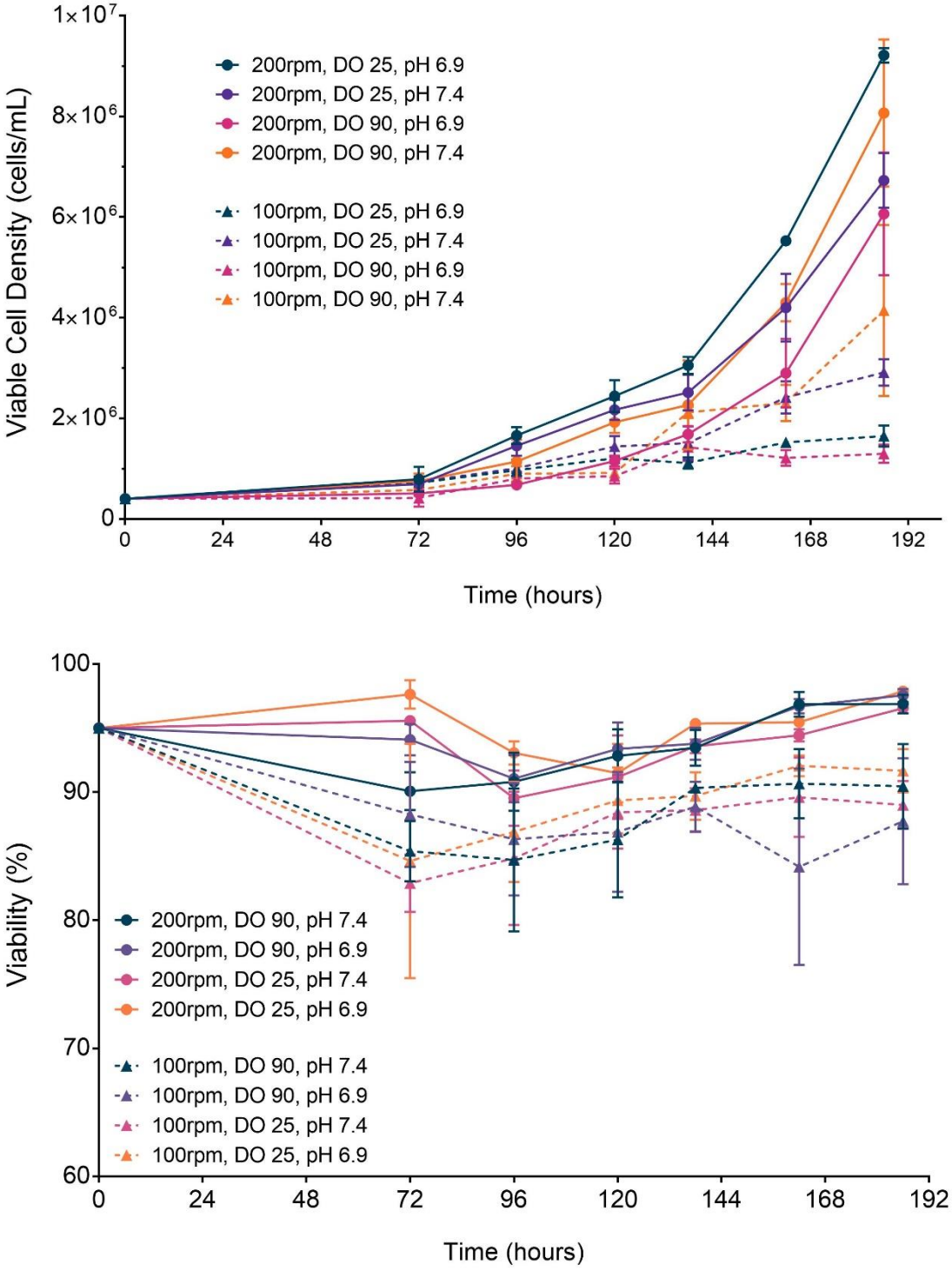

Figure 6.6: Growth (top) and viability (bottom) of primary T cells of three healthy donors grown in the micro-Matrix at shaking speeds of 100 and 200 rpm, pH levels of 6.9 and 7.4, and DO levels of 25 and 90%. The working volume was 2 mL throughout the experiments and the temperature was controlled at 37°C. Cells were cultivated using a perfusion-mimic approach with a VVD of 0.5 (day 3 to 4) and 1.0 (day 5 to 6). Error bars represent one standard deviation about the mean (n ≥ 7).

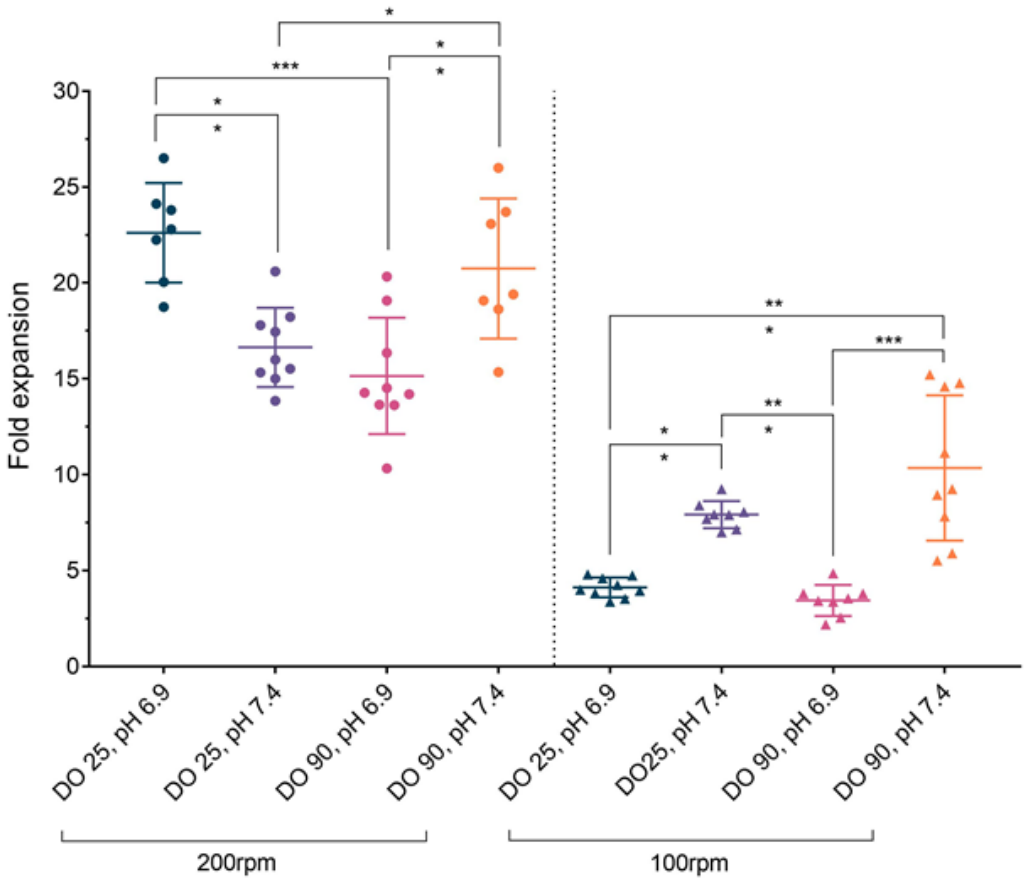

Figure 6.7: Fold expansion of primary T cells of three healthy donors grown in the micro-Matrix at shaking speeds of 100 and 200 rpm, pH levels of 6.9 and 7.4, and DO levels of 25 and 90%. The working volume was 2 mL throughout the experiments and the temperature was controlled at 37°C. Cells were cultivated using a perfusion-mimic approach with a VVD of 0.5 (day 3 to 4) and 1.0 (day 5 to 6). Mean ± SD (n ≥ 7). Significance is indicated when $p \leq 0.05$ (*), 0.01 (**), 0.001 (***), Tukey's test.

In addition to a favourable mixing and oxygen transfer environment, the expansion of primary T cells *in vitro* is reliant upon their activation through Dynabeads (Kershaw, Westwood and Darcy, 2013). This growth stimulus is based on the stochastic event that cells and beads collide in the medium. As Costariol *et al.* (2019) pointed out, the frequency of this event occurring can be increased with higher agitation rates. A combination of differences in mixing and frequency of bead-cell interactions, likely forms the basis for the differences in growth behaviour between the shaking speeds used here. At a low shaking speed of 100 rpm, the cells tended to form large aggregates at the bottom of the well that could be identified from visual observation (data not shown). Such cell clusters can significantly limit the transport of nutrients and oxygen, as shown

for other cell types (Sutherland, 1988; Han *et al.*, 2006), and in consequence lead to the generation of microenvironments within the cultivation vessel. The cultivation conditions in such clusters are essentially uncontrolled and may not reflect the ideal conditions for expansion. Furthermore, the interaction between Dynabeads and cells would be reduced within the aggregate, leading to a lack of activation.

The culture pH had a less pronounced effect on the cell proliferation. At 200 rpm, an interaction effect between the pH and the DO was observed, while at a low shaking speed of 100 rpm, a low pH set point limited cell growth. Literature regarding the effect of varying pH levels on the proliferation of T cells is scarce and direct comparisons are further complicated as most studies were performed with static cultures grown under incubator conditions. Carswell and Papoutsakis (2000) tested T cell growth in T-flasks at pH levels between 7.0 - 7.4 and found that the highest cell densities were achieved for pH values of less than 7.4. Later, Bohnenkamp et al. (2002) demonstrated an inhibited proliferation of T cells expanded in a STR at pH 6.7 and recommended a pH range of 7.0 – 7.3. Calcinotto et al. (2012) tested pH levels between 6.5 – 7.4 and reiterated worse T cell proliferation under acidic conditions.

However, it must be noted that CO_2 was used in order to control the pH. Particularly in the beginning of the cultivation, the concentration differences of dissolved CO_2 in the medium between the high and the low pH set point would have been greatest. Subsequently, the acidification of the medium through the production of lactate would progressively reduce the amount of CO_2 necessary to control the pH. The effect of varying pCO_2 levels on cellular behaviour of other mammalian cell types has been investigated extensively (Kimura and Miller, 1996; Zhu *et al.*, 2008; Darja *et al.*, 2016; Xu *et al.*, 2018). Yet, due to the small sample volumes, no measurements of the pCO_2 were possible as part of the experiments shown here.

As mentioned above, the effect of the DO at a shaking speed of 200 rpm was dependent on the pH level, while at 100 rpm the DO had no effect on the final cell number. The available literature regarding the effect of the DO set point on the expansion of T cells is similarly mixed. Bohnenkamp et al. (2002) observed improved proliferation of T cells grown in spinner flasks at a DO range of

5 – 50% compared to 75%, while another study suggests that atmospheric DO levels favour the proliferation of T cells compared to a physiological DO environment (Atkuri, Herzenberg and Herzenberg, 2005; Atkuri *et al.*, 2007). A later study also found improved growth at atmospheric DO concentrations and attributed this effect to a build-up of cAMP at low DO levels. A build-up of cAMP was further linked to an inhibition of lymphocyte-specific protein tyrosine kinase, which in turn inhibited T cell activation (Larbi *et al.*, 2010). A more recent study by Berahovich et al. (2019) found no difference in the proliferative capacity of CAR-T cells grown under atmospheric and physiological DO conditions.

Figure 6.8 shows the glucose concentrations for each condition throughout the experiment. Samples were taken of the spent medium, prior to each media exchange. Particularly at a shaking speed of 100 rpm, glucose was consumed rapidly and in one case (pH 7.4 and DO 25%) could not be maintained above depletion level. For a combination of 100 rpm, pH 6.9, and DO 90%, the glucose concentration increased towards the end of the experiment, probably because the cells had entered the stationary phase and were no longer expanding. For a shaking speed of 200 rpm, the glucose consumption was slower, and the glucose concentration was maintained above depletion level for most of the tested conditions.

Especially with regards to the specific glucose consumption rates (Figure 6.10), it becomes clear that the environmental conditions had a marked effect on the metabolism of the primary T cells. The conditions that promoted slow cell growth (100 rpm) showed an increased glucose consumption, whereas rapid proliferation coincided with a downregulated glucose consumption. The metabolic state appeared to be a good predictor of the proliferative capacity of the cell population, as the condition with the highest fold expansion (200 rpm, DO 25%, pH 6.9) showed the lowest q_{Gluc} and the condition with the lowest fold expansion (100 rpm, DO 90%, pH 6.9) showed the highest q_{Gluc}.

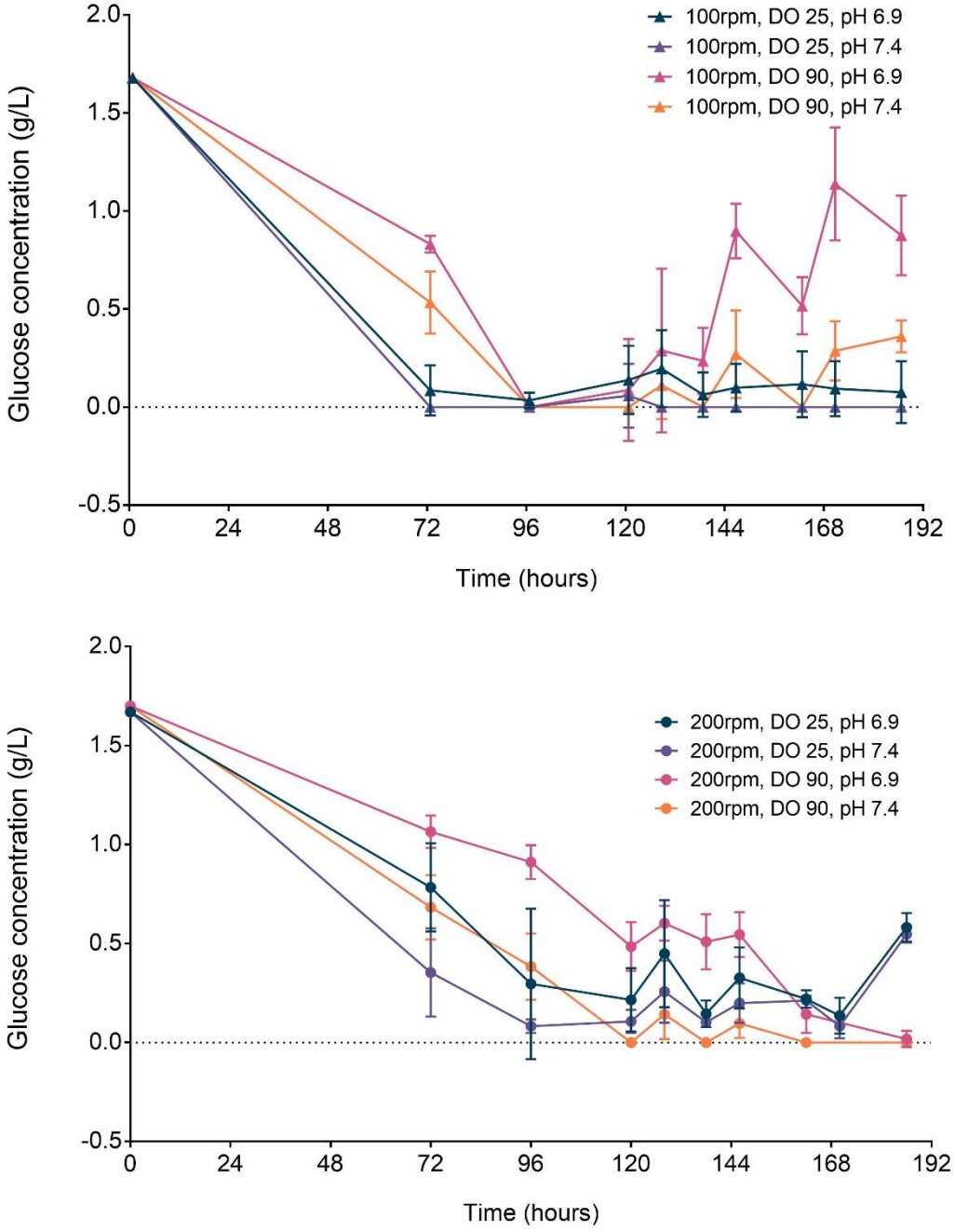

Figure 6.8: Progression of the glucose concentration over the course of the cultivation of primary T cells of three healthy donors grown in the micro-Matrix at shaking speeds of 100 (top) and 200 rpm (bottom), pH levels of 6.9 and 7.4, and DO levels of 25 and 90%. The working volume was 2 mL throughout the experiments and the temperature was controlled at 37°C. Cells were cultivated using a perfusion-mimic approach with a VVD of 0.5 (day 3 to 4) and 1.0 (day 5 to 6). Samples were taken of the spent medium. Error bars represent one standard deviation about the mean (n ≥ 7).

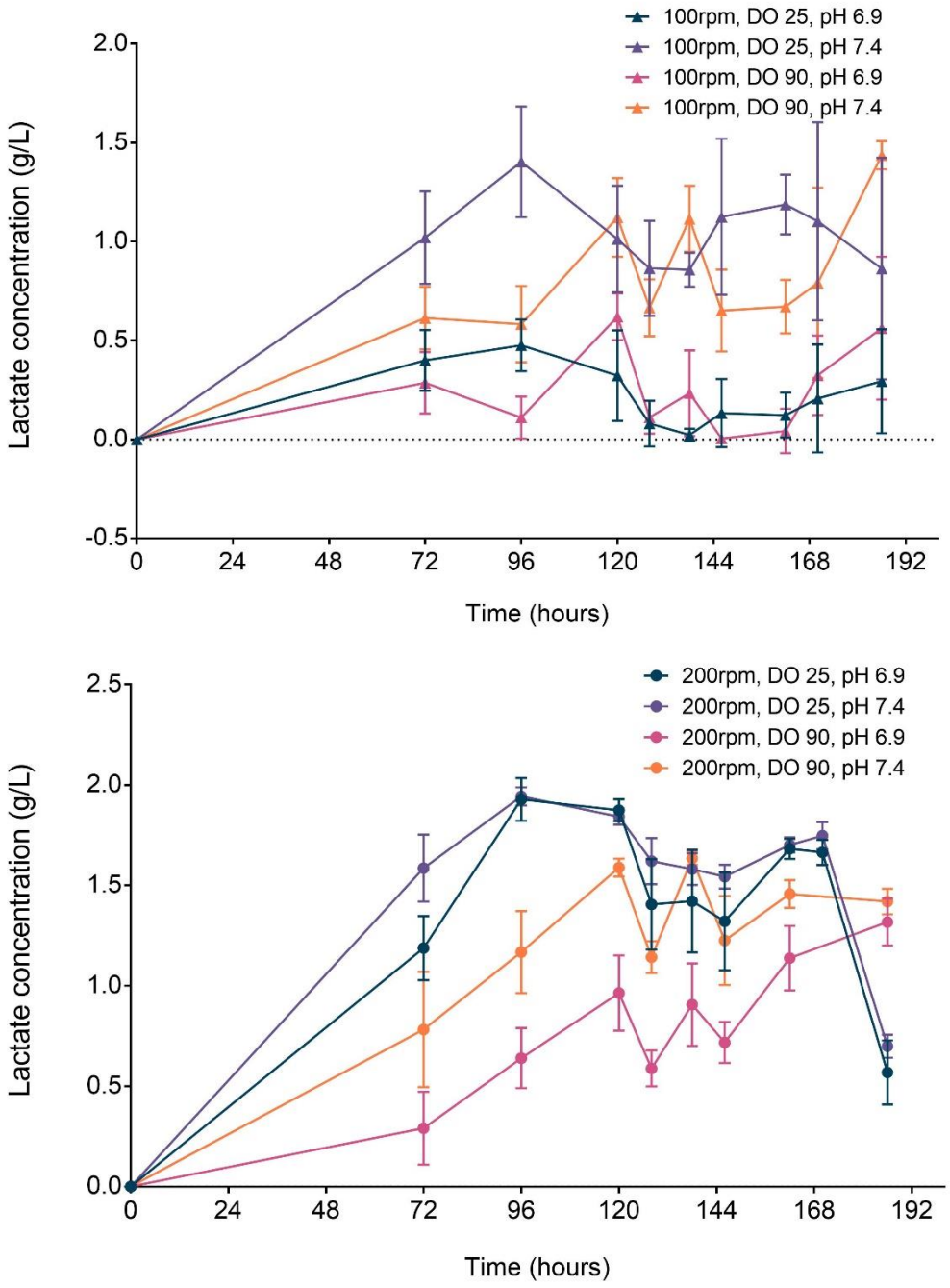

Figure 6.9: Progression of the lactate concentration over the course of the cultivation of primary T cells of three healthy donors grown in the micro-Matrix at shaking speeds of 100 (top) and 200 rpm (bottom), pH levels of 6.9 and 7.4, and DO levels of 25 and 90%. The working volume was 2 mL throughout the experiments and the temperature was controlled at 37°C. Cells were cultivated using a perfusion-mimic approach with a VVD of 0.5 (day 3 to 4) and 1.0 (day 5 to 6). Samples were taken of the spent medium. Error bars represent one standard deviation about the mean ($n \geq 7$).

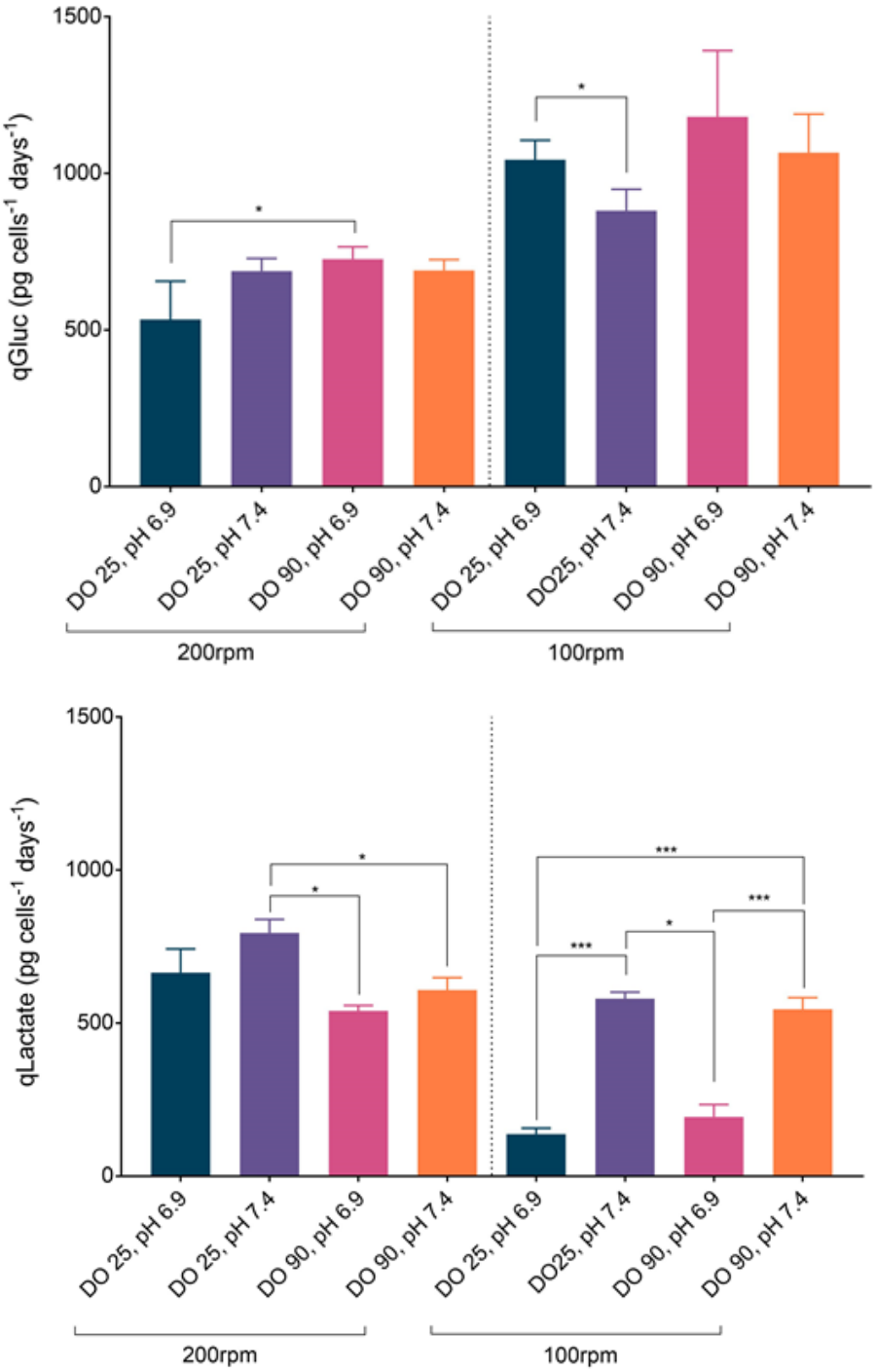

Figure 6.10: Cell specific glucose consumption (top) and lactate production (bottom) of primary T cells of three healthy donors grown in the micro-Matrix at shaking speeds of 100 and 200 rpm, pH levels of 6.9 and 7.4, and DO levels of 25 and 90%. The working volume was 2 mL throughout the experiments and the temperature was controlled at 37°C. Cells were cultivated using a perfusion-mimic approach with a VVD of 0.5 (day 3 to 4) and 1.0 (day 5 to 6). Mean ± SD (n ≥ 7). Significance is indicated when $p \leq 0.05$ (*), 0.01 (**), 0.001 (***),Tukey's test.

The generation of lactate (Figure 6.9) was shown to be lower when a shaking speed of 100 rpm was used. Particularly a low pH set point of 6.9, showed comparatively low concentrations of lactate throughout the cultivation. This relationship becomes more obvious with consideration of the specific lactate production rate (q_{Lac}) in Figure 6.10, which shows that a low pH set point caused a significant reduction of q_{Lac} at a shaking speed of 100 rpm. A reduction of the glycolytic activity of T cells through an acidic culture environment was also found by Pilon-Thomas et al. (2016). Similar observations for other mammalian cell types suggest that a possible mechanism of action could be found in the inhibition of the enzyme phosphofructokinase by elevated proton concentrations, which would in turn downregulate glycolysis (Trivedi and Danforth, 1966; Halperin *et al.*, 1969; Dobson, Yamamoto and Hochachka, 1986; Erecińska, Deas and Silver, 2002). At 200 rpm, the production of lactate was more rapid, but the maximum concentration of lactate did not exceed 2 g L^{-1} in any of the tested conditions. For 200 rpm, no correlation between the pH and the metabolic state of the cells could be established.

Both, q_{Lac} and q_{Gluc}, showed considerable differences between the shaking speeds, where a lower shaking speed generally led to a higher uptake of glucose and a lower lactate formation. The low cell viability at a shaking speed of 100 rpm suggests that the cells were subject to a higher level of stress. A similar stress response was demonstrated in a study by Keane, Ryan and Gray (2003), where CHO cells were stressed using shear, which resulted in a 42% increase of the q_{Gluc} and a reduction of q_{Lac} by 50%.

6.3.3. Phenotypic analysis

The percentage of central memory T cells (T_{CM}) and effector memory T cells (T_{EM}) in the harvest population of each condition on day 7 was analysed via flow cytometry (Figure 6.11). The phenotypic distribution of the cell population was used as a product quality marker, as it has been shown that less differentiated T_{CM} cells exhibit improved proliferative capacity, longevity, and persistence *in vivo* compared to T_{EM} cells (Sallusto *et al.*, 1999; Louis *et al.*, 2011; Kochenderfer *et al.*, 2017). For a shaking speed of 200 rpm, the highest percentage of T_{CM} cells was 32.6 ± 11.3% for a combination of high pH and low DO. However, the T_{CM} data for this condition

show a marked discrepancy between donors. This suggests that the differentiation may be prone to patient-to-patient variability at this condition.

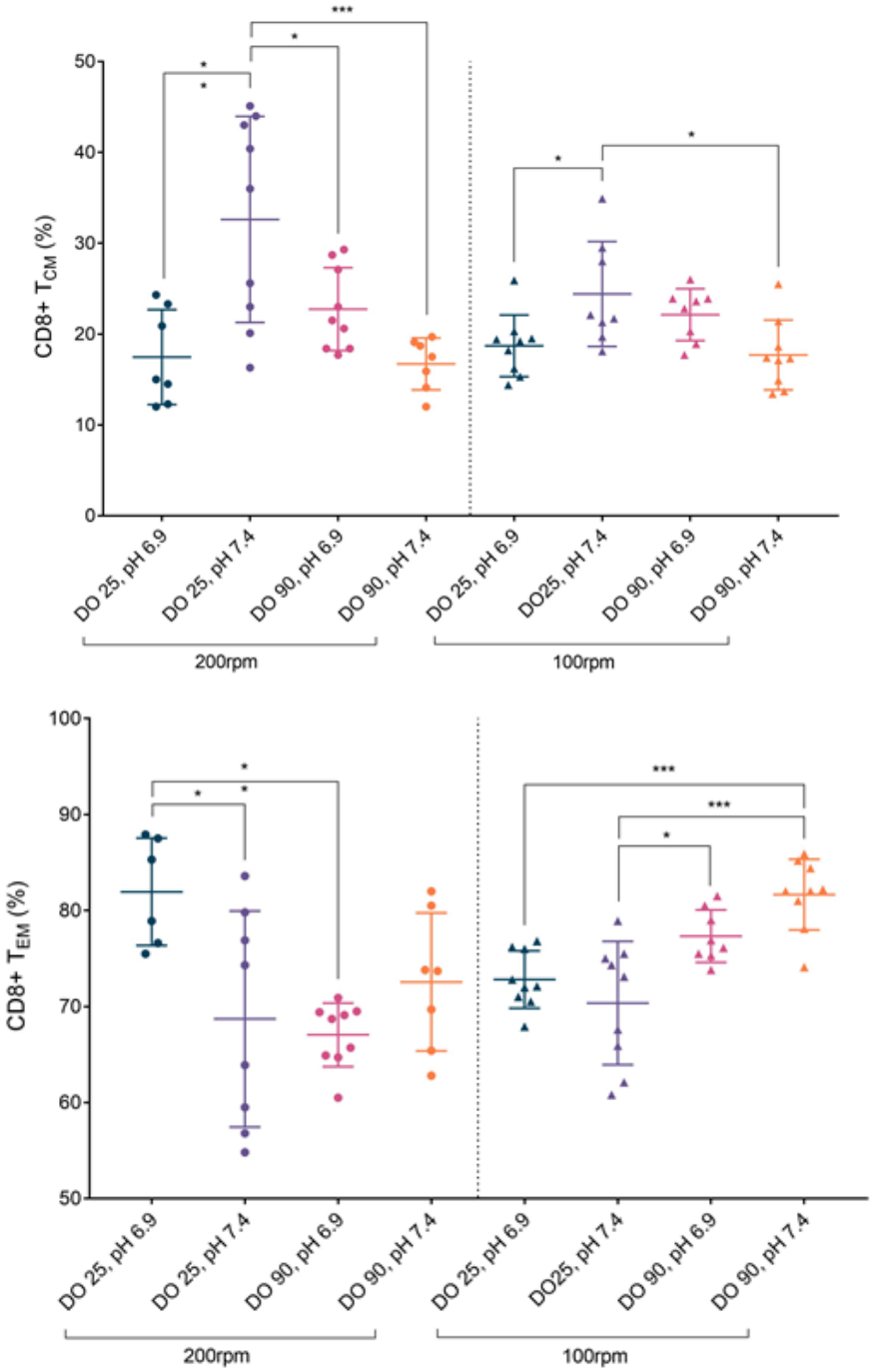

Figure 6.11: Percentage of T_{CM} (top) and T_{EM} (bottom) cells in the harvest population of primary T cells grown in the micro-Matrix at shaking speeds of 100 and 200 rpm, pH levels of 6.9 and 7.4, and DO levels of 25 and 90%. The working volume was 2 mL throughout the experiments and the temperature was controlled at 37°C. Cells were cultivated using a perfusion-mimic approach with a VVD of 0.5 (day 3 to 4) and 1.0 (day 5 to 6). Mean ± SD (n ≥ 7). Significance is indicated when $p \leq 0.05$ (*), 0.01 (**), 0.001 (***),Tukey's test.

A combination of high pH and low DO also yielded the highest percentage of T_{CM} cells at a shaking speed of 100 rpm (24.4 ± 5.8%). Furthermore, the lowest percentage of T_{CM} cells at a shaking speed of 200 rpm correlated with the conditions that showed the highest fold expansion. Between the shaking speeds, the phenotypic distribution was largely comparable. As expected, the percentage of T_{EM} cells follows a similar, but inverse, pattern. T_{EM} cells are further differentiated than T_{CM} cells so that the majority of cells that are not registered as T_{CM} cells, will have assumed a T_{EM} phenotype.

The observed phenotypic distributions were comparable to data published by Costariol *et al.* (2019), who reported a percentage of roughly 20% T_{CM} cells in the harvest population, which was found to be independent of the cultivation platform and rate of agitation. Furthermore, studies by Atkuri *et al.* (2007) and Berahovich *et al.* (2019), who investigated the effect of varying DO set points under incubator conditions, also reported no effect of the DO on the differentiation of T cells.

In the following section, the generated growth and differentiation data were used to create a model based on the environmental conditions to predict the optimal T Cell expansion conditions.

6.3.4. DoE models and optimal cultivation conditions

The contour plots for the predictive models of the final VCC and the final percentage of T_{CM} cells are shown in Figure 6.12. The correlation matrix illustrated in Figure A 7 of Appendix II provides further detail regarding the relation of input and output factors. For the model of the VCC (Table 6.4), shaking speed and pH were found to be significant factors, whereas the DO was excluded from the model. The VCC increased rapidly with an increase of the shaking speed, while the effect of the pH was found to be strongest at lower shaking speeds, where a high pH set point favoured increased final VCCs.

The predictive model for T_{CM} cells (Table 6.5) was significantly affected by the set points of pH and DO, whereas the shaking speed was not found to be a significant term and was thus removed from the model. Figure 6.12 shows that within the investigated design space, the percentage of

T_{CM} cells only varied slightly. The highest percentages of T_{CM} cells were predicted for a combination of high pH and low DO as well as low pH and high DO.

Overall, the models largely reflect the experimental findings of the previous sections (see 6.3.2 and 6.3.3) in which potential underlying causes have been discussed.

Table 6.4: ANOVA table of the viable cell concentration DoE model after natural log transformation.

Adjusted ANOVA for selected factorial model						
Analysis of variance table [Partial sum of squares - Type III]						
	Sum of		**Mean**	**F**	**p-value**	
Source	**Squares**	**df**	**Square**	**Value**	**Prob > F**	
Model	28.22	3	9.41	187.56	< 0.0001	significant
A-pH	*3.18*	*1*	*3.18*	*63.48*	*< 0.0001*	
C-Shaking speed	*21.57*	*1*	*21.57*	*430.16*	*< 0.0001*	
AC	*2.93*	*1*	*2.93*	*58.39*	*< 0.0001*	
Curvature	7.39	1	7.39	147.41	< 0.0001	
Residual	3.86	77	0.050			
Lack of Fit	*1.20*	*4*	*0.30*	*8.21*	*< 0.0001*	*significant*
Pure Error	*2.66*	*73*	*0.036*			
Cor Total	39.47	81				

Table 6.5: ANOVA table of the CD8+ T-CM DoE model after natural square root transformation.

Adjusted ANOVA for selected factorial model						
Analysis of variance table [Partial sum of squares - Type III]						
	Sum of		**Mean**	**F**	**p-value**	
Source	**Squares**	**df**	**Square**	**Value**	**Prob > F**	
Model	0.028	3	9.442E-003	13.24	< 0.0001	significant
A-pH	*8.386E-004*	*1*	*8.386E-004*	*1.18*	*0.2815*	
B-DO	*2.305E-003*	*1*	*2.305E-003*	*3.23*	*0.0761*	
AB	*0.024*	*1*	*0.024*	*33.14*	*< 0.0001*	
Curvature	0.12	1	0.12	172.21	< 0.0001	
Residual	0.055	77	7.129E-004			
Lack of Fit	*2.860E-003*	*4*	*7.149E-004*	*1.00*	*0.4117*	*not significant*
Pure Error	*0.052*	*73*	*7.128E-004*			
Cor Total	0.21	81				

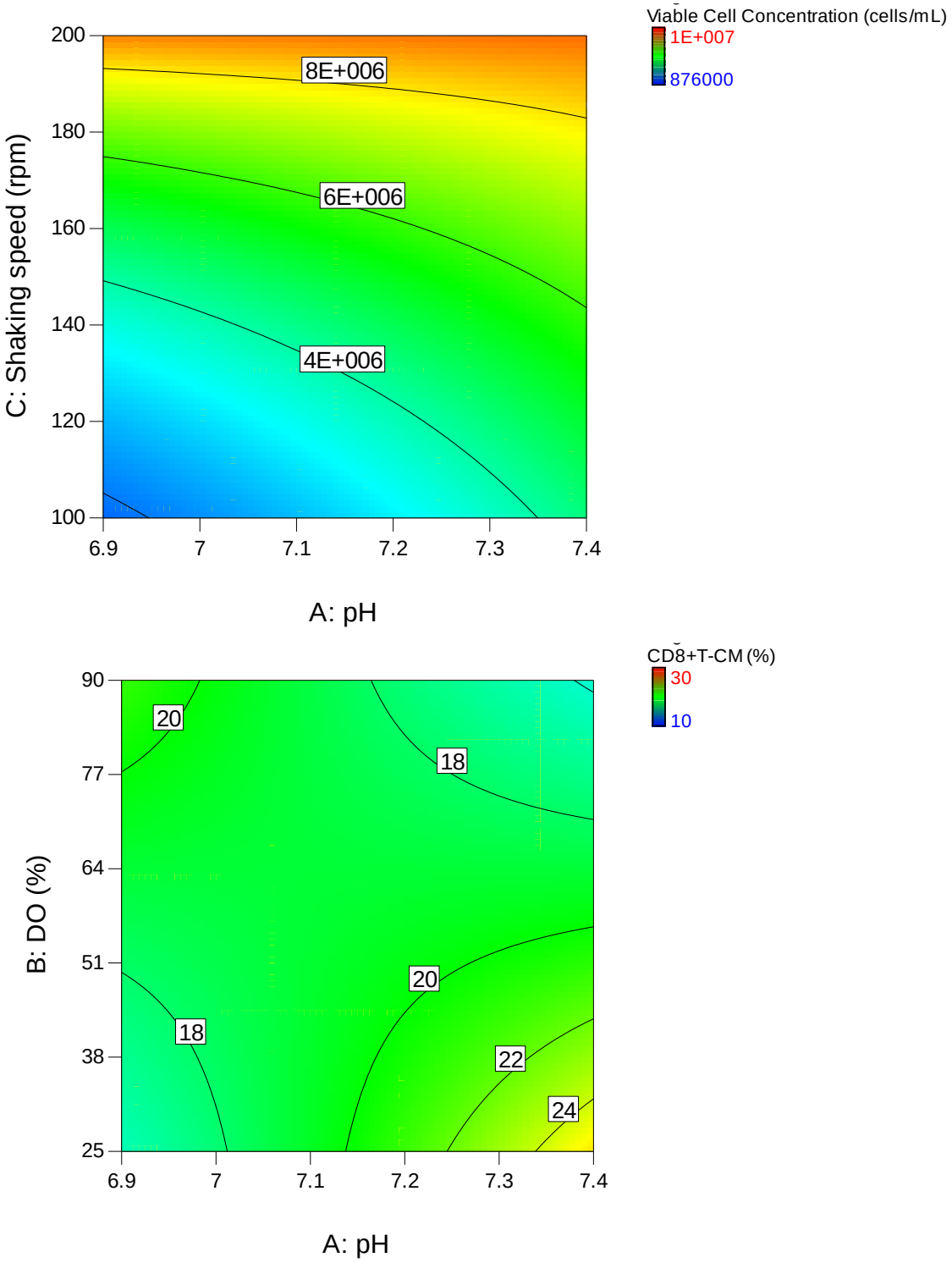

Figure 6.12: Contour plots of predictive models for the final viable cell concentration (top) and percentage of T_{CM} cells (bottom) as part of a full-factorial design. Variables that are not shown are fixed at the centre point.

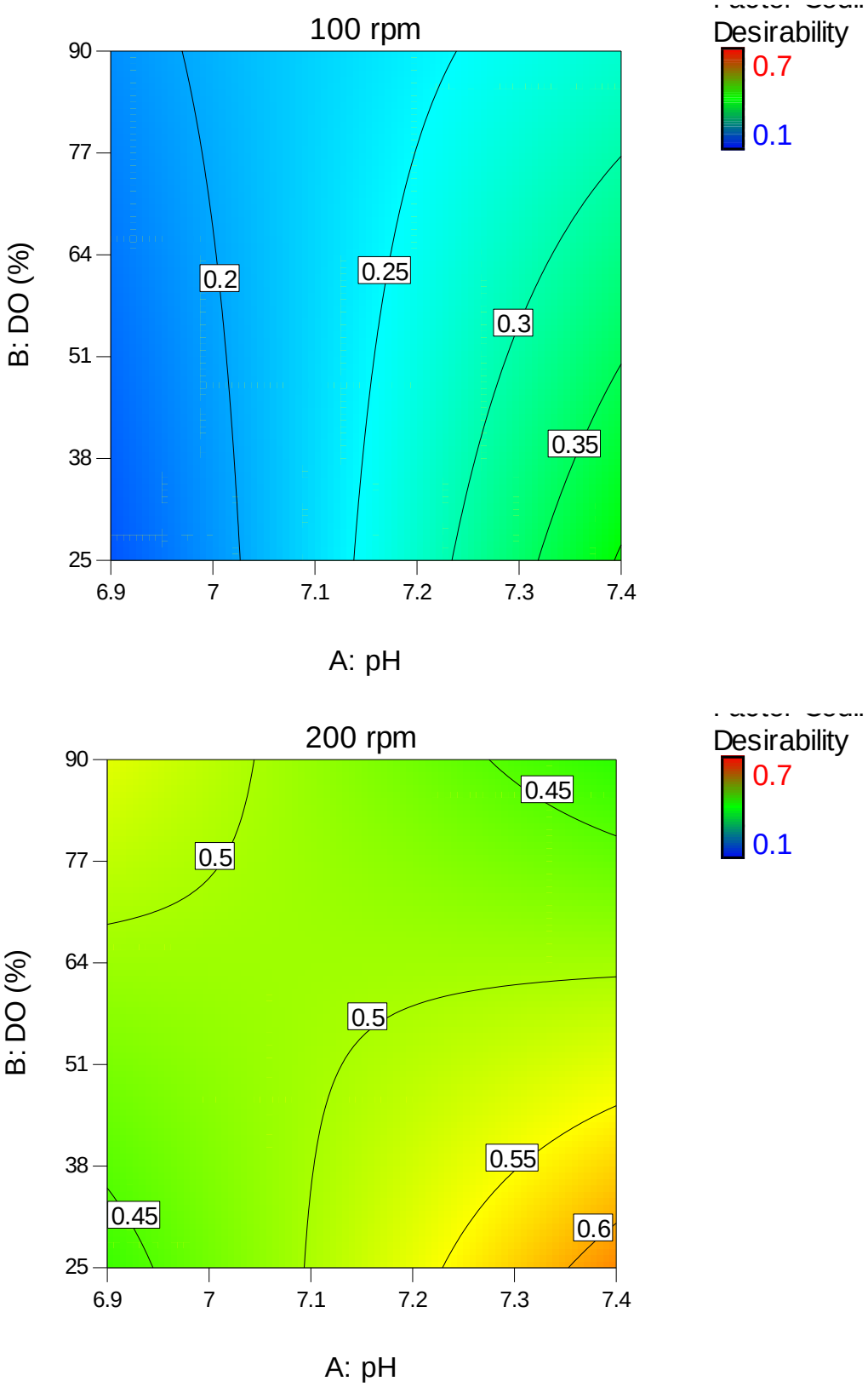

Figure 6.13: Contour plots of the desirability functions for a shaking speed of 100 rpm (top) and 200 rpm (bottom) as part of a numerical optimisation in which final VCC and percentage of T_{CM} cells were considered with equal importance.

The predictive models derived from the full-factorial design were used to perform a numerical optimisation of the T cell expansion process. As the final VCC and the percentage of T_{CM} cells are important parameters for an efficacious therapeutic T cell product, both were included in equal weighting in the desirability function. The desirability function combines both responses and generates values between zero (least desirable) and one (most desirable) that depend on the magnitude of the input parameters. Design Expert's numerical optimisation tool was used to find the combination of process parameters that yielded the highest desirability. Contour plots of the desirability function at a shaking speed of 100 rpm and 200 rpm are shown in Figure 6.13. The numerical optimisation identified that the ideal cultivation conditions within the investigated design space are predicted for a shaking speed of 200 rpm, a pH of 7.4, and a DO of 25%. However, as indicated by the contour plots shown in Figure 6.12, further improvement of the final VCC and the final percentage of T_{CM} cells may be possible by shifting the design space towards higher shaking speeds and higher pH levels.

6.4. Conclusion

Current manufacturing processes of adoptive T cell therapies are still prohibitively expensive (Roddie *et al.*, 2019). A key variable in driving down the cost of goods is an efficient T cell expansion process, which meets the dose-dependent number of cells in a short time span and results in a clinically efficacious distribution of T cell phenotypes.

This chapter investigated the influence of the cultivation parameters shaking speed, pH, and DO on the proliferation and differentiation of T cells in the micro-Matrix. Initial experiments identified growth limitations caused by a rapid depletion of glucose. Nutrient limitations were thereupon alleviated using a perfusion-mimic approach, which also proved beneficial in maintaining lactate concentrations low. Within a full-factorial design, increased agitation rates were established as a main contributor to an improved final VCC, while the formation of aggregates at low shaking speeds appeared to inhibit growth. The investigated pH and DO environments affected the process to a lesser extent. Interestingly, low pH set points were found to shift the T cell metabolism to a less glycolytic state and consequently reduced the formation of lactate. If continuous removal of lactate from the cultivation broth is not feasible, a low pH set point may therefore be used to

inhibit its formation. Furthermore, the DO was found to affect the final percentage of T_{CM} cells with best results obtained for a DO of 25%. Therefore, commonly used “normoxic” expansion conditions inside incubators should be reviewed, as they may not be ideal to achieve a desirable phenotypic distribution.

Finally, an ideal parameter combination within the investigated design space was proposed at a shaking speed of 200 rpm, a pH of 7.4, and a DO of 25% based on a numerical optimisation using predictive DoE models. Further improvement upon the final VCC and percentage of T_{CM} cells may be attainable for shaking speeds exceeding 200 rpm and pH levels more alkaline than 7.4, which could be explored by expanding the existing design space.

Chapter 7. Conclusions and future work

7.1. Conclusions

The aim of the work presented in this thesis was to evaluate whether the micro-Matrix microbioreactor is a suitable tool for mammalian cell culture process development. Using an IgG4 producing GS-CHO cell line as representative organism, it was shown that the micro-Matrix is capable of providing an environment that supports growth of mammalian cells, which by extension is comparable to larger scale STR systems and therefore scalable.

Initial work outlined in Chapter 3 sought to characterise the cultivation environment created within the micro-Matrix under a range of operating conditions. The Dual Indicator Method for Mixing Time revealed micro-Matrix mixing times similar to conditions found in conventional STRs (Barrett *et al.*, 2010), the µ24 (Betts *et al.*, 2014), and ambr® 15 microbioreactor (Nienow *et al.*, 2013). The k_La on the other hand was generally significantly higher compared to larger scale STRs (Nienow, 2006) and was therefore ruled out as a suitable scaling criterion, as a matched k_La would lead to insufficient mixing in the micro-Matrix. The P/V, which is typically challenging to determine experimentally for shaken systems, was derived through CFD simulations and found to be comparable to STR systems configured for mammalian cell cultivation.

Preliminary cell cultivations highlighted excessive evaporation and lack of well-to-well reproducibility as major limitations of the micro-Matrix system. Inhomogeneous and excessive evaporation is a common problem in small-scale cultivation systems (Martuza *et al.*, 1976; Deshpande, Wittmann and Heinzle, 2004). A novel method was developed in which reoccurring volume corrections with dH_2O were performed based on the concentration of sodium ions in the cell broth. Implementation of this method successfully reduced overall liquid loss below 10% per well and concurrently decreased well-to-well variability.

Based on the micro-Matrix engineering characterisation in Chapter 3 and in line with previous work by Silk (2014), a matched mixing time was chosen as scaling criterion in order to scale down a fed-batch process from a 5 L STR to the micro-Matrix. The initial scale-down experiments

revealed that the cell line's growth kinetics were negatively affected by low pCO_2 levels. Such a behaviour has not been reported for CHO cells previously. The CO_2 addition profile was therefore also matched between the microbioreactor and the STR. A tailored scaling strategy is not out of the ordinary and can be required to take the specific characteristics of the cells, the process, or the cultivation system into account (Kelly *et al.*, 2018).

Using this augmented scaling strategy, growth, IgG4 production, and the glycoprofile were for the first time shown to behave analogously in the micro-Matrix and a benchtop-scale STR. Further scale-down to 24 SRW microtitre plates proved challenging and evoked major differences in growth, metabolism, IgG4 galactosylation and the percentage of terminal sialic acid moieties compared to the cultivation systems that were pH and DO controlled. These deviations were hypothesised to have mainly arisen from a lack of active pH control in the 24 SRW format, which caused the cells to spend prolonged periods in a comparatively acidic environment (Naciri, Kuystermans and Al-Rubeai, 2008; Toussaint, Henry and Durocher, 2016; Jiang, Chen and Xu, 2018).

After the micro-Matrix was established as a scale-down model for fed-batch GS-CHO cultivations in the 5 L STR, the high-throughput of the micro-Matrix was leveraged to optimise the feeding regime in the micro-Matrix in two experiments. Feeding strategies are highly dependent on the cell line in use (Lu *et al.*, 2013) and it can often be necessary to choose continuous feed additions over bolus feeding (Bibila and Robinson, 1995). Therefore, several modes of bolus and semi-continuous feed additions were first compared with the help of the micro-Matrix feeding module, which allowed for the automated addition of feed. As no improvements were found for gradual additions over bolus feeding, further optimisation was based on the manual addition of bolus shots of feed medium. As a result, the feeding module was used instead for automated base additions, which permitted tighter control of the CO_2 addition profile, which as demonstrated in section 4.5, is pivotal to assure scalability for this cell line.

A circumscribed central composite optimisation design was used to explore the effect of three feeding parameters on the space-time-yield (STY) of the process. The time point at which the

feeding was started, the total feed volume and the rate at which this volume was added were investigated over five levels in 20 experimental conditions, including 6 centre point replicates. The optimum STY was captured within the design space and predicted for a feed start after 5 days and a feed volume of 64% of the initial working volume, divided into 6 additions on consecutive days. The prediction was affirmed by a highly replicated scale-down experiment and then successfully scaled up to the 5 L STR. Compared to the standard feeding regime, the optimised variation achieved a 25.0% higher final titre, a 25.4% increase of the STY, and a reduction of the run time by 1 day.

To explore the applicability of the micro-Matrix as process development tool for other processes such as the production of advanced therapy medicinal products (ATMP) processes, it was used for the cultivation of T cells. In the literature, T cells are often expanded under static incubator conditions (Zhan *et al.*, 2013; Bajgain *et al.*, 2014; Mock *et al.*, 2016; Vormittag *et al.*, 2018). Under these conditions, key parameters such as pH and DO are neither monitored nor controlled and no comprehensive study has been reported that explores the effect of DO and pH process conditions on the expansion and differentiation of primary T cells.

In an initial experiment, it was shown that agitation of the immortalised T cell line Jurkat could prompt improved growth kinetics over static cultivation. Further experiments with primary T cells revealed that frequent media exchanges and ideally a perfusion mode of operation helped to support growth and maintain high cell viabilities. The perfusion process was then taken forward and used to investigate a design space of pH, DO and agitation setpoints on the expansion and differentiation of primary T cells as part of a full-factorial design. Increased agitation rates were established as a main contributor to an improved final VCC, while the formation of aggregates at low shaking speeds appeared to inhibit growth. Importantly, this finding is in contradiction with T cells' shear sensitivity that has been reported previously by Chen *et al.* (2019) and supports the findings reported by Costariol *et al.* (2019), which render primary T cells shear resistant and overall positively affected by increased agitation. The investigated pH and DO environments affected the process to a lesser extent. Although the DoE models indicated that the optimal operating conditions are situated outside the investigated design space, an ideal parameter

combination within the design space was proposed for a shaking speed of 200 rpm, a pH of 7.4, and a DO of 25%.

7.2. Limitations and future work

Although the utility of the micro-Matrix as process development tool in the biotechnology industry and its advantages over alternative formats such as benchtop scale STRs and microtitre plates has been demonstrated in two exemplary applications, several aspects remain that would have benefited from further experimentation.

The images and videos obtained during colorimetric mixing time experiments were analysed using visual observation. Image analysis of this kind can be automated using software such as MATLAB as demonstrated by Li, Ducci and Micheletti (2020). An automated approach removes bias and can benefit consistency of the resulting analysis.

Mixing time and k_La measurements were each performed using only a single method. Although a comparison to literature of similar systems showed equivalent behaviour of these parameters in the micro-Matrix, validation with alternative methods as described in Marques, Cabral and Fernandes (2010) would have been a valuable confirmation of the validity of these parameters.

Similarly, further validation of results obtained as part of CFD simulations would be helpful to add confidence to the validity of these simulations and to understand their limitations. To do so, fluid flow within the micro-Matrix well could for instance be investigated using particle image velocimetry (Thomas *et al.*, 2017) and compared to the simulated flow patterns. An alternative and less experimentally complex validation approach could be the simulation of mixing experiments for a range of shaking speeds as well as working volumes and comparison of the resulting simulated mixing times to the experimentally determined values (Figure 3.2). Furthermore, the P/V values derived from CFD simulations could be evaluated as a scaling criterion instead of mixing time. The benefit of a P/V-based scaling strategy is that it can be applied to pilot scale systems as well, whereas mixing times typically increase drastically with increasing scale (Tissot *et al.*, 2010).

Although scalability between the micro-Matrix and the 5 L STR was achieved by indirectly modulating the CO_2 addition profile, future work would benefit from measurements of the pCO_2 in the cell broth throughout the cultivation in order to characterise with more granularity what minimum concentration of CO_2 is necessary to achieve a certain peak cell density. This could in turn inform process decisions such as the CO_2 fraction in the inflowing gas that is required to position the process away from an “edge of failure”. Furthermore, improved control technologies like a mass flow controller could be used to better control and fine-tune the CO_2 fraction of the inflowing gas.

The micro-Matrix’s high throughput is not only suited for rapid optimisation approaches, but also lends itself to screening designs in combination with advanced data analytical tools. Further work could therefore include early-stage process development such as clone screening (Fink *et al.*, 2021) or supplement and media screenings (Brühlmann *et al.*, 2017) in combination with a multivariate data analytical approach. As part of a collaborative project, cell cultivations of the micro-Matrix and a benchtop-scale STR were already captured by a modelling approach, where model parameter distributions were then used to evaluate scalability of the systems (Arndt *et al.*, 2021). In further studies, the mathematical models could be used for *in silico* process optimisation.

Manual handling of the micro-Matrix cassette and manual liquid handling remain major bottlenecks especially in view of more complex applications such as supplementation studies. While manual steps increase labour costs, they can also increase the risk of contamination and operator-dependent variability. Future work could encompass the partial or full automation of the experimental workflow. Similar studies have been conducted for microtitre plates (Markert and Joeris, 2017) and have demonstrated to greatly facilitate the workflow and in turn increase the experimental output (Markert *et al.*, 2019). As the micro-Matrix cassette is covered by a firmly fitted top plate and a closed hood is necessary to control the temperature inside the wells, integration of the device with a pipetting robot would not be feasible without major design changes of the micro-Matrix hardware. More realistically, the cassette could be equipped with microfluidic channels to achieve automated sampling and at-line analytics.

The small working volumes of the micro-Matrix make it an ideal candidate as unit operation in an ultra scale-down (USD) process. Changes in the upstream process can affect the outcome of downstream unit operations in an unanticipated fashion. These interactions often go unnoticed until a process is scaled up and the resulting batch is fully processed in subsequent unit operations. A number of USD technologies already exist (Rayat *et al.*, 2016) and further processing the harvested material from the micro-Matrix in USD mid- and downstream unit operations has the potential of rapidly generating a wealth of holistic process knowledge early in the development timeline.

Within the scope of T cell process development, experiments were only performed using primary T cells of healthy donors. However, in a clinical setting primary T cells are isolated from cancer patients, which would constitute starting material with a different cellular and chemical composition. The transferability of results obtained in this thesis to a clinical setting has not been investigated here, but should be considered as part of further experimentation. Additionally, in order for the isolated and expanded primary T cells to become an efficacious medicinal product, the cells have to be transduced with the chimeric antigen receptor (CAR) specific to the targeted cancer. It would be crucial to gain a better understanding in how far results obtained for the expansion and differentiation of primary T cells are indicative for the growth, differentiation, transduction efficiency, and treatment efficacy of CAR-T cells.

Lastly, the micro-Matrix microbioreactor would not be an ideal platform for the production of CAR-T cells, as the working volumes are limited and the risk for cross-contamination between wells is high. Therefore, further studies could investigate whether the results obtained in this thesis can be translated to upstream technologies that are already in use under manufacturing conditions (Vormittag *et al.*, 2018). In view of emerging allogeneic CAR-T cell therapies, process scalability to conventional STR systems, as done by Costariol *et al.* (2019), presents a particularly interesting area of further research. In a collaborative project and as extension of the primary T cell expansion optimisation in the micro-Matrix, first experiments have already been conducted in glass and single-use STR systems. At a working volume of 100 mL these experiments

investigated the effect of various aeration strategies on the expansion and differentiation of primary and CAR T cells.

Appendix I. Industrial implementation of the parallel microbio-reactor system for cell culture process development

I.1. Introduction and aim

With full monitoring and control capabilities at the millilitre scale, microbioreactors offer a clear advantage over conventional cell culture platforms such as microtitre plates, shake flasks, and STRs by maintaining a high information density per experiment, while considerably reducing equipment footprint. The optimisation case study presented in Chapter 5 shows how the micro-Matrix system can be used as a process development tool. This chapter aims to outline the conceptual implementation of the device as such a tool in an industrial setting with consideration of the economic, practical, safety, and environmental impact.

Chapter aims and objectives:

- Assess the implementation of the micro-Matrix in an industrial process development setting
- Evaluate the economic potential of the micro-Matrix in comparison to conventional process development tools
- Examine practical, safety, and environmental aspects

I.2. Assessing the implementation of the micro-Matrix in an industrial process development setting

As illustrated by Hemmerich *et al.* (2018) (Figure 1.3), the traditional upstream bioprocess development workflow is limited by the inverse correlation between information and throughput. While microtitre plate cultures under incubator conditions can be highly parallelised and have a small footprint, which allows for a high throughput, the information density for each of the conditions tested in such a setting is limited. The small volume only allows for a restricted range of measurements and the lack of active pH and DO control often constitutes significant differences

to the larger scale systems, which may precipitate in a lack of scalability and in turn challenges the value of information generated in this way.

The micro-Matrix microbioreactor can be a valuable addition to the bioprocess development workflow in early- as well as mid-stage process development. In early-stage process development, large numbers of clones are typically screened in microtitre plates and selected based on parameters such as the final titre or specific productivity. Moving this screening procedure into a controlled and scalable cultivation environment such as the micro-Matrix, increases the probability of identifying suitable clones for at-scale manufacturing. In turn, moving benchtop scale process optimisation to the microbioreactor scale can increase throughput by dramatically decreasing footprint and setup time compared to conventional STRs. A higher throughput at this stage of the process development allows for more complex experimental designs and the investigation of larger design spaces. By extension, the increased throughput allows for a higher replication of experimental conditions, which can increase the statistical power of the experimental designs.

Although the theoretical advantages of a microbioreactor system over its benchtop-scale and microtitre plate counterparts is evident, its applied utility may not always be unequivocal. From a scientific perspective, the first step in assessing the implementation of a tool such as the micro-Matrix is by evaluating whether its capabilities and characteristics sufficiently match the requirements of the process that it is supposed to accommodate. For instance, the optical pH sensors support a relatively narrow range of pH levels (pH 5.5 – 8.5), which may in niche cases be situated outside the cell culture process specifications. Similarly, the process may not rely on an active control of the pH and DO, in which case a transfer to a microbioreactor may not be necessary. Recent developments in process intensification often entail additional technologies and ancillaries such as cell retention devices, which the micro-Matrix may not be able to approximate. Finally, characteristics specific to the cell line need to be taken into account. The square and therefore baffled nature of the micro-Matrix wells may for instance promote shear rates that are incompatible with the cell type.

Once a thorough assessment of the practical utility of the micro-Matrix has been performed, its implementation requires an economic assessment.

I.3. Economic evaluation

Table A 1 outlines the expense that is required per condition over a range of scales based on the capital cost and consumable pricing detailed in Table A 2. Even in comparison to the 10 L single-use benchtop-scale, the economic advantage of small-scale cultivation systems is considerable. With further increase of the working volume, the proportion of media cost gains increasing importance. Such differences would be even more pronounced in situations where costly raw materials are screened.

The stark contrast in cost per condition between small scale cultivation systems and the larger scale systems illustrates the economic value of scale-down models. Although the price per condition tested in shake flasks is about half compared to the micro-Matrix, the lack of monitoring, control, and automation in shake flasks can drastically limit their applicability in upstream process development. For instance, results obtained in rounds of screenings or process optimisations performed in shake flasks may not be scalable. These limitations may lead to a manufacturing process that is run under suboptimal conditions or a delay in the process development timeline. Both cases entail the loss of substantial amounts of revenue.

Table A 1: Economic evaluation of upstream process development systems.

	Single-use cell culture systems					
	3.4 mL 24 SRW	**125 mL Shake Flask**	**10 mL micro-Matrix**	**3 L STR**	**100 L STR**	**1000 L STR**
Throughput per system and experiment	720	24	24	1	1	1
Batches per year (14 days per run + 1 day turnaround)	24	24	24	24	24	24
Total number of conditions per year	17280	576	576	24	24	24
*Capital cost per condition over 10 year lifespan (£)***	0.1	3.7	26.9	83.3	270.8	291.7
Consumables and media cost per condition (£)	0.8	18.6	21.2	1509.0	23180.0	187800.0
Total cost per condition (£)	**1.0**	**22.3**	**48.1**	**1592.3**	**23450.8**	**188091.7**

*) Assuming a maximum capacity of 30 microtitre plates per incubator

**) $\frac{Capital\ cost}{10\ years \cdot Number\ of\ conditions\ per\ year}$

Table A 2: Capital and consumables pricing per run.

	Price (£)	***Source***
Incubator	21510.0	(Simaria *et al.*, 2014)
24 SRW	20.3	Quote
Shake Flask	8.5	Quote
micro-Matrix	155000.0	Quote
micro-Matrix consumables	498.4	Quote
3 L STR	20000.0	Quote
3 L STR vessel	600.0	Quote
100 L STR	65000.0	Quote
100 L STR bag	5000.0	Quote
1000 L STR	70000.0	Quote
1000 L STR bag	6000.0	Quote
CD CHO (L)	101.0	Quote

Yet, an ultra-scale-down model in microtitre plates may still be a worthwhile investment in addition to a microbioreactor system despite the decreased information density per experiment. A microtitre plate-based model could be particularly useful to dissolve bottlenecks in throughput that would be challenging to address even with several microbioreactor systems running in parallel. For instance, in a single incubator 17,280 conditions can be tested in 24-SRW microtitre plates annually. Reaching the same number of conditions would require 30 micro-Matrix systems. However, this economic evaluation does not include the cost of labour required for setup, operation and turnaround of each system and it would undoubtedly require several operators or considerable capital investment in an automated cell culture platform to manage a microtitre plate experiment run at full capacity.

I.4. Practical, safety, and environmental aspects

Following the economic feasibility assessment of the micro-Matrix' implementation in an industrial setting, it has to be evaluated whether the implementation can be realised practically. A suitable lab-space with the required footprint and connections for electricity and gas lines needs to be provided. As part of a demo and in close cooperation with the manufacturer of the device, suitable test conditions have to be established and a representative process should be run using the micro-Matrix. Ideally, an existing process would be scaled down from the benchtop or

manufacturing scale to the micro-Matrix. During the run, all critical process parameters (CPPs) will be monitored and controlled. After the run, a range of critical quality attributes (CQAs) will be measured to assess process scalability to the micro-Matrix. In case the system is used as a screening tool, scalability to other cultivation systems may not be priority. It could, however, be tested whether screening outputs derived from a pre-existing screening platform hold true when the same screening is performed using the micro-Matrix.

Before installation and operation of the micro-Matrix, a risk assessment will be carried out and its environmental impact will be assessed. In terms of safety, operation of the micro-Matrix entails similar hazards to other bioreactor systems. Gas connections require regular checking to prevent any leaks of gases that could be potentially toxic, flammable, or asphyxiant. Additionally, the liquid addition bottle is pressurised and should therefore be inspected frequently for leaks, especially if it is supposed to hold caustic solutions.

After the system has been delivered, the micro-Matrix needs to undergo an installation qualification to ensure that the equipment has been setup and configured appropriately. Subsequently, an operational qualification is performed to ensure that the system is operating within the ranges specified by the manufacturer. Finally, a performance qualification is carried out to evaluate whether the system performs as expected under experimental conditions.

Additionally, environmental impacts of the micro-Matrix are of similar nature compared to other single-use cell cultivation systems. Harvested material that does not require further processing needs to be inactivated before disposal. Soiled single-use components need to be disposed of according to regulations. Compared to the benchtop scale, the amount of plastic and energy required for each experiment is markedly reduced. Therefore, the implementation of the micro-Matrix represents a significant reduction of the environmental burden.

Appendix II. Supplementary material

II.1. Exemplary micro-Matrix online data

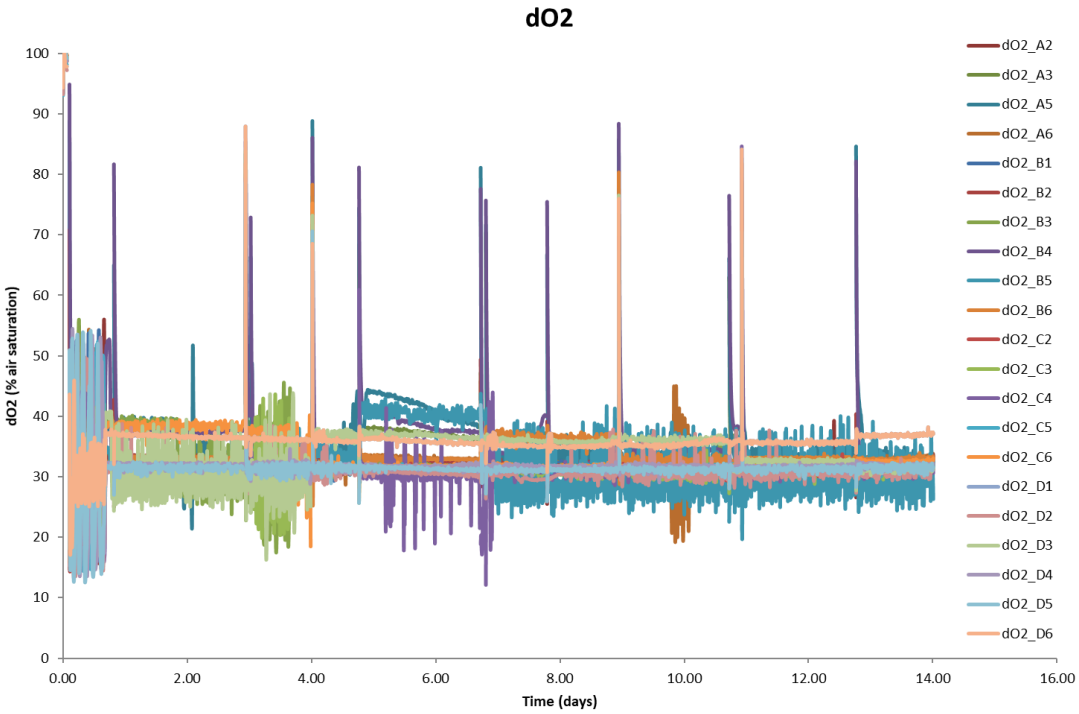

Figure A 1: Dissolved oxygen profile of the micro-Matrix cultivation detailed in section 3.2.3.

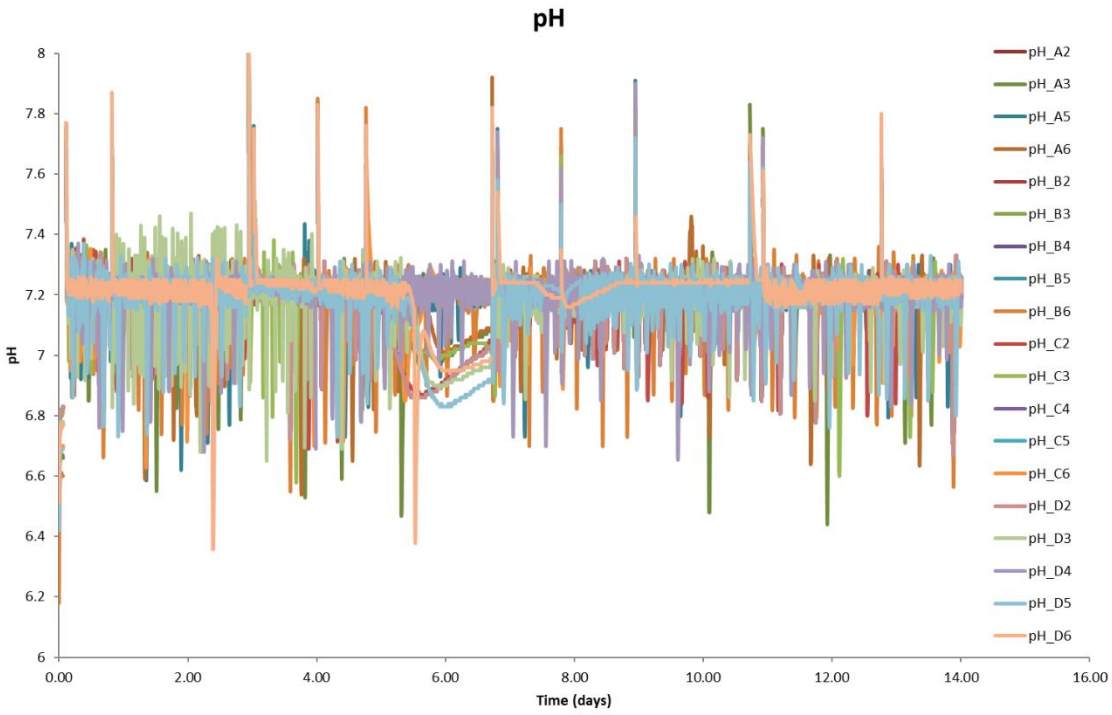

Figure A 2: pH profile of the micro-Matrix cultivation detailed in section 3.2.3.

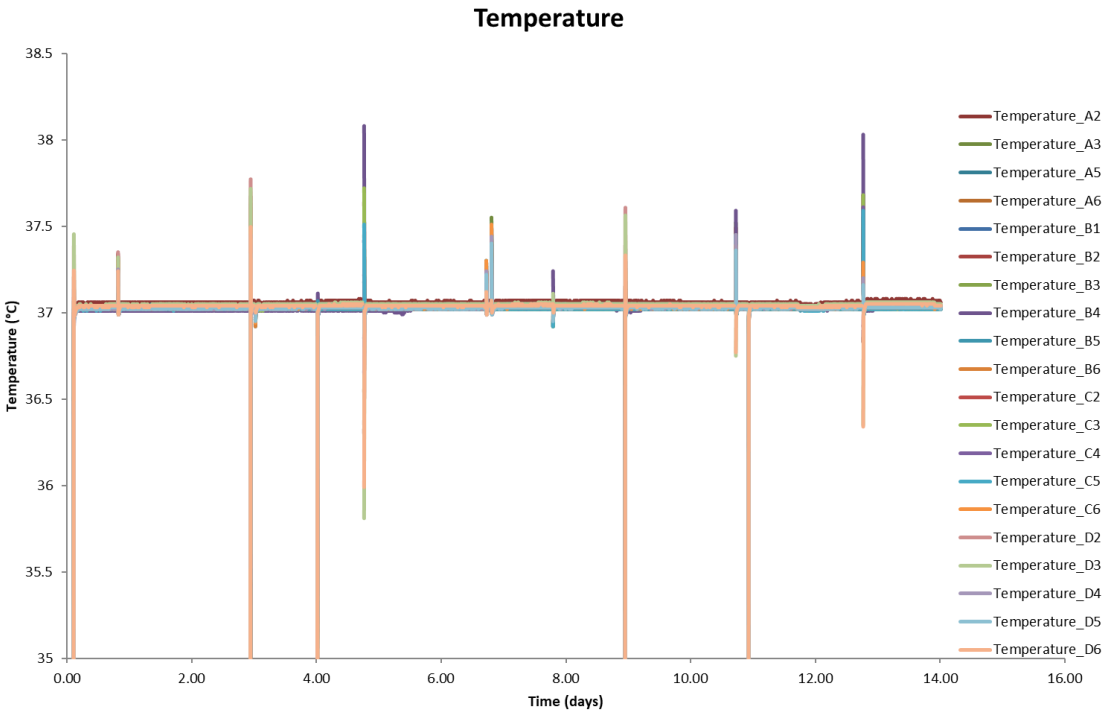

Figure A 3: Temperature profile of the micro-Matrix cultivation detailed in section 3.2.3.

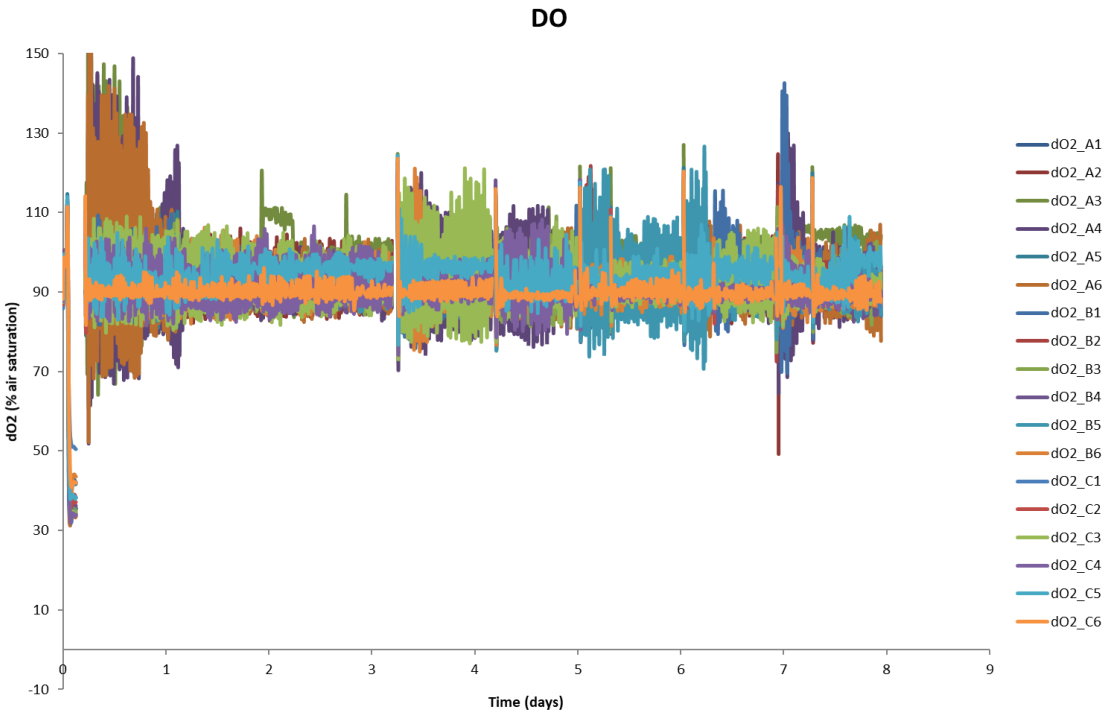

Figure A 4: DO profile of the micro-Matrix cultivation detailed in section 6.3.2. The DO setpoint for this experiment was 90%.

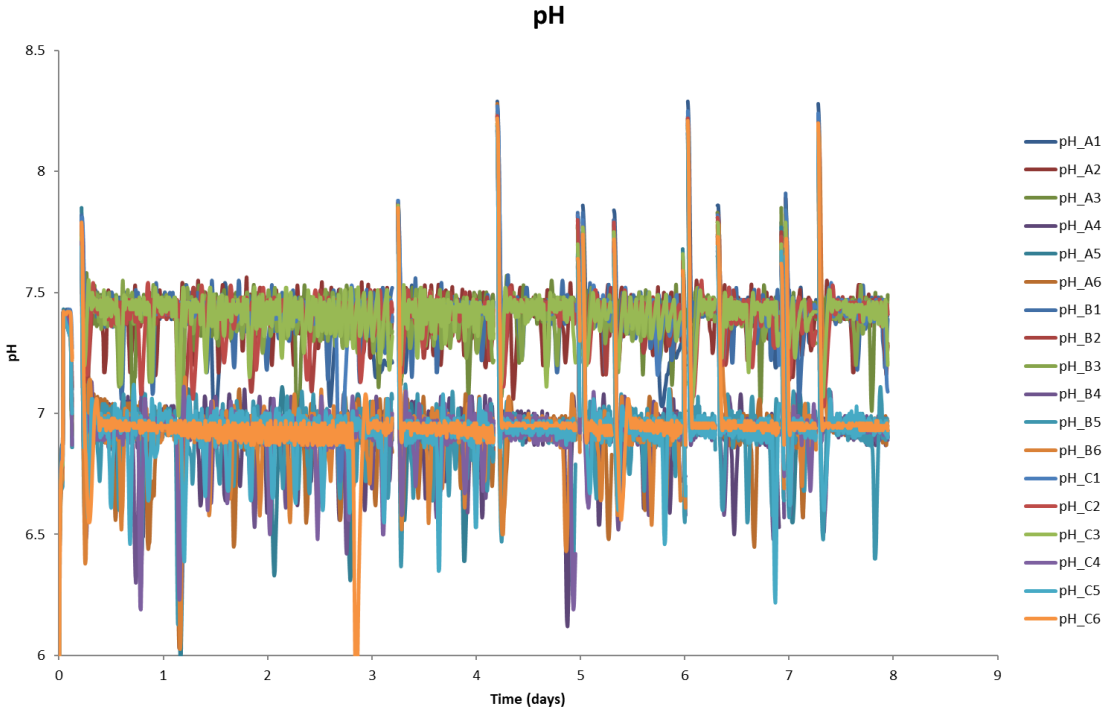

Figure A 5: pH profile of the micro-Matrix cultivation detailed in section 6.3.2. The pH setpoints for this experiment were 6.9 and 7.4.

II.2. Correlation matrices

	Feed volume	Feed start	Feed additions	Final Titre	Yield	STY
Feed volume	1.0000	0.0000	-0.0000	0.6689	0.6631	0.4943
Feed start	0.0000	1.0000	-0.0000	0.4137	0.4221	0.1814
Feed additions	-0.0000	-0.0000	1.0000	0.1593	0.1543	-0.0426
Final Titre	0.6689	0.4137	0.1593	1.0000	0.9707	0.7964
Yield	0.6631	0.4221	0.1543	0.9707	1.0000	0.7629
STY	0.4943	0.1814	-0.0426	0.7964	0.7629	1.0000

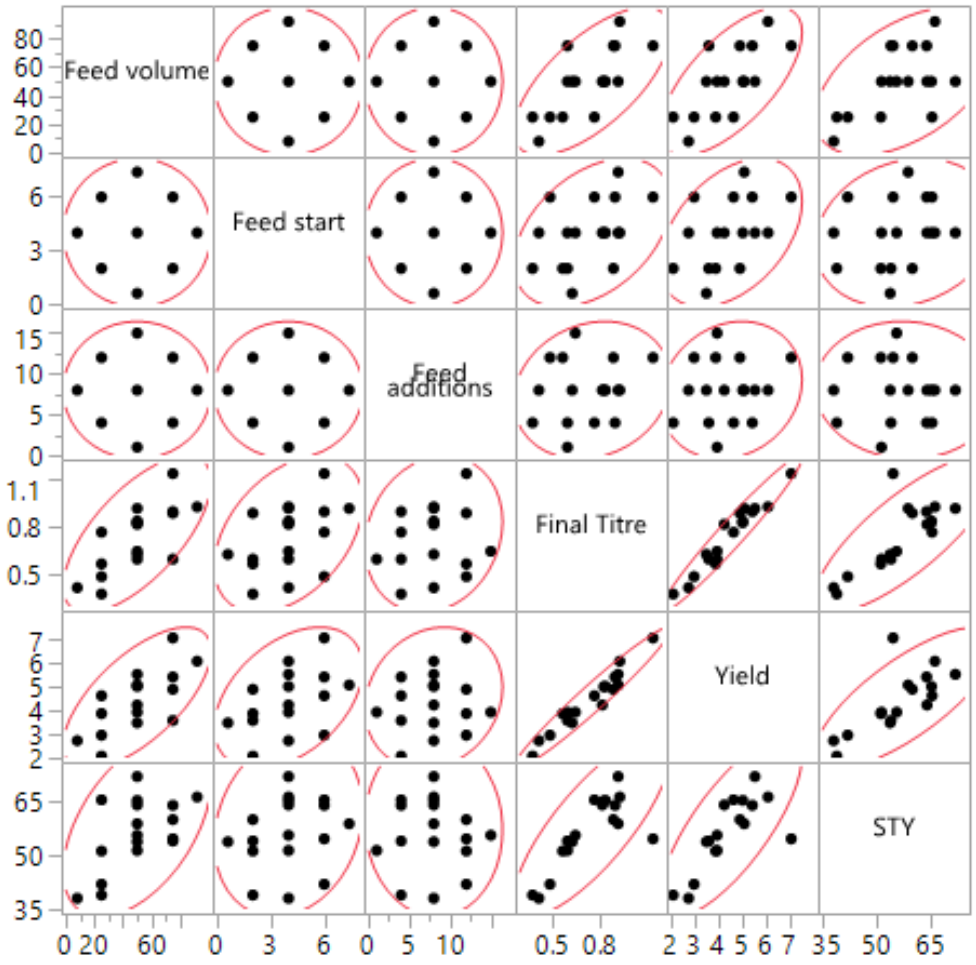

Figure A 6: Correlation matrix of central composite design input and output factors detailed in section 5.3.2.

	pH	DO	Shaking speed	Viable Cell Concentration	CD4+ T-CM (%)	CD8+T-CM (%)
pH	1.0000	-0.0303	-0.0000	0.1696	-0.3247	0.1549
DO	-0.0303	1.0000	0.0000	-0.0114	0.3501	-0.2030
Shaking speed	-0.0000	0.0000	1.0000	0.7289	-0.3447	0.1278
Viable Cell Concentration	0.1696	-0.0114	0.7289	1.0000	-0.7412	-0.3163
CD4+ T-CM (%)	-0.3247	0.3501	-0.3447	-0.7412	1.0000	0.4267
CD8+T-CM (%)	0.1549	-0.2030	0.1278	-0.3163	0.4267	1.0000

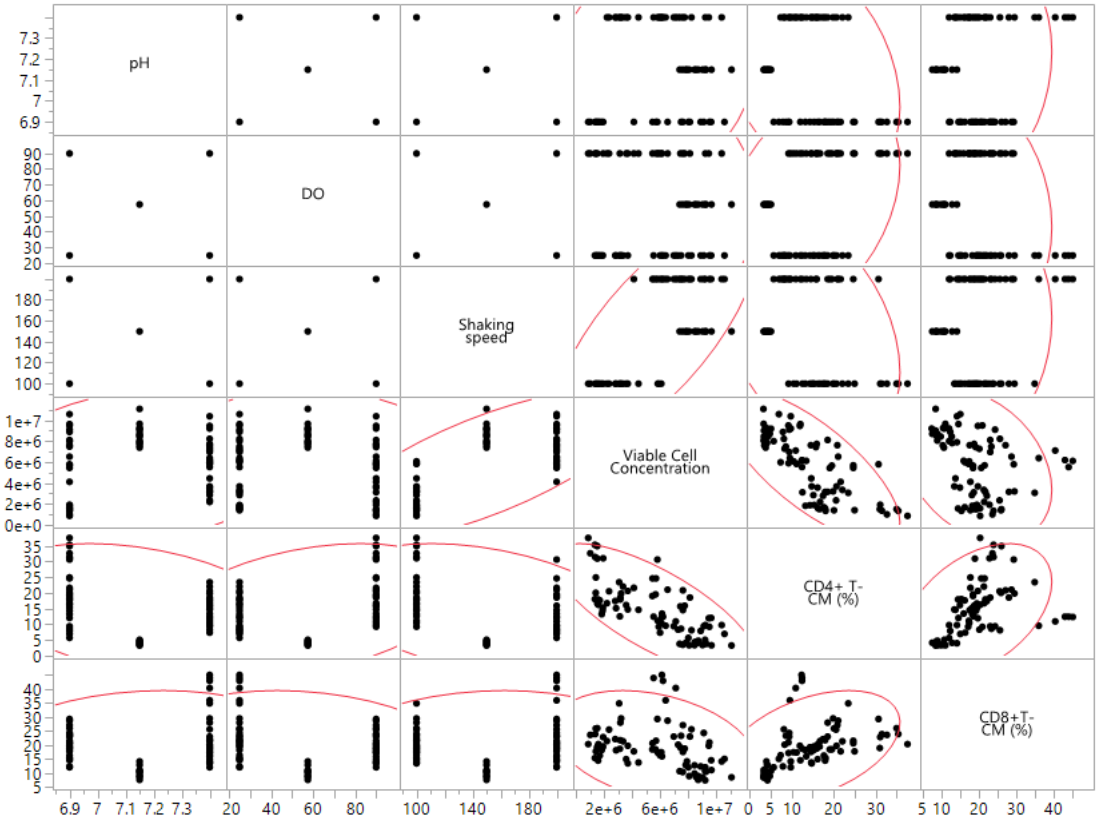

Figure A 7: Correlation matrix of full factorial design input and output factors detailed in section 6.3.1.

References

Abraham, R. T. and Weiss, A. (2004) 'Jurkat T cells and development of the T-cell receptor signalling paradigm', *Nature Reviews Immunology*. Nature Publishing Group, pp. 301–308. doi: 10.1038/nri1330.

Ahmed, S. U. *et al.* (2010) 'Computational fluid dynamics modeling of gas dispersion in multi impeller bioreactor', *Journal of Bioscience and Bioengineering*. doi: 10.1016/j.jbiosc.2009.11.014.

Ahn, W. S. *et al.* (2008) 'Effect of culture temperature on erythropoietin production and glycosylation in a perfusion culture of recombinant CHO cells', *Biotechnology and Bioengineering*, 101(6), pp. 1234–1244. doi: 10.1002/bit.22006.

Alfieri, R. R. and Petronini, P. G. (2007) 'Hyperosmotic stress response: comparison with other cellular stresses.', *Pflügers Archiv : European Journal of Physiology*, 454(2), pp. 173–85. doi: 10.1007/s00424-006-0195-x.

Allen, M. J. *et al.* (2008) 'Identification of novel small molecule enhancers of protein production by cultured mammalian cells.', *Biotechnology and Bioengineering*, 100(6), pp. 1193–204. doi: 10.1002/bit.21839.

Altamirano, C. *et al.* (2004) 'Strategies for fed-batch cultivation of t-PA producing CHO cells: substitution of glucose and glutamine and rational design of culture medium', *Journal of Biotechnology*, 110(2), pp. 171–179. doi: 10.1016/j.jbiotec.2004.02.004.

Altamirano, C. *et al.* (2006) 'Considerations on the lactate consumption by CHO cells in the presence of galactose.', *Journal of Biotechnology*, 125(4), pp. 547–56. doi: 10.1016/j.jbiotec.2006.03.023.

Amini, A. *et al.* (2020) 'Bioprocess considerations for T-cell therapy: Investigating the impact of agitation, dissolved oxygen, and pH on T-cell expansion and differentiation', *Biotechnology and Bioengineering*, 117(10), pp. 3018–3028. doi: 10.1002/bit.27468.

Applikon (2016) *Brochure: micro-Matrix 24 bioreactors in a convenient microtiter forma*. Available at: http://www.applikon-biotechnology.us/images/download/micro-matrix/micro-Matrix-leaflet.pdf (Accessed: 30 January 2017).

Arndt, L. *et al.* (2021) 'Model-based workflow for scale-up of process strategies developed in miniaturized bioreactor systems', *Biotechnology Progress*. doi: 10.1002/btpr.3122.

Atkuri, K. R. *et al.* (2007) 'Importance of culturing primary lymphocytes at physiological oxygen levels', *Proceedings of the National Academy of Sciences of the United States of America*. National Academy of Sciences, 104(11), p. 4547. doi: 10.1073/PNAS.0611732104.

Atkuri, K. R., Herzenberg, Leonard A and Herzenberg, Leonore A (2005) 'Culturing at atmospheric oxygen levels impacts lymphocyte function.', *Proceedings of the National Academy of Sciences of the United States of America*. National Academy of Sciences, 102(10), pp. 3756–9. doi: 10.1073/pnas.0409910102.

Bailey, J. E. and Ollis, D. F. (1986) *Biochemical engineering fundamentals*. McGraw-Hill.

Bajgain, P. *et al.* (2014) 'Optimizing the production of suspension cells using the G-Rex "M" series', *Molecular Therapy - Methods & Clinical Development*. Cell Press, 1, p. 14015. doi: 10.1038/MTM.2014.15.

Baker, M. (2005) 'Upping the ante on antibodies.', *Nature Botechnology*. Nature Publishing Group, 23(9), pp. 1065–72. doi: 10.1038/nbt0905-1065.

Bareither, R. and Pollard, D. (2011) 'A review of advanced small-scale parallel bioreactor technology for accelerated process development: Current state and future need', *Biotechnology Progress*, 27(1), pp. 2–14. doi: 10.1002/btpr.522.

Barrett, T. A. *et al.* (2010) 'Microwell engineering characterization for mammalian cell culture process development', *Biotechnology and Bioengineering*, 105(2), pp. 260–275. doi: 10.1002/bit.22531.

Bausch, M., Schultheiss, C. and Sieck, J. B. (2019) ‘Recommendations for Comparison of Productivity Between Fed-Batch and Perfusion Processes’, *Biotechnology Journal*, 14(2), p. 1700721. doi: 10.1002/biot.201700721.

Bebbington, C. R. *et al.* (1992) ‘High-Level Expression of a Recombinant Antibody from Myeloma Cells Using a Glutamine Synthetase Gene as an Amplifiable Selectable Marker’, *Bio/Technology*. Nature Publishing Group, 10(2), pp. 169–175. doi: 10.1038/nbt0292-169.

Becker, M. *et al.* (2019) ‘The Less the Better: How Suppressed Base Addition Boosts Production of Monoclonal Antibodies With Chinese Hamster Ovary Cells’, *Frontiers in Bioengineering and Biotechnology*. Frontiers, 7, p. 76. doi: 10.3389/fbioe.2019.00076.

Berahovich, R. *et al.* (2019) ‘Hypoxia Selectively Impairs CAR-T Cells In Vitro.’, *Cancers*, 11(5). doi: 10.3390/cancers11050602.

Bertout, J. A., Patel, S. A. and Simon, M. C. (2008) ‘The impact of O2 availability on human cancer’, *Nature Reviews Cancer Rev Cancer*, 8(12), pp. 967–975.

Betts, J. I. *et al.* (2006) ‘Miniature bioreactors: current practices and future opportunities’, *Microbial Cell Factories*. BioMed Central, 5(1), p. 21. doi: 10.1186/1475-2859-5-21.

Betts, J. I., Doig, S. D. and Baganz, F. (2006) ‘Characterization and Application of a Miniature 10 mL Stirred-Tank Bioreactor, Showing Scale-Down Equivalence with a Conventional 7 L Reactor’, *Biotechnology Progress*, 22(3), pp. 681–688. doi: 10.1021/bp050369y.

Betts, J. P. J. *et al.* (2014) ‘Impact of aeration strategies on fed-batch cell culture kinetics in a single-use 24-well miniature bioreactor’, *Biochemical Engineering Journal*, 82, pp. 105–116. doi: 10.1016/j.bej.2013.11.010.

Biasco, L. *et al.* (2015) ‘In vivo tracking of T cells in humans unveils decade-long survival and activity of genetically modified T memory stem cells.’, *Science translational medicine*, 7(273), p. 273ra13. doi: 10.1126/scitranslmed.3010314.

Bibila, T. A. and Robinson, D. K. (1995) 'In pursuit of the optimal fed-batch process for monoclonal antibody production', *Biotechnology Progress*, 11(1), pp. 1–13. doi: 10.1021/bp00031a001.

Birch, J. R. and Racher, A. J. (2006) 'Antibody production', *Advanced Drug Delivery Reviews*, 58(5–6), pp. 671–685. doi: 10.1016/j.addr.2005.12.006.

Bohnenkamp, H., Hilbert, U. and Noll, T. (2002) 'Bioprocess development for the cultivation of human T-lymphocytes in a clinical scale', *Cytotechnology*, 38(1/3), pp. 135–145. doi: 10.1023/A:1021174619613.

Bollati-Fogolín, M. *et al.* (2008) 'Temperature Reduction in Cultures of hGM-CSF-expressing CHO Cells: Effect on Productivity and Product Quality', *Biotechnology Progress*. American Chemical Society, 21(1), pp. 17–21. doi: 10.1021/bp049825t.

Boyd, P. N., Lines, A. C. and Patel, A. K. (1995) 'The effect of the removal of sialic acid, galactose and total carbohydrate on the functional activity of Campath-1H', *Molecular Immunology*, 32(17–18), pp. 1311–1318. doi: 10.1016/0161-5890(95)00118-2.

Brentjens, R. J. *et al.* (2013) 'CD19-targeted T cells rapidly induce molecular remissions in adults with chemotherapy-refractory acute lymphoblastic leukemia.', *Science translational medicine*. NIH Public Access, 5(177), p. 177ra38. doi: 10.1126/scitranslmed.3005930.

Brown, C. E. and Mackall, C. L. (2019) 'CAR T cell therapy: inroads to response and resistance', *Nature Reviews Immunology*. Nature Publishing Group, 19(2), pp. 73–74. doi: 10.1038/s41577-018-0119-y.

Brühlmann, D. *et al.* (2017) 'Parallel experimental design and multivariate analysis provides efficient screening of cell culture media supplements to improve biosimilar product quality', *Biotechnology and Bioengineering*. John Wiley & Sons, Ltd, 114(7), pp. 1448–1458. doi: 10.1002/bit.26269.

Brunner, M. *et al.* (2018) 'Elevated pCO2 affects the lactate metabolic shift in CHO cell culture processes', *Engineering in Life Sciences*. John Wiley & Sons, Ltd, 18(3), pp. 204–214. doi: 10.1002/elsc.201700131.

Büchs, J. *et al.* (2000) ‘Power consumption in shaking flasks on rotary shaking machines: I. Power consumption measurement in unbaffled flasks at low liquid viscosity’, *Biotechnology and Bioengineering*. John Wiley & Sons, Inc., 68(6), pp. 589–593. doi: 10.1002/(SICI)1097-0290(20000620)68:6<589::AID-BIT1>3.0.CO;2-J.

Büchs, J. (2001) ‘Introduction to advantages and problems of shaken cultures’, *Biochemical Engineering Journal*, 7(2), pp. 91–98. doi: 10.1016/S1369-703X(00)00106-6.

Büchs, J., Lotter, S. and Milbradt, C. (2001) ‘Out-of-phase operating conditions, a hitherto unknown phenomenon in shaking bioreactors’, *Biochemical Engineering Journal*, 7, pp. 135–141.

Bujalski, W. *et al.* (1999) ‘Suspension and Liquid Homogenization in High Solids Concentration Stirred Chemical Reactors’, *Chemical Engineering Research and Design*. Elsevier, 77(3), pp. 241–247. doi: 10.1205/026387699526151.

Burky, J. E. *et al.* (2007) ‘Protein-free fed-batch culture of non-GS NS0 cell lines for production of recombinant antibodies.’, *Biotechnology and Bioengineering*, 96(2), pp. 281–93. doi: 10.1002/bit.21060.

Butler, M. (2004) *Animal Cell Culture and Technology*. BIOS Scientific Publishers.

Butler, M. (2005) ‘Animal cell cultures: recent achievements and perspectives in the production of biopharmaceuticals.’, *Applied microbiology and biotechnology*. Springer-Verlag, 68(3), pp. 283–91. doi: 10.1007/s00253-005-1980-8.

Calcinotto, A. *et al.* (2012) ‘Modulation of Microenvironment Acidity Reverses Anergy in Human and Murine Tumor-Infiltrating T Lymphocytes’, *Cancer Research*. American Association for Cancer Research, 72(11), pp. 2746–2756. doi: 10.1158/0008-5472.CAN-11-1272.

Caldwell, C. C. *et al.* (2001) ‘Differential effects of physiologically relevant hypoxic conditions on T lymphocyte development and effector functions.’, *Journal of immunology*. American Association of Immunologists, 167(11), pp. 6140–9. doi: 10.4049/jimmunol.167.11.6140.

Capriotti, T. (2001) ‘Monoclonal antibodies: Drugs that combine pharmacology and biotechnology’, *Medsurg Nursing*. ProQuest Central pg, 10(2).

Carswell, K. S. and Papoutsakis, E. T. (2000) ‘Extracellular pH Affects the Proliferation of Cultured Human T Cells and Their Expression of the Interleukin-2 Receptor’, *Journal of Immunotherapy*, 23(6), pp. 669–674.

Chapman, A. E. and Calhoun, J. C. (1988) ‘Effects of glucose starvation and puromycin treatment on lipid-linked oligosaccharide precursors and biosynthetic enzymes in Chinese hamster ovary cells in vivo and in vitro’, *Archives of Biochemistry and Biophysics*, 260(1), pp. 320–333. doi: 10.1016/0003-9861(88)90456-0.

Chartrain, M. and Chu, L. (2008) ‘Development and production of commercial therapeutic monoclonal antibodies in mammalian cell expression systems: an overview of the current upstream technologies.’, *Current Pharmaceutical Biotechnology*, 9(6), pp. 447–67.

Chaturvedi, K. *et al.* (2014) ‘Comparison of the behavior of CHO cells during cultivation in 24-square deep well microplates and conventional shake flask systems’, *Biotechnology Reports*, 1–2(2), pp. 22–26. doi: 10.1016/j.btre.2014.04.001.

Chee Furng Wong, D. *et al.* (2005) ‘Impact of dynamic online fed-batch strategies on metabolism, productivity and N-glycosylation quality in CHO cell cultures’, *Biotechnology and Bioengineering*. John Wiley & Sons, Ltd, 89(2), pp. 164–177. doi: 10.1002/bit.20317.

Chen, S. *et al.* (2019) ‘Expandable Bioreactor for the culture of immune cells’, *Cytotherapy*. Elsevier BV, 21(5), p. S43. doi: 10.1016/j.jcyt.2019.03.386.

Chu, L. and Robinson, D. K. (2001) ‘Industrial choices for protein production by large-scale cell culture’, *Current Opinion in Biotechnology*, 12(2), pp. 180–187. doi: 10.1016/S0958-1669(00)00197-X.

Chua, F. K., Yap, M. G. and Oh, S. K. (1994) ‘Hyper-stimulation of monoclonal antibody production by high osmolarity stress in eRDF medium.’, *Journal of biotechnology*, 37(3), pp. 265–75.

Chudasama, V., Maruani, A. and Caddick, S. (2016) 'Recent advances in the construction of antibody–drug conjugates', *Nature Chemistry*. Nature Publishing Group, 8(2), pp. 114–119. doi: 10.1038/nchem.2415.

Clincke, M.-F. *et al.* (2013) 'Very high density of CHO cells in perfusion by ATF or TFF in WAVE bioreactor™. Part I. Effect of the cell density on the process.', *Biotechnology Progress*, 29(3), pp. 754–67. doi: 10.1002/btpr.1704.

Collier, R. (2009) 'Drug development cost estimates hard to swallow.', *CMAJ : Canadian Medical Association journal = journal de l'Association medicale canadienne*. Canadian Medical Association, 180(3), pp. 279–80. doi: 10.1503/cmaj.082040.

Cooper, C. M., Fernstrom, G. A. and Miller, S. A. (1944) 'Performance of Agitated Gas-Liquid Contactors', *Industrial & Engineering Chemistry*. American Chemical Society, 36(6), pp. 504–509. doi: 10.1021/ie50414a005.

Corbet, C. and Feron, O. (2017) 'Tumour acidosis: from the passenger to the driver's seat', *Nature Reviews Cancer*. Nature Publishing Group, 17(10), pp. 577–593. doi: 10.1038/nrc.2017.77.

Costariol, E. *et al.* (2019) 'Establishing the scalable manufacture of primary human T-cells in an automated stirred-tank bioreactor', *Biotechnology and Bioengineering*. John Wiley & Sons, Ltd, p. bit.27088. doi: 10.1002/bit.27088.

Dankckwerts, P. V. and Litt, M. (1971) *Gas-liquid reactions*, *AIChE Journal*. American Institute of Chemical Engineers. doi: 10.1002/aic.690170204.

Darja, O. *et al.* (2016) 'Responses of CHO cell lines to increased pCO2 at normal (37 °C) and reduced (33 °C) culture temperatures', *Journal of Biotechnology*. Elsevier, 219, pp. 98–109. doi: 10.1016/J.JBIOTEC.2015.12.013.

DeBerardinis, R. J. *et al.* (2007) 'Beyond aerobic glycolysis: transformed cells can engage in glutamine metabolism that exceeds the requirement for protein and nucleotide synthesis.', *Proceedings of the National Academy of Sciences of the United States of America*, 104(49), pp. 19345–50. doi: 10.1073/pnas.0709747104.

Depil, S. *et al.* (2020) '"Off-the-shelf" allogeneic CAR T cells: development and challenges', *Nature Reviews Drug Discovery*. Nature Research, pp. 185–199. doi: 10.1038/s41573-019-0051-2.

Deshpande, R. R., Wittmann, C. and Heinzle, E. (2004) 'Microplates with integrated oxygen sensing for medium optimization in animal cell culture', *Cytotechnology*, 46(1), pp. 1–8.

Dillman, R. O. (2001) 'Monoclonal Antibody Therapy for Lymphoma. An Update', *Cancer Practice*. Blackwell Science Inc, 9(2), pp. 71–80. doi: 10.1046/j.1523-5394.2001.009002071.x.

Dobson, G. P., Yamamoto, E. and Hochachka, P. W. (1986) 'Phosphofructokinase control in muscle: nature and reversal of pH-dependent ATP inhibition', *American Journal of Physiology-Regulatory, Integrative and Comparative Physiology*, 250(1), pp. R71–R76. doi: 10.1152/ajpregu.1986.250.1.R71.

Doig, S. D. *et al.* (2005) 'Modelling surface aeration rates in shaken microtitre plates using dimensionless groups', *Chemical Engineering Science*, 60(10), pp. 2741–2750. doi: 10.1016/j.ces.2004.12.025.

Doran, P. M. (2013) *Bioprocess engineering principles*. Academic Press.

Dübel, S. and Reichert, J. M. (2014) *Handbook of Therapeutic Antibodies*. Wiley. Available at: https://books.google.de/books?id=I9k8BAAAQBAJ.

Duetz, W. A. *et al.* (2000) 'Methods for intense aeration, growth, storage, and replication of bacterial strains in microtiter plates.', *Applied and environmental microbiology*. American Society for Microbiology, 66(6), pp. 2641–6. doi: 10.1128/AEM.66.6.2641-2646.2000.

Duetz, W. A. (2007) 'Microtiter plates as mini-bioreactors: miniaturization of fermentation methods', *Trends in Microbiology*, 15(10), pp. 469–475. doi: 10.1016/j.tim.2007.09.004.

Duetz, W. A. and Witholt, B. (2001) 'Effectiveness of orbital shaking for the aeration of suspended bacterial cultures in square-deepwell microtiter plates', *Biochemical Engineering Journal*, 7(2), pp. 113–115. doi: 10.1016/S1369-703X(00)00109-1.

Duetz, W. A. and Witholt, B. (2004) ‘Oxygen transfer by orbital shaking of square vessels and deepwell microtiter plates of various dimensions’, *Biochemical Engineering Journal*, 17(3), pp. 181–185. doi: 10.1016/S1369-703X(03)00177-3.

Dunn, I. J. and Einsele, A. (1975) ‘Oxygen transfer coefficients by the dynamic method’, *Journal of Applied Chemistry and Biotechnology*. John Wiley & Sons, Ltd, 25(9), pp. 707–720. doi: 10.1002/jctb.5020250910.

Dürauer, A. *et al.* (2016) ‘Mixing at the microscale: Power input in shaken microtiter plates’, *Biotechnology Journal*, 11(12), pp. 1539–1549. doi: 10.1002/biot.201600027.

Ecker, D. M., Jones, S. D. and Levine, H. L. (2015) ‘The therapeutic monoclonal antibody market.’, *mAbs*. Taylor & Francis, 7(1), pp. 9–14. doi: 10.4161/19420862.2015.989042.

El-Enshasy (2007) ‘Effects of Different Osmotic Pressure of the Cultivation Media on hybridoma Cell Growth and Monoclonal Antibody Production Kinetics in Batch Culture’, *Biotechnology*, 6(2), pp. 202–209.

Elmahdi, I. *et al.* (2003) ‘pH control in microwell fermentations of S. erythraea CA340: influence on biomass growth kinetics and erythromycin biosynthesis’, *Biochemical Engineering Journal*, 16(3), pp. 299–310. doi: 10.1016/S1369-703X(03)00073-1.

Enzyscreen (1999) *System Duetz*. Available at: http://www.enzyscreen.com/sandwich_covers_24_mtps.htm (Accessed: 10 May 2017).

Erecińska, M., Deas, J. and Silver, I. A. (2002) ‘The Effect of pH on Glycolysis and Phosphofructokinase Activity in Cultured Cells and Synaptosomes’, *Journal of Neurochemistry*, 65(6), pp. 2765–2772. doi: 10.1046/j.1471-4159.1995.65062765.x.

Erra Díaz, F., Dantas, E. and Geffner, J. (2018) ‘Unravelling the interplay between extracellular acidosis and immune cells’, *Mediators of Inflammation*. Hindawi Limited. doi: 10.1155/2018/1218297.

Erstad, B. L. (2003) ‘Osmolality and Osmolarity: Narrowing the Terminology Gap’, *Pharmacotherapy*, 23(9), pp. 1085–1086. doi: 10.1592/phco.23.10.1085.32751.

Fenge, C. *et al.* (1993) ‘Agitation, aeration and perfusion modules for cell culture bioreactors’, *Cytotechnology*. Kluwer Academic Publishers, 11(3), pp. 233–244. doi: 10.1007/BF00749874.

Fink, M. *et al.* (2021) ‘High-throughput microbioreactor provides a capable tool for early stage bioprocess development’, *Scientific Reports*. Nature Research, 11(1), pp. 1–10. doi: 10.1038/s41598-021-81633-6.

Fletcher, T. (2005) ‘Designing culture media for recombinant protein production: A rational approach’, *BioProcess International*, 3(1), pp. 30–36.

François Cabaret *et al.* (2007) ‘Mixing Time Analysis Using Colorimetric Methods and Image Processing’. American Chemical Society. doi: 10.1021/IE0613265.

Freshney, R. I. (2010) *Culture of Animal Cells*. Hoboken, NJ, USA: John Wiley & Sons, Inc. doi: 10.1002/9780470649367.

Funke, M. *et al.* (2009) ‘The baffled microtiter plate: Increased oxygen transfer and improved online monitoring in small scale fermentations’, *Biotechnology and Bioengineering*, 103(6), pp. 1118–1128. doi: 10.1002/bit.22341.

Gagnon, M. *et al.* (2011) ‘High-End pH-controlled delivery of glucose effectively suppresses lactate accumulation in CHO Fed-batch cultures’, *Biotechnology and Bioengineering*. John Wiley & Sons, Ltd, 108(6), pp. 1328–1337. doi: 10.1002/bit.23072.

Gagnon, M. *et al.* (2019) ‘Novel, linked bioreactor system for continuous production of biologics’, *Biotechnology and Bioengineering*. John Wiley & Sons, Ltd, 116(8), p. bit.26985. doi: 10.1002/bit.26985.

Galleguillos, S. N. *et al.* (2017) ‘What can mathematical modelling say about CHO metabolism and protein glycosylation?’, *Computational and Structural Biotechnology Journal*. Elsevier, 15, pp. 212–221. doi: 10.1016/J.CSBJ.2017.01.005.

Garcia-Ochoa, F. and Gomez, E. (2008) 'Bioreactor scale-up and oxygen transfer rate in microbial processes: An overview', *Biotechnology Advances*, 27, pp. 153–176. doi: 10.1016/j.biotechadv.2008.10.006.

Gatenby, R. A. and Gillies, R. J. (2004) 'Why do cancers have high aerobic glycolysis?', *Nature Reviews Cancer*, 4(11), pp. 891–899. doi: 10.1038/nrc1478.

Gattinoni, L. *et al.* (2011) 'A human memory T cell subset with stem cell–like properties', *Nature Medicine*. Nature Publishing Group, 17(10), pp. 1290–1297. doi: 10.1038/nm.2446.

Gerweck, L. E. and Seetharaman, K. (1996) 'Cellular pH gradient in tumor versus normal tissue: potential exploitation for the treatment of cancer.', *Cancer research*, 56(6), pp. 1194–8. Available at: http://www.ncbi.nlm.nih.gov/pubmed/8640796 (Accessed: 29 October 2019).

Gigout, A., Buschmann, M. D. and Jolicoeur, M. (2008) 'The fate of Pluronic F-68 in chondrocytes and CHO cells.', *Biotechnology and bioengineering*, 100(5), pp. 975–87. doi: 10.1002/bit.21840.

Goldrick, S. *et al.* (2019) 'Multivariate Data Analysis Methodology to Solve Data Challenges Related to Scale-up Model Validation and Missing Data on a Micro-Bioreactor System', *Biotechnology Journal*. John Wiley & Sons, Ltd, p. 1800684. doi: 10.1002/biot.201800684.

Gouble, A. *et al.* (2014) 'In Vivo Proof of Concept of Activity and Safety of UCART19, an Allogeneic "Off-the-Shelf" Adoptive T-Cell Immunotherapy Against CD19+ B-Cell Leukemias', *Blood*, 124(21). Available at: http://www.bloodjournal.org/content/124/21/4689 (Accessed: 14 August 2019).

Goudar, C. T. *et al.* (2007) 'Decreased pCO2 accumulation by eliminating bicarbonate addition to high cell-density cultures', *Biotechnology and Bioengineering*. Wiley Subscription Services, Inc., A Wiley Company, 96(6), pp. 1107–1117. doi: 10.1002/bit.21116.

Gramer, M. J. *et al.* (2011) 'Modulation of antibody galactosylation through feeding of uridine, manganese chloride, and galactose', *Biotechnology and Bioengineering*. Wiley Subscription Services, Inc., A Wiley Company, 108(7), pp. 1591–1602. doi: 10.1002/bit.23075.

Grilo, A. L. and Mantalaris, A. (2019) ‘The Increasingly Human and Profitable Monoclonal Antibody Market’, *Trends in Biotechnology*. Elsevier Current Trends, 37(1), pp. 9–16. doi: 10.1016/J.TIBTECH.2018.05.014.

Gross, G., Waks, T. and Eshhar, Z. (1989) ‘Expression of immunoglobulin-T-cell receptor chimeric molecules as functional receptors with antibody-type specificity’, *Proceedings of the National Academy of Sciences of the United States of America*. National Academy of Sciences, 86(24), pp. 10024–10028. doi: 10.1073/pnas.86.24.10024.

Gu, X. and Wang, D. I. (1998) ‘Improvement of interferon-gamma sialylation in Chinese hamster ovary cell culture by feeding of N-acetylmannosamine.’, *Biotechnology and bioengineering*, 58(6), pp. 642–8. Available at: http://www.ncbi.nlm.nih.gov/pubmed/10099302 (Accessed: 20 October 2015).

Guy, H. M. *et al.* (2013) ‘Characterization of Lentiviral Vector Production Using Microwell Suspension Cultures of HEK293T-Derived Producer Cells’, *Human Gene Therapy Methods*, 24(2), pp. 125–139. doi: 10.1089/hgtb.2012.200.

Halperin, M. L. *et al.* (1969) ‘Factors that control the effect of pH on glycolysis in leukocytes.’, *The Journal of biological chemistry*, 244(2), pp. 384–90. Available at: http://www.ncbi.nlm.nih.gov/pubmed/4237582 (Accessed: 11 September 2019).

Han, Y. *et al.* (2006) ‘Cultivation of Recombinant Chinese hamster ovary cells grown as suspended aggregates in stirred vessels’, *Journal of Bioscience and Bioengineering*. Elsevier, 102(5), pp. 430–435. doi: 10.1263/jbb.102.430.

Hanson, M. A. *et al.* (2007) ‘Comparisons of optical pH and dissolved oxygen sensors with traditional electrochemical probes during mammalian cell culture’, *Biotechnology and Bioengineering*, 97(4), pp. 833–841. doi: 10.1002/bit.21320.

Haque, N. *et al.* (2013) ‘Hypoxic Culture Conditions as a Solution for Mesenchymal Stem Cell Based Regenerative Therapy’, *The Scientific World Journal*. Hindawi Publishing Corporation. doi: 10.1155/2013/632972.

Hartley, F. *et al.* (2018) ‘Mechanisms driving the lactate switch in Chinese hamster ovary cells’, *Biotechnology and Bioengineering*. Wiley-Blackwell, 115(8), pp. 1890–1903. doi: 10.1002/bit.26603.

Hay, K. A. and Turtle, C. J. (2017) ‘Chimeric Antigen Receptor (CAR) T Cells: Lessons Learned from Targeting of CD19 in B-Cell Malignancies’, *Drugs*. Springer International Publishing, 77(3), pp. 237–245. doi: 10.1007/s40265-017-0690-8.

Hegde, S. *et al.* (2012) ‘Controlled release of nutrients to mammalian cells cultured in shake flasks’, *Biotechnology Progress*. American Chemical Society (ACS), 28(1), pp. 188–195. doi: 10.1002/btpr.729.

Hemmerich, J. *et al.* (2018) ‘Microbioreactor Systems for Accelerated Bioprocess Development’, *Biotechnology Journal*. Wiley-Blackwell, 13(4), p. 1700141. doi: 10.1002/biot.201700141.

Hermann, R., Lehmann, M. and Büchs, J. (2003) ‘Characterization of gas-liquid mass transfer phenomena in microtiter plates’, *Biotechnology and Bioengineering*. Wiley Subscription Services, Inc., A Wiley Company, 81(2), pp. 178–186. doi: 10.1002/bit.10456.

Hewitt, C. J. and Nienow, A. W. (2007) ‘The Scale-Up of Microbial Batch and Fed-Batch Fermentation Processes’, *Advances in Applied Microbiology*, 62, pp. 105–135. doi: 10.1016/S0065-2164(07)62005-X.

Hsu, P. P. and Sabatini, D. M. (2008) ‘Cancer cell metabolism: Warburg and beyond.’, *Cell*, 134(5), pp. 703–7. doi: 10.1016/j.cell.2008.08.021.

Hsu, W.-T. *et al.* (2012) ‘Advanced microscale bioreactor system: a representative scale-down model for bench-top bioreactors.’, *Cytotechnology*, 64(6), pp. 667–78. doi: 10.1007/s10616-012-9446-1.

Hunter, M. C., Teijeira, A. and Halin, C. (2016) ‘T cell trafficking through lymphatic vessels’, *Frontiers in Immunology*. Frontiers Media S.A., p. 613. doi: 10.3389/fimmu.2016.00613.

Invitrogen (2007) *CHO CD EfficientFeed™ Kit User Manual*. Available at: https://assets.thermofisher.com/TFS-Assets/LSG/manuals/CHO_CD_EfficientFeed_man.pdf (Accessed: 18 March 2020).

Isett, K. *et al.* (2007) 'Twenty-four-well plate miniature bioreactor high-throughput system: Assessment for microbial cultivations', *Biotechnology and Bioengineering*. Wiley Subscription Services, Inc., A Wiley Company, 98(5), pp. 1017–1028. doi: 10.1002/bit.21484.

Islam, R. S. *et al.* (2007) 'Framework for the Rapid Optimization of Soluble Protein Expression in Escherichia coli Combining Microscale Experiments and Statistical Experimental Design', *Biotechnology Progress*. American Chemical Society, 23(4), pp. 785–793. doi: 10.1021/bp070059a.

Islam, R. S. *et al.* (2008) 'Scale-up ofEscherichia coli growth and recombinant protein expression conditions from microwell to laboratory and pilot scale based on matchedkLa', *Biotechnology and Bioengineering*. Wiley Subscription Services, Inc., A Wiley Company, 99(5), pp. 1128–1139. doi: 10.1002/bit.21697.

Ivarsson, M. *et al.* (2014) 'Evaluating the impact of cell culture process parameters on monoclonal antibody N-glycosylation', *Journal of Biotechnology*. Elsevier, 188, pp. 88–96. doi: 10.1016/J.JBIOTEC.2014.08.026.

Ivarsson, M. *et al.* (2015) 'Insights into pH-induced metabolic switch by flux balance analysis', *Biotechnology Progress*. American Chemical Society (ACS), 31(2), pp. 347–357. doi: 10.1002/btpr.2043.

Iyer, R. K. *et al.* (2018) 'Industrializing Autologous Adoptive Immunotherapies: Manufacturing Advances and Challenges', *Frontiers in Medicine*. Frontiers, 5, p. 150. doi: 10.3389/fmed.2018.00150.

Janas, M. *et al.* (2015) 'Perfusion's Role in Maintenance of High-Density T-Cell Cultures', *BioProcess International*, 13(1), pp. 18–26.

Jefferis, R. (2005) 'Glycosylation of recombinant antibody therapeutics.', *Biotechnology progress*, 21(1), pp. 11–6. doi: 10.1021/bp040016j.

Jefferis, R. (2007) ‘Antibody therapeutics: isotype and glycoform selection.’, *Expert opinion on biological therapy*, 7(9), pp. 1401–13. doi: 10.1517/14712598.7.9.1401.

Jefferis, R. (2009) ‘Glycosylation as a strategy to improve antibody-based therapeutics.’, *Nature reviews. Drug discovery*. Nature Publishing Group, 8(3), pp. 226–34. doi: 10.1038/nrd2804.

Jiang, R., Chen, H. and Xu, S. (2018) ‘pH excursions impact CHO cell culture performance and antibody N-linked glycosylation’, *Bioprocess and Biosystems Engineering*. Springer Verlag, 41(12), pp. 1731–1741. doi: 10.1007/s00449-018-1996-y.

Jo, E.-C. *et al.* (1990) ‘Balanced nutrient fortification enables high-density hybridoma cell culture in batch culture’, *Biotechnology and Bioengineering*. Wiley Subscription Services, Inc., A Wiley Company, 36(7), pp. 717–722. doi: 10.1002/bit.260360709.

Jo, E.-C. *et al.* (1993) ‘Repeated fed-batch culture of hybridoma cells in nutrient-fortified high-density medium’, *Biotechnology and Bioengineering*. Wiley Subscription Services, Inc., A Wiley Company, 42(10), pp. 1229–1237. doi: 10.1002/bit.260421013.

Jöbses, I., Martens, D. and Tramper, J. (1991) ‘Lethal events during gas sparging in animal cell culture’, *Biotechnology and Bioengineering*, 37(5), pp. 484–490. doi: 10.1002/bit.260370510.

John, G. *et al.* (2003) ‘pH-Sensing 96-well micrtotiter plates for the characterisation of acid production by dairy starter cultures.’, *J.Dairy Res*, 70, pp. 327–333.

Jordan, M. *et al.* (2013) ‘Cell culture medium improvement by rigorous shuffling of components using media blending’, *Cytotechnology*. Springer, 65(1), pp. 31–40. doi: 10.1007/s10616-012-9462-1.

Juran, J. M. (1992) *Juran on quality by design : the new steps for planning quality into goods and services*. Free Press.

Kaiser, A. D. *et al.* (2015) ‘Towards a commercial process for the manufacture of genetically modified T cells for therapy’, *Cancer Gene Therapy*. Nature Publishing Group, 22(2), pp. 72–78. doi: 10.1038/cgt.2014.78.

Kaisermayer, C. *et al.* (2016) ‘Biphasic cultivation strategy to avoid Epo-Fc aggregation and optimize protein expression’, *Journal of Biotechnology*, 227, pp. 3–9. doi: 10.1016/j.jbiotec.2016.03.054.

Kalos, M. *et al.* (2011) ‘T cells with chimeric antigen receptors have potent antitumor effects and can establish memory in patients with advanced leukemia.’, *Science translational medicine*. American Association for the Advancement of Science, 3(95), p. 95ra73. doi: 10.1126/scitranslmed.3002842.

Keane, J. T., Ryan, D. and Gray, P. P. (2003) ‘Effect of shear stress on expression of a recombinant protein by Chinese hamster ovary cells’, *Biotechnology and Bioengineering*. John Wiley & Sons, Ltd, 81(2), pp. 211–220. doi: 10.1002/bit.10472.

Keen, M. J. and Steward, T. W. (1995) ‘Adaptation of cholesterol-requiring NS0 mouse myeloma cells to high density growth in a fully defined protein-free and cholesterol-free culture medium.’, *Cytotechnology*, 17(3), pp. 203–11. doi: 10.1007/BF00749658.

Kelly, W. *et al.* (2018) ‘Optimizing performance of semi-continuous cell culture in an ambr15™ microbioreactor using dynamic flux balance modeling’, *Biotechnology Progress*. American Chemical Society (ACS), 34(2), pp. 420–431. doi: 10.1002/btpr.2585.

Kennett, R. H. (1981) ‘Hybridomas: a new dimension in biological analyses.’, *In vitro*, 17(12), pp. 1036–50. Available at: http://www.ncbi.nlm.nih.gov/pubmed/6172364 (Accessed: 2 November 2016).

Kensy, F., Engelbrecht, C. and Büchs, J. (2009) ‘Scale-up from microtiter plate to laboratory fermenter: evaluation by online monitoring techniques of growth and protein expression in Escherichia coli and Hansenula polymorpha fermentations’, *Microbial Cell Factories*. BioMed Central, 8(1), p. 68. doi: 10.1186/1475-2859-8-68.

Kerdouss, F. *et al.* (2008) ‘Two-phase mass transfer coefficient prediction in stirred vessel with a CFD model’, *Computers and Chemical Engineering*. doi: 10.1016/j.compchemeng.2007.10.010.

Kershaw, M. H., Westwood, J. A. and Darcy, P. K. (2013) ‘Gene-engineered T cells for cancer therapy’, *Nature Reviews Cancer*. Nature Publishing Group, 13(8), pp. 525–541. doi: 10.1038/nrc3565.

Khang, S. J. and Levenspiel, O. (1976) ‘New scale-up and design method for stirrer agitated batch mixing vessels’, *Chemical Engineering Science*, 31(7), pp. 569–577. doi: 10.1016/0009-2509(76)80020-6.

Kimura, R. and Miller, W. M. (1996) ‘Effects of elevated pCO2 and/or osmolality on the growth and recombinant tPA production of CHO cells’, *Biotechnology and Bioengineering*, 52(1), pp. 152–160. doi: 10.1002/(SICI)1097-0290(19961005)52:1<152::AID-BIT15>3.0.CO;2-Q.

Klarer, A. *et al.* (2018) ‘Demonstrating Scalable T-Cell Expansion in Stirred-Tank Bioreactors’, *Bioprocess International*, 16(6), pp. 6–14. Available at: https://bioprocessintl.com/manufacturing/cell-therapies/demonstrating-scalable-t-cell-expansion-in-stirred-tank-bioreactors/ (Accessed: 29 October 2019).

Klöckner, W. *et al.* (2012) ‘Power input correlation to characterize the hydrodynamics of cylindrical orbitally shaken bioreactors’, *Biochemical Engineering Journal*. Elsevier, 65, pp. 63–69. doi: 10.1016/J.BEJ.2012.04.007.

Klöckner, W. and Büchs, J. (2012) ‘Advances in shaking technologies’, *Trends in Biotechnology*, 30(6), pp. 307–314. doi: 10.1016/j.tibtech.2012.03.001.

Kochenderfer, J. N. *et al.* (2017) ‘Lymphoma Remissions Caused by Anti-CD19 Chimeric Antigen Receptor T Cells Are Associated With High Serum Interleukin-15 Levels.’, *Journal of clinical oncology : official journal of the American Society of Clinical Oncology*. American Society of Clinical Oncology, 35(16), pp. 1803–1813. doi: 10.1200/JCO.2016.71.3024.

Köhler, G. and Milstein, C. (1975) ‘Continuous cultures of fused cells secreting antibody of predefined specificity.’, *Nature*, 256(5517), pp. 495–7. Available at: http://www.ncbi.nlm.nih.gov/pubmed/1172191 (Accessed: 2 November 2016).

Konno, Y. *et al.* (2012) ‘Fucose content of monoclonal antibodies can be controlled by culture medium osmolality for high antibody-dependent cellular cytotoxicity.’, *Cytotechnology*, 64(3), pp. 249–65. doi: 10.1007/s10616-011-9377-2.

Kou, T.-C. *et al.* (2011) ‘Increasing the productivity of TNFR-Fc in GS-CHO cells at reduced culture temperatures’, *Biotechnology and Bioprocess Engineering*. The Korean Society for Biotechnology and Bioengineering, 16(1), pp. 136–143. doi: 10.1007/s12257-010-0157-1.

Kreye, S. *et al.* (2019) ‘A novel scale-down mimic of perfusion cell culture using sedimentation in an automated microbioreactor (SAM)’, *Biotechnology Progress*. John Wiley and Sons Inc., 35(5). doi: 10.1002/btpr.2832.

Kumar, N., Gammell, P. and Clynes, M. (2007) ‘Proliferation control strategies to improve productivity and survival during CHO based production culture’, *Cytotechnology*. Springer Netherlands, 53(1–3), pp. 33–46. doi: 10.1007/s10616-007-9047-6.

Kumar, S., Wittmann, C. and Heinzle, E. (2004) ‘Minibioreactors’, *Biotechnology Letters*, 26, pp. 1–10. Available at: https://link.springer.com/content/pdf/10.1023%2FB%3ABILE.0000009469.69116.03.pdf (Accessed: 16 August 2017).

Larbi, A. *et al.* (2010) ‘Induction of HIF-1α and the glycolytic pathway alters apoptotic and differentiation profiles of activated human T cells’, *Journal of Leukocyte Biology*. John Wiley & Sons, Ltd, 87(2), pp. 265–273. doi: 10.1189/jlb.0509304.

Lattermann, C. and Büchs, J. (2015) ‘Microscale and miniscale fermentation and screening’, *Current Opinion in Biotechnology*, 35, pp. 1–6. doi: 10.1016/j.copbio.2014.12.005.

Lattermann, C. and Büchs, J. (2016) ‘Design and Operation of Microbioreactor Systems for Screening and Process Development’, in *Bioreactors*. Weinheim, Germany: Wiley-VCH Verlag GmbH & Co. KGaA, pp. 35–76. doi: 10.1002/9783527683369.ch2.

Lavery, M. and Nienow, A. W. (1987) ‘Oxygen transfer in animal cell culture medium’, *Biotechnology and Bioengineering*. John Wiley & Sons, Ltd, 30(3), pp. 368–373. doi: 10.1002/bit.260300307.

Li, F. *et al.* (2010) ‘Cell culture processes for monoclonal antibody production’, *mAbs*. Taylor & Francis, 2(5), pp. 466–479. doi: 10.4161/mabs.2.5.12720.

Li, Y., Ducci, A. and Micheletti, M. (2020) ‘Study on mixing characteristics in shaken microwell systems’, *Biochemical Engineering Journal*. Elsevier, 153, p. 107392. doi: 10.1016/J.BEJ.2019.107392.

Lim, H. C. and Shin, H. S. (2013) *Fed-Batch Cultures: Principles and Applications of Semi-Batch Bioreactors*. Cambridge University Press (Cambridge Series in Chemical Engineering). Available at: https://books.google.co.uk/books?id=qVpobOmhOHsC.

Linek, V. and Vacek, V. (1988) ‘Volumetric mass transfer coefficient in stirred reactors’, *Chemical Engineering & Technology - CET*. WILEY-VCH Verlag, 11(1), pp. 249–251. doi: 10.1002/ceat.270110133.

Link, T. *et al.* (2004) ‘Bioprocess development for the production of a recombinant MUC1 fusion protein expressed by CHO-K1 cells in protein-free medium’, *Journal of Biotechnology*. Elsevier, 110(1), pp. 51–62. doi: 10.1016/J.JBIOTEC.2003.12.008.

Liu, Y.-S., Wu, J.-Y. and Ho, K. (2006) ‘Characterization of oxygen transfer conditions and their effects on Phaffia rhodozyma growth and carotenoid production in shake-flask cultures’, *Biochemical Engineering Journal*, 27(3), pp. 331–335. doi: 10.1016/j.bej.2005.08.031.

Ljunggren, J. and Häggström, L. (1994) ‘Catabolic control of hybridoma cells by glucose and glutamine limited fed batch cultures.’, *Biotechnology and bioengineering*, 44(7), pp. 808–18. doi: 10.1002/bit.260440706.

Louis, C. U. *et al.* (2011) ‘Antitumor activity and long-term fate of chimeric antigen receptor-positive T cells in patients with neuroblastoma’, *Blood*, 118(23), pp. 6050–6056. doi: 10.1182/blood-2011-05-354449.

Lu, F. *et al.* (2013) ‘Automated dynamic fed-batch process and media optimization for high productivity cell culture process development’, *Biotechnology and Bioengineering*, 110(1), pp. 191–205. doi: 10.1002/bit.24602.

Luan, Y. T., Mutharasan, R. and Magee, W. E. (1987) ‘Strategies to extend longevity of hybridomas in culture and promote yield of monoclonal antibodies’, *Biotechnology Letters*. Kluwer Academic Publishers, 9(10), pp. 691–696. doi: 10.1007/BF01024599.

Ma, N. *et al.* (2004) ‘Quantitative studies of cell-bubble interactions and cell damage at different pluronic F-68 and cell concentrations’, *Biotechnology Progress*. American Chemical Society (ACS), 20(4), pp. 1183–1191. doi: 10.1021/bp0342405.

Maier, U. and Büchs, J. (2001) ‘Characterisation of the gas-liquid mass transfer in shaking bioreactors’, in *Biochemical Engineering Journal*. Elsevier, pp. 99–106. doi: 10.1016/S1369-703X(00)00107-8.

Mandenius, C. F. (2016) ‘Design-of-Experiments for Development and Optimization of Bioreactor Media’, in *Bioreactors*. Weinheim, Germany: Wiley-VCH Verlag GmbH & Co. KGaA, pp. 421–452. doi: 10.1002/9783527683369.ch15.

Markert, S. *et al.* (2019) ‘Automated and enhanced clone screening using a fully automated microtiter plate-based system for suspension cell culture’, *Biotechnology Progress*. American Chemical Society (ACS), 35(2), p. e2760. doi: 10.1002/btpr.2760.

Markert, S. and Joeris, K. (2017) ‘Establishment of a fully automated microtiter plate-based system for suspension cell culture and its application for enhanced process optimization’, *Biotechnology and Bioengineering*, 114(1), pp. 113–121. doi: 10.1002/bit.26044.

Marques, M. P. C., Cabral, J. M. S. and Fernandes, P. (2010) ‘Bioprocess scale-up: quest for the parameters to be used as criterion to move from microreactors to lab-scale’, *Journal of Chemical Technology & Biotechnology*. John Wiley & Sons, Ltd., 85(9), pp. 1184–1198. doi: 10.1002/jctb.2387.

Martuza, R. L. *et al.* (1976) ‘Evaporation as a cause of positional differences in cell plating and growth in microtiter plates’, *Transplantation*, 21(3), pp. 271–273. doi: 10.1097/00007890-197603000-00016.

Maude, S. L. *et al.* (2014) ‘Chimeric Antigen Receptor T Cells for Sustained Remissions in Leukemia’, *New England Journal of Medicine*. Massachusetts Medical Society, 371(16), pp. 1507–1517. doi: 10.1056/NEJMoa1407222.

McCracken, N. A., Kowle, R. and Ouyang, A. (2014) ‘Control of galactosylated glycoforms distribution in cell culture system.’, *Biotechnology progress*, 30(3), pp. 547–53. doi: 10.1002/btpr.1906.

McQueen, A. and Bailey, J. E. (1990) ‘Effect of ammonium ion and extracellular pH on hybridoma cell metabolism and antibody production’, *Biotechnology and Bioengineering*, 35(11), pp. 1067–1077. doi: 10.1002/bit.260351102.

Melton, L. A. *et al.* (2002) ‘Dismt - Determination of mixing time through color changes’, *Chemical Engineering Communications*. Taylor & Francis Group , 189(3), pp. 322–338. doi: 10.1080/00986440212077.

Michaels, J. D., Mallik, A. K. and Papoutsakis, E. T. (1996) ‘Sparging and agitation-induced injury of cultured animals cells: Do cell-to-bubble interactions in the bulk liquid injure cells?’, *Biotechnology and Bioengineering*. Wiley Subscription Services, Inc., A Wiley Company, 51(4), pp. 399–409. doi: 10.1002/(SICI)1097-0290(19960820)51:4<399::AID-BIT3>3.0.CO;2-D.

Micheletti, M. *et al.* (2006) ‘Fluid mixing in shaken bioreactors: Implications for scale-up predictions from microlitre-scale microbial and mammalian cell cultures’, *Chemical Engineering Science*, 61(9), pp. 2939–2949. doi: 10.1016/j.ces.2005.11.028.

Micheletti, M. and Lye, G. J. (2006) ‘Microscale bioprocess optimisation’, *Current Opinion in Biotechnology*, 17(6), pp. 611–618. doi: 10.1016/j.copbio.2006.10.006.

Mock, U. *et al.* (2016) ‘Automated manufacturing of chimeric antigen receptor T cells for adoptive immunotherapy using CliniMACS Prodigy’, *Cytotherapy*. Elsevier, 18(8), pp. 1002–1011. doi: 10.1016/J.JCYT.2016.05.009.

Montes, F. J., Catalán, J. and Galán, M. A. (1999) ‘Prediction of kLa in yeast broths’, *Process Biochemistry*, 34(6), pp. 549–555. doi: 10.1016/S0032-9592(98)00125-3.

Moore, A. *et al.* (1997) ‘Effects of temperature shift on cell cycle, apoptosis and nucleotide pools in CHO cell batch cultues’, *Cytotechnology*. Kluwer Academic Publishers, 23(1/3), pp. 47–54. doi: 10.1023/A:1007919921991.

Mora, A. *et al.* (2018) ‘Sustaining an efficient and effective CHO cell line development platform by incorporation of 24-deep well plate screening and multivariate analysis’, *Biotechnology Progress*. American Chemical Society (ACS), 34(1), pp. 175–186. doi: 10.1002/btpr.2584.

Mordon, S. *et al.* (1992) ‘Characterization of tumorous and normal tissue using a pH-sensitive fluorescence indicator (5,6-carboxyfluorescein) in vivo’, *Journal of Photochemistry and Photobiology, B: Biology*, 13(3–4), pp. 307–314. doi: 10.1016/1011-1344(92)85070-B.

Mostafa, S. S. and Gu, X. S. (2003) ‘Strategies for Improved dCO2 Removal in Large-Scale Fed-Batch Cultures’, *Biotechnology Progress*. American Chemical Society (ACS), 19(1), pp. 45–51. doi: 10.1021/bp0256263.

Mulukutla, B. C., Gramer, M. and Hu, W.-S. (2012) ‘On metabolic shift to lactate consumption in fed-batch culture of mammalian cells’, *Metabolic Engineering*, 14(2), pp. 138–149. doi: 10.1016/j.ymben.2011.12.006.

Muntari, B. *et al.* (2012) ‘Recombinant bromelain production in Escherichia coli: Process optimization in shake flask culture by response surface methodology’, *AMB Express*. Springer Verlag, 2(1), pp. 1–9. doi: 10.1186/2191-0855-2-12.

Murphy, K. M. (2011) *Janeway’s Immunobiology*. Taylor & Francis Group. Available at: https://books.google.de/books?id=WDMmAgAAQBAJ.

Müthing, J. *et al.* (2003) ‘Effects of buffering conditions and culture pH on production rates and glycosylation of clinical phase I anti-melanoma mouse IgG3 monoclonal antibody R24’, *Biotechnology and Bioengineering*. John Wiley & Sons, Ltd, 83(3), pp. 321–334. doi: 10.1002/bit.10673.

Naciri, M., Kuystermans, D. and Al-Rubeai, M. (2008) ‘Monitoring pH and dissolved oxygen in mammalian cell culture using optical sensors’, *Cytotechnology*. Springer Netherlands, 57(3), pp. 245–250. doi: 10.1007/s10616-008-9160-1.

Nagata, S. (1975) *Mixing: principles and applications*. Kodansha (Kodansha scientific books). Available at: https://books.google.co.uk/books?id=j75TAAAAMAAJ.

Nguyen Dang, A. *et al.* (2019) 'Interaction of cell culture process parameters for modulating mAb afucosylation', *Biotechnology and Bioengineering*. John Wiley & Sons, Ltd, p. bit.26908. doi: 10.1002/bit.26908.

Nienow, A. W. (1997) 'On impeller circulation and mixing effectiveness in the turbulent flow regime', *Chemical Engineering Science*, 52(15), pp. 2557–2565. doi: 10.1016/S0009-2509(97)00072-9.

Nienow, A. W. (2006) 'Reactor Engineering in Large Scale Animal Cell Culture', *Cytotechnology*. Springer Netherlands, 50(1–3), pp. 9–33. doi: 10.1007/s10616-006-9005-8.

Nienow, A. W. *et al.* (2013) 'The physical characterisation of a microscale parallel bioreactor platform with an industrial CHO cell line expressing an IgG4', *Biochemical Engineering Journal*, 76, pp. 25–36. doi: 10.1016/j.bej.2013.04.011.

Nienow, A. W. (2015) 'Aeration in Biotechnology', in *Kirk-Othmer Encyclopedia of Chemical Technology*. Hoboken, NJ, USA: John Wiley & Sons, Inc., pp. 1–23. doi: 10.1002/0471238961.0209152014090514.a01.pub3.

Odeleye, A. O. O. *et al.* (2014) 'On the fluid dynamics of a laboratory scale single-use stirred bioreactor.', *Chemical engineering science*. Elsevier, 111(100), pp. 299–312. doi: 10.1016/j.ces.2014.02.032.

Oh, S. K., Chua, F. K. and Choo, A. B. (1995) 'Intracellular responses of productive hybridomas subjected to high osmotic pressure.', *Biotechnology and bioengineering*, 46(6), pp. 525–35. doi: 10.1002/bit.260460605.

Oh, S. K. W. *et al.* (1989) 'The effects of agitation intensity with and without continuous sparging on the growth and antibody production of hybridoma cells', *Journal of Biotechnology*. Elsevier, 12(1), pp. 45–61. doi: 10.1016/0168-1656(89)90128-4.

Oh, S. K. W. *et al.* (1992) ‘Further studies of the culture of mouse hybridomas in an agitated bioreactor with and without continuous sparging’, *Journal of Biotechnology*, 22(3), pp. 245–270. doi: 10.1016/0168-1656(92)90144-X.

Oosterhuis, N. M. G. and Kossen, N. W. F. (1981) ‘Power input measurements in a production scale bioreactor’, *Biotechnology Letters*. Kluwer Academic Publishers, 3(11), pp. 645–650. doi: 10.1007/BF00158694.

Ozturk, S. and Hu, W. S. (2005) *Cell Culture Technology for Pharmaceutical and Cell-Based Therapies*. CRC Press (Biotechnology and Bioprocessing). Available at: https://books.google.de/books?id=KIRTCpMHU28C.

P&S Market Research (2015) *Global Biopharmaceuticals Market Size, Share, Development, Growth and Demand Forecast to 2020 – Industry Insights by Type and by Application*. Available at: https://www.reportbuyer.com/product/3605399/global-biopharmaceuticals-market-size-share-development-growth-and-demand-forecast-to-2020-industry-insights-by-type-and-by-application.html.

De Palma, A. (2014) ‘Single-Use Bioreactors Dare to Scale’, *Genetic Engineering & Biotechnology News*, 34(14), pp. 24, 26–27. doi: 10.1089/gen.34.14.12.

Phillips, P. J. *et al.* (1991) ‘An analysis of some batch and continuous kinetic data of specific monoclonal antibody production from hybridomas’, *Cytotechnology*, 6, pp. 189–195.

Pilon-Thomas, S. *et al.* (2016) ‘Neutralization of Tumor Acidity Improves Antitumor Responses to Immunotherapy’, *Cancer Research*. American Association for Cancer Research, 76(6), pp. 1381–1390. doi: 10.1158/0008-5472.CAN-15-1743.

Porter, D. L. *et al.* (2015) ‘Chimeric antigen receptor T cells persist and induce sustained remissions in relapsed refractory chronic lymphocytic leukemia’, *Science Translational Medicine*. American Association for the Advancement of Science, 7(303). doi: 10.1126/scitranslmed.aac5415.

Raju, T. S. (2003) ‘Glycosylation variations with expression systems’, *BioProcess International*, 9(2), pp. 44–53.

Rameez, S. *et al.* (2014) ‘High-throughput miniaturized bioreactors for cell culture process development: Reproducibility, scalability, and control’, *Biotechnology Progress*, 30(3), pp. 718–727. doi: 10.1002/btpr.1874.

Rao, G., Moreira, A. and Brorson, K. (2009) ‘Disposable bioprocessing: The future has arrived’, *Biotechnology and Bioengineering*, 102(2), pp. 348–356. doi: 10.1002/bit.22192.

Rathore, A. S., Kanwar Shekhawat, L. and Loomba, V. (2016) ‘Computational Fluid Dynamics for Bioreactor Design’, in *Bioreactors*. Weinheim, Germany: Wiley-VCH Verlag GmbH & Co. KGaA, pp. 295–322. doi: 10.1002/9783527683369.ch10.

Raval, K., Kato, Y. and Büchs, J. (2007) ‘Comparison of torque method and temperature method for determination of power consumption in disposable shaken bioreactors’, *Biochemical Engineering Journal*, 34(3), pp. 224–227. doi: 10.1016/j.bej.2006.12.017.

Rayat, A. C. *et al.* (2016) ‘Ultra scale-down approaches to enhance the creation of bioprocesses at scale: impacts of process shear stress and early recovery stages’, *Current Opinion in Chemical Engineering*. Elsevier Ltd, pp. 150–157. doi: 10.1016/j.coche.2016.09.012.

Reichert, J. M. *et al.* (2005) ‘Monoclonal antibody successes in the clinic’, *Nature Biotechnology*. Nature Publishing Group, 23(9), pp. 1073–1078. doi: 10.1038/nbt0905-1073.

Reichert, J. M. (2016) ‘Antibodies to watch in 2016’, 8(2), pp. 197–204. doi: 10.1080/19420862.2015.1125583.

Reichert, J. M. and Valge-Archer, V. E. (2007) ‘Development trends for monoclonal antibody cancer therapeutics’, *Nature Reviews Drug Discovery*. Nature Publishing Group, 6(5), pp. 349–356. doi: 10.1038/nrd2241.

Rillahan, C. D. *et al.* (2012) ‘Global metabolic inhibitors of sialyl- and fucosyltransferases remodel the glycome.’, *Nature chemical biology*, 8(7), pp. 661–8. doi: 10.1038/nchembio.999.

Roddie, C. *et al.* (2019) ‘Manufacturing chimeric antigen receptor T cells: issues and challenges’, *Cytotherapy*. Elsevier, 21(3), pp. 327–340. doi: 10.1016/J.JCYT.2018.11.009.

Rodrigues, M. E. *et al.* (2010) ‘Technological progresses in monoclonal antibody production systems.’, *Biotechnology progress*, 26(2), pp. 332–51. doi: 10.1002/btpr.348.

Rodriguez, G. *et al.* (2014) ‘On the measurement and scaling of mixing time in orbitally shaken bioreactors’, *Biochemical Engineering Journal*, 82, pp. 10–21. doi: 10.1016/j.bej.2013.10.021.

Rowland-Jones, R. C. and Jaques, C. (2019) ‘At-line raman spectroscopy and design of experiments for robust monitoring and control of miniature bioreactor cultures’, *Biotechnology Progress*. American Chemical Society (ACS), 35(2), p. e2740. doi: 10.1002/btpr.2740.

Sallusto, F. *et al.* (1999) ‘Two subsets of memory T lymphocytes with distinct homing potentials and effector functions’, *Nature*, 401(6754), pp. 708–712. doi: 10.1038/44385.

Sandner, V. *et al.* (2019) ‘Scale-Down Model Development in ambr systems: An Industrial Perspective’, *Biotechnology Journal*, 14(4), p. 1700766. doi: 10.1002/biot.201700766.

Sarkar, J. *et al.* (2016) ‘CFD of mixing of multi-phase flow in a bioreactor using population balance model’, *Biotechnology Progress*. John Wiley and Sons Inc., 32(3), pp. 613–628. doi: 10.1002/btpr.2242.

Schaber, S. D. *et al.* (2011) ‘Economic Analysis of Integrated Continuous and Batch Pharmaceutical Manufacturing: A Case Study’, *Ind. Eng. Chem. Res*, 50, pp. 10083–10092. doi: 10.1021/ie2006752.

Schirrmann, T. *et al.* (2011) ‘Phage Display for the Generation of Antibodies for Proteome Research, Diagnostics and Therapy’, *Molecules*. Molecular Diversity Preservation International, 16(12), pp. 412–426. doi: 10.3390/molecules16010412.

Schneider, U., Schwenk, H.-U. and Bornkamm, G. (1977) ‘Characterization of EBV-genome negative “null” and “T” cell lines derived from children with acute lymphoblastic leukemia and leukemic transformed non-Hodgkin lymphoma’, *International Journal of Cancer*. John Wiley & Sons, Ltd, 19(5), pp. 621–626. doi: 10.1002/ijc.2910190505.

Schumpe, A. (1993) ‘The estimation of gas solubilities in salt solutions’, *Chemical Engineering Science*, 48(1), pp. 153–158. doi: 10.1016/0009-2509(93)80291-W.

Seo, J. S. *et al.* (2013) ‘Effect of culture pH on recombinant antibody production by a new human cell line, F2N78, grown in suspension at 33.0 °C and 37.0 °C’, *Applied Microbiology and Biotechnology*. Springer-Verlag, 97(12), pp. 5283–5291. doi: 10.1007/s00253-013-4849-2.

Sever, J. L. (1962) ‘Application of a microtechnique to viral serological investigations.’, *Journal of immunology (Baltimore, Md. : 1950)*. American Association of Immunologists, 88(3), pp. 320–9. Available at: http://www.ncbi.nlm.nih.gov/pubmed/13910995 (Accessed: 9 August 2018).

Sewell, D. J. *et al.* (2019) ‘Enhancing the functionality of a microscale bioreactor system as an industrial process development tool for mammalian perfusion culture’, *Biotechnology and Bioengineering*. John Wiley & Sons, Ltd, 116(6), pp. 1315–1325. doi: 10.1002/bit.26946.

Sharma, C., Malhotra, D. and Rathore, A. S. (2011) ‘Review of Computational fluid dynamics applications in biotechnology processes’, *Biotechnology Progress*. American Chemical Society (ACS), 27(6), pp. 1497–1510. doi: 10.1002/btpr.689.

Shuler, M. L. and Kargi, F. (1992) *Bioprocess engineering : basic concepts*. Prentice Hall.

Silk, N. (2014) *High throughput approaches to mammalian cell culture process development*, *Doctoral thesis*. London, UCL (University College London). Available at: https://discovery.ucl.ac.uk/id/eprint/1420214/ (Accessed: 10 November 2019).

Silk, N. J. *et al.* (2010) ‘Fed-batch operation of an industrial cell culture process in shaken microwells’, *Biotechnology Letters*. Springer Netherlands, 32(1), pp. 73–78. doi: 10.1007/s10529-009-0124-0.

Simaria, A. S. *et al.* (2014) ‘Allogeneic cell therapy bioprocess economics and optimization: Single-use cell expansion technologies’, *Biotechnology and Bioengineering*. John Wiley & Sons, Ltd, 111(1), pp. 69–83. doi: 10.1002/bit.25008.

Simons, A. *et al.* (2013) ‘Chemotherapy and monoclonal antibodies’, in *Haematology Nursing*. West Sussex, UK: John Wiley & Sons, Ltd., pp. 275–286. doi: 10.1002/9781118702949.ch19.

Sinacore, M. S. *et al.* (1996) ‘CHO DUKX cell lineages preadapted to growth in serum-free suspension culture enable rapid development of cell culture processes for the manufacture of recombinant proteins’, *Biotechnology and Bioengineering*, 52(4), pp. 518–528. doi: 10.1002/(SICI)1097-0290(19961120)52:4<518::AID-BIT7>3.0.CO;2-S.

Snee, R. D. (2011) ‘Think Strategically for Design of Experiments Success’, pp. 18–26.

Spens, E. and Häggström, L. (2007) ‘Defined protein and animal component-free NS0 fed-batch culture.’, *Biotechnology and bioengineering*, 98(6), pp. 1183–94. doi: 10.1002/bit.21509.

Street, T. O., Bolen, D. W. and Rose, G. D. (2006) ‘A molecular mechanism for osmolyte-induced protein stability.’, *Proceedings of the National Academy of Sciences of the United States of America*, 103(38), pp. 13997–4002. doi: 10.1073/pnas.0606236103.

Sumino, Y., Akiyama, S. and Fukuda, H. (1972) ‘Performance of the shaking flask (I) power consumption’, *J Ferment Technol*, 50, pp. 203–208.

Sutherland, R. M. (1988) ‘Cell and environment interactions in tumor microregions: The multicell spheroid model’, *Science*. American Association for the Advancement of Science, pp. 177–184. doi: 10.1126/science.2451290.

Tait, A. S. *et al.* (2013) ‘Differential response in downstream processing of CHO cells grown under mild hypothermic conditions’, *Biotechnology Progress*. American Chemical Society (ACS), 29(3), pp. 688–696. doi: 10.1002/btpr.1726.

Takagi, M., Hayashi, H. and Yoshida, T. (2000) ‘The effect of osmolarity on metabolism and morphology in adhesion and suspension chinese hamster ovary cells producing tissue plasminogen activator.’, *Cytotechnology*. Springer, 32(3), pp. 171–9. doi: 10.1023/A:1008171921282.

Tang, Y.-J., Ohashi, R. and Hamel, J.-F. P. (2007) ‘Perfusion culture of hybridoma cells for hyperproduction of IgG(2a) monoclonal antibody in a wave bioreactor-perfusion culture system.’, *Biotechnology progress*, 23(1), pp. 255–64. doi: 10.1021/bp060299a.

Thitilertdecha, P. *et al.* (2018) ‘A closed-culture system using a GMP-grade culture bag and anti-CD3/28 coated bead stimulation for CD4+ T cell expansion from healthy and HIV-infected donors’, *Journal of Immunological Methods*. Elsevier B.V., 460, pp. 17–25. doi: 10.1016/j.jim.2018.06.004.

Thomas, J. M. D. *et al.* (2017) ‘Validation of a CFD model of an orbiting culture dish with PIV and analytical solutions’, *AIChE Journal*. John Wiley and Sons Inc., 63(9), pp. 4233–4242. doi: 10.1002/aic.15762.

Tissot, S. *et al.* (2010) ‘Determination of a scale-up factor from mixing time studies in orbitally shaken bioreactors’, *Biochemical Engineering Journal*. Elsevier, 52(2–3), pp. 181–186. doi: 10.1016/J.BEJ.2010.08.005.

Toussaint, C., Henry, O. and Durocher, Y. (2016) ‘Metabolic engineering of CHO cells to alter lactate metabolism during fed-batch cultures’, *Journal of Biotechnology*. Elsevier, 217, pp. 122–131. doi: 10.1016/J.JBIOTEC.2015.11.010.

Tregidgo, M., Micheletti, M. and Pollard, D. (2017) ‘Ultra scale-down mimics for perfusion culture: Experimental study for rapid biopharmaceutical process development’, *Integrated Continuous Biomanufacturing III*. Available at: https://dc.engconfintl.org/biomanufact_iii/49 (Accessed: 18 April 2020).

Trivedi, B. and Danforth, W. H. (1966) ‘Effect of pH on the kinetics of frog muscle phosphofructokinase.’, *The Journal of biological chemistry*, 241(17), pp. 4110–2. Available at: http://www.ncbi.nlm.nih.gov/pubmed/4224144 (Accessed: 11 September 2019).

Trummer, E. *et al.* (2006) ‘Process parameter shifting: Part I. Effect of DOT, pH, and temperature on the performance of Epo-Fc expressing CHO cells cultivated in controlled batch bioreactors’, *Biotechnology and Bioengineering*, 94(6), pp. 1033–1044. doi: 10.1002/bit.21013.

van der Valk, J. *et al.* (2004) 'The humane collection of fetal bovine serum and possibilities for serum-free cell and tissue culture.', *Toxicology in vitro : an international journal published in association with BIBRA*, 18(1), pp. 1–12. Available at: http://www.ncbi.nlm.nih.gov/pubmed/14630056 (Accessed: 18 September 2015).

van der Valk, J. *et al.* (2010) 'Optimization of chemically defined cell culture media – Replacing fetal bovine serum in mammalian in vitro methods', *Toxicology in Vitro*, 24(4), pp. 1053–1063. doi: 10.1016/j.tiv.2010.03.016.

Vallée, C., Durocher, Y. and Henry, O. (2014) 'Exploiting the metabolism of PYC expressing HEK293 cells in fed-batch cultures', *Journal of Biotechnology*. Elsevier, 169, pp. 63–70. doi: 10.1016/J.JBIOTEC.2013.11.002.

Van't Riet, K. (1979) 'Review of Measuring Methods and Results in Nonviscous Gas-Liquid Mass Transfer in Stirred Vessels', *Industrial & Engineering Chemistry Process Design and Development*. American Chemical Society, 18(3), pp. 357–364. doi: 10.1021/i260071a001.

Velez-Suberbie, M. L. *et al.* (2018) 'High throughput automated microbial bioreactor system used for clone selection and rapid scale-down process optimization', *Biotechnology Progress*. American Chemical Society (ACS), 34(1), pp. 58–68. doi: 10.1002/btpr.2534.

VelezSuberbie, M. L. *et al.* (2013) 'Impact of aeration strategy on CHO cell performance during antibody production', *Biotechnology Progress*. Wiley Subscription Services, Inc., A Wiley Company, 29(1), pp. 116–126. doi: 10.1002/btpr.1647.

Visuri, O., Laakkonen, M. and Aittamaa, J. (2007) 'A Digital Imaging Technique for the Analysis of Local Inhomogeneities from Agitated Vessels', *Chemical Engineering & Technology*. WILEY-VCH Verlag, 30(12), pp. 1692–1699. doi: 10.1002/ceat.200700306.

Voncken, R. M., Holmis, D. B. and Den Hartog, H. W. (1964) 'Fluid flow in turbine-stirred, bailled tanks-II Dispersion during circulation', *Chemical Engineering Science*. Pergamon Press Ltd, 19, pp. 209–213.

Vormittag, P. *et al.* (2018) 'A guide to manufacturing CAR T cell therapies', *Current Opinion in Biotechnology*, 53, pp. 164–181. doi: 10.1016/j.copbio.2018.01.025.

Walsh, G. (2014) ‘Biopharmaceutical benchmarks 2014’, *Nature Biotechnology*. Nature Research, 32(10), pp. 992–1000. doi: 10.1038/nbt.3040.

Wang, X. *et al.* (2016) ‘Phase 1 studies of central memory-derived CD19 CAR T-cell therapy following autologous HSCT in patients with B-cell NHL.’, *Blood*. The American Society of Hematology, 127(24), pp. 2980–90. doi: 10.1182/blood-2015-12-686725.

Warikoo, V. *et al.* (2012) ‘Integrated continuous production of recombinant therapeutic proteins’, *Biotechnology and Bioengineering*. Wiley Subscription Services, Inc., A Wiley Company, 109(12), pp. 3018–3029. doi: 10.1002/bit.24584.

Waymouth, C. (1970) ‘Osmolality of mammalian blood and of media for culture of mammalian cells’, *In Vitro*, 6(2), pp. 109–127. doi: 10.1007/BF02616113.

Weiner, L. M., Surana, R. and Wang, S. (2010) ‘Monoclonal antibodies: versatile platforms for cancer immunotherapy’, *Nature Reviews Immunology*. Nature Publishing Group, 10(5), pp. 317–327. doi: 10.1038/nri2744.

Weinhouse, S. *et al.* (1956) ‘On Respiratory Impairment in Cancer Cells’, *Science*, 124(3215), pp. 267–272. doi: 10.1126/science.124.3215.267.

Weissenborn, P. K. and Pugh, R. J. (1996) ‘Surface Tension of Aqueous Solutions of Electrolytes: Relationship with Ion Hydration, Oxygen Solubility, and Bubble Coalescence’, *Journal of Colloid and Interface Science*, 184(2), pp. 550–563. doi: 10.1006/jcis.1996.0651.

Wenger, R. *et al.* (2015) ‘Frequently asked questions in hypoxia research’, *Hypoxia*. Dove Medical Press Ltd., p. 35. doi: 10.2147/hp.s92198.

Weuster-Botz, D., Stevens, S. and Hawrylenko, A. (2002) *Parallel-operated stirred-columns for microbial process development*, *Biochemical Engineering Journal*. doi: 10.1016/S1369-703X(02)00010-4.

Whitman, W. G. (1923) ‘The Two-Film Theory of Gas Absorption It Seems to Explain Satisfactorily the Well-Recognized Differences of Absorption Rate for Varying Concentrations’, *Chemical And Metallurgical Engineering*, 29(4).

Wiegmann, V. *et al.* (2019) ‘Towards the development of automated fed-batch cell culture processes at microscale’, *BioTechniques*. Future Science Ltd London, UK, p. btn-2019-0063. doi: 10.2144/btn-2019-0063.

Wiegmann, V., Martinez, C. B. and Baganz, F. (2018) ‘A simple method to determine evaporation and compensate for liquid losses in small-scale cell culture systems’, *Biotechnology Letters*, 40(7), pp. 1029–1036. doi: 10.1007/s10529-018-2556-x.

Wiegmann, V., Martinez, C. B. and Baganz, F. (2020) ‘Using a Parallel Micro-Cultivation System (Micro-Matrix) as a Process Development Tool for Cell Culture Applications’, *Methods in molecular biology (Clifton, N.J.)*. NLM (Medline), 2095, pp. 69–81. doi: 10.1007/978-1-0716-0191-4_5.

Wlaschin, K. F. and Hu, W.-S. (2006) ‘Fedbatch Culture and Dynamic Nutrient Feeding’, in. Springer, Berlin, Heidelberg, pp. 43–74. doi: 10.1007/10_015.

Wolf, M. K. F. *et al.* (2019) ‘Process design and development of a mammalian cell perfusion culture in shake-tube and benchtop bioreactors’, *Biotechnology and Bioengineering*. John Wiley & Sons, Ltd, 116(8), p. bit.26999. doi: 10.1002/bit.26999.

Woof, J. M. and Burton, D. R. (2004) ‘Human antibody–Fc receptor interactions illuminated by crystal structures’, *Nature Reviews Immunology*, 4(2), pp. 89–99. doi: 10.1038/nri1266.

Wu, P., Ray, N. G. and Shuler, M. L. (1993) ‘A computer model for intracellular pH regulation in Chinese hamster ovary cells’, *Biotechnology Progress*, 9(4), pp. 374–384. doi: 10.1021/bp00022a004.

Wurm, F. M. (2004) ‘Production of recombinant protein therapeutics in cultivated mammalian cells.’, *Nature biotechnology*, 22(11), pp. 1393–8. doi: 10.1038/nbt1026.

Wutz, J. *et al.* (2018) ‘Establishment of a CFD-based $k_L a$ model in microtiter plates to support CHO cell culture scale-up during clone selection’, *Biotechnology Progress*. American Chemical Society (ACS), 34(5), pp. 1120–1128. doi: 10.1002/btpr.2707.

Xie, L. *et al.* (2002) ‘Serum-free suspension cultivation of PER.C6® cells and recombinant adenovirus production under different pH conditions’, *Biotechnology and Bioengineering*. Wiley Subscription Services, Inc., A Wiley Company, 80(5), pp. 569–579. doi: 10.1002/bit.10443.

Xing, Z. *et al.* (2009a) ‘Scale-up analysis for a CHO cell culture process in large-scale bioreactors’, *Biotechnology and Bioengineering*. Wiley Subscription Services, Inc., A Wiley Company, 103(4), pp. 733–746. doi: 10.1002/bit.22287.

Xing, Z. *et al.* (2009b) ‘Scale-up analysis for a CHO cell culture process in large-scale bioreactors’, *Biotechnology and Bioengineering*. John Wiley & Sons, Ltd, 103(4), pp. 733–746. doi: 10.1002/bit.22287.

Xing, Z. *et al.* (2017) ‘A carbon dioxide stripping model for mammalian cell culture in manufacturing scale bioreactors’, *Biotechnology and Bioengineering*, 114(6), pp. 1184–1194. doi: 10.1002/bit.26232.

Xu, S. *et al.* (2017) ‘A practical approach in bioreactor scale-up and process transfer using a combination of constant P / V and vvm as the criterion’, *Biotechnology Progress*. American Chemical Society (ACS), 33(4), pp. 1146–1159. doi: 10.1002/btpr.2489.

Xu, S. *et al.* (2018) ‘Probing lactate metabolism variations in large-scale bioreactors’, *Biotechnology Progress*. American Chemical Society (ACS), 34(3), pp. 756–766. doi: 10.1002/btpr.2620.

Yao, W. . *et al.* (1998) ‘Mixing performance experiments in impeller stirred tanks subjected to unsteady rotational speeds’, *Chemical Engineering Science*, 53(17), pp. 3031–3040. doi: 10.1016/S0009-2509(98)00116-X.

Yoon, S. K. *et al.* (2005) ‘Effect of culture pH on erythropoietin production by Chinese hamster ovary cells grown in suspension at 32.5 and 37.0°C’, *Biotechnology and Bioengineering*. Wiley Subscription Services, Inc., A Wiley Company, 89(3), pp. 345–356. doi: 10.1002/bit.20353.

Yoon, S. K., Ahn, Y.-H. and Han, K. (2001) ‘Enhancement of recombinant erythropoietin production in CHO cells in an incubator without CO2 addition’, *Cytotechnology*. Kluwer Academic Publishers, 37(2), pp. 119–132. doi: 10.1023/A:1019905319224.

Zagari, F. *et al.* (2013) ‘Lactate metabolism shift in CHO cell culture: the role of mitochondrial oxidative activity’, *New Biotechnology*, 30(2), pp. 238–245. doi: 10.1016/j.nbt.2012.05.021.

Zhan, H. *et al.* (2013) ‘Production and First-in-Man Use of T Cells Engineered to Express a HSVTK-CD34 Sort-Suicide Gene’, *PLoS ONE*. Edited by E. Alici. Public Library of Science, 8(10), p. e77106. doi: 10.1371/journal.pone.0077106.

Zhang, H. *et al.* (2005) ‘Computational-fluid-dynamics (CFD) analysis of mixing and gas–liquid mass transfer in shake flasks’, *Biotechnology and Applied Biochemistry*. Blackwell Publishing Ltd, 41(1), p. 1. doi: 10.1042/BA20040082.

Zhang, H. *et al.* (2008) ‘Engineering characterisation of a single well from 24-well and 96-well microtitre plates’, *Biochemical Engineering Journal*, 40(1), pp. 138–149. doi: 10.1016/j.bej.2007.12.005.

Zhang, Y. (2009) ‘Approaches to optimizing animal cell culture process: substrate metabolism regulation and protein expression improvement.’, *Advances in biochemical engineering/biotechnology*, 113, pp. 177–215. doi: 10.1007/10_2008_19.

Zhou, M. *et al.* (2011) ‘Decreasing lactate level and increasing antibody production in Chinese Hamster Ovary cells (CHO) by reducing the expression of lactate dehydrogenase and pyruvate dehydrogenase kinases’, *Journal of Biotechnology*, 153(1), pp. 27–34. doi: 10.1016/j.jbiotec.2011.03.003.

Zhou, W., Rehm, J. and Hu, W.-S. (1995) ‘High viable cell concentration fed-batch cultures of hybridoma cells through on-line nutrient feeding’, *Biotechnology and Bioengineering*. John Wiley & Sons, Ltd, 46(6), pp. 579–587. doi: 10.1002/bit.260460611.

Zhu, M. M. *et al.* (2008) ‘Effects of Elevated pCO2 and Osmolality on Growth of CHO Cells and Production of Antibody-Fusion Protein B1: A Case Study’, *Biotechnology Progress*. American Chemical Society (ACS), 21(1), pp. 70–77. doi: 10.1021/bp049815s.

Zoro, B. (2016) ‘Micro-Scale Bioreactors in Fed-batch Microbial Screening’, *Biopharm International*, 29(8), pp. 27–32.